Arsenic and Fluoride Contamination in the Independence Basin Aquifer System of Guanajuato, Mexico

by

Forest Thomas Shepherd

B.S., Appalachian State University, 2016

A THESIS

submitted in partial fulfillment of the requirements for the degree

MASTER OF SCIENCE

Department of Geology
College of Arts and Sciences

KANSAS STATE UNIVERSITY
Manhattan, Kansas

2018

Approved by:

Major Professor
Dr. Saugata Datta

Copyright

Abstract

Elevated concentrations of arsenic (As) and fluoride (F) have been documented within the volcano-sedimentary aquifers of the Independence Basin Aquifer System in Guanajuato, Mexico which lies in the Mesa Central (MC) physiographic province on the northern edge of the Trans Mexican Volcanic Belt (TVMB). The geogenic sources of these contaminants are not well understood. This study adds to the existing record of the distribution of As and F contamination in the major aquifers of the basin by analyzing 24 water samples from five urban and rural areas. The mean As and F concentrations in the Cuenca Alto Rio Laja (CARL) aquifer on the western side of the basin were ~10 µg/L (median = 36 µg/L) and ~0.5 mg/L (median = 0.8 mg/L), respectively. In contrast, the mean As and F concentrations in the Laguna Seca (LS) aquifer on the eastern side of the basin were ~44 µg/L (median = 11 µg/L) and ~5.8 mg/L (2.6 mg/L), respectively. The high sodium, alkalinity, and low calcium concentrations observed in both aquifers are typical for fractured acid volcanic geothermal systems which have been observed in many Mexican states. Boron, lithium, and groundwater temperature showed positive correlations with As (R^2 = 0.47, 0.68, and 0.55) and F (R^2 = 0.31, 0.73, and 0.57) concentrations. These trace elements and elevated groundwater temperatures are indicators of water with hydrothermal origins. The drill cuttings from two boreholes ~500 m in depth were analyzed by X-ray diffraction, petrographic, and elemental analysis. This work revealed that the volcanic rocks of the CARL aquifer are primarily comprised of plagioclase, quartz, potassium-feldspar, calcite, volcanic glass, apatite, and iron oxyhydroxides. Additionally, there are layers of volcanic rocks comprised of pyroxene, plagioclase, quartz; amphibole, biotite, and apatite. The sedimentary rocks of the LS aquifer are comprised primarily of plagioclase, potassium feldspar, muscovite, biotite, volcanic glass, apatite, calcite, and quartz. These sedimentary rocks were deposited on volcanic rocks comprised of plagioclase, pyroxene, quartz, calcite, apatite, olivine, amphibole, hematite, chlorite, biotite, and ilmenite. To determine source zones the distribution of leachable F from the drill cuttings of both boreholes was examined through batch reactors. The leached F concentration profile revealed that the upper 140 m and lower 400 m of the western and eastern sides of the basin were the dominant source zones of leachable F. Overpumping in the IBAS has caused water table levels in this aquifer the decline over time. As these groundwater wells continue to be constructed to deeper depths to reach groundwater the release of As and F from these sources and the mechanisms controlling As

and F from these subsurface lithologies needs to be understood. The release of both As and F from the rocks of the western and eastern side of the basin at 400 to ~500 m depths were examined through pH-adjusted batch reactors with groundwater from the CARL which contained initial As and F concentrations of ~7.9 µg/L and ~0.8 mg/L; respectively. The dissolution of F-bearing minerals and adsorption reactions with iron oxyhydroxides display a dominant control on the changes in As and F concentrations in the groundwater of the CARL aquifer. At pH 5, the rocks from the 400 – 500 m depth within the CARL aquifer reduced the initial concentrations of As and F to values of ~5.8 µg/L and ~0.5 mg/L, respectively, after 200 hours. Whereas at a pH of 9 these rocks leached F increasing its concentration to ~0.9 mg/L. The As concentration was reduced to ~6.3 µg/L. In contrast to the CARL aquifer rocks, the rocks of the LS aquifer released F at all three pH values as F-bearing minerals dissolved. Alongside F-bearing mineral dissolution, adsorption on to iron oxyhydroxide surfaces could be occurring as F concentrations continuously decreased after 50 hours of reaction. The As concentrations in the rocks from the 400 – 550 m depths of the LS aquifer released minor amounts of As at pH 7 and 9, increasing the concentration slightly until 50 hours of reaction. During the remaining 150 hours of reaction the As concentrations displayed a continuous decrease in concentration. At pH 5, however, As concentrations decreased to ~5.7 µg/L after 200 hours of reaction. The spatial and kinetic leaching patterns observed in this study, combined with the mapping of known As- and F-bearing minerals within major rock aquifer groups on the east and west side of the basin, will suggest initial release or mobilization mechanisms to future researchers. The mechanisms of initial release and transport of As and F through aquifers of the Independence Basin should be studied through a combination of laboratory experiments and reactive flow and transport modeling to determine the migration of As and F from source rocks to groundwater wells.

Table of Contents

List of Figures viii
List of Tables xiii
Acknowledgements xvii
Dedication xviii
Chapter 1 - Introduction 1
1.1 Arsenic and Fluoride Contamination in Mexico 1
1.2 Arsenic Chemistry 3
1.3 Fluoride chemistry 4
1.4 Co-occurrence of Arsenic and Fluoride 5
1.5 Dissolution Studies 9
1.6 Research objectives 9
Chapter 2 - Geologic History 10
2.1 Regional Geologic History 10
2.2 Hydrogeology of the IBAS 12
Chapter 3 - Methods and Materials 16
3.1 Fieldwork 16
3.2 Ion Chromatography 18
3.3 Stable Isotopes 19
3.4 Dissolved Organic Carbon 19
3.5 Powder X-ray Diffraction 19
General settings 19
Arrastres Drill Cuttings 20
Lourdes Drill Cuttings 20
X-Ray Diffraction Data Analysis 20
3.6 X-ray Fluorescence 21
3.7 Optical Microscopy 21
3.8 Preliminary Batch Experiment 22
Batch Reactor Configuration 22
Water Sample Analysis 22

3.9 Dissolution Experiments 23
Reactor Construction and Groundwater 23
Rock Sample Preparation 24
Extraction of Water Samples for Analysis 24
3.10 Inductively Coupled Optical Emission Spectroscopy and Inductively Coupled Plasma Mass Spectroscopy 25
3.11 Geochemical Modeling of Batch Reactor Systems 26
Chapter 4 - Results 28
4.1 The Physicochemical Parameters of the Wells Sampled in the Field 28
Urban and Rural Groundwater Wells 28
Hand-Dug Wells 29
Waste Water Treatment Plant Dolores Hidalgo 30
4.2 The Water Chemistry of the Wells Sampled in the Field 33
Urban and Rural Groundwater Wells 33
Hand-dug Wells 34
Waste Water Treatment Plant Dolores Hidalgo 34
4.3 Laboratory Results of the IBAS Water Samples 36
Urban and Rural Groundwater Wells Cations 36
Urban and Rural Groundwater Wells Anions 37
Hand-Dug Wells Major Ions 38
Waste Water Treatment Plant Major Ions 38
Groundwater Water Types 40
Urban and Rural Groundwater Wells Trace Ions 42
Hand-Dug Wells Trace Ions 44
Waste Water Treatment Plant Trace Ions 44
4.4 Oxygen ($\delta^{18}O$) and Deuterium ($\delta^{2}H$) Isotopic Ratios of IBAS Groundwater 46
4.5 Dissolved Organic Carbon in the IBAS Water Sample 50
4.6 X-Ray Diffraction of the Drill Cuttings from the IBAS 51
Western Side of Basin (Arrastres) 51
Eastern Side of the Basin (Lourdes) 52
4.7 Surface Samples of Rocks and Sediments 53

4.8 Petrographic Analysis Results on Thin Sections of the Drill Cuttings 57
Arrastres Drill Cuttings 57
Lourdes Drill Cuttings 58
4.9 X-ray fluorescence Results of Drill Cuttings 61
Arrastres Drill Cuttings: 61
Lourdes Drill Cuttings: 63
4.10 Depth Dependent Distribution of Leachable Fluoride in the Basin 65
Overview 65
Fluoride Leaching from Arrastres Drill Cutting in DI Waters: 65
Fluoride Leaching from Lourdes Drill Cuttings in DI Water: 65
Fluoride Leaching from the Arrastres Drill Cuttings in Groundwater: 67
Fluoride Leaching from the Lourdes Drill Cuttings in Groundwater: 67
4.11 Time and pH dependent Water-Rock Interactions 69
Overview 69
Arrastres Drill Cuttings and Groundwater Interaction Experiment 69
Lourdes Drill Cuttings and Groundwater Interaction Experiment 71
4.12 Rate Const ant Calculations 79
4.13 Geochemical Modeling of Batch Reactor Results 80
Chapter 5 - Discussion 82
5.1 How Water Chemistry Influences Elemental Mobilities in IBAS 82
5.2 How Dominant Lithologies affect the Water Chemistry and Reactions in IIBAS 87
5.3 Leaching of Major and Trace Elements from Rocks of the Arrastres and Lourdes Cores . 90
Chapter 6 - Conclusions 95
References 97
Appendix A - Supplementary Data 107

List of Figures

Figure 1.1 Location of the IBAS with respect to Mexico and the state of Guanajuato. Areas of black indicate major urban areas with connecting roads and basin limits outlined (Navarro de Leon et al., 2005). 3

Figure 1.2 Distribution of main hydrothermal areas in Mexico. Main geothermal areas are named, and the feasibility of their potential for hydrothermal production are indicated in legend (alta = high, media = medium, baja = low) (Flores-Armenta et al., 2011). This studies area outlined in a black square. 6

Figure 2.1 The physiographic provinces of Mexico which include the SMOc, SMOr, TMVB, and the MC. The SW – NE trending striped areas outline the Sierra Madre Occidental Volcanic Province of the mid-Tertiary period which represents a large rhyolitic volcanic event (Orozco-Esquivel et al., 2002). The SE – NW trending striped area represents Oligocene – Miocene volcanic rocks (Nieto-Samaniego, 1999). The black box is used to indicate this study's field area (Orozco-Esquivel et al., 2002)..... 11

Figure 2.2 Chronostratigraphic section of the IBAS (Mahlknecht et al., 2004). 12

Figure 2.3 Geologic Map of the IBAS with the basin limit outlined in blue, faults defined by purple lines, and green circles which indicate major cities (Loza-Aguirre I., work in progress; Nieto-Samaniego et al., 2007). 14

Figure 2.4 The sampling locations for this study and the location of the two borehole drill cuttings used in this study identified by black hexagons. Simplified geologic map (Muehlberger, 1985-1990; Ortega-Gutierrez, 1992; Padilla y Sanchez et al., 1994; as cited by USGS, Geologic Map of North America). WWTP: Waste water treatment plant, TC: Terreros de la Concepciones 15

Figure 3.1 Images of production wells sampled, the preparation of field kits for conducting analysis, and collecting depth to water measurements in the IBAS in Mexico (Images curtesy of William Thurston at Caminos del Agua). 18

Figure 3.2 Conceptual model of the batch reactors used in this study. 23

Figure 4.1 Piper diagram displaying the major water types observed in the basin. 40

Figure 4.2 Range of values in major ions from groundwater wells, hand-dug wells, and water treatment effluent water samples with mean value designated with the symbol x. Interior and outlier points a denoted alongside the four quartiles. 41
Figure 4.3 Range of values in trace ions from groundwater, hand dug, and water treatment effluent water samples with mean value designated with the symbol x. Interior and outlier points a denoted alongside the four quartiles. 45
Figure 4.4 Oxygen and deuterium isotopes for all water samples from the IBAS. The solid black line represents the global meteoric water line (GMWL: $\delta^2H = 8\ \delta^{18}O + 10$) (Craig H., 1961), the dashed lines represent the regional meteoric water line (RMWL: $\delta^2H = 7.97\delta^{18}O + 11.03$) and groundwater impacted by mixing between the western and eastern sides of the basin (Mixing & Evaporation: $\delta^2H = 6.97\delta^{18}O - 4.40$) (Mahlknecht et al., 2004)..... 48
Figure 4.5 Oxygen and deuterium isotopic composition of wells sampled in the IBAS since 2008. The black triangles represent samples collected in the basin directly west of the IBAS by Horst et al. (2008). The dashed lines represent: groundwater impacted by mixing between the western and eastern sides of the basin (Mixing & Evaporation: $\delta^2H = 6.97\delta^{18}O - 4.40$) (Mahlknecht et al., 2004), the global meteoric water line (GMWL: $\delta^2H = 8\ \delta^{18}O + 10$) (Craig H., 1961), and the regional meteoric water line (RMWL: $\delta^2H = 7.97\delta^{18}O + 11.03$) (Cortes et al., 1989). The black circles and the black dashed line represents the local meteoric water line (LMWL: $\delta^2H = 7.37\delta^{18}O + 4.31$) developed by Knappett et al. (2018). 48
Figure 4.6 Oxygen and deuterium isotope ratios for San Luis de la Paz (SLP) and flow path. (GMWL: $\delta^2H = 8\ \delta^{18}O + 10$) (Craig H., 1961), (Mixing & Evaporation: $\delta^2H = 6.97\delta^{18}O - 4.40$) 49
Figure 4.7 The DOC concentrations in groundwater wells with respect to the depth of the well (A). The distribution of DOC values in the water samples collected from the IBAS (B). The water treatment plant effluent water (16.18 mg/L) was excluded from the box and whisker plot as it skewed the average concentration (B). 50
Figure 4.8 Stratigraphic column of the Arrastres drill cuttings from the western side of the basin. 51

Figure 4.9 Stratigraphic column of the Lourdes drill cuttings from the eastern side of the basin. Clinoptilolite was identified at the 180 m and hornblende between 240 and 280 m. Magnetite was identified at the 420 m depth. 52
Figure 4.10 The location of the four field samples collected in the IBAS. 54
Figure 4.11 Sample one collected from the IBAS 54
Figure 4.12 Sample two collected from the IBAS 55
Figure 4.13 Sample four collected from the IBAS 55
Figure 4.14 Sample seven collected from the IBAS 56
Figure 4.15 Images of the mineralogy observed in the ~20 m (A) ~160 m (B) ~340 m depth (C) and ~440 m depth (D) of the Arrastres drill cuttings Images shown in transmitted light with crossed polars. Images of the minerology observed in the ~540 m depth (E) of the Lourdes drill cuttings and the ~440 m depth (F) of the Arrastres drill cuttings shown in reflected light. 59
Figure 4.16 Images of the mineralogy of the Lourdes drill cuttings from images of the mineralogy observed in the ~140 m (A), ~220 m (B) ~360 m (C) depth with crossed polars, and ~540 m (D) ~540 m depth (E and F). Images shown in transmitted light. 60
Figure 4.17 The major and trace element concentration profiles with depth for the Arrastres drill cuttings with the blue line expressing the average value and horizontal lines expressing the standard deviation calculated in Excel between the three measurements taken at each depth. 62
Figure 4.18 The major and trace element concentration profiles with depth for the Lourdes drill cuttings with the blue line expressing the average value and horizontal lines expressing the standard deviation calculated in Excel between the three measurements taken at each depth. 64
Figure 4.19 Leachable F concentrations from the Arrastres drill cuttings (A) and Lourdes drill cuttings (B). Reactors used DI water, were run alongside a set of duplicates (red circles) with measurements by IC (green X) Dashed lines represent the WHO safe drinking water limit of 1.5 mg/L for F. 66
Figure 4.20 Leachable F concentration measurements for the Arrastres and Lourdes drill cuttings. Reactors used groundwater from the rural wells CDW (C) and LS-0178 (D). Red line indicates the initial F concentration of the groundwater. These reactors were run with

duplicates (red circles) and IC (green X) the dashed line represents the WHO Safe Drinking Water Limit 1.5 mg/L for F. 68
Figure 4.21 The F concentration changes from the Arrastres drill cuttings on the western side of the basin reacting with groundwater (A and B). The WHO safe drinking water limit for F 1.5 mg/L (A) and 0.79 mmol/L (B). 72
Figure 4.22 The F concentration changes from the Lourdes drill cuttings on the eastern side of the basin reacting with groundwater (C and D). The WHO safe drinking water limit for F 1.5 mg/L (A) and 0.79 mmol/L (A). 72
Figure 4.23 The As concentration changes from the Arrastres drill cuttings on the western side of the basin reacting with groundwater (E and F). The WHO safe drinking water limit for F 10 µg/L (A) and 0.13 µmol/L (B). 73
Figure 4.24 The As concentration changes from the Lourdes drill cuttings on the eastern side of the basin reacting with groundwater (E and F). The WHO safe drinking water limit for F 10 µg/L (A) and 0.13 µmol/L (B). 73
Figure 4.25 Dissolved Ca concentration changes from the Arrastres drill cuttings on the western side of the basin. 74
Figure 4.26 Dissolved Ca concentration changes from the Lourdes drill cuttings on the eastern side of the basin. 74
Figure 4.27 Dissolved Na concentration changes from the Arrastres drill cuttings (M) from the western side of the basin. Reactors impacted by the addition of NaOH were removed. 75
Figure 4.28 Dissolved Na concentration changes from the Lourdes drill cuttings from the eastern side of the basin. Reactors impacted by the addition of NaOH were removed. 75
Figure 4.29 Dissolved B concentration changes from the Arrastres drill cuttings from the western side of the basin. 76
Figure 4.30 Dissolved B concentration changes from the Lourdes drill cuttings from the eastern side of the basin. 76
Figure 4.31 Dissolved Li concentration changes from the Arrastres drill cuttings from the western side of the basin. 77
Figure 4.32 Dissolved Li concentration changes from the Lourdes drill cuttings from the eastern side of the basin. 77

Figure 4.33 Dissolved Fe concentration changes from the Arrastres drill cuttings from the western side of the basin. 78
Figure 4.34 Dissolved Fe concentration changes from the Lourdes drill cuttings from the eastern side of the basin. 78
Figure 4.35 Bivariant plot representing the change in F concentrations with respect to time during the initial 50 hours of reaction. 80
Figure 4.36 Modeling simulation output of fluorite dissolution and adsorption of F onto iron oxyhydroxide mineral surfaces (A) pH = 9, (B) pH = 7, (C) pH = 5 81
Figure 4.37 Modeling simulation output of arsenic adsorption onto iron oxyhydroxide mineral surfaces (D) pH = 9, (E) pH = 7, (F) pH = 5. 81
Figure 5.1 Bivariate plots which represents the relationship between boron and lithium in groundwater wells. Markers with red fill are groundwater wells with water temperatures greater than 30 C^{o} 83
Figure 5.2 F and Ca concentration from the groundwater wells sampled in the Independence Basin with dashed line representing fluorite saturation calculated from the equilibrium constant provided by Brown and Roberson (1977). 85

List of Tables

Table 1.1 Arsenic and F contamination studies conducted in the Central Plateau region of Mexico. PG = possibly geogenic, G = Geogenic, A = Anthropogenic, GT = Geothermal, U = Unknown. Table modified from Reyes-Gomez et al., 2013 with data sources from: Martinez-Prado et al., 2013; Gonzalez-Horta et al., 2015; Westerhoff et al., 2004; Hernandez-Montoya et al., 2003; Navarro et al., 2017; Carrillo-Rivera et al., 2002; Razo et al., 2004; Armienta and Segovia, 2008; Ortega-Guerrero, 2009; Birkle and Merkel, 2000; Hurtado-Jimenez and Gardea Torresdey, 2006; ESF-DMAE, 2006; Pinon-Miramontes et al., 2003; Gonzalez D., 2011; Hurtado-Jimenez and Gardea-Torresdey, 2004; Mahlknecht et al., 2008; Planer-Friedrich et al., 2001..... 7

Table 1.2 Health risks studies conducted in the Central Plateau region of Mexico. Data sources include: Betancourt-Lineares et al., 2013; Monroy-Torres et al., 2009; Smeester et al., 2011; Wyatt et al., 1998; Mendez et al., 2016; Hurtado-Jimenez et al., 2006; Hurtado-Jimenez and Gardea-Torresdey, 2005; Rodriguez-Dozal et al., 2005; Aguilar-Díaz et al., 2016; Pontigo-Loyola et al., 2008; Hernández-Montoya et al., 2003; Castro de Esparza M.L., 2006; Carrizalesa et al., 2006; Mendoza et al., 2011. 8

Table 3.1 List of field kits used to measure chemical parameters of groundwater samples..... 17

Table 3.2 Adsorption reactions used in the Geochemist Workbench Software (*indicates estimated values). The >(w) represents weak surface sites. 27

Table 4.1 The water chemistry data collected in the field alongside locations of wells sampled within the IBAS. The city designation is based on the wells proximity to a major city and type is used to separate urban wells versus rural wells. (n.a.) indicates the measurement were not available or determined. 31

Table 4.2 Specific conductance calculated from the EC and temperature values measured in the field with the following calculation SC = EC/(1+0.0191*(T-25^{o}C). ORP was corrected for the use of an Ag/AgCl probe by adding 199 to the value measured in the field. 32

Table 4.3 Ranges of the physicochemical parameters and water chemistries measured in the five major cities in the basin. 34

Table 4.4 The groundwater chemical parameters measured in the field from the five urban areas All units expressed as mg/L. 35

Table 4.5 Major ions in the groundwater of the IBAS. Nitrite was only detectable in sample CDW at 0.28 mg/L. 39
Table 4.6 Ranges of values measured major ions for the five different municipalities. All values are expressed as mg/L. HCO3- is expressed as mg/L as CaCO3 40
Table 4.7 The averages and ranges of trace ions in only the groundwater samples collected from the IBAS. 44
Table 4.8 Average values for selected trace ion concentrations that were detectable around each of the five major municipalities in the basin. All values are expressed as µg/L. 44
Table 4.9 Range of values for selected trace ion concentrations that were detectable around each of the five major municipalities in the basin. All values are expressed as µg/L. 45
Table 4.10 Range of values for trace ion concentrations in the rural and urban wells near two major urban areas in the IBAS. All values are expressed as µg/L. 45
Table 4.11 Oxygen and Deuterium isotopic ratios for water samples from the IBAS. 47
Table 4.12 Oxygen and deuterium isotopic ranges and averages for the major urban areas. All units are expressed as ‰VSMOW 47
Table 4.13 Summary of the DOC measured near major urban areas. 50
Table 4.14 Rock samples collected in the field and analyzed by XRD. 53
Table 4.15 Minerals observed in the thin sections of the Arrastres drill cuttings. 57
Table 4.16 Minerals observed in the thin sections of the Lourdes drill cuttings. 58
Table 4.17 Range of elemental concentrations for the Arrastres Drill cuttings from 0 – 500 m. All values are reported as parts per million (mg/kg). 61
Table 4.18 Range of elemental concentrations for the Lourdes Drill cuttings from 0 – 550 m. All values are reported as parts per million (mg/kg). 63
Table 4.19 Water Chemistry of the groundwater used in the leaching experiments. 65
Table 4.20 Water chemistry of the basin 69
Table 4.21 Table of rate constant values 79
Table 5.1 R^2 Correlation matrix between physiochemical parameters and trace and major elements. Values in bold have p-values below 0.05. 83
Table A.1 Field measurement collected in the IBAS. (Bdl) indicates below detection limit. (nm) indicates no measurement. 107
Table A.2 Field measurements continued. (nm) indicates no measurement. 108

Table A.3 Trace elements for the groundwater samples collected from the IBAS. The (n.a.) symbol indicates vales are not available. 109
Table A.4 Dissolved organic carbon values for all wells in the IBAS. The values without highlighting are DOC values for samples that were acidified with 10.2 M HCl in the field. The values highlighted yellow are from samples not acidified in the field. 113
Table A.5 Arrastres rock drill cuttings: data collected from the target batch reactor for F using DI water. 114
Table A.6 Arrastres Drill cuttings: Ion chromatography anion results from the DI batch reactors. 114
Table A.7 Arrastres Drill cuttings: Ion chromatography cation results from the DI batch reactors. 115
Table A.8 Arrastres Drill cuttings: Duplicates using DI water batch reactor. 115
Table A.9 Arrastres rock drill cuttings: The F values from batch reactor using groundwater from the rural well (CDW). 116
Table A.10 Arrastres Drill cuttings: Ion chromatography anion results from the GW batch reactors. 116
Table A.11Arrastres Drill cuttings: Ion chromatography cation results from the GW batch reactors. 117
Table A.12 Arrastres Drill cuttings: Duplicates using groundwater from CDW. 117
Table A.13 The initial measurements of the waters in the F targeting batch reactor. 117
Table A.14 Controls used for the experiment after 200 hours. 117
Table A.15 Lourdes rock drill cuttings: data collected from the target batch reactor for F using DI water. 118
Table A.16 Lourdes Drill cuttings: Ion chromatography anion results from the DI batch reactors. 118
Table A.17 Lourdes Drill cuttings: Ion chromatography cation results from the DI batch reactors. 119
Table A.18 Lourdes Drill cuttings: Duplicates for DI water batch reactor 119
Table A.19 Lourdes rock drill cuttings: data collected from the target batch reactor for F using groundwater. 120

Table A.20 Lourdes Drill cuttings: Ion chromatography anion results from the GW batch reactors 120
Table A.21 Lourdes Drill Cuttings: Ion chromatography cation results from the GW batch reactors 121
Table A.22 Lourdes Drill Cuttings: Ion chromatography cation results from the DI batch reactors 121
Table A.23 Lourdes Drill cuttings: Duplicates for GW batch reactor 121
Table A.24 Lourdes Drill Cuttings physicochemical parameters. 121
Table A.25 Major anion analysis of pH adjusted batch reactor. 122
Table A.26 Major cation result from pH adjusted batch reactor 125
Table A.27 Major and trace results from pH-adjusted batch reactor 128
Table A.28 Trace element data for the pH adjusted batch reactors. 134
Table A.29 Trace elements results from the pH adjusted batch reactors. 136
Table A.30 Control De-ionized water and groundwater used in the pH adjusted reactor. 138
Table A.31 Fluorite saturation index calculation for the pH-adjusted batch reactors 139

Acknowledgements

During the initial days of this work the support I received in the field from Viridiana Gonzalez, Manuel Jasso, Dulce Torres, Rodrigo Rodriguez, and William Thurston. They were patient with me during the first few days and by the end we were sharing stories and working well as a team. They took time out of their days and worked extremely hard to ensure this work would be a success. I would also like to acknowledge the support I received from Dr. Yanmei Li and Dr. Horacio Hernandez. They kept me in their house, feed me amazing food, and shared their life with me while I was in Mexico. Once I returned to Kansas State University, I received support from all the faculty in the department of geology. My fellow graduate students also helped me immensely.

I would also like to thank Dr. Parameswaran, Dr. Nippert, and Dr. Kirk for allowing use of their instruments to analyze water samples and for their helpful and thought-provoking discussions. Patrick Manselle was an amazing colleague who aided in properly identifying and teaching me about the minerology of the minerals found in the drill cuttings.

Dr. Ganga Hettiarachchi, you were always open to discussions and your time invested in me will not be forgotten. Your input and discussions were critical both as a professor and mentor. You were a great addition to the team and thank you.

Dr. Peter Knappett, I would not be where I am today if it was not for you and your efforts to help the communities of Guanajuato. Collaborative meetings and your ability to bring such a large group of professionals together made this project a success and I owe a lot to you for your time and guidance.

Dr. Pamela Kempton, your conversations and input to help me understand the geology and mineralogy of the basin which aided in my understanding and thoughts as I worked. Your guidance over the geology department allowed me to access all the tools and equipment, as well as, professors which helped me make this work a success.

Lastly, I would like to address my mentor and friend, Dr. Saugata Datta. You gave me knowledge, life lessons, and opened my eyes to the complex and difficult world of geochemistry. Your support and guidance has brought out the best in this work. You are a great mentor and I was lucky to be able to work with you.

Dedication

The people of Guanajuato, Mexico.

Chapter 1 - Introduction

1.1 Arsenic and Fluoride Contamination in Mexico

The Independence Basin Aquifer System (IBAS) in the state of Guanajuato, Mexico, spans a surface area of 6840 km^2 and supplies groundwater for agriculture, industry, and drinking to approximately half a million people in the urban areas of San Miguel de Allende, San Luis de La Paz, San Felipe, San Diego de la Union, and Dolores Hidalgo (Mahlknecht et al., 2004; Navarro de Leon et al., 2005) (Figure 1.1). The IBAS is primarily composed of fractured rhyolitic ignimbrite deposits that are overlain by alluvial and lacustrine sedimentary deposits with interstratified layers of volcanoclastic conglomerates and volcanic ash (Mahlknecht et al., 2004). The groundwater wells emplaced in the sedimentary deposits supply ~80% of the groundwater used by the inhabitants of the IBAS, while the remaining ~20% of the population extracts groundwater from fractured rhyolite units (Ortega-Guerrero, 2009). Several studies have conducted chemical analyses on samples obtained from groundwater wells emplaced in this aquifer system and found dissolved arsenic (As) and dissolved fluoride (F) concentrations that are above the World Health Organization's (WHO) provisional guidelines of 0.010 mg/L and 1.5 mg/L, respectively (Ortega-Guerrero et al., 2002; Mahlknecht et al., 2003; Mahlknecht et al., 2004; Ortega-Guerrero, 2009). These water samples have also surpassed the Mexican drinking water standard for As at 0.025 mg/L (Ortega-Guerrero, 2009). The prolonged consumption of these two harmful contaminants can result in a plethora of health-related problems. The harmful effect of consuming As at concentrations greater than the 10 µg/L include, but are not limited to, various forms of cancer and reproductive effects (Bissen and Frimmel, 2003; WHO, 2004; Kapaj et al., 2006). The consumption of F above 1.5 mg/L can result in both dental and skeletal fluorosis (Chouhan and Flora, 2010).

The studies conducted in the IBAS have aided in determining the distribution of elevated As and F concentrations and the link between the geology of the basin and groundwater. Ortega-Guerrero et al. (2002) found elevated concentrations of As and F in the IBAS which ranged from 0.010 – 0.120 mg/L and 1.5 – 16.0 mg/L, respectively. The rural communities living the northeastern extent of the basin are exposed to the highest concentrations of both these contaminants (Ortega-Guerrero et al., 2002; Ortega-Guerrero, 2009). Investigations by Mahlknecht et al. (2004) on the groundwater of the IBAS included chemical, isotopic, petrographic, and mineralogical analyses and concluded through inverse geochemical modeling

that the extraction of paleogroundwater, oxidation of As -bearing sulfides, and the dissolution of volcanic rocks were the sources of As and F. Almost two decades after these initial measurements were conducted, Knappett et al. (2018) re-sampled 22 of the groundwater wells sampled by Mahlknecht et al. (2004) and Ortega-Guerrero (2009). This study suggested increasing F concentrations in drinking water wells were driven by deeper groundwater extraction, increased pumping rates, and irrigation return flow which enriches F concentrations through evaporation. Although these investigations have brought awareness to the presence of these two contaminants in the region, the specific source rocks and minerals have not been confirmed directly and the mechanisms controlling these two contaminants in groundwater has not been investigated through controlled laboratory experiments.

In many states surrounding the state of Guanajuato, aquifers have been identified which contain elevated As and F concentrations, including: Zacatecas (Navarro et al., 2017), San Luis Potosi (Jarquin-Yanez et al., 2015), Durango (Martinez-Prado et al., 2013), as well as many other states (Armienta and Segoiva, 2008) (Table 1.1). Groundwater is the primary source of drinking water in these states with arid and semi-arid climates. The health-risks from consuming As and F laden groundwater are increased, relative to more temperate climates, as drier climates induce increased consumption (Apambire et al., 1997). Furthermore, physical laborers, such as poor farmers, for example, are likely to consume much more water in a day than people with more sedentary office jobs. Additionally, the heterogeneous distribution of these two contaminants also presents a challenge in documenting and managing the health risks (Armienta and Segoiva, 2008; Mazziotti-Tagliani et al., 2012). The rural populations that are impacted by these contaminants are especially difficult to monitor as few funding sources support investigations into the water quality and health of these impacted communities (Kapaj et al., 2006).

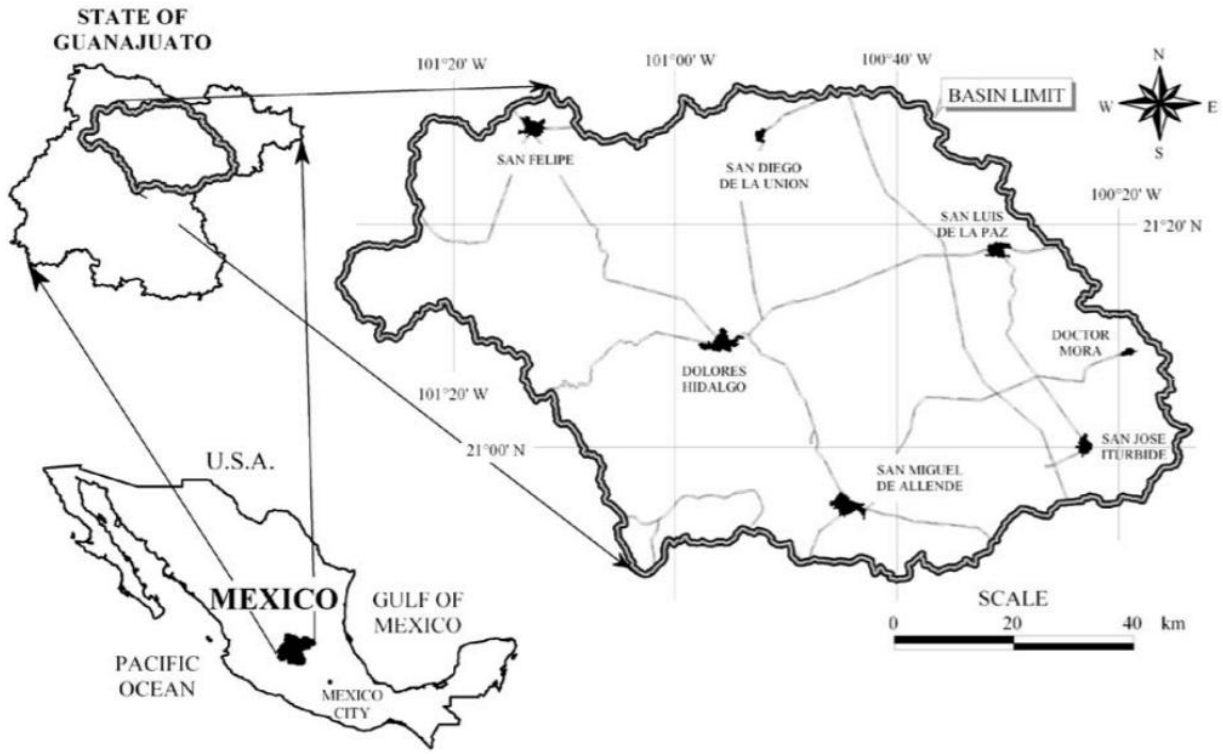

Figure 1.1 Location of the IBAS with respect to Mexico and the state of Guanajuato. Areas of black indicate major urban areas with connecting roads and basin limits outlined (Navarro de Leon et al., 2005).

1.2 Arsenic Chemistry

Arsenic is a toxic metalloid that can bond with many other elements to form both inorganic and organic compounds (Bissen and Frimmel, 2003). These compounds are then released into the environment from both anthropogenic and natural sources. Anthropogenic sources of As include mining, fossil fuels, smelting plants, phosphate fertilizers, and pesticides (Smedley and Kinniburgh, 2002; Kapaj et al., 2006). The natural sources of As include iron (Fe), manganese (Mn), and aluminum (Al) oxides; some silicate minerals; chlorite; As – bearing sulfides like arsenopyrite (FeAsS); and over 200 other As-bearing minerals (Simons and Mapes-Vazquez, 1956; Smedley and Kinniburgh, 2002; Smedley et al., 2008; Masuda et al., 2012).

When these anthropogenic and natural sources of As chemically interact with groundwater they can mobilize As into the environment. The mechanisms that mobilize As include adsorption/desorption reactions involving Fe (Dixit and Hering, 2003; Kumar et al., 2016), Mn, and Al oxides; clay minerals; dissolved organic carbon (Smedley and Kinniburgh, 2002); hydrothermal fluids (Lopez et al., 2012); and the dissolution of As-bearing minerals (Smedley and Kinniburgh, 2002). Once in groundwater, As can occur in multiple oxidation states, including -3,

0, +3, and +5, although it commonly occurs in the two oxidation states: arsenite (As^{III}) and arsenate (As^{V}) (Smedley and Kinniburgh, 2002; Bissen and Frimmel, 2003). The different oxidation states of As are capable of protonation through bonding with oxygen and hydrogen to create various oxyanions depending on the potential hydrogen (pH), redox potential (Eh), and the chemical composition of an aqueous environment (Hinkle and Polette, 1999; Stollenwerk et al., 2007). In oxidizing aquifers below a neutral pH value (pH < 6.9), the arsenate species H_3AsO_4 and $H_2AsO_4^-$ are dominant whereas the least protonated arsenate species $HAsO_4^{2-}$ becomes dominant at pH values greater than 6.9 (Smedley and Kinniburgh, 2002; Bissen and Frimmel, 2003). In reducing aquifers with a pH below 9.2, arsenite (H_3AsO_3) is the dominant species with H_2AsO^{3-}, $HAsO_3^{2-}$, and AsO_3^{3-} becoming dominant at high pH values (Smedley and Kinniburgh, 2002; Bissen and Frimmel, 2003). The arsenite species of As is typically more toxic to humans than arsenate (Reimann et al., 2009).

The WHO established the provisional guideline of 10 µg/L for As based on studies of skin cancer risks (Kapaj et al., 2006). Prolonged consumption of As can result in both acute and chronic health-related effects. The acute health effects include vomiting, dryness of the mouth and throat, muscle cramps, tingling of the hands and feet, circulatory disorders, nervousness, and weakness (Bissen and Frimmel, 2003). The chronic health effects include loss of reflexes, weariness, gastritis, colitis, weight and hair loss, hyperkeratosis, hyperpigmentation, cardiovascular disease, nervous system effects, various forms of cancers, and reproductive effects (Table 1.2; Bissen and Frimmel, 2003; WHO, 2004; Kapaj et al., 2006). Individuals who are unaccustomed to consuming As will die upon ingestion of 0.1 – 0.3 g/d (Bissen and Frimmel, 2003).

1.3 Fluoride chemistry

Fluorine is the 13th most common element in the earth's crust with an average concentration of 0.3 g/kg (McBride, 1994; Lennon et al., 2004; WHO, 2004). It is the most electronegative element which is why in water, fluorine forms F ions with a charge of -1. Anthropogenic sources of F include aluminum smelters, ceramics, brick, glass, and fertilizer factories (Gago et al., 2014). Natural sources of F include fluorite (CaF_2), topaz ($Al_2SiO_4(F,OH)_2$), fluorapatite ($Ca_5(PO_4)_3(OH,F,Cl)$ and many accessory minerals (Gaciri and Davies, 1993; Apambire et al., 1997; WHO, 2004;). F is also known to become part of the lattice structure in micas through isomorphic substitution, which involves the F ion replacing an ion with a similar charge and radius, such as the hydroxyl (OH) ion to form F-rich biotite ($KFe_3(AlSi_3)O_{10}F_2$),

phlogopite ($KMg_3(AlSi_3)O_{10}F_2$), and amphibole (Apambire et al., 1997; Madhavan, 2002; Garcia and Borgnino, 2015). Additionally, F can be incorporated into fluorite as a replacement mineral on calcium carbonate surfaces (Baer and Lewin, 1970).

The concentrations of F in ground waters is dependent on temperature, pH, abundance of complexing ions, solubility of F-bearing minerals, anion exchange capacity of the aquifer material, the extent and composition of the geology, and the residence time in the aquifer (Apambire et al., 1997). The adsorption/desorption mechanisms for F range from electrostatic attraction, anion exchange, and ligand exchange with surface OH groups and water molecules (Harrington et al., 2003). The degree of adsorption is affected by pH, grain size, F concentration, and salinity (Sivasankar et al., 2016).

In acidic (pH < 7) environments, F tends to form complexes with aluminum (AlF^{2+}, AlF_2^+, AlF_3, AlF_4^-), ferric iron (FeF_2^+, FeF_2^+, FeF_3), hydrogen (HF, HF_2^-), and silicon (SiF_4, SiF_6^{2-}) (Gaciri and Davies, 1993, McBride, 1994; WHO, 2003; Viero et al., 2008;). At pH > 7, F ions are released from aluminum and ferric iron in exchange for hydroxide ions, which form gibbsite ($Al(OH)_3$), goethite (FeO(OH)) and ferrihydrite ($Fe_{10}O_{15}•9H_2O$) (WHO, 2003; Viero et al., 2008;). In alkaline (pH > 7) environments, the most stable form of F is fluorite, although the low solubility tends to release F from this crystal structure (WHO, 2003). Additionally, F can remain in solution as calcium tends to form complexes with carbonates and sulfates (Nordstrom and Jenne, 1977). In alkaline environments, F can be prevented from adsorbing onto clays and oxyhydroxide minerals (Viero et al., 2008).

In low concentrations, F can improve dental health (WHO, 2003). Although, when F is consumed above 1.5 mg/L it has been linked to health-related diseases, including dental and skeletal fluorosis (Table 1.2; WHO, 2003). The acute health risks of consuming F include nausea, vomiting, diarrhea, and abdominal pain (Chouhan and Flora, 2010). The long-term health related risks are emaciation, stiffness of joints, and fluorosis; which is related to bone hardening and abnormal enamel growth on teeth (Chouhan and Flora, 2010).

1.4 Co-occurrence of Arsenic and Fluoride

Geogenic As contamination of groundwater has impacted millions of inhabitants in many areas of the world; including China, Argentina, Vietnam, Romania, Chile, Bangladesh, and India (Welch et al., 2000; Smedley and Kinniburgh, 2002; Alarcon-Herrera et al., 2013). Elevated concentrations of F have been identified alongside As in the groundwater of areas including China,

Argentina, Chile, India, and Mexico (Mahlknecht et al., 2004; Chaouhan and Flora 2010; Alarcon-Herrera et al., 2013; Kumar et al, 2016).

The first occurrence of chronic As contamination in Mexico was documented in 1958 by Cebrián et al. (1994) (as cited in Armienta and Segoiva, 2008). The primary sources and processes causing elevated dissolved levels of As and F concentrations are still debated for these regions but speculated sources in the groundwaters of Mexico include dissolution of As- and F-bearing minerals, hydrothermal influence, and anthropogenic input through mining activity (Armienta and Segovia, 2008; Lopez et al. 2012).

In 27 of the 32 Mexican states, low to medium temperature (28 – 200ºC) hydrothermal conditions exist due to the volcanic activity and the fault structure of the TMVB and the Sierra Madre Occidental (SMOc) (Lopez et al., 2012) (Figure 1.2). Although these conditions are known, water chemistry data related to As in these hydrothermal areas is poorly understood (Lopez et al. 2012). Examination of wells in these hydrothermal areas has found As concentrations ranging from 0.25 – 73.6 mg/L (Lopez et al., 2012). In many of these geothermal settings F is a common co-occurring ion in solution.

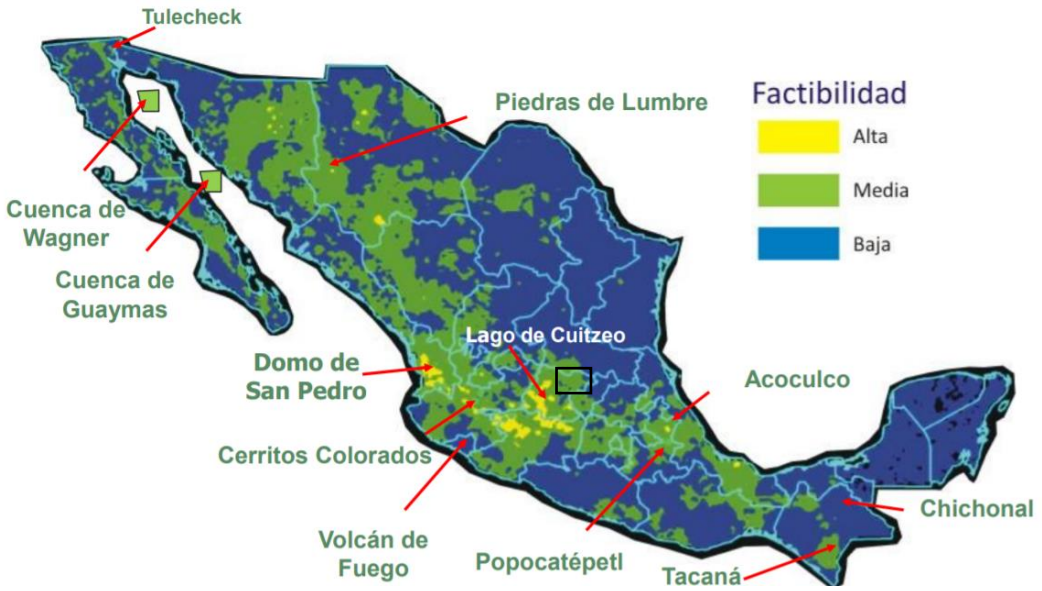

Figure 1.2 Distribution of main hydrothermal areas in Mexico. Main geothermal areas are named, and the feasibility of their potential for hydrothermal production are indicated in legend (alta = high, media = medium, baja = low) (Flores-Armenta et al., 2011). This studies area outlined in a black square.

Table 1.1 Arsenic and F contamination studies conducted in the Central Plateau region of Mexico. PG = possibly geogenic, G = Geogenic, A = Anthropogenic, GT = Geothermal, U = Unknown. Table modified from Reyes-Gomez et al., 2013 with data sources from: Martinez-Prado et al., 2013; Gonzalez-Horta et al., 2015; Westerhoff et al., 2004; Hernandez-Montoya et al., 2003; Navarro et al., 2017; Carrillo-Rivera et al., 2002; Razo et al., 2004; Armienta and Segovia, 2008; Ortega-Guerrero, 2009; Birkle and Merkel, 2000; Hurtado-Jimenez and Gardea Torresdey, 2006; ESF-DMAE, 2006; Pinon-Miramontes et al., 2003; Gonzalez D., 2011; Hurtado-Jimenez and Gardea-Torresdey, 2004; Mahlknecht et al., 2008; Planer-Friedrich et al., 2001.

Mexico States	Arsenic (µg/L)	Fluoride (mg/L)	Speculated Sources
Sonora (Northern Mexico)	18 – 62	0.5 – 3.5	PG
Chihuahua (Northern Mexico)	52 – 627	0.5 – 3.3	PG
Durango (Northern Mexico)	80 – 150	1.1 – 17.8	G, PG, A
Zacatecas (Central Mexico)	3.3 –75	0.35 – 3.6	G, A
Aguascalientes (Central Mexico)	N/A	1.5 – 12	PG
San Luis Potosi (Central Mexico)	1 – 120	0.001 – 16	G, PG, A
Hidalgo (Central Mexico)	59 – 400	N/A	G, A
Michoacán (Central Mexico)	1 – 800	1.3 – 16	GT
Jalisco (Central Mexico)	14 – 260	1.66 – 18.5	G, A
Guanajuato (Study Area)	1 – 93	0.3 – 15	G, A

Table 1.2 Health risks studies conducted in the Central Plateau region of Mexico. Data sources include: Betancourt-Lineares et al., 2013; Monroy-Torres et al., 2009; Smeester et al., 2011; Wyatt et al., 1998; Mendez et al., 2016; Hurtado-Jimenez et al., 2006; Hurtado-Jimenez and Gardea-Torresdey, 2005; Rodriguez-Dozal et al., 2005; Aguilar-Díaz et al., 2016; Pontigo-Loyola et al., 2008; Hernández-Montoya et al., 2003; Castro de Esparza M.L., 2006; Carrizalesa et al., 2006; Mendoza et al., 2011.

Mexico States	Symptoms of Arsenic Poisoning	Dental Fluorosis [Age] (mild – severe)
Sonora (Northern Mexico)	Several high levels of arsenic in urine	[12] 1.1 – 0.5% [15] 3.8 – 0.6%
Chihuahua (Northern Mexico)	Increased cardiometabolic risk	[12] 4.2– 0.1% [15] 6.4 – 1.0%
Durango (Northern Mexico)	Skin cancer, HPV, Immune system risks	[12] 23.1 – 13.9% [15] 24.1 - 14%
Zacatecas (North of Guanajuato)	80% inhabitants at risk for arsenic-related diseases	[12] 10.5 – 10% [15] 7.7 – 9.2%
Aguascalientes (NW of Guanajuato)	Chronic kidney disease in infants	[12] 6.9 – 1.6% [15] 7.6 – 3.3%
San Luis Potosi (Northeast of Guanajuato)	Arsenic levels in urine of children: 30% > 50 µg/g creatinine (critical action) and 7% > 100 µg/g creatinine (WHO limit)	[12] 13.5 – 4.2% [15] 10 – 2%
Hidalgo (Southeast of Guanajuato)	Arsenic-related cancer, heart disease, and diabetes	[12] 0.7 – 0.3% [15] 1.2 – 0%
Michoacán (South of Guanajuato)	n.a.	[12] 0.6 – 0% [15] 0 – 0%
Jalisco (West of Guanajuato)	Possible risks of skin disease, gastrointestinal effects, neurological damage, cardiovascular problems, and hematological effects	[12] 5.9 – 4.9% [15] 5.4 – 4.5%
Guanajuato (Study Area)	Arsenic levels in hair 1.3 mg/kg (0.05 mg/kg), did not investigate arsenicosis	[12] 2.9 – 6.4% [15] 5.4 – 4.5%

1.5 Dissolution Studies

A prior investigation conducted by Orozco-Esquivel et al., (2002) studied the F content of volcanic rocks in the southern extent of Mesa Central (MC) and found that F content ranges from 207 – 7603 mg/kg in the Oligocene rhyolite sequences, greatly enriched over the average crustal abundance of 0.3 mg/kg. To the authors knowledge, the As contents of the rocks of this region have not been investigated, but typical As concentrations in rhyolites, andesites, and volcanic glasses of 4.3, 2.7, and 5.9 mg/kg, respectively, have been reported by others (Smedley and Kinniburgh, 2002). These As concentrations are comparatively higher than the average As content of 1.5 mg/kg for igneous rocks quoted by Ure and Berrow (1982) (as cited by Smedley and Kinniburgh, 2002). The chemical composition of these rocks is affected by purity, size, and texture (Hem, 1985).

As rocks undergo chemical weathering the elements held in the lattice structures of their constituent minerals transition to free ions which become part of the natural waters (Hem, 1985). In the IBAS, it is hypothesized that the sources of As and F are weathering reactions of arsenopyrite and F-rich rhyolites (Mahlknecht et al., 2004). To investigate the leaching of As and F from rocks to natural waters, studies must use laboratory-scale batch reactors. Similar studies have been implemented with rocks of Argentina (Borgnino et al., 2013; Bia et al., 2014), Brazil (Kohler et al., 2005), South Korea (Chae et al., 2006), and Germany (Yinian et al., 2003) to determine the mechanisms, sources, and rate of reactions for rocks releasing ions into solution.

1.6 Research objectives

- Verify and expand the existing state-of-knowledge of the spatial distribution of As and F contamination across the IBAS through detailed testing with water chemistry, isotopic ratios, and dissolved organic carbon
- Identify the mineralogy comprising different representative rock types within the basin by analyzing drill cuttings from two boreholes of ~500 m by petrographic and x-ray analysis
- Experimentally derive the kinetic rates and mechanisms controlling As and F release from representative rocks within the IBAS

Chapter 2 - Geologic History

2.1 Regional Geologic History

The IBAS is in the southeastern region of the Mesa Central (MC) physiographic province of the Mexican Central Plateau. This physiographic province is surrounded by the SMOc province to the west, the Sierra Madre Oriental (SMOr) province to the north and east, and the TMVB province to the south (Mahknecht et al., 2004) (Figure 2.1). The mountainous SMOc province formed during the Late Jurassic - Early Cretaceous period as the Guerrero Composite Terrane accreted to the mainland of Gondwana during subduction of the Farallon plate (Nieto-Samaniego et al., 1999; Aranda-Gomez et al. 2003; Ortiz-Hernandez et al., 2003; Ferrari et al., 2007; Centeno-Garcia, 2008). The contact between the Guerrero Composite Terrane and the edge of Gondwana is expressed to the west of the Independence Basin as an overturned marine structure called the Arperos basin (Freydier et al., 2000; Palacios-Garcia and Martini, 2014). Prior to the Early Cretaceous arc accretion, the marine platform of the SMOr province was considered the western passive margin of Gondwana (Ortega-Gutierrez et al., 1995; Nieto-Samaniego et al., 1999; Nieto-Samaniego et al., 2007; Centeno-Garcia, 2008).

The TMVB province formed during the Middle Miocene - Holocene epochs as volcanism progressed across Mexico from the Pacific coastline to the Gulf of Mexico (Ferrari et al., 2012). In addition to these bounding physiographic provinces, the MC is surrounded by a series of normal faulted structures including: the El Bajio (lowlands) Fault System, which runs along the southern boundary; the Taxco-San Miguel de Allende Fault System along the eastern boundary; the Aguascalientes Fault System, which forms the southern portion of the western boundary; and the San Luis – Tepehuanes Fault System, which forms the northern portion of the western boundary and separates the MC province into northern and southern regions (Nieto-Samaniego et al., 1999; Nieto-Samaniego et al., 2007).

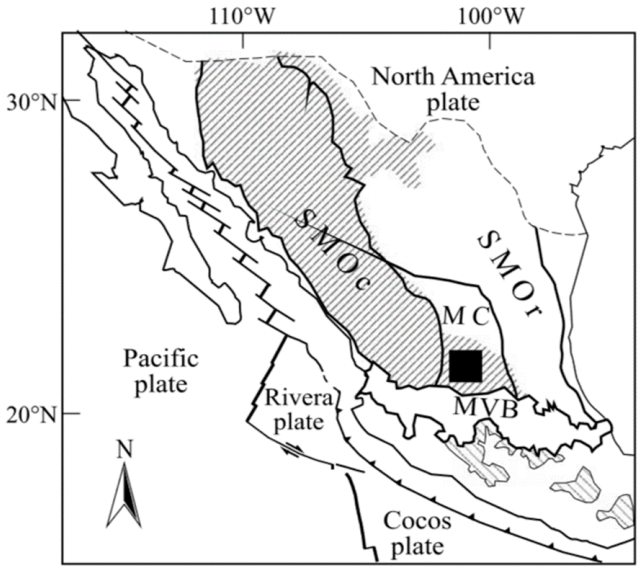

Figure 2.1 The physiographic provinces of Mexico which include the SMOc, SMOr, TMVB, and the MC. The SW – NE trending striped areas outline the Sierra Madre Occidental Volcanic Province of the mid-Tertiary period which represents a large rhyolitic volcanic event (Orozco-Esquivel et al., 2002). The SE – NW trending striped area represents Oligocene – Miocene volcanic rocks (Nieto-Samaniego, 1999). The black box is used to indicate this study's field area (Orozco-Esquivel et al., 2002).

Triassic – Early Jurassic period turbidite deposits define the eastern margin of the MC province identified in the city of San Luis de Potosi called the Zacatecas Formation (Barboza-Gudino et al., 2012). These marine deposits are unconformably overlain by Early – Middle Jurassic period continental deposits of sandstones, conglomerates, and volcanic rocks which define the first appearance of the MC province (Nieto-Samaniego et al., 2007). Late Jurassic limestone, chert, and mudstones which formed across the entire MC province until the Early Cretaceous period overlies the Middle Jurassic period continental deposits (Nieto-Samaniego et al., 2007). The Early – Late Cretaceous period is characterized by thick marine sedimentary deposits across the entire basin alongside volcanosedimentary rock on the western edge of the MC (Nieto-Samaniego et al., 2007).

During the Paleocene – Middle Eocene epochs layers of conglomerates were deposited and unconformably overlain by mafic and felsic composition volcanic rocks (Nieto-Samaniego et al., 2007). There are no rocks expressed in the basin of the Middle Eocene - Oligocene epochs; an angular unconformity stratigraphically defines these ages (Nieto-Samaniego et al., 2007). In the Early Oligocene, large volcanic events emplaced andesitic and rhyolitic composition rocks over

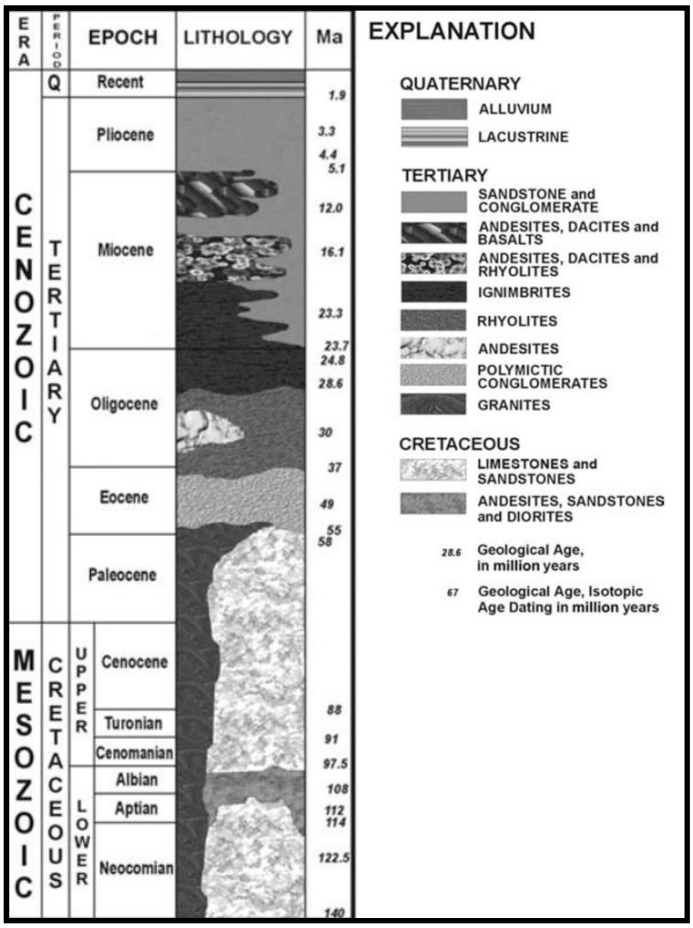

Figure 2.2 Chronostratigraphic section of the IBAS (Mahlknecht et al., 2004).

the Mesozoic era basement rocks (Orozco-Esquivel et al., 2002). A second pulse of Oligocene epoch volcanism generated chemically distinct rhyolites rich in silica and F followed by ignimbrites containing quartz, sanidine, and minor biotite (Orozco-Esquivel et al., 2002). Stratigraphically above the Oligocene epoch volcanic rocks are mafic to intermediate composition rocks from the TMVB (Orozco-Esquivel et al., 2002; Nieto-Samaniego et al. 2007; Mahlknecht et al., 2004). The last occurrence of volcanism is linked to the Early Miocene epoch which emplaced ignimbrite and vein deposits (Camprubi, 2013). As in the Basin and Range province of the western United States, multiple normal faulting events during the Miocene epoch generated a horst and graben structure throughout the IBAS (Mahlknecht et al., 2004). Numerous normal faults, volcanic rocks, and sedimentary deposits shaped the present-day landscape of the MC province (Mahlknecht et al., 2004) (Figure 2.3 and 2.4).

2.2 Hydrogeology of the IBAS

The IBAS is in the southeastern region of the MC province. This aquifer system is primarily composed of the CARL aquifer on the western side of the basin and the LS aquifer on the eastern side of the basin, although other minor aquifers exist. The basin relief ranges from 1,900 – 2,100 m above sea level, and has a semi-arid climate, and a shrubby/thorny vegetated landscape (Nieto-Samaniego et al., 1999; Navarro de Leon et al., 2005; Nieto-Samaniego et al., 2007; INEGI, 2015). Average rainfall in the basin is 35 – 86 mm/month (Mahlknecht et al., 2006). This rainfall primarily occurs between May through October and is followed by the dry season (Mahlknecht et al., 2006).

The lowest amount of rainfall occurs in the northeastern corner of the basin (Navarro de Leon et al., 2005). The average temperature in the basin is 16 ^{o}C and potential evaporation is 1,828 mm/yr. (Navarro de Leon et al., 2005). Groundwater recharge to the IBAS originates along the mountainous margins of the basin and flows towards the center of the basin. Prior to groundwater development much of this groundwater likely discharged to the Rio Laja River which eventually discharged through a canyon in the southern end of the basin (Navarro de Leon et al., 2005; Mahlknecht et al., 2006). Based on radiocarbon dating, estimates of the residence time of groundwater in this basin range from 11,000 years to modern (Mahlknecht et al., 2006). Currently, the rate of groundwater extraction exceeds the recharge rate, resulting in rapidly declining water tables (Knappett et al., 2018). Evaluating future water supplies for this region is beyond the scope of this work, however, water scarcity may drive declining groundwater quality in the future (Navarro et al., 2005; Knappett et al., 2018).

Mahlknecht et al. (2006) separated the IBAS into two distinct lithologies. The lowermost lithology is composed of fractured volcanic and sedimentary rocks composed of ignimbrites, rhyolites, andesites, and conglomerates (Mahlknecht et al., 2006). The upper lithology is composed of siltstone and sandstone alluvium deposits (Mahlknecht et al., 2006). Petrographic analysis conducted by Mahlknechht (2003) determined the sedimentary aquifer material is composed of albite, quartz, feldspar, kaolinite, Ca-montmorillonite, and hematite, cemented together with calcite. The same study found that the tuff and rhyolite rocks of the basin consisted of albite, potassium-mica, potassium-feldspar, plagioclase, anorthite, and quartz (Mahlknecht, 2003).

Three hydrostratigraphic units have been identified within the basin: a lowermost unit of Early Jurassic – Late Cretaceous age marine deposits and volcanic rocks, a middle unit of Tertiary age mafic volcanic rocks, and an upper unit of Late Tertiary - Quaternary age volcanic rocks and sediments (Mahlknecht et al., 2004). These sedimentary deposits are a result of Cenozoic extension which created depressions throughout the basin that are filled with 100 - 500 m of volcanoclastic deposits and volcanic tuff (Navarro de Leon et al., 2005; Mahlknecht et al., 2006). These sedimentary deposits are heavily exploited, as the storage capacity and permeability are optimum for groundwater production (Mahlknecht et al., 2004).

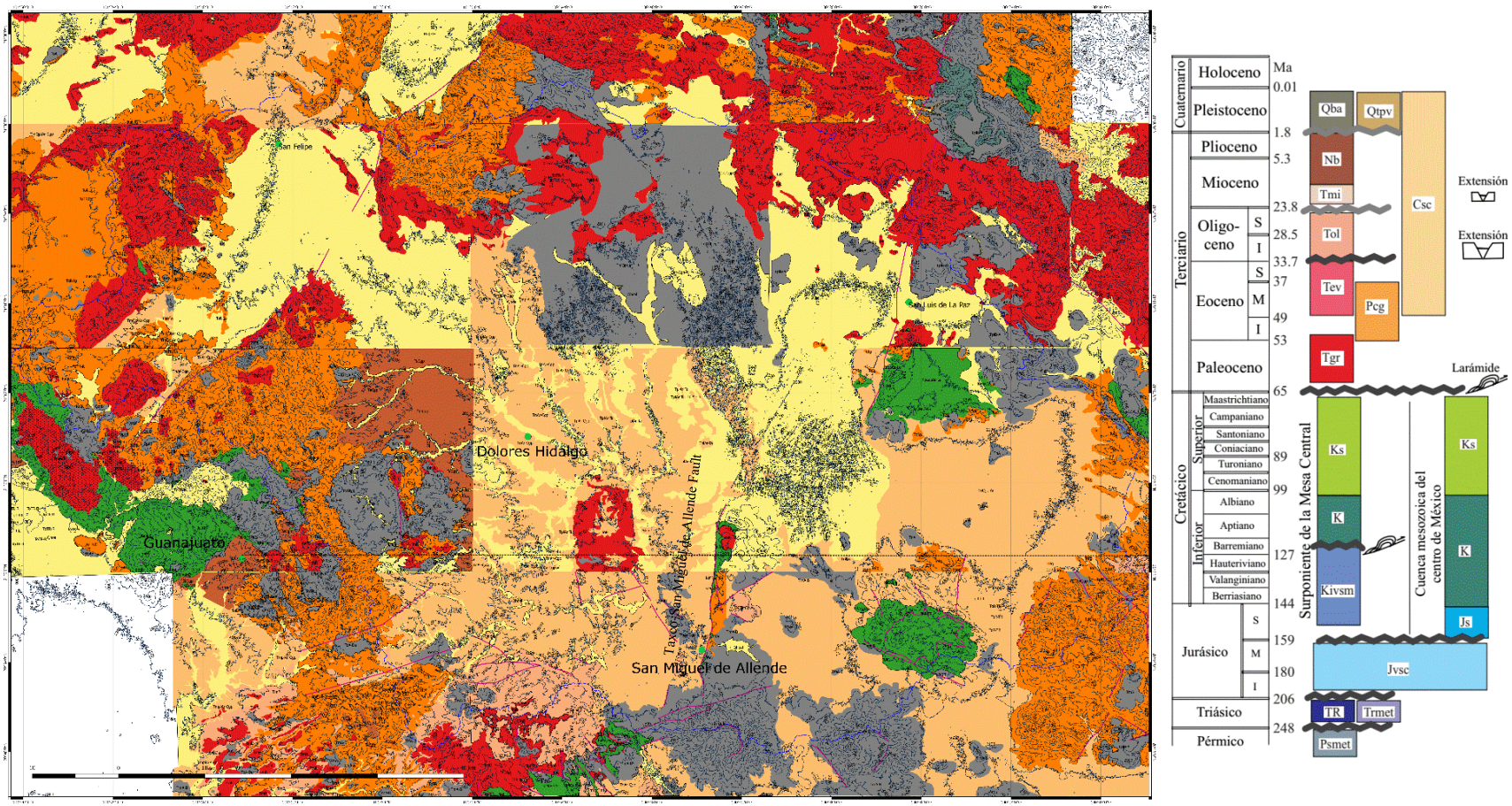

Qba—Quaternary basalt; Qtpv—Quaternary-Pliocene volcanic rock; Nb—Neogene basalt; Tmi—Miocene ignimbrite; Csc—Cenozoic continental strata; Tol—Oligocene rhyolitic rocks; Tev—Eocene volcanic rocks; Pcg—Paleogene continental conglomerate; Tgr—Tertiary granite; Ks—Upper Cretaceous marine strata; K— Lower Cretaceous marine strata; Kivsm—Upper Jurassic-Lower Cretaceous volcanosedimentary marine strata; Js—Upper Jurassic marine strata; Jvsc—Middle Jurassic volcanosedimentary continental strata; TR—Triassic marine strata; Trmet—Triassic metamorphic rocks; Psmet—Paleozoic metamorphic rocks

Figure 2.3 Geologic Map of the IBAS with the basin limit outlined in blue, faults defined by purple lines, and green circles which indicate major cities (Loza-Aguirre I., work in progress; Nieto-Samaniego et al., 2007).

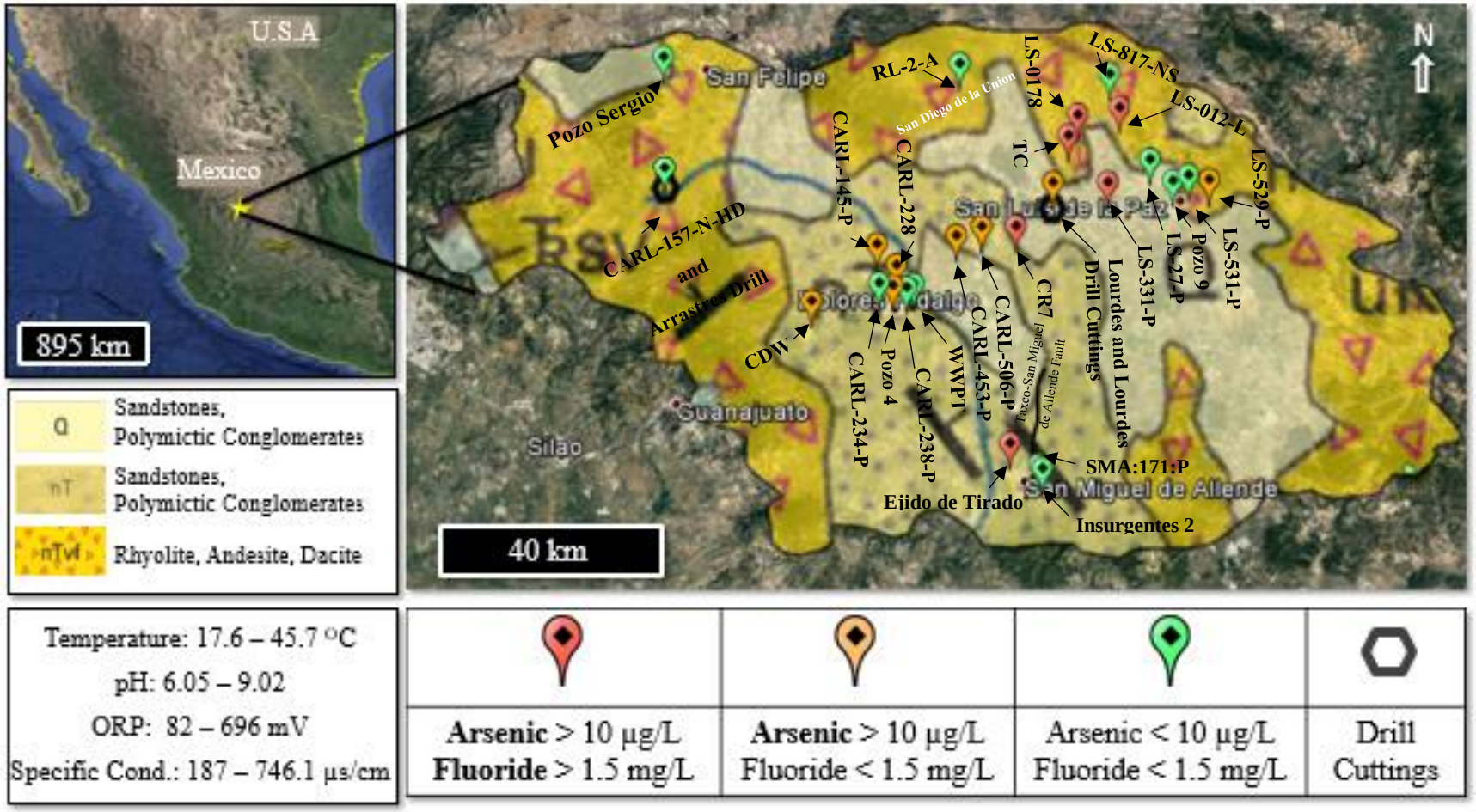

Figure 2.4 The sampling locations for this study and the location of the two borehole drill cuttings used in this study identified by black hexagons. Simplified geologic map (Muehlberger, 1985-1990; Ortega-Gutierrez, 1992; Padilla y Sanchez et al., 1994; as cited by USGS, Geologic Map of North America). WWTP: Waste water treatment plant, TC: Terreros de la Concepciones

Chapter 3 - Methods and Materials

3.1 Fieldwork

In this study the geographical position, depth to water (DTW) table, and information regarding the well constructions were collected from well managers (when well managers were available) at all 24 groundwater wells visited (Figure 2.4). Groundwater wells were purged for 15 minutes to displace at least three well volumes of groundwater prior to taking samples and conducting in-situ chemical analysis. Furthermore; pH, electrical conductivity (EC), temperature, and oxidation-reduction potential (ORP) were monitored during pumping to ensure stabilization prior to sampling. The hand-dug wells and groundwater wells were sampled from a clean bucket and waste water treatment effluent waters were sampled directly from the discharge location. The water samples were stored in a cooler on ice and then placed in a refrigerator at 4^{o}C until all samples were transported back to Kansas State University (KSU). Temperature (^{o}C), EC (µs/cm), ORP (mV), pH, and F (mg/L) were measured on-site by an HQ40d Portable pH, Conductivity, ORP (Ag/AgCl), and F ion selective electrode (FISE) Multi-Parameter Meter (HACH, Loveland, CO). The temperature, EC, pH, and ORP probes were calibrated with 500 µs/cm standard solution; 220 mV Zobells solution; and 4 pH, 7 pH, and 10 pH standard solutions, respectively. The FISE calibration required calibration by mixing 0.5, 1, 2, and 10 mg/L concentration standard solutions with one total ionic strength adjustment buffer powder packet for every 25 mg/L of standard solution. All probes and spectrophotometer and colorimeter materials were cleaned daily with de-ionized (DI) water and soap to ensure no cross contamination. At every sampling location multiple field kits were used including: vacu-vials with the V-2000 Multi-Analyte Photometer (CHEMetrics, Inc., Midland, VA) and TNT vial tests with the DR 1900 Portable Spectrophotometer (HACH) (Table 3.1; Figure 3.1).

Table 3.1 List of field kits used to measure chemical parameters of groundwater samples.

Measured parameter	Field Kit
Alkalinity as $CaCO_3$	Alkalinity (Total), TNTplus Vial Test (25-400 mg/L $CaCO_3$), and Alkalinity (total) — Titrets® Titration Cells Range: 10-100 mg/L – CHEMetrics
Total dissolved arsenic (As)	EZ Arsenic High Range Test Kit – HACH
Total dissolved manganese ($Mn_)$	Manganese Test Kit, Model MN-5 – HACH
Nitrate (NO_3^- - N)	Nitrate TNTplus Vial Test, LR (0.2-13.5 mg/L NO_3^--N) – HACH
Nitrite (NO_2^- - N)	Nitrite TNTplus Vial Test, HR (0.6-6.0 mg/L NO_2^{2-}-N) – HACH
Total dissolved iron (Fe)	Iron TNTplus Vial Test (0.2-6.0 mg/L Fe) – HACH
Sulfate (SO_4)	Pocket Colorimeter™ II, Sulfate Turbidimetric – HACH
Phosphate (PO_4)	Phosphate Test Kit Total Ortho-/Meta-, Model PO-24 HACH
Chloride (Cl)	Chloride Test Kit, Model CD-51 – HACH
Ammonia (NH_4)	Ammonia — CHEMets® Kit
Sulfide (S)	Sulfide — CHEMets® Visual Kit
Bromide (Br)	Bromine — CHEMets® Visual Kit
Dissolved silica (SiO_2)	Silica Test Kit, Model SI-5 - HACH

Groundwater samples were collected in high-density polyethylene (HDPE) bottles, glass containers, and polypropylene (PP) centrifuge tubes which were rinsed in-situ three times with groundwater from the well site. Sample bottle was filled completely with sample to remove any headspace and minimize reactions during storage before being transported back to the laboratory at KSU. At 12 of the wells visited, a two-gallon sample was collected, stored in a cold and dark area, and then transported to KSU for use in future reactor studies.

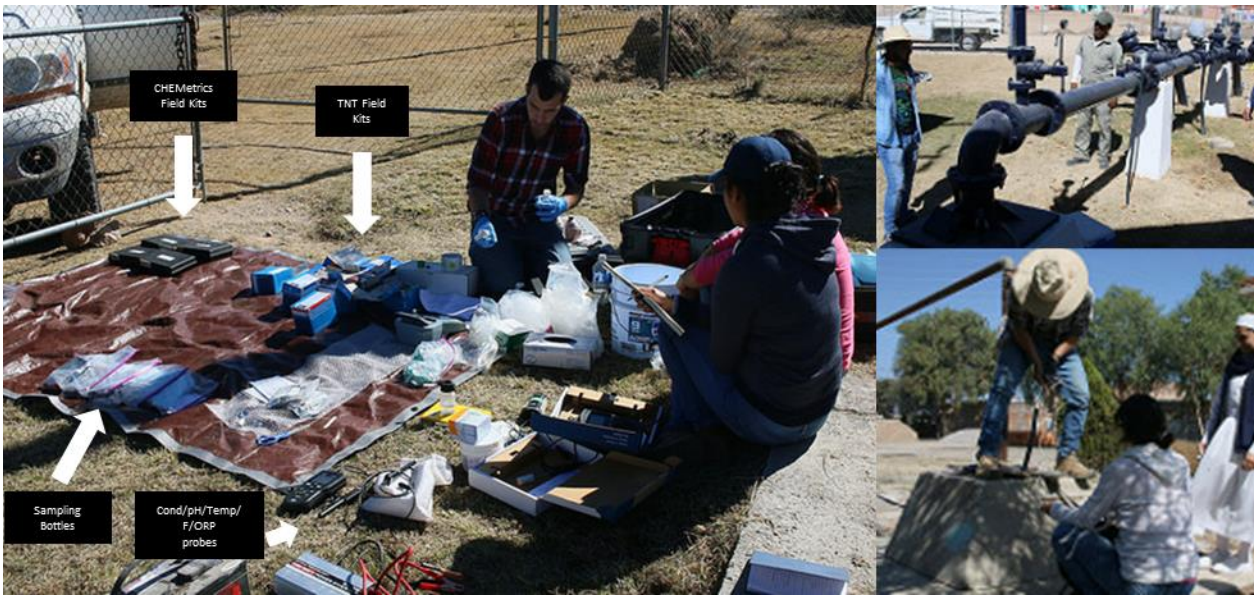

Figure 3.1 Images of production wells sampled, the preparation of field kits for conducting analysis, and collecting depth to water measurements in the IBAS in Mexico (Images curtesy of William Thurston at Caminos del Agua).

3.2 Ion Chromatography

The water samples for the determination of major cations (Na, K, NH_4, Mg, Ca, and Sr) were collected in 250 ml HDPE amber bottles following filtration with a 0.45 µm nitrocellulose filter (Whatman, Maidstone, UK). These samples were then acidified with 0.2 (w/v) ultrapure nitric acid (HNO_3) to reduce the pH to a value less than 2, which stabilizes the samples. Water samples for major anions (F, Cl, NO_2, Br, NO_3, SO_4, and PO_4) were collected in 50-ml PP centrifuge tubes following filtration through a 0.45 µm nitrocellulose filter. Major element water chemistries were measured at KSU. The water samples from twenty-one groundwater wells, two hand-dug wells (Norias), and a waste water treatment plant in the basin were poured into clean 0.5 ml clear vials and plugged with 0.2 µm filter caps. The vials were then loaded into a carousal auto sampler alongside a set of cation and anion standard solutions of known concentrations (mg/l): Na (5, 10, 25, 50), K (2.5, 5, 10, 20), NH_4 (1, 2.5, 5, 10), Mg (2.5, 5, 10, 20), Ca (2.5, 5, 10, 20), Sr (2.5, 5, 10, 20) F (0.5, 1, 2, 4), Cl (10, 15, 30, 60), NO_2 (0.5, 1, 1.5, 4), Br (0.5, 1, 2, 4), NO_3 (1.5, 2.5, 5, 10), PO_4 (0.5, 1, 2, 4), and SO_4 (5, 10, 20, 40). Additionally, vials filled with 18-ohm ultra-pure water (Millipore, Burlington, MA) were loaded in between every five samples. These served as blanks and to purge and clean the system. A sample from one of the wells sampled was re-run following each 10 measurements measure analytical precision for field samples.

3.3 Stable Isotopes

Water samples collected in 60 ml clear glass bottles from the IBAS that were not filtered or acidified were used to determine the oxygen and deuterium isotopic ratios. These water samples were analyzed with a Picarro WS-CRDS isotopic water analyzer (L1102-I, Santa Clara, CA) in the Department of Biology at KSU. The working standards used to create the regression line range for these measurements are from glacial water (depleted) to evaporated water (enriched), with two additional working standards between the depleted and enriched standards. The oxygen ($\delta^{18}O$) and deuterium ($\delta^{2}H$) ratios are then reported as compared to the international standard of Vienna Standard Mean Ocean Water (VSMOW) and results from investigation in the IBAS. Oxygen and deuterium isotopic ratios often reflect the origin and amount of evaporation rainfall underwent before recharge and is therefore influenced by climatic effects and possible mixing between groundwater flow paths in the IBAS.

3.4 Dissolved Organic Carbon

The groundwater samples for dissolved organic carbon (DOC) analysis were collected in 250 ml glass amber bottles after filtration with 0.45 µm nitrocellulose filters and acidified with 10.2 M hydrochloric acid (HCl) and stored in a refrigerator at 4°C to prevent further microbial activity. These samples were then analyzed for DOC concentrations with a TOC-5000 analyzer (Sigma-Aldrich, St. Louis, MO) in the Department of Civil Engineering at KSU. This device measures DOC by converting all the organic material in solution to carbon dioxide (CO_2) and measuring the CO_2 produced. An additional batch of filtered and unacidified samples was run alongside the acidified samples to examine the extent of microbial activity in the samples that were unacidified in the field.

3.5 Powder X-ray Diffraction

General settings

Drill cuttings from two boreholes from the western (Arrastres) and eastern sides (Lourdes) of the basin were provided to KSU by the University of Guanajuato. These two boreholes measured ~500 m on the western side of the basin and ~550 m on the eastern side of the basin. A sample at each ~20 m interval along each set of borehole drill cuttings was selected for analysis by X-ray Diffraction (XRD) using the following method. A small amount of the drill cuttings was crushed by hand in an agate mortar and pestle to a fine-grained grain size. This powder was then back-loaded into a stainless-steel sample holder with a diameter of 27 mm. A Panalytical Empyrean X-

ray diffractometer (PanAnalytical Empyrean, Malvern, UK) was then used to analyze the powders in the reflection transmission spinner rotating at 4 rev/s Two different scan configurations were used in this study to understand the major and trace phases of the two borehole drill cuttings. Since the Lourdes drill cuttings were closer to the area of highest As and F contamination in the basin, it was deemed necessary to examine their drill cuttings for trace phases, while the Arrastres drill cuttings were far from the As and F contaminated area and only a major phase analysis was necessary.

Arrastres Drill Cuttings

The Arrastres drill cuttings analysis was conducted with measurements at 45 kV and 40 mA using copper (Cu) radiation, a $1/8^{th}$ anti-scatter slit, a 10 mm incident beam mask, and 0.04 rad soller slits. The scan ranged between 5^o and 70^o 2θ with a 0.0066 step size and 42.075 s/step. A large beta nickel filter was used on the diffracted side of the instrument to attenuate the beta x-rays from the profile to reduce the additive effects of alpha and beta reflections. This configuration was chosen for the identification of major phases present in the drill cuttings with a maximum peak from a reflection greater than 1000 counts (personal communication, Panalytical).

Lourdes Drill Cuttings

The Lourdes drill cuttings analysis was conducted at 45 kV and 40 mA using Cu radiation, a $1/8^{th}$ anti-scatter slit, a 10 mm incident beam mask, and 0.04 rad soller slits. The scan ranged between 5^o and 70^o 2θ with a 0.0066 step size and 179 s/step. A large beta nickel filter was used on the diffracted side of the instrument to attenuate the beta x-rays from the profile to reduce the additive effects of alpha and beta reflections. The increased time per step was chosen for the analysis of major and trace phases based on the presence of a maximum peak from a reflection greater than 10,000 counts (personal communication, Panalytical).

X-Ray Diffraction Data Analysis

The results of the scans from both borehole drill cuttings were loaded into Highscore Plus and matched to the reference card database from the International Centre for Diffraction Data (ICDD). The peaks were matched using the following parameters of quality: the reference cards were not deleted from the database by ICDD, the reference cards were of star or indexed quality, and the reference cards data was collected at ambient temperature and pressure. Mineral reference cards were determined to match the scan results when the top five most relative intense peaks (I/I_o)

from each of the reference cards was examined and determined to be a match based on the intensity, position, and location within the context of the geology of the basin.

3.6 X-ray Fluorescence

X-ray Fluorescence (XRF) (Bruker Tracer III, Billercia, MA) analysis was used to determine the elemental weight percentage of the two borehole drill cuttings using a Bruker Tracer III Handheld XRF. The X-rays emitted from the XRF penetrate the shale standard to a certain depth and measurements are collected from the unknown sample at this same depth. The data collected by the XRF is then compared in Microsoft Excel with calibrated chemical data for a standard of Woodford shale (Rowe et al., 2012). The calibrated measurements were then used to determine the elemental weight percentages. The drill cuttings were prepared by separating each 20-meter interval of the ~500 m depth and sieved through a 250-micron grain size sieve and loaded into Funnelshape SpectroMicro XRF sample cup (Chemex, Chicopee, MA) with 1.5-micron Prolene Thin-Film (Chemex) and a XRF sample cup lid on either end. The samples were measured in triplicates for both major and trace elements. Between each measurement the samples were shaken and tapped on a flat surface to mix and compact the samples. The major element analysis required a vacuum pump, a voltage of 15 kV and 25 μA, no filter, and a measurement time of 180 s to allow the spectrum to stabilize. The pump was turned off for trace element analysis and a yellow filter (12 mil Al + 1 mil Ti) was installed into the XRF. The voltage was set to 40 kV and 12.4 μA and the analysis was run for 120 s to allow the spectrum to stabilize.

3.7 Optical Microscopy

A total of four drill cutting samples from the Arrastres drill cuttings (20 – 22 m, 160 – 162 m, 340 – 342 m, and 440 – 442 m) and five drill cutting samples from the Lourdes drill cuttings (18 – 20 m, 140 – 142 m, 220 – 222 m, 360 – 362 m, and 540 – 542 m) were shipped to Spectrum petrographic to be made into 27 X 46 mm polished thin sections. At spectrum, the samples were submerged in a quartz epoxy and allowed to solidify while glued to a glass slide. The thin sections were then ground down to a 30 μm size shipped back to KSU. These thin sections were then examined by optical microscopy and reflected light microscopy and images were taken with a camera attached to the petrographic microscope.

3.8 Preliminary Batch Experiment

Batch Reactor Configuration

The following method was used to determine which sections of the drill cuttings would be used for the long-term batch reactor study. Initially the ~500 m borehole drill cuttings were separated into 20 m sections. These 20 m sections were then divided into 2 m sections. A portion of each 2 m section was then crushed in an agate mortar and pestle and sieved down to a grain size less than 63 µm. The 20 m sections produced a mass of 10 g which were thoroughly mixed by shaking in a PP centrifuge tube for 5 minutes to homogenize the samples and then separated into 5 g subsamples and placed in new 50 mL PP centrifuge tubes. In the case of duplicates, the previously mentioned method generated 20 g of sample. The less than 63 µm grain size fraction was used for the experiment, because the higher surface area of the particles and the potential to facilitate the water – rock reactions. A reaction time of 200 hrs. was used based on studies of dissolution reactions with granite conducted by Chae et al. (2006). These PP centrifuge tubes were then either filled with DI or groundwater collected from the eastern or western side the IBAS (well IDs: CDW and LS-0178). The chemistry of the groundwaters used in this experiment is included in the results section (Table 4.20). A weight of rocks to volume of water ratio of 1:5 (g/mL) was used for this experiment. Once all PP centrifuge tubes were filled with 5 g of rocks and 25 mL of DI or groundwater, they were vortexed for 1 s to initialize the reaction. The PP centrifuge tubes were then laterally shaken at a rate of 250 shakes per min for a total of 200 hours. After 200 hrs. the PP centrifuge tubes were placed in a centrifuge for three minutes at 6000 rpm.

Water Sample Analysis

Water samples from each reaction vessel was extracted by syringe and filtered through a 0.45 µm nitrocellulose filter into three different PP centrifuge tubes. The three PP centrifuge tubes were then used accordingly: 22 ml filled one PP centrifuge tube for F measurements by FISE, 1.5 ml was separated for cation analysis and acidified with 0.2% (w/v) HNO_3, and 1.5 ml was separated for anion analysis by Ion Chromatograph (IC). The temperature (^oC), EC (µs/cm), ORP (mv), pH, and F (mg/L) concentration were measured with an HQ40d Portable Multi-Parameter Meter equipped with pH, EC, ORP (Ag/AgCl), and FISE probes. The EC probe was calibrated with 500-µs/cm standard solution. The ORP was calibrated with a 220-mV standard solution. The pH probe was calibrated with 4 pH, 7 pH, and 10 pH solutions. The FISE probe was calibrated with a set of 0.5, 1, 2, and 10 mg/L standard solutions. A total ionic strength adjustment buffer pack was added

to the 22 ml samples prior to measuring the F concentration with the FISE. A series of duplicate samples was measured using the previously mentioned method to determine the accuracy of this method. Two controls were used (one with DI water in a PP centrifuge tube and one with groundwater from the IBAS) to determine if storage in the PP centrifuge tubes influenced the water chemistry. The methods were altered in the case of the groundwater from the eastern side of the basin (well ID: LS-0178) as the F concentrations were higher than the calibration range for the FISE probe. In this case only 11 ml of reacted water was removed from the PP centrifuge tubes after 200 hrs. A one to one dilution with DI water was then used to bring the volume of the water analyzed to 22 ml and to bring the F concentrations within the calibration range of the FISE.

3.9 Dissolution Experiments

Reactor Construction and Groundwater

A Form Lab-2 3D printer (Form Labs, Somerville, MA) was used to create eighteen reactor cells composed of photopolymer resin (Tough-2) at KSU (Figure 3.2).

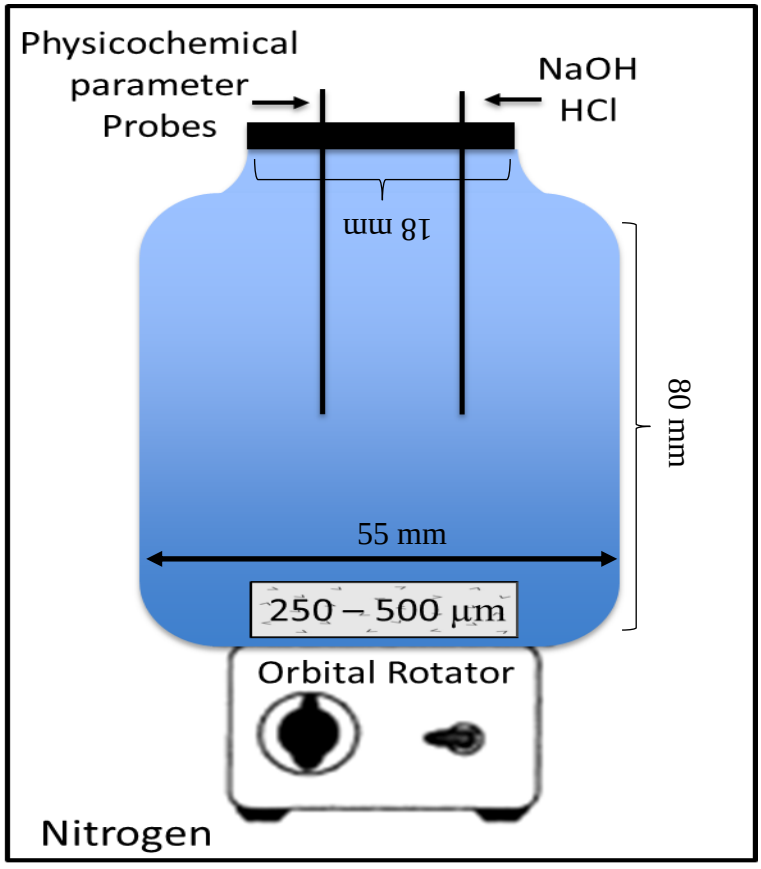

Figure 3.2 Conceptual model of the batch reactors used in this study.

These reactor cells were then cleaned using an acid bath in the following series 1:1 nitric acid; tap water; 1:1 HCl acid; tap water; and then the reagent water. The reagent water selected for this experiment was groundwater from the recharge area of the IBAS (RL-2-A), which had a similar chemical composition to the average water chemistry measured within the basin, based on measurements in this study (Table 4.21). A total of 100 mL of groundwater from the IBAS was used to fill each of the reactor cells. These reactors were then loaded into a glovebox with an oxygen percentage which ranged from 10.4 – 11.0%. The pH of the groundwater in each of the reactor cells was then adjusted to either 5, 7, or 9 with 0.015M HCl acid or 0.025M NaOH. These reactors were the loaded with drill cuttings from the Arrastres and Lourdes boreholes.

Rock Sample Preparation

The sediments used in the experiment were selected from the 400 – 500 m depths of the Arrastres drill cuttings and the 400 – 550 m depths of the Lourdes drill cuttings. These depths were selected based on the quantity of sample available and prior F-leaching experimental results. The drill cuttings were then sieved through a decreasing sieve stack consisting of brass American Standard for Testing Materials (ASTM) sieves with a stainless-steel mesh of 1000, 850, 710, 500, 425, 355, 300, and 250 µm apertures. The grains collected in the 425, 355, 300, and 250 sieves were weighed in folded Fisherbrand 6 x 6 weighing papers. These four different grain sizes from the 400 – ~500 m sections of the drill cuttings were then separately mixed in PP centrifuge tubes end over end for 5 minutes. The homogenized sediment sample sizes were then distributed evenly into each reactor cell at a constant weight ratio of 4.44 g of 250-micron, 4.44g of 300-micron, 5.11g of 355-microns, and 6.01g of 425-micron grains. This created a 1:5 (g/mL) weight of sediment to volume of groundwater ratio amongst the reactor cells.

Extraction of Water Samples for Analysis

Once the sediments were added to the groundwater the reactor cells were capped with clean number 3 rubber stoppers and placed on an orbital rotator to be stirred at 100 rpm. At 25, 50, 100, 150, and 200 hrs. ten ml of reacted water was extracted, filtered with a 0.45 µm nitrocellulose filter, pumped in a 20 mL glass vial, acidified with nitric acid at 0.2% (w/v), capped with a septum, and crimped closed with a crimp cap. A total of 5 mL was then filter into two separate new 15 mL PP centrifuge tubes at 2.5 mL each with one sample being acidified with 0.02% (w/v) HNO_3^- to stabilize the sample for cation analysis and the other sample was not acidified for anions analysis by IC. These samples were then placed in a refrigerator at 4^{o}C until analysis. The EC (µs/cm) and

ORP (mv) were measured with a HQ40d Portable Multi-Parameter Meter (HACH) equipped with EC and ORP (Ag/AgCl) probes and the pH and temperature were measured with a Mettler Toledo equipped with a Mettler Toledo pro-ISM pH probe (Mettler Toledo, Greifensee, Switzerland). The EC probe was calibrated with a 500-µs/cm standard solution. The ORP probe was calibrated with a 220-mV standard solution. The pH probe was calibrated with 4 pH, 7 pH, and 10 pH standard solutions. These measurements were then collected in triplicate. The water extracted from each rector was then replaced with RL-2-A groundwater and the pH of the reactor was re-adjusted to either 5, 7, or 9 using either 0.015 M HCl or 0.025 M sodium hydroxide (NaOH). IC analysis for major cations and anions was then conducted at KSU.

3.10 Inductively Coupled Optical Emission Spectroscopy and Inductively Coupled Plasma Mass Spectroscopy

The major elements (Na, K, Ca, Mg, Ba and P) were determined by inductively coupled plasma optical emission spectroscopy (ICP-OES) using a Perkin Elmer Spectro CirOS instrument equipped with an axial torch. Internal standards (Yb, In and Cs) were introduced samples and calibration standards to compensate for instrument drift. Four calibration standards and a blank were used for calibration, with an independent check standard. Calculated analytical precision was within 0.4-4% RSD for the range of major elements measured. Cesium chloride (CsCl) was used as the ionization buffer for the ‘easily ionization effect’ due to axial torch. Analytical quality control was maintained using a NIST SRM 1640a.

Trace and ultra-trace elements (Li, Be, B, Al, Mn, Co, Ni, Cu, Zn, Sr, Mo, Ag, Cd, Sn, Sb, Ba, Tl, Pb, Th, U, Cr, Fe, Ni, Se, As and V) were determined by Inductively Coupled Plasma Mass Spectrometry (ICP-MS) analysis using a Perkin-Elmer/Sciex Elan DRCII instrument with Axial Field Technology, equipped with a dynamic reaction cell to remove molecular ion interferences. Samples were brought to a final acid strength of approximately 1-2% nitric acid prior to analysis. Analyses were performed in standard mode, oxide mode, and dynamic reaction cell mode at the same time. For the “reaction cell” mode, ammonia was used as a reaction cell gas to remove molecular ArO+ interference.

Internal standards were added to all samples and calibration standards to compensate for instrument drift and viscosity and surface tension differences between samples and standards. Calibration was performed with external standards using a blank and four calibration standards

and was evaluated with an independent check standard. The mass of analyte per sample was calculated by multiplying the observed concentration by the volume to which the sample was diluted. A set of multi-elemental standards (Inorganic Ventures, USA) and blanks re-run throughout the sequence of samples allow precise quantification and correction for machine drift. Analytical precision on individual samples was <5% RSD for all the elements (3 repeat measurements). Method Detection Limits (MDL) varied by run for each of the elements but were generally <0.01 ppb. Duplicate values were considered valid when average concentration was not less than 3 × MDL. Analytical quality controls with GLP were regularly practiced using a commercial SRM material for trace elements in natural waters (SRM 1640a, NIST, USA). The reproducibility on a frequently run interval laboratory standard was also recorded (±0.2–0.5%). Laboratory Control Samples (LCS) recovery was within 97-104 % and spike recovery was within 94-103%, provided values were considered valid when the observed concentration was not less than 3 × MDL.

3.11 Geochemical Modeling of Batch Reactor Systems

Modeling simulations of the reactor cells was conducted via Geochemist Workbench Software using the termo.tdat thermodynamic database and the FeOH+.dat adsorption database from Dzombak and Morel (1990). The FeOH+.dat database incorporates adsorption reactions with the strong and weak bonding sites on goethite mineral surfaces. The surface area was assumed as the default value of 600 m^2/g. The site density of goethite was 0.005 mol/mol for strong bonding sites and 0.200 mol/mol for weak bonding sites. The modeled reactions are summarized in Table 3.2. The water chemistry of the groundwater used (Well ID: RL-2-A) in the batch reactor experiment is loaded as the basis species with 0.05 mg of fluorite to facilitate the release of F ions into solution and 0.05 g of goethite. No As -bearing species was modeled as no As-bearing minerals were observed in mineralogical analyses. The groundwater was allowed to react with the iron oxyhydroxide mineral surface over an 8-day period.

Table 3.2 Adsorption reactions used in the Geochemist Workbench Software (*indicates estimated values). The >(w) represents weak surface sites.

Reaction	Log(k)
>(w)FeOH + H^+ + F^- → >(w)FeF + H_2O	-8.7*
>(w)FeOH + F^- → >(w)FeOHF^-	-1.6*
>(w)FeOH + AsO_4^{3-} + 3 H^+ → >(w)FeH_2AsO_3 + H_2O	-29.31
>(w)FeOH + AsO_4^{3-} + 2H^+ → >(w)FeHAsO_4^- + H_2O	-25.39
>(w)FeOH + AsO_4^{3-} → >(w)FeOHAsO_4^{3-}	-10.58

Chapter 4 - Results

4.1 The Physicochemical Parameters of the Wells Sampled in the Field

Urban and Rural Groundwater Wells

The geospatial information and physico-chemical parameters of 23 urban (n = 10) and rural (n = 13) groundwater wells was collected in this study (Table 4.1, 4.2). A summary of the ranges of values measured in each rural and urban area is found in Table 4.3. The physico-chemical parameters of the groundwater wells sampled in the IBAS are described with respect to the nearby major urban areas. These four major urban areas are used to facilitate a spatial understanding of the variations observed in the groundwater chemistries. Dolores Hidalgo is located on the western side of the basin, whereas San Diego de la Union is in the northern extent of the basin, San Luis de la Paz is located on the eastern side of the basin, and San Miguel de Allende is located on the southern extent of the basin (Figure 2.4). Additional data collected from field is included in the Appendix A.1. In total these groundwater wells ranged in depth from 140 – 550 m. These wells are typically cased to a depth of ~15 m (personal communication with Dr. Yanmei Li). The depths of six out of the 23 groundwater wells are unknown, but four of these six wells had a DTW greater than 158 m, indicating that they are constructed beyond the measured DTW value. The groundwater wells near San Luis de la Paz, Dolores Hidalgo, San Miguel de Allende were constructed to depths ranging from 140 – 550 m, greater than 170 – 500 m, and 195 – 300 m; respectively (Table 4.1). The depth of the single groundwater well sampled in San Diego de La Union is unknown and it was not possible to determine in the field.

The groundwater around the four urban areas of the IBAS showed differences in water physicochemical parameters (Table 4.3). Additionally, differences were observed between the urban and rural wells located near the San Luis de la Paz and Dolores Hidalgo. The groundwater temperature observed around the four major urban areas of San Luis de la Paz, Dolores Hidalgo, San Miguel de Allende, and San Diego de la Union ranged from 20.1 – 45.7 ^{o}C. The highest groundwater temperatures were recorded in the rural wells near San Luis de La Paz. The lowest groundwater temperature was measured in an urban well of San Luis de La Paz. The urban and rural groundwater wells near the cities of Dolores Hidalgo and San Miguel de Allende ranged in temperature from 23.3 – 34.5 ^{o}C and 25.7 – 31.1 ^{o}C, respectively. Only one well from San Diego

de la Union was measured in this study and had a groundwater temperature of 32.0 ºC (Table 4.3). The average groundwater temperature across the basin was 29 ºC.

The pH values measured in groundwater wells across the basin ranged from neutral (7.05) to alkaline (9.02). The rural and urban wells of San Luis de la Paz had a pH range from 7.49 – 9.02. The rural wells near this city had four of the highest pH values recorded in the basin. The groundwater wells near Dolores Hidalgo had pH values ranging from 7.05 – 7.85. The lowest groundwater pH was measured in a rural well near Dolores Hidalgo (Well ID: CDW). The city of San Miguel de Allende had a pH range from 7.83 – 8.13. The rural well sampled in San Diego de La Union had a pH of 7.42. The basin had an average pH value of 7.72.

The EC measurements were converted to specific conductance (SC) for all groundwater samples. The SC ranged from 186 – 746 µs/cm in groundwater samples from the four major urban areas. The groundwater wells near the city of San Luis de la Paz had the highest SC values. The SC measured in the urban and rural wells near San Luis de la Paz ranged from 385.2 – 746.1 µs/cm (Table 4.3). The urban wells of Dolores Hidalgo and San Miguel de Allende had similar SC ranges of 187.0 – 622.1 µs/cm and 264.2 – 425.3 µs/cm, respectively (Table 4.3). The lowest SC value was measured in a rural well to the west of Dolores Hidalgo (Well ID: CDW = 187 µs/cm). The highest SC value measured in a rural well near Dolores Hidalgo correlated with the well installed to the greatest depth (CR7). The one San Diego de La Union rural well had a SC of 435.2 µs/cm (Table 4.2). The average SC value for the basin was 447 µs/cm.

The ORP values measured across the aquifer indicate oxic conditions (82.3 – 696.0 mV) (Table 4.3). The ORP values for the urban and rural wells of San Luis de la Paz ranged from 82.3 – 698 mV, respectively. The groundwater wells from the urban and rural wells near Dolores Hidalgo ranged from 404.5 – 570.0 mV. San Miguel de Allende had ORP values that ranged from 404.5 – 570.0 mV. The ORP value for San Diego de la Union was 416.0 mV. The average ORP value for groundwater wells in the basin was 457 mV.

Hand-Dug Wells

Two hand-dug wells were sampled from the IBAS near San Felipe. The temperature of Well ID: CARL-157-N-HD was 17.6 ºC. The pH and SC of this well were 6.45 and 208.0 µs/cm, respectively. The measured ORP for Well ID: CARL-157-N-HD was 383 mV. The Well ID: Pozo Sergio of San Felipe had a water temperature of 17.8 ºC (Table 4.2). The pH and SC of this well were 6.05 and 202.9 µs/cm, respectively (Table 4.2). The ORP value for this well was 371.5 mV.

Waste Water Treatment Plant Dolores Hidalgo

The waste water treatment plant of Dolores Hidalgo named Planta San Pablo was sampled at the discharge location of the plant. The temperature of the effluent water was 21.7 ºC. The pH and SC were 7.60 and 1495.2 µs/cm, respectively. The ORP value for this effluent was 317.0 mV.

Table 4.1 The water chemistry data collected in the field alongside locations of wells sampled within the IBAS. The city designation is based on the wells proximity to a major city and type is used to separate urban wells versus rural wells. (n.a.) indicates the measurement were not available or determined.

Well ID	City	Latitude (DD)	Longitude (DD)	Well Depth (m)	DTW (m)
Rural					
Lourdes	San Luis de la Paz	21.2888	-100.7047	550	151.00
LS-331-P	San Luis de la Paz	21.2891	-100.6238	200	>170.00
LS-012-L	San Luis de la Paz	21.3916	-100.6068	>158	158.00
LS-0178	San Luis de la Paz	21.3815	-100.6684	275	n.a.
Terreros de la Concepciones	San Luis de la Paz	21.3533	-100.6822	n.a.	n.a.
CARL-453-P	Dolores Hidalgo	21.2154	-100.8469	>171	171.00
CARL-506-P	Dolores Hidalgo	21.2279	-100.8095	170	n.a.
CR7	Dolores Hidalgo	21.2287	-100.7592	500	>170.00
CARL-145-P	Dolores Hidalgo	21.2035	-100.9638	n.a.	n.a.
CDW	Dolores Hidalgo	21.1251	-101.0597	280	>200.00
RL-2-A	San Diego de la Union	21.4516	-100.8426	> 94	94.00
Urban					
Pozo 9	San Luis de la Paz	21.2911	-100.5282	180	n.a.
LS-531-P	San Luis de la Paz	21.2989	-100.5050	180	180.00
LS-529-P	San Luis de la Paz	21.2926	-100.4747	140	145.00
CARL-228	Dolores Hidalgo	21.1748	-100.9350	240	114.00
Pozo 4	Dolores Hidalgo	21.1467	-100.9399	200	n.a.
CARL-238-P	Dolores Hidalgo	21.1442	-100.9197	210	n.a.
CARL-234-P	Dolores Hidalgo	21.1503	-100.9604	210	88.86
Ejido de Tirado	San Miguel de Allende (W of fault)	20.9304	-100.7675	300	n.a.
Insurgentes 2	San Miguel de Allende (E of fault)	20.8962	-100.7196	295	>195.00
SMA:171:P	San Miguel de Allende (E of fault)	20.9012	-100.7247	195	n.a.
Waste Water Treatment Plant					
Planta San Pablo	Dolores Hidalgo	21.1489	-100.9096	n.a.	n.a.
Hand-Dug Well					
CARL-157-N-HD	San Felipe	21.3153	-101.2746	n.a.	n.a.
Pozo Sergio	San Felipe	21.4594	-101.2795	n.a.	1.80
Extra Wells Not Sampled					
LS-27-P (No Sample)	San Luis de la Paz	21.4594	-101.2795	n.a.	n.a.
LS-817-NS (No Sample)	San Luis de la Paz	21.3207	-100.5616	n.a.	19.27

Table 4.2 Specific conductance calculated from the EC and temperature values measured in the field with the following calculation SC = EC/(1+0.0191*(T-25ºC). ORP was corrected for the use of an Ag/AgCl probe by adding 199 to the value measured in the field.

Well ID	City	T (ºC)	pH	EC_{raw} (µs/cm)	SC (µs/cm)	ORP_{raw} (mV)	ORP Ag/AgCl (mV)
Rural							
Lourdes	San Luis de la Paz	31.0	7.69	527.0	471.8	376.0	575.0
LS-331-P	San Luis de la Paz	25.2	9.02	749.0	746.1	-117.0	82.3
LS-012-L	San Luis de la Paz	39.1	8.28	489.0	385.2	419.0	618.0
LS-0178	San Luis de la Paz	45.7	8.27	550.0	394.2	327.9	526.9
Terreros de la Concepciones	San Luis de la Paz	29.2	8.30	670.0	620.2	338.8	537.8
CARL-453-P	Dolores Hidalgo	32.9	7.36	475.0	412.7	255.7	454.7
CARL-506-P	Dolores Hidalgo	27.4	7.40	521.0	498.2	480.4	679.4
CR7	Dolores Hidalgo	34.5	7.85	735.0	622.1	133.1	332.1
CARL-145-P	Dolores Hidalgo	34.2	7.05	343.0	291.7	497.0	696.0
CDW	Dolores Hidalgo	33.2	7.21	216.4	187.0	217.0	416.0
RL-2-A	San Diego de la Union	32.2	7.42	495.0	435.2	173.0	372.0
Urban							
Pozo 9	San Luis de la Paz	20.1	7.77	500.0	551.1	-43.6	155.4
LS-531-P	San Luis de la Paz	26.3	7.49	707.0	689.9	139.9	338.9
LS-529-P	San Luis de la Paz	26.6	7.64	679.0	658.9	224.1	423.1
CARL-228	Dolores Hidalgo	27.6	7.63	334.0	318.2	169.1	368.1
Pozo 4	Dolores Hidalgo	25.7	7.52	300.0	296.0	199.4	398.4
CARL-238-P	Dolores Hidalgo	23.3	7.42	336.0	347.3	201.9	400.9
CARL-234-P	Dolores Hidalgo	27.8	7.27	295.0	280.0	195.6	394.6
Ejido de Tirado	San Miguel de Allende	31.1	8.13	295.0	264.2	205.5	404.5
Insurgentes 2	San Miguel de Allende	26.3	8.11	369.0	360.1	244.7	443.7
SMA:171:P	San Miguel de Allende	25.7	7.83	431.0	425.3	371.0	570.0
Waste Water Treatment Plant							
Planta San Pablo	Dolores Hidalgo	21.7	7.60	1401.0	1495.2	118.0	317.0
Hand-Dug Well							
CARL-157-N-HD	San Felipe	17.6	6.45	178.6	208.0	184.2	383.2
Pozo Sergio	San Felipe	17.8	6.05	175.0	202.9	172.5	371.5
Extra Wells Not Sampled							
LS-27-P (No Sample)	San Luis de la Paz	28.9	7.80	524.0	487.7	469.3	668.3
LS-817-NS (No Sample)	San Luis de la Paz	31.0	7.69	530.0	577.4	446.8	645.8

4.2 The Water Chemistry of the Wells Sampled in the Field

Urban and Rural Groundwater Wells

The complete data set for the field measurements can be found in Table 4.4 and Appendix A.1. Dissolved oxygen (DO) values ranged from less than 1 to greater than 15 mg/L indicating most groundwater wells contain oxygenated groundwater. In the rural wells surrounding San Luis de la Paz DO ranged from 4.837 – 8.877 mg/L. In urban wells of the same municipality the DO ranged from 11.440 – 14.950 mg/L. Dolores Hidalgo had similar DO levels ranging from 4.694 – 14.730 mg/L in rural wells and 5.537 – 9.758 mg/L in the urban wells. The DO content in San Miguel de Allende was similar to the urban wells of San Luis de la Paz, ranging from 13.850 – 14.080 mg/L. The groundwater well in San Diego de la Union had DO levels greater than 15.0 mg/L.

Dissolved nitrate (NO_3 – N) in the groundwater wells near San Luis de la Paz ranged from 0.24 – 5.91 mg/L with an average value of 2.7 mg/L. The NO_3-N measured in the groundwater wells near Dolores Hidalgo ranged from 0.32 – 3.82 mg/L. The NO_3-N measured in San Miguel de Allende ranged from 0.82 – 6.16 mg/L. The one groundwater well sampled in San Diego de la Union had a NO3 – N value of 2.23 mg/L.

The highest dissolved sulfate (SO_4) was measured near the city of San Luis de la Paz ranging from 53.4 – 71.0 mg/L. Dolores Hidalgo had a slightly lower range of SO_4 concentrations ranging from 20.0 – 59.5 mg/L. San Miguel de Allende has the lowest SO_4 concentration range with values from 19.0 – 27.0 mg/L. The one groundwater well sampled in San Diego de la Union had dissolved SO concentrations less than 20 mg/L.

Dissolved silica (SiO_2) for groundwater wells near San Luis de la Paz ranged from 80 – 160 mg/L. Dolores Hidalgo had a similar range from 40 – 160 mg/L. The SiO_2 values measured in San Miguel de Allende ranged from 100 – 140 mg/L. The SiO_2 in the groundwater well from San Diego de la Union measured 180 mg/L.

Dissolved nitrite (NO_2-N) measurements were all below the detection limit of 0.6 mg/L. Field measurements of sulfide (S) and Mn were also below detection limits. Additionally, total Fe for all groundwater samples, except one from an urban well of San Luis de la Paz (Well ID: Pozo 9, Fe = 0.281 mg/L), were below the detection limit of 0.2 mg/L. Ammonia values for the basin were low with only six wells registering detectable levels between 0.043 and 0.128 mg/L.

Hand-dug Wells

Dissolved oxygen for Well ID: CARL-145-N-HD was 1.627 mg/L. Alkalinity values for this well was 100 mg/L measured as $CaCO_3$. The SiO_2 in the water of this well was 80 mg/L. Dissolved NO3 – N and dissolved SO_4 in the water of this well was less than 0.2 mg/L and less than 20 mg/L; respectively. The NO_2-N value for this well was below detection limit of 0.6 mg/L. Field measurements of S and manganese were below detection limits. The total Fe in this well was below the detection limit of 0.2 mg/L.

Dissolved oxygen for Well ID: Pozo Sergio was 7.5 mg/L. Dissolved silica in the groundwater of this well was 160 mg/L. The dissolved NO3 – N and dissolved SO_4 of the water in this well was 3.0 mg/L and less than 20 mg/L. The NO_2-N value for this well was below detection limit of 0.6 mg/L. Field measurements of S and Mn were below detection limits. The Fe in this well was 0.20 mg/L.

Waste Water Treatment Plant Dolores Hidalgo

Dissolved oxygen for the effluent was 2.6 mg/L. Dissolved silica in the effluent was 160 mg/L. The dissolved NO3 – N and dissolved SO_4 was less than 0.2 mg/L and less than 20 mg/L. The nitrite value for this effluent was below detection limit of 0.6 mg/L. Field measurements of S and Mn were below detection limits. The Fe concentration of the effluent was 0.23 mg/L.

Table 4.3 Ranges of the physicochemical parameters and water chemistries measured in the five major cities in the basin.

Physicochemical Parameter	San Luis de la Paz	Dolores Hidalgo	San Miguel de Allende	San Felipe	San Diego de la Union
Well Depth (m)	140 – 550	170 – 500	195 – 300	n.a.	n.a.
Depth to Water (m)	145.00 – 180.00	88.86 – >200.00	n.a.	n.a.	n.a.
Temperature (C°)	20.1 – 45.7	23.3 – 34.5	25.7 – 31.1	17.6 – 17.8	32.0
pH	7.49 – 9.02	7.05 – 7.85	7.83 – 8.13	6.05 – 6.45	7.42
Spec. Cond. (µs/cm)	385.2 – 746.1	187.0 – 622.1	264.2 – 425.3	202.9 – 208.0	435.2
ORP (mV)	82.3 – 618.0	332.1 – 696.0	404.5 – 570.0	371.5 – 383.2	416.0
DO (mg/L)	4.837 – 14.950	4.694 – > 15.000	13.850 – 14.080	1.6 – 7.5	< 15
NO_3-N (mg/L)	0.24 – 5.91	0.32 – 3.82	0.82 – 6.16	n.a.	n.a.
SO_4^{2-} (mg/L)	53.4 – 71.0	20.0 – 59.5	19.0 – 27.0	n.a.	n.a.

Table 4.4 The groundwater chemical parameters measured in the field from the five urban areas All units expressed as mg/L.

Well ID	City	DO	NO_3-N	SO_4	SiO_2
Rural					
Lourdes	San Luis de la Paz	5.491	1.22	71.0	100
LS-331-P	San Luis de la Paz	8.877	0.24	63.9	80
LS-012-L	San Luis de la Paz	4.837	3.16	57.0	80
LS-0178	San Luis de la Paz	< 1.000	0.96	70.0	120
Terreros de la Concepciones	San Luis de la Paz	4.879	2.33	60.0	100
CARL-453-P	Dolores Hidalgo	4.694	1.41	58.0	120
CARL-506-P	Dolores Hidalgo	5.574	3.82	58.0	140
CR7	Dolores Hidalgo	> 15.000	0.45	59.5	160
CARL-145-P	Dolores Hidalgo	5.322	0.70	20.0	120
CDW	Dolores Hidalgo	14.730	0.32	< 20.0	120
RL-2-A	San Diego de la Union	> 15.000	2.23	< 20.0	180
Urban					
Pozo 9	San Luis de la Paz	11.440	< 0.2	< 20.0	160
LS-531-P	San Luis de la Paz	14.950	5.91	53.4	160
LS-529-P	San Luis de la Paz	14.630	5.17	63.3	160
CARL-228	Dolores Hidalgo	6.055	0.92	< 20.0	160
Pozo 4	Dolores Hidalgo	5.527	1.32	< 20.0	180
CARL-238-P	Dolores Hidalgo	7.107	1.44	< 20.0	180
CARL-234-P	Dolores Hidalgo	9.758	0.69	< 20.0	40
Ejido de Tirado	San Miguel de Allende	13.850	0.82	19.0	100
Insurgentes 2	San Miguel de Allende	n.a.	1.99	< 20.0	120
SMA:171:P	San Miguel de Allende	14.080	6.16	27.0	140
Waste Water Treatment Plant					
Planta San Pablo	Dolores Hidalgo	2.580	< 0.2	< 20.0	160
Hand-Dug Well					
CARL-157-N-HD	San Felipe	1.627	< 0.2	16.0	80
Pozo Sergio	San Felipe	7.482	3.04	< 20.0	200
Extra Wells Not Sampled					
LS-27-P (No Sample)	San Luis de la Paz	5.568	1.28	57.0	n.a.
LS-817-NS (No Sample)	San Luis de la Paz	6.638	11.75	45.0	n.a.

4.3 Laboratory Results of the IBAS Water Samples

Urban and Rural Groundwater Wells Cations

A total of 21 groundwater well samples (10 rural and 11 urban) were brought back to the lab for major ion analyses by ion chromatography (Table 4.5). Summaries of the ranges and averages for the five major urban areas can be found in Table 4.6.

The highest sodium (Na) concentrations were found in the rural groundwater wells northwest of San Luis de la Paz (Table 4.4). The Na concentrations measured in four of these five rural wells of San Luis de la Paz were about twice (118.52 – 175.55 mg/L) the average Na concentrations measured in the basin. The urban and rural wells of Dolores Hidalgo had four of the lowest Na concentrations measured in the basin (out of 21 wells). In contrast the highest Na concentration was measured near Dolores Hidalgo in a rural well drilled to a depth of 500 m (Well ID: CR7 = 161.06 mg/L), which is much deeper than the typical well depths (median = 210 m). The urban wells of San Miguel de Allende also had relatively low Na concentrations (Table 4.6). An urban groundwater well located on the western side of the Taxco-San Miguel de Allende Fault of San Miguel de Allende had higher Na concentrations (Well ID: Ejido de Tirado = 64.61 mg/L) compared to urban wells on the eastern side of the fault (Well ID: Insurgentes 2 = 43.87 mg/L and Well ID: SMA:171:P = 43.09 mg/L). The Na concentration measured in the rural well of San Diego de la Union was 66.39 mg/L

The potassium (K) concentrations were variable across the basin. The highest K concentrations were measured in rural wells between San Luis de la Paz and Dolores Hidalgo with values of 21.17 and 22.37 mg/L. The K concentrations observed in the rural wells of San Luis de La Paz were typically lower than the urban wells of San Luis de la Paz. The urban wells of Dolores Hidalgo and San Miguel de Allende had similar ranges for K concentrations (Table 4.6). The K concentration of the groundwater well sampled in San Diego de la Union was 19.61 mg/L.

The magnesium (Mg), calcium (Ca), and strontium (Sr) values were highest in the urban wells of San Luis de la Paz. The lowest values of Mg, Ca, and Sr were measured in the rural wells of San Luis de la Paz. The urban areas of Dolores Hidalgo and San Miguel de Allende had similar averages and ranges for Mg, Ca, and Sr (Table 4.6)

Ammonium was only detectable in two samples from San Luis de la Paz and one from Dolores Hidalgo ranging in value from 0.42 – 1.96 mg/L with the highest values recorded in a rural well of San Luis de la Paz (Table 4.4).

Urban and Rural Groundwater Wells Anions

The highest F concentrations measured in the basin occurred in the rural wells near San Luis de la Paz in the eastern half of the basin (Well ID: LS-331-P = 3.70 mg/L, Well ID: LS-012-L = 5.80 mg/L, Well ID: LS-0178 = 15.24 mg/L, and Well ID: Terreros de la Concepciones = 12.04 mg/L). The F concentrations in the rural wells contrast starkly to the F values measured in the urban wells of San Luis de la Paz which were all less than 1.5 mg/L. The F concentrations measured in the groundwater wells of Dolores Hidalgo and San Miguel de Allende had similar ranges (Table 4.6). A high F concentration (3.35 mg/L) was measured in an urban well of San Miguel de Allende located on the western side of the Taxco-San Miguel de Allende Fault System that dissects this urban area (Figure 2.4). A high F concentration (3.54 mg/L) was measured in a rural well near Dolores Hidalgo drilled to a depth of 500 m (Well ID: CR7). The average F values measured in the basin is 2.70 mg/L.

The SO_4 values were similar for both the urban and rural wells of the San Luis de la Paz area. The lowest SO_4 values were found near Dolores Hidalgo and San Miguel de Allende (Table 4.4). The SO_4 concentration measured in San Diego de la Union was 34.41 mg/L. The highest chloride (Cl) concentrations measured in the basin were in the urban wells of San Luis de la Paz. The lowest concentrations of Cl were observed in the urban and rural wells near Dolores Hidalgo and the urban wells of San Miguel de Allende. The well sampled from San Diego de la Union had a Cl concertation of 11.54 mg/L. Nitrite (NO_2) was only detectable in one rural well between the cities of San Luis de la Paz and Dolores Hidalgo (Well ID: CDW). The highest bromide (Br) concentrations were found in the rural and urban wells of San Luis de la Paz. The lowest Br concentrations occurred in the urban areas of Dolores Hidalgo and San Miguel de Allende. The Br concentration of the groundwater well of San Diego de la Union was 0.12 mg/L. Nitrate (NO_3) concentrations were variable across the basin with the highest concentrations measured in the urban wells of San Luis de la Paz (Well ID: Pozo 9 = 23.67 mg/L and Well ID: LS-531-P = 25.86 mg/L) and San Miguel de Allende (Well ID: SMA:171:P = 26.05 mg/L). The phosphate (PO_4) concentrations in all groundwater samples from the region were all below one mg/L with the

highest concentration (Well ID: LS-012-L = 0.93 mg/L) observed in a rural well near San Luis de la Paz.

Alkalinity values were measured in the field and the data can be found in Table 4.5. Alkalinity is the major anion in the groundwaters of the IBAS. The highest alkalinity was measured in San Luis de la Paz. The lowest alkalinity values were measured near Dolores Hidalgo. The deepest well in the center of the basin (Well ID: CR7 = 331.80 mg/L as $CaCO_3$) had higher alkalinity values than the values measured in the urban area of Dolores Hidalgo. San Miguel de Allende had an alkalinity values ranging from 165.0 – 182.0 mg/L as $CaCO_3$. In San Diego de la Union the alkalinity was 193.4 mg/L as CaCO3.

Hand-Dug Wells Major Ions

The two hand dug wells from San Felipe (Well ID's: CARL-157-N-HD and Pozo Sergio) had relatively low concentrations of F (0.30 and 0.25 mg/L), Cl (5.87 and 8.24 mg/L), NO_3 (0.19 and 13.37 mg/L), SO_4 (11.23 and 27.15 mg/L), Na (12.60 and 30.45 mg/L), K (8.39 and 10.49 mg/L), Ca (21.47 and 5.58 mg/L), Mg (5.35 and 1.64 mg/L), Sr (0.62 and bdl mg/L), and alkalinity (100 and 40 mg/L as $CaCO_3$) values compared to groundwater wells of the basin.

Waste Water Treatment Plant Major Ions

The waste water treatment plant was sampled at the discharge location of the plant. The water had high Cl (118.59 mg/L), PO_4 (3.37 mg/L), SO_4 (84.85 mg/L), Na (153.08 mg/L), NH_4 (68.03 mg/L), K (33.06 mg/L), Ca (41.39 mg/L), and alkalinity (394.1 mg/L as $CaCO_3$) concentrations compared to the groundwater wells of the basin. The F (0.54 mg/L), Mg (5.56 mg/L), and Sr (1.03 mg/L) were relatively low compared to the groundwater wells of the basin.

Table 4.5 Major ions in the groundwater of the IBAS. Nitrite was only detectable in sample CDW at 0.28 mg/L.

Well ID	Na mg/L	NH_4 mg/L	K mg/L	Mg mg/L	Ca mg/L	Sr mg/L	F mg/L	Cl mg/L	Br mg/L	NO_3 mg/L	PO_4 mg/L	SO_4 mg/L	HCO_3 mg/L
Rural													
Lourdes	86.34	bdl	21.17	4.44	30.01	0.93	1.20	16.94	0.26	9.16	0.74	47.71	163.9
LS-331-P	175.44	1.96	8.70	bdl	2.34	bdl	3.70	17.56	0.21	0.78	0.69	52.93	313.9
LS-012-L	118.52	bdl	2.40	bdl	7.50	0.25	5.80	22.93	0.26	11.72	0.93	40.36	210.0
LS-0178	132.13	bdl	2.39	bdl	5.04	0.22	15.24	24.04	0.30	3.35	0.64	44.12	250.0
Terreros de la Concepciones	175.55	bdl	3.81	0.89	3.76	0.21	12.04	22.10	0.30	10.38	0.60	43.72	360.0
CARL-453-P	77.05	0.35	14.16	2.14	35.52	0.92	1.37	15.14	0.18	8.65	0.56	37.85	169.8
CARL-506-P	79.82	bdl	22.37	2.91	38.18	1.20	1.05	12.50	0.16	13.48	bdl	48.65	210.0
CR7	161.06	bdl	13.51	1.79	16.01	0.57	3.54	17.01	0.16	4.95	bdl	41.64	331.8
CARL-145-P	59.10	bdl	10.25	2.95	22.22	0.62	0.93	6.70	bdl	3.23	0.57	11.06	210.0
CDW	33.74	bdl	3.43	0.66	16.02	0.33	1.18	4.76	bdl	2.11	0.37	7.87	115.0
RL-2-A	66.39	bdl	19.61	5.24	24.16	0.77	0.75	11.54	0.12	11.32	bdl	34.41	193.4
Urban													
Pozo 9	55.72	bdl	14.82	23.76	50.20	1.96	1.05	43.19	0.37	23.67	0.57	45.16	298.9
LS-531-P	56.90	bdl	14.86	24.33	52.29	1.90	1.10	43.10	0.41	25.86	0.69	49.56	236.1
LS-529-P	77.53	0.42	18.40	18.86	34.38	1.66	1.41	34.38	0.41	17.18	0.65	52.80	200.0
CARL-228	41.62	bdl	15.16	2.53	25.18	0.76	0.84	6.44	bdl	4.02	0.51	13.57	142.2
Pozo 4	31.91	bdl	8.00	4.01	26.93	0.63	0.52	4.79	bdl	5.14	0.74	15.28	53.7
CARL-238-P	31.15	bdl	10.10	5.38	31.62	0.93	0.40	4.76	bdl	5.55	0.60	20.86	126.6
CARL-234-P	23.84	bdl	8.96	4.57	30.17	0.83	0.37	4.74	bdl	3.09	0.56	16.72	133.7
Ejido de Tirado	64.61	bdl	7.28	0.83	10.88	0.27	3.35	5.00	bdl	3.99	bdl	12.29	165.0
Insurgentes 2	43.87	bdl	12.69	10.32	31.37	1.14	0.40	5.80	bdl	10.43	bdl	11.07	175.0
SMA:171:P	43.09	bdl	13.70	11.97	43.02	1.46	0.39	9.36	0.11	26.05	bdl	16.72	182.0
Waste Water Treatment Plant													
Planta San Pablo	153.08	68.03	33.06	5.56	41.39	1.03	0.54	118.59	bdl	bdl	3.37	84.85	394.1
Hand-Dug Well													
CARL-157-N-HD	12.60	bdl	8.39	5.35	21.47	0.62	0.30	5.87	bdl	0.19	bdl	11.23	100.0
Pozo Sergio	30.45	bdl	10.49	1.64	5.58	bdl	0.25	8.24	bdl	13.37	bdl	27.15	40.0

Table 4.6 Ranges of values measured major ions for the five different municipalities. All values are expressed as mg/L. HCO3- is expressed as mg/L as CaCO3

Major Ions	San Luis de la Paz	Dolores Hidalgo	San Miguel de Allende	San Felipe	San Diego de la Union
Na	55.72 – 175.55	23.84 – 161.06	43.00 – 64.61	12.60 – 30.45	66.39
NH_4	0.42 – 1.96	0.35	Bdl	Bdl	Bdl
K	2.39 – 21.17	3.43 – 22.37	7.28 – 13.70	8.39 – 10.49	19.61
Mg	0.89 – 24.33	0.66 – 5.38	0.83 – 11.97	1.64 – 5.35	5.24
Ca	2.34– 52.29	16.01 – 38.18	10.88 – 43.02	5.58 – 21.47	24.16
Sr	0.21- 1.96	0.33 – 1.2	0.27 – 1.46	0.62	0.77
F	1.05 – 15.24	0.37 – 3.54	0.39 – 3.35	0.25 – 0.30	0.75
Cl	16.94 – 43.19	4.74 – 17.01	5.00 – 9.36	5.87 – 8.24	11.54
Br	0.21 – 0.41	0.16 – 0.18	0.11	Bdl	0.12
NO_3	0.78 – 25.86	2.11 – 13.48	3.99 – 26.05	0.19 – 13.37	11.32
SO_4	40.36 – 52.93	7.87 – 48.65	11.07 – 16.72	11.23 – 27.15	34.41
PO_4	0.57 – 0.93	0.37 – 0.74	Bdl	Bdl	Bdl
HCO_3	163.9 – 360	53.7 – 331.8	165.0 – 182.0	40.0 – 100.0	193.4

Groundwater Water Types

The high Na, F, and As concentrations observed in the rural wells of the northeastern corner of the basin display a stark contrast to the urban wells (Figure 4.1). In the IBAS urban wells are dominantly Ca-Mg-Na-HCO_3 rich water types while rural wells are Na-HCO_3^- rich water types which correlate with elevated F and As (Figure 4.1). The distribution of major ions in the IBAS are displayed as box and whisker plots (Figure 4.2).

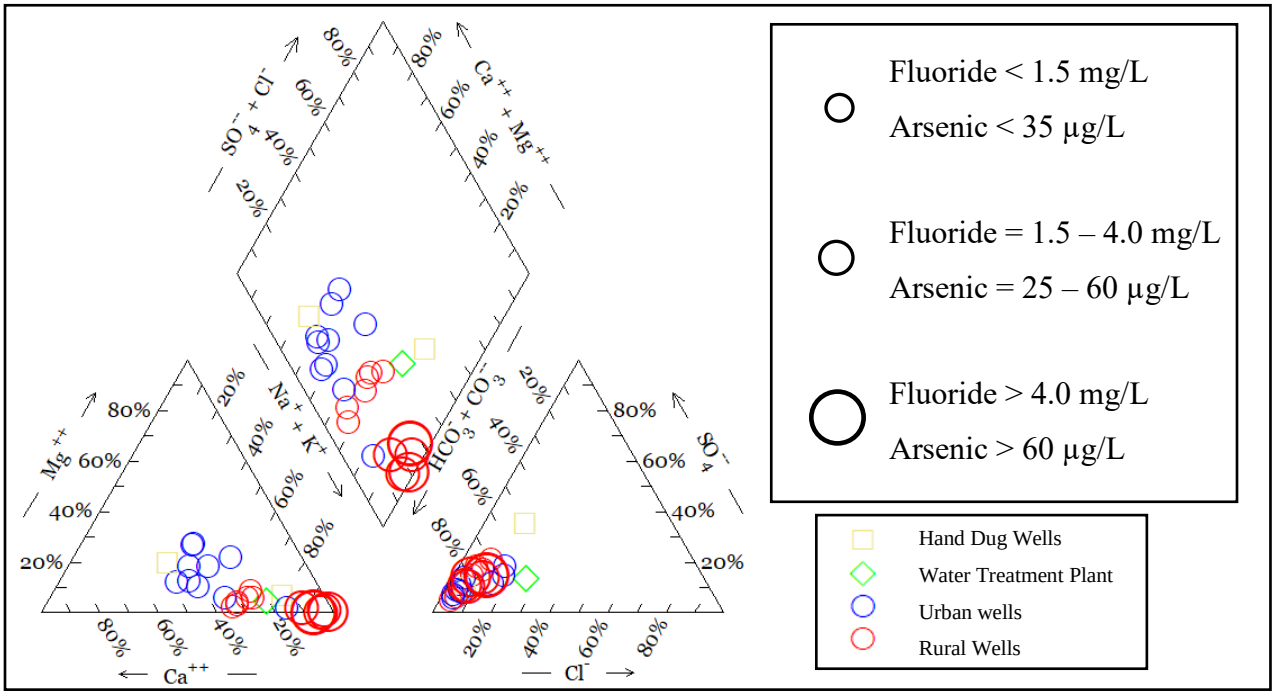

Figure 4.1 Piper diagram displaying the major water types observed in the basin.

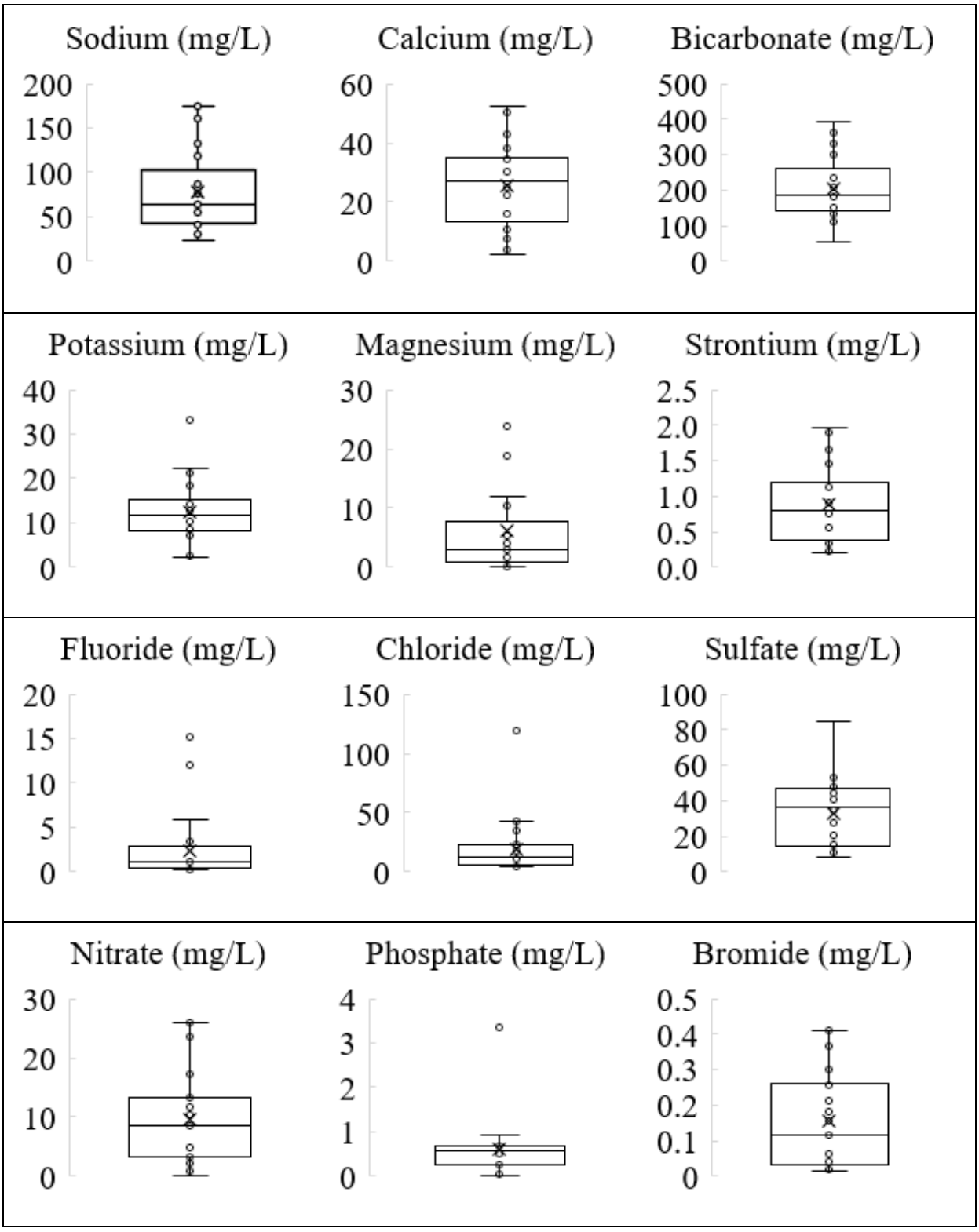

Figure 4.2 Range of values in major ions from groundwater wells, hand-dug wells, and water treatment effluent water samples with mean value designated with the symbol x. Interior and outlier points a denoted alongside the four quartiles.

Urban and Rural Groundwater Wells Trace Ions

A total of 21 groundwater well water samples (10 rural and 11 urban) were brought back to KSU for analysis by ICP-MS and retested with ACTlabs. A summary of the average and ranges of selected trace elements can be found in Tables 4.7, 4.8, 4.9, 4.10, and Figure 4.3. The complete dataset can be found in Appendix A.3.

The highest average As concentrations were found in the rural wells on the eastern side of the basin near San Luis de la Paz (Table 4.8). Additionally, a well sampled in the center of the basin near Dolores Hidalgo (Well ID: CR7) had relatively high As concentrations at 40.3 µg/L. The range of As concentrations measured San Luis de la Paz displayed the widest range of values (Table 4.9). Specifically, the rural wells of San Luis de la Paz are in stark contrasts to the urban wells of San Luis de la Paz (Table 4.10). The rural wells near Dolores Hidalgo on the western side also had relatively low As concentrations compared to the San Luis de la Paz. The As concentrations in the rural wells and the urban wells of Dolores Hidalgo also displayed different ranges in values (Table 4.10). The urban wells of San Miguel de Allende had the lowest average As concentrations (Table 4.8). The urban wells of San Miguel de Allende showed different As values spatially as the groundwater well located on the western side of the Taxco-San Miguel de Allende fault had higher concentrations compared to the urban wells on the eastern side of the fault. In the urban well sampled in San Diego de la Union the As concentration measured 7.93 µg/L. The As concentrations measured in the basin was 21.5 µg/L with a range of values between 3.0 and 93.5 µg/L (Table 4.8).

The highest average dissolved boron (B) concentrations were found in the rural wells near San Luis de la Paz which had B values ranging from 189.0 – 410.0 µg/L (Table 4.9). The range of B values found in the urban wells of San Luis de la Paz (60.3 – 95.1 µg/L) were similar to the urban wells of Dolores Hidalgo (35.7 – 101.8 µg/L) (Table 4.10). The rural wells surrounding Dolores Hidalgo had a drastically different range of values compared to the nearby rural wells (Table 4.10). The 697.0 µg/L value for B was the highest concentration measured in the basin, this was also the deepest well (Well ID: CR7) installed near Dolores Hidalgo at 500 m depth. San Miguel de Allende had average B concentration that was less than half of the average B concentrations measured in San Luis de la Paz and Dolores Hidalgo (Table 4.8). The one well measured in San Diego de la Union had relatively low B concentrations (Table 4.8). Boron values

measured across the basin ranged from 9.7 µg/L – 697 µg/L with an average of 157.1 µg/L (Table 4.9).

The total dissolved Fe concentrations were only detectable in 16 out of 24 wells as the other eight wells were below detection limit of 1 µg/L. The wells Well ID: Lourdes and Well ID: LS-331-P have detectable Fe concentrations with values of 58 µg/L and 11 µg/L, respectively. The urban wells in the city of San Luis de la Paz ranged in Fe concentrations from 22.3 µg/L – 41.4 µg/L. The rural and urban wells of Dolores Hidalgo ranged in Fe concentrations from 28.0 µg/L – 138.0 µg/L and 7.9 µg/L – 22.3 µg/L, respectively. The Fe concentrations was detectable in two of the three urban wells in San Miguel de Allende. These urban wells had the lowest average Fe concentrations with values ranging from 8.5 – 20.0 µg/L (Table 4.8 and 4.9). The Fe concentration in the urban well of San Diego de la Union was below detection limit of 1 µg/L. The Fe concentrations measured in the basin ranged from 7.6 µg/L – 196.8 µg/L with an average value of 45.8 µg/L (Table 4.8).

The dissolved lithium (Li) concentrations measured in the rural wells of San Luis de la Paz had the highest average concentrations and displayed the largest range of values (Table 4.8 and Table 4.9). The range of Li concentrations in the rural wells of Dolores Hidalgo was comparable to the range observe in the rural wells of San Luis de la Paz (Table 4.9). The highest Li value measured in Dolores Hidalgo was observed in the rural well (Well ID: CR7). The urban wells of San Luis de la Paz had significantly less Li on average and displayed a narrow range of values (Table 4.10). The range of Li concentrations observed in the urban wells of Dolores Hidalgo were comparable to the range of values in the urban wells of San Luis de la Paz (Table 4.10). The urban wells of San Miguel de Allende had Li concentrations ranging from 2.3 – 83.4 µg/L with an average Li concentration of 44.6 µg/L. The highest Li concentrations in the San Miguel de Allende was observed in the groundwater well located on the western side of the fault line. The urban well of San Diego de la Union had a Li concentration of 107.0 µg/L. The average Li concentration measured in the basin was 109.4 µg/L and ranged from 1.8 – 454.0 µg/L.

The dissolved Mn concentration was detectable in one of the five rural wells from San Luis de la Paz at 1.3 µg/L. The urban wells of San Luis de la Paz had Mn concentrations ranging from 0.6 – 6.4 µg/L. Mn concentrations were detectable in eight of the nine urban wells and rural wells of Dolores Hidalgo. These wells had the three highest Mn concentrations measured in the basin. In the rural and urban wells of Dolores Hidalgo, Mn ranges where 0.7 – 159.2 µg/L and 1.2 – 36.2

µg/L, respectively. The urban wells of San Miguel de Allende had Mn concentrations which ranged from 0.7 µg/L – 9.9 µg/L. The urban well of San Diego de la Union had a Mn concentration of 5.7 µg/L. The average Mn measured in the basin was 16.4 µg/L with values ranging from 0.6 – 159.0 µg/L (Table 4.7).

Hand-Dug Wells Trace Ions

The two hand dug wells had low As concentrations (Appendix A.3). The two hand dug wells of San Felipe had the lowest B concentrations measured in the basin at values of 9.7 and 12.7 µg/L. These wells had Fe concentrations of 127 µg/L – 197 µg/L. The hand-dug wells of San Felipe had Li concentrations of 1.9 – 27.3 µg/L. These wells had Mn values ranging from 0.5 – 8.2 µg/L.

Waste Water Treatment Plant Trace Ions

The water treatment plant of Dolores Hidalgo had an As concentration of 8.26 µg/L, a B concentration of 161 µg/L, an Fe concentration of 48 µg/L, a Li concentration of 60 µg/L, and Mn concentration that was below the detection limit of 0.05 µg/L.

Table 4.7 The averages and ranges of trace ions in only the groundwater samples collected from the IBAS.

Trace Ions	Detectable Measurements	Range (µg/L)	Average (µg/L)
As	n = 21	3 – 93.5	23.2
B	n = 21	22.9 – 697	171
Fe	n = 14	7.6 – 196.8	29.2
Li	n = 21	1.8 – 454	118.5
Mn	n = 15	0.6 – 159	18

Table 4.8 Average values for selected trace ion concentrations that were detectable around each of the five major municipalities in the basin. All values are expressed as µg/L.

Trace Ions (µg/L)	San Luis de la Paz	Dolores Hidalgo	San Miguel de Allende	San Felipe	San Diego de la Union
As	36.7	17.1	10.7	3.3	7.9
B	198.9	190.7	72.7	11.2	65.1
Fe	33.8	30.2	14.3	161.9	n.a.
Li	175.0	94.1	44.6	14.6	107.2
Mn	3.6	33.6	4.8	4.4	5.7

Table 4.9 Range of values for selected trace ion concentrations that were detectable around each of the five major municipalities in the basin. All values are expressed as µg/L.

Trace Ions (µg/L)	San Luis de la Paz	Dolores Hidalgo	San Miguel de Allende	San Felipe	San Diego de la Union
As	6.4 – 93.5	6.4 – 40.3	3.0 – 25.5	1.4 – 5.2	7.3
B	60.3 – 410	35.8 – 697	22.9 – 171	9.7 – 12.7	65.1
Fe	11 – 58	7.6 – 138	8.5 – 20	127 – 196.9	<1
Li	24.4 – 454	1.8 – 333	2.3 – 83.4	1.9 – 27.3	107.2
Mn	0.6 – 6.4	0.7 – 159	0.7 – 9.9	0.5 – 8.2	5.7

Table 4.10 Range of values for trace ion concentrations in the rural and urban wells near two major urban areas in the IBAS. All values are expressed as µg/L.

Municipality	San Luis de la Paz		Dolores Hidalgo	
Land Use Type	Urban	Rural	Urban	Rural
Trace Ions	(µg/L)	(µg/L)	(µg/L)	(µg/L)
As	6.4 – 11.3	13.1 – 93.5	6.4 – 15.2	11.3 – 19.3
B	60.3 – 95.1	189 - 410	35.7 – 101.8	99.7 – 697
Fe	22.3 – 41.4	11 – 58	7.9 – 22.3	28 – 138
Li	24.4 – 126	89.7 – 454	1.8 – 128	38 – 333
Mn	0.63 – 6.4	1.3	0.7 – 159.2	1.2 – 36.2

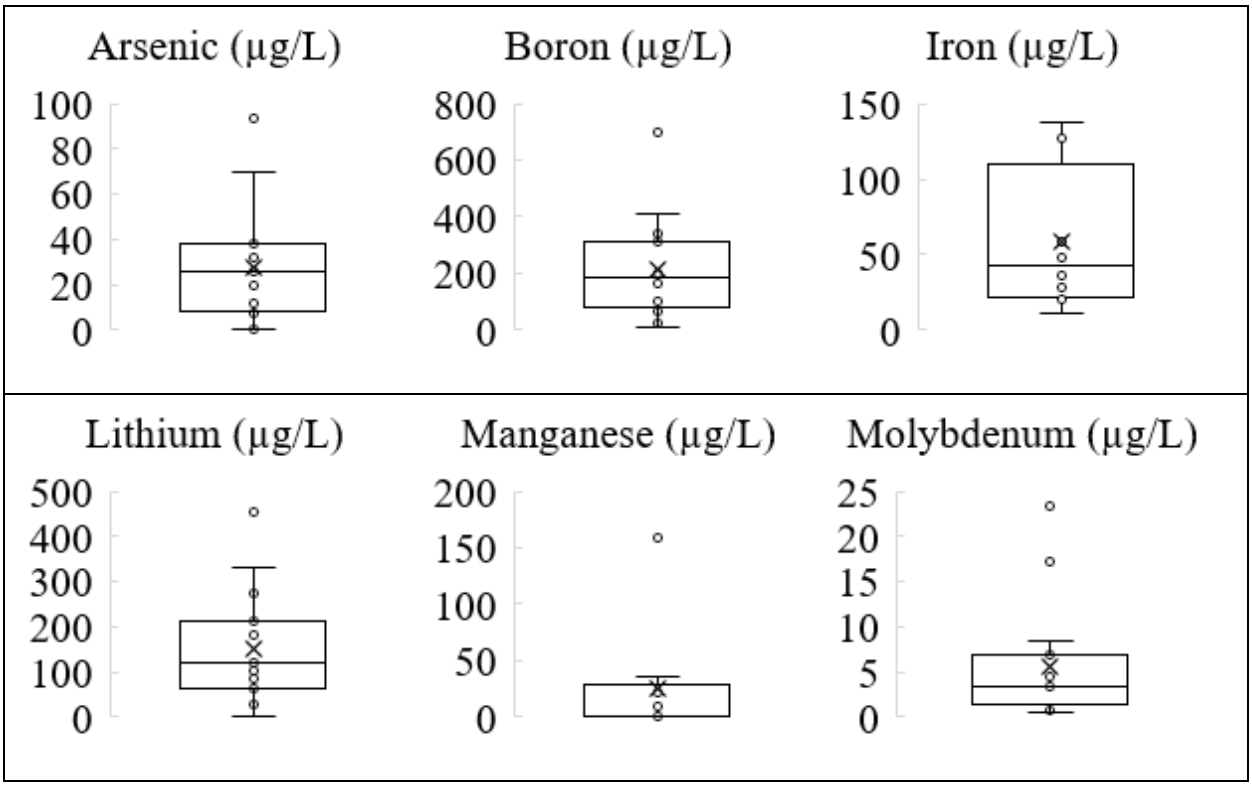

Figure 4.3 Range of values in trace ions from groundwater, hand dug, and water treatment effluent water samples with mean value designated with the symbol x. Interior and outlier points a denoted alongside the four quartiles.

4.4 Oxygen ($\delta^{18}O$) and Deuterium ($\delta^{2}H$) Isotopic Ratios of IBAS Groundwater

A total of 24 water samples was brought back to the lab for isotopic analysis. The complete dataset can be found in Table 4.11. The urban and rural groundwater wells sampled in the study have an oxygen ($\delta^{18}O$) ratios between -8.7 – -10.2 ‰ and -7.9 – -9.6 ‰, respectively. The deuterium ($\delta^{2}H$) ratios for the urban and rural groundwater wells is between -67 – -78 ‰ and -61 – -72 ‰, respectively. The ranges of $\delta^{18}O$ and $\delta^{2}H$ for the five urban areas are in Table 4.12. The hand dug wells sampled in this region have $\delta^{18}O$ ratios of -7.6 ‰ and -6.4 ‰ and $\delta^{2}H$ ratios of -57 ‰ and -52‰ (Table 4.14). The distribution of oxygen and deuterium isotopic ratios were similar to the study conducted by Knappett et al. 2018 (Figure 4.4). The water samples isotopic ratios cluster along the mixing and evaporation line generated by Mahlknecht et al., (2004) reflects the contribution of rainfall from the Sierra de Guanajuato to the west and rainfall created from the Atlantic to the east with evaporation effects because of irrigation from framing which alters the isotopic ratios (Figure 4.5). The groundwater wells of the urban area of San Luis de la Paz have the most isotopically enriched groundwater, whereas the rural wells near this city have the most depleted groundwater isotopic ratios (Figure 4.6). The water treatment effluent water has $\delta^{18}O$ and $\delta^{2}H$ ratios of -8.9 and -69 ‰, respectively.

Table 4.11 Oxygen and Deuterium isotopic ratios for water samples from the IBAS.

Well Sampled	City	δ^2H ‰ VSMO	$\delta^{18}O$ ‰ VSMO
Rural			
Lourdes	San Luis de la Paz	-62	-7.9
LS-331-P	San Luis de la Paz	-66	-8.4
LS-012-L	San Luis de la Paz	-70	-9.4
LS-0178	San Luis de la Paz	-70	-9.6
Terreros de la Concepciones	San Luis de la Paz	-72	-9.5
CARL-453-P	Dolores Hidalgo	-61	-7.9
CARL-506-P	Dolores Hidalgo	-66	-8.2
CR7	Dolores Hidalgo	-71	-9
CDW	Dolores Hidalgo	-69	-8.8
CARL-145-P	Dolores Hidalgo	-68	-9.1
RL-2-A	San Diego de la Union	-71	-9.3
Urban			
Pozo 9	San Luis de la Paz	-75	-10
LS-531-P	San Luis de la Paz	-78	-10
LS-529-P	San Luis de la Paz	-79	-10.2
CARL-228	Dolores Hidalgo	-67	-8.7
Pozo 4	Dolores Hidalgo	-72	-9.2
CARL-238-P	Dolores Hidalgo	-72	-9.3
CARL-234-P	Dolores Hidalgo	-73	-9.4
Ejido de Tirado	San Miguel de Allende	-68	-9
Insurgentes 2	San Miguel de Allende	-71	-9.4
SMA:171:P	San Miguel de Allende	-71	-9.5
Waste Water Treatment Plant			
Planta San Pablo	Dolores Hidalgo	-69	-8.9
Hand Dug Well			
CARL-157-N-HD	San Felipe	-52	-6.4
Pozo Sergio	San Felipe	-57	-7.6

Table 4.12 Oxygen and deuterium isotopic ranges and averages for the major urban areas. All units are expressed as ‰VSMOW.

Isotopes	San Luis de la Paz	Dolores Hidalgo	San Miguel de Allende	San Felipe	San Diego de la Union
δ^2H‰	(-79) – (-62)	(-73) – (-61)	(-71) – (-68)	(-57) – (-52)	(-69)
$\delta^{18}O$‰	(-10.2) – (-7.9)	(-9.4) – (-7.9)	(-9.5) – (-9.0)	(-7.6) – (-6.4)	(-8.8)
Mean δ^2H‰	-71.5	-69	-70	-54.5	n.a.
Mean $\delta^{18}O$‰	-9.4	-8.9	-9.3	-7.0	n.a.

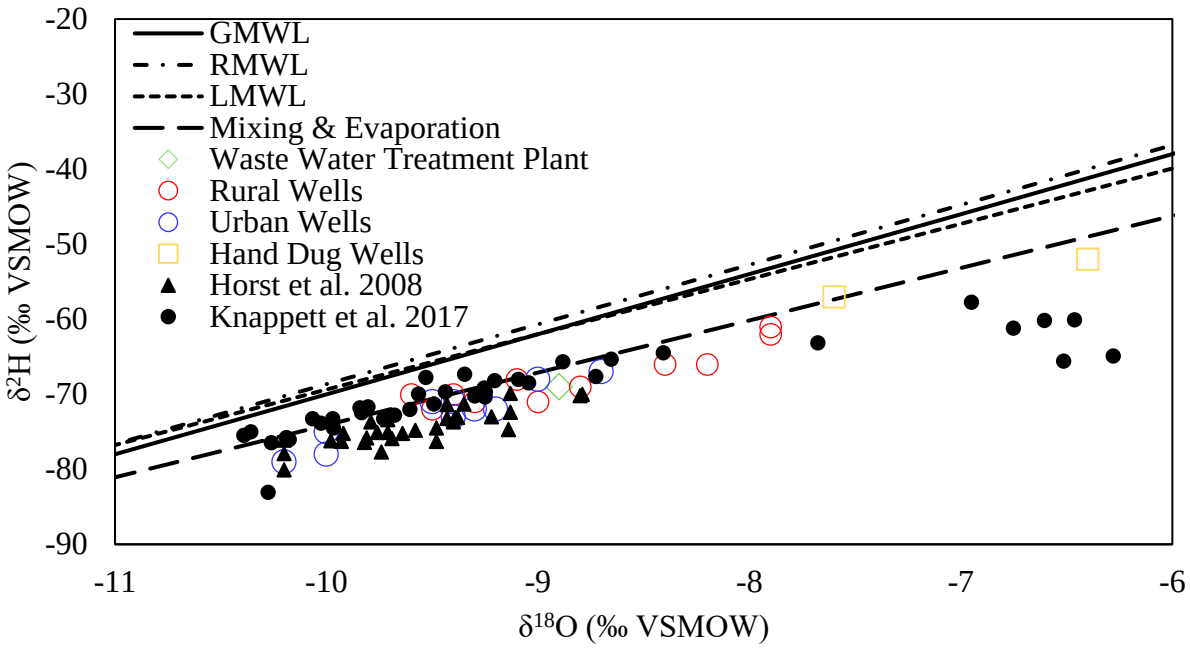

Figure 4.4 Oxygen and deuterium isotopes for all water samples from the IBAS. The solid black line represents the global meteoric water line (GMWL: $\delta^2H = 8\ \delta^{18}O + 10$) (Craig H., 1961), the dashed lines represent the regional meteoric water line (RMWL: $\delta^2H = 7.97\delta^{18}O + 11.03$) and groundwater impacted by mixing between the western and eastern sides of the basin (Mixing & Evaporation: $\delta^2H = 6.97\delta^{18}O - 4.40$) (Mahlknecht et al., 2004).

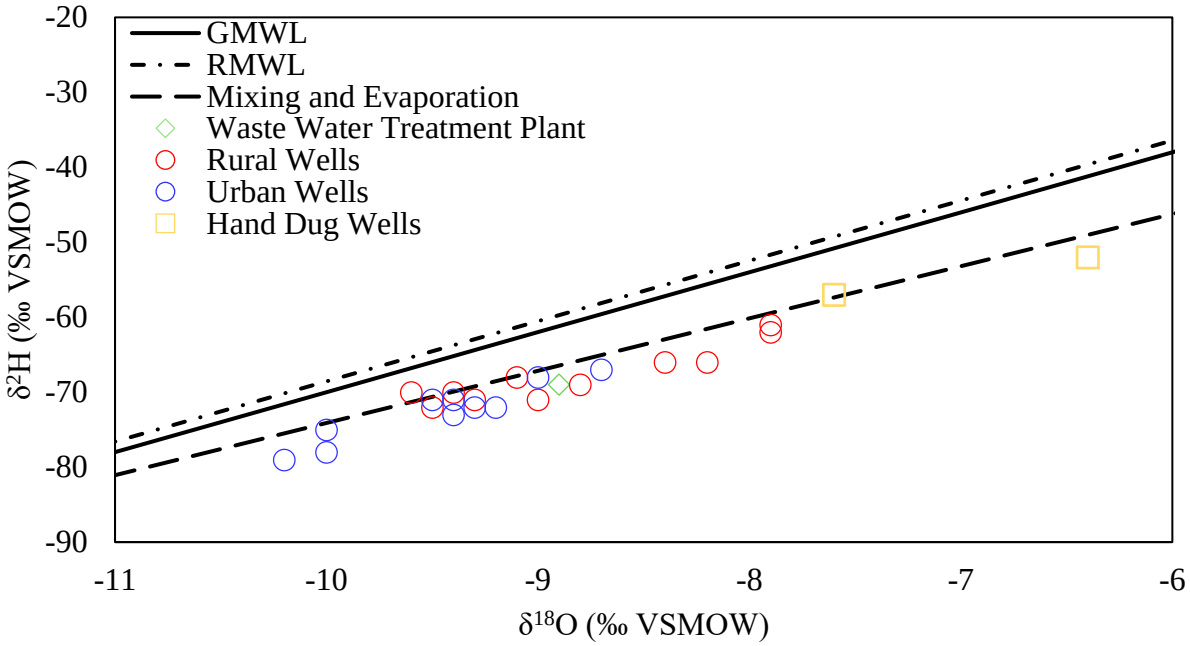

Figure 4.5 Oxygen and deuterium isotopic composition of wells sampled in the IBAS since 2008. The black triangles represent samples collected in the basin directly west of the IBAS by Horst et al. (2008). The dashed lines represent: groundwater impacted by mixing between

the western and eastern sides of the basin (Mixing & Evaporation: $\delta^2H = 6.97\delta^{18}O - 4.40$) (Mahlknecht et al., 2004), the global meteoric water line (GMWL: $\delta^2H = 8\ \delta^{18}O + 10$) (Craig H., 1961), and the regional meteoric water line (RMWL: $\delta^2H = 7.97\delta^{18}O + 11.03$) (Cortes et al., 1989). The black circles and the black dashed line represents the local meteoric water line (LMWL: $\delta^2H = 7.37\delta^{18}O + 4.31$) developed by Knappett et al. (2018).

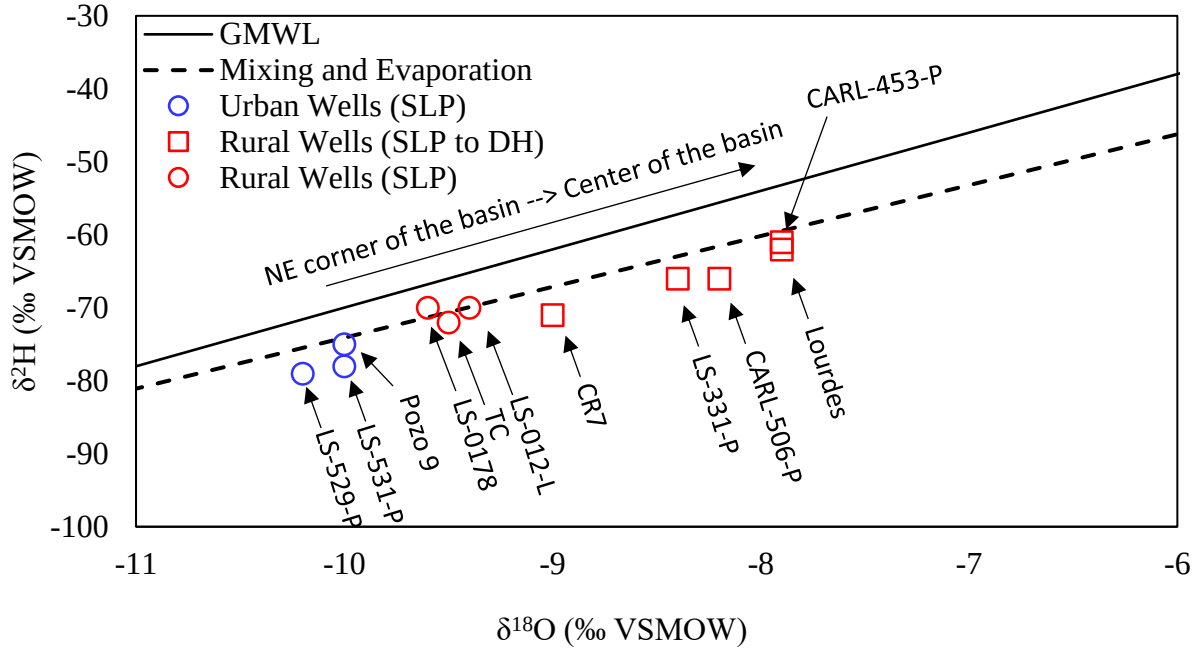

Figure 4.6 Oxygen and deuterium isotope ratios for San Luis de la Paz (SLP) and flow path. (GMWL: $\delta^2H = 8\ \delta^{18}O + 10$) (Craig H., 1961), (Mixing & Evaporation: $\delta^2H = 6.97\delta^{18}O - 4.40$)

4.5 Dissolved Organic Carbon in the IBAS Water Sample

A total of 24 samples was brought back to the lab for DOC analysis. The complete dataset can be found in Appendix A.4. The DOC concentrations measured throughout the basin are typical for groundwater and did not show any correlation with respect to depth (Figure 4.7A). The DOC values for all groundwater wells sampled ranged from 0.39 – 1.93 mg/L (Figure 4.7B). The highest groundwater DOC concentration is (Well ID: CDW = 1.93 mg/L) on the eastern side of the basin installed at a depth of 280 m. The hand dug wells (Well ID: CARL-157-HD and Well ID: Pozo Sergio) are more representative of surface water with higher concentrations of DOC's than the groundwater wells with values of 2.961 and 5.093 mg/L (Table 4.13). The waste water treatment plant had the highest DOC values of all the samples with a concentration of 16.18 mg/L.

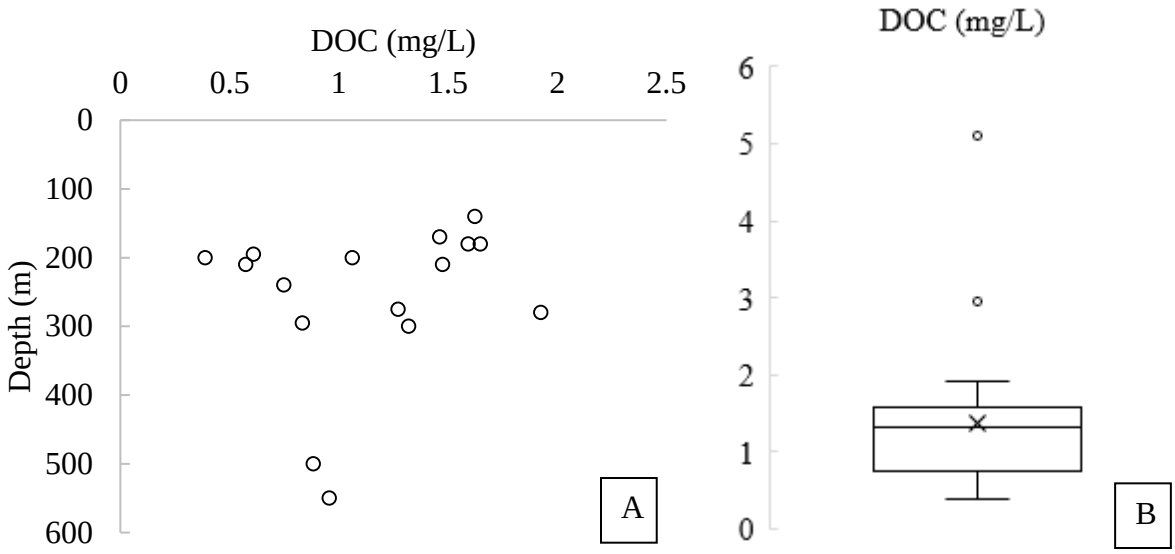

Figure 4.7 The DOC concentrations in groundwater wells with respect to the depth of the well (A). The distribution of DOC values in the water samples collected from the IBAS (B). The water treatment plant effluent water (16.18 mg/L) was excluded from the box and whisker plot as it skewed the average concentration (B).

Table 4.13 Summary of the DOC measured near major urban areas.

DOC	San Luis de la Paz	Dolores Hidalgo	San Miguel de Allende	San Felipe	San Diego de la Union
Average (mg/L)	1.37	1.05	0.92	4.03	0.48
Range (mg/L)	0.96 – 1.65	0.39 – 1.93	0.61 – 1.32	2.96 – 5.09	n.a.

4.6 X-Ray Diffraction of the Drill Cuttings from the IBAS

Western Side of Basin (Arrastres)

The 500-meters of drill cuttings from the Arrastres borehole on the western side of the basin was analyzed through powder XRD. The XRD analyses results can be found in Appendix A.32 – A.57. Summaries of the results for the Arrastres borehole can be found in Figure 4.8. The first 0 – 40 m of the Arrastres drill cuttings are composed of plagioclase, pyroxene, and quartz. The 40 – 220 m of the drill cuttings are composed of plagioclase, potassium feldspar, and quartz. The 220 – 400 m of the drill cuttings are composed of plagioclase, pyroxene, and quartz. The 400 – 500 m of the drill cuttings are composed of plagioclase, potassium feldspar, and quartz.

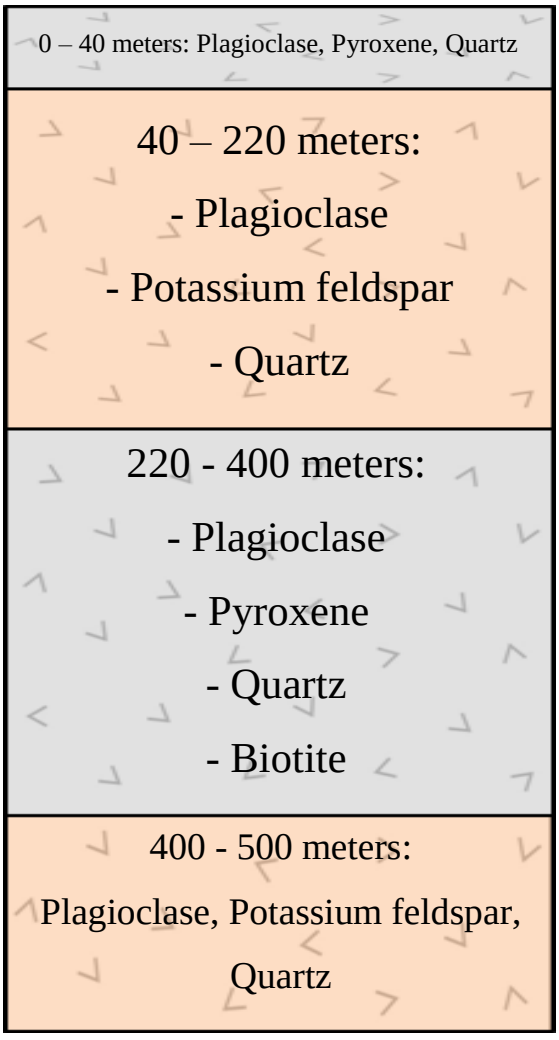

DEPTH (m)	PLAGIOCLASE	QUARTZ	K-FELDSPAR	PYROXENE	CLINOPTILOLITE	NONTRONITE	BIOTITE
10	X	X		X		X	
20	X	X		X		X	
40	X	X	X			X	
60	X	X	X		X	X	
80	X	X	X			X	
100	X	X	X		X	X	
120	X	X	X		X	X	
140	X	X	X		X	X	
160	X	X	X			X	
180	X	X	X			X	
200	X	X	X		X	X	
220	X	X	X	X		X	X
240	X	X		X			
260	X	X	X	X		X	
280	X		X	X		X	
300	X		X	X		X	
320	X	X		X		X	X
340	X	X		X		X	
360	X	X		X		X	X
384	X		X	X		X	
400	X	X		X	X		X
420	X	X	X		X		
430	X	X	X		X		
452	X	X	X		X		
480	X	X	X		X		
500	X	X	X		X		

Figure 4.8 Stratigraphic column of the Arrastres drill cuttings from the western side of the basin.

Eastern Side of the Basin (Lourdes)

The 550-meters of drill cuttings from Lourdes borehole on the eastern side of the basin were examined and results of the analysis can be found in Appendix A.58 – A.84. The 0 – 300 m of the drill cuttings are composed of plagioclase, potassium feldspar, quartz, muscovite, and calcite (Figure 4.9). The 300 – 550 m of the drill cuttings are composed of plagioclase, pyroxene, and quartz. At 220 m depth a single mineral was found to be composed of fluorite (Appendix A.69).

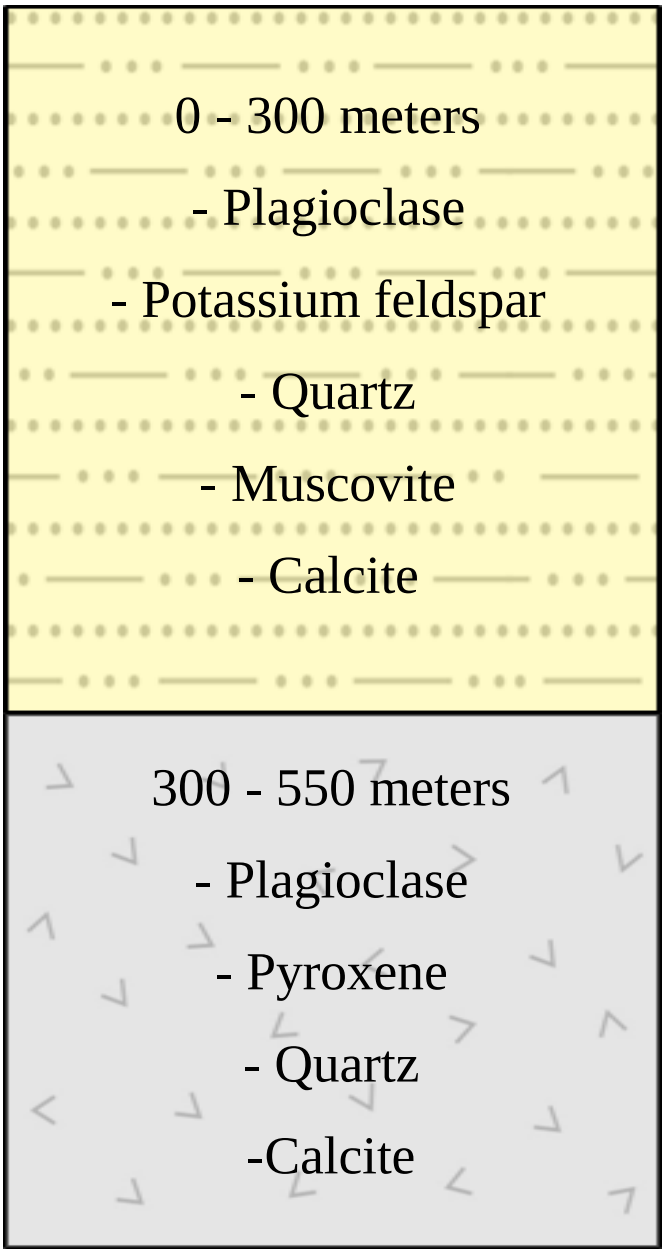

DEPTH (m)	PLAGIOCLASE	QUARTZ	K-FELDSPAR	CALCITE	MUSCOVITE	PYROXENE	MONTMORILLONITE
20	X	X	X	X	X		
40	X	X	X	X	X		
60	X	X	X	X	X		
80	X	X	X	X			
100	X	X	X	X			
120	X	X	X	X	X		
140	X	X	X	X	X		
160	X	X	X	X	X		
180	X	X	X	X	X		
200	X	X	X	X	X		
220	X	X	X		X		
240	X	X	X	X	X		
260	X	X	X	X	X		
280	X	X	X	X			
300	X	X	X			X	X
320	X	X		X		X	X
340	X	X				X	X
360	X	X				X	X
400	X	X		X		X	X
420	X	X		X		X	X
440	X	X				X	X
460	X	X				X	X
480	X	X				X	X
500	X	X				X	X
520	X	X		X		X	X
540	X			X		X	X

Figure 4.9 Stratigraphic column of the Lourdes drill cuttings from the eastern side of the basin. Clinoptilolite was identified at the 180 m and hornblende between 240 and 280 m. Magnetite was identified at the 420 m depth.

4.7 Surface Samples of Rocks and Sediments

During a trip in January of 2018, four field samples were by collected and analyzed by XRD and XRF at the University of Guanajuato by Dr. Datta (Table 4.14, Figure 4.10, Figure 4.11, Figure 4.12, Figure 4.13, and Figure 4.14). The XRF data is available in Appendix A.85. The samples consisted of felsic volcanic rocks of ignimbrite and rhyolite composition, along with sedimentary conglomerates and fine-grained sandstone.

Table 4.14 Rock samples collected in the field and analyzed by XRD.

SAMPLE	ROCK TYPE	QUARTZ	CALCITE	K-FELDSPAR	MUSCOVITE	PLAGIOCLASE	MONTMORILLONITE	KAOLINITE	HEMATITE
Sample 1	n.a.	X	X		X		X		
Sample 2	Ignimbrite -or- Rhyolite	X		X			X		
Sample 4	Eocene Conglomerate	X		X		X		X	
Sample 7	Ignimbrite	X		X		X			X

Figure 4.10 The location of the four field samples collected in the IBAS.

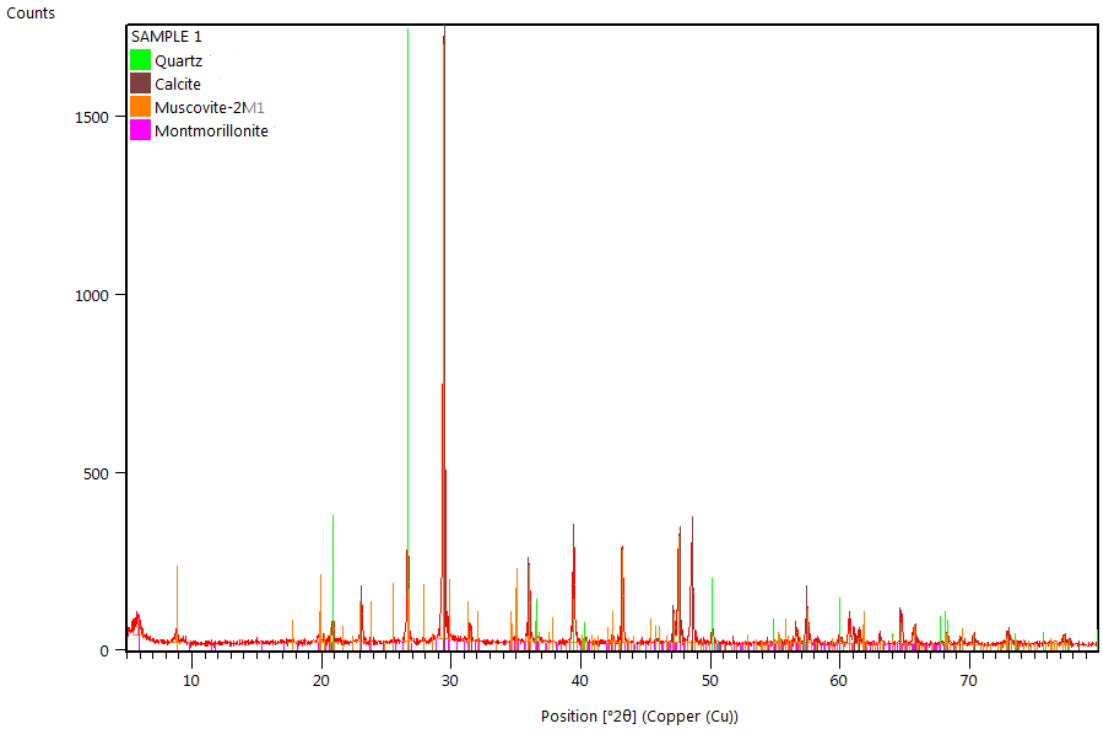

Figure 4.11 Sample one collected from the IBAS

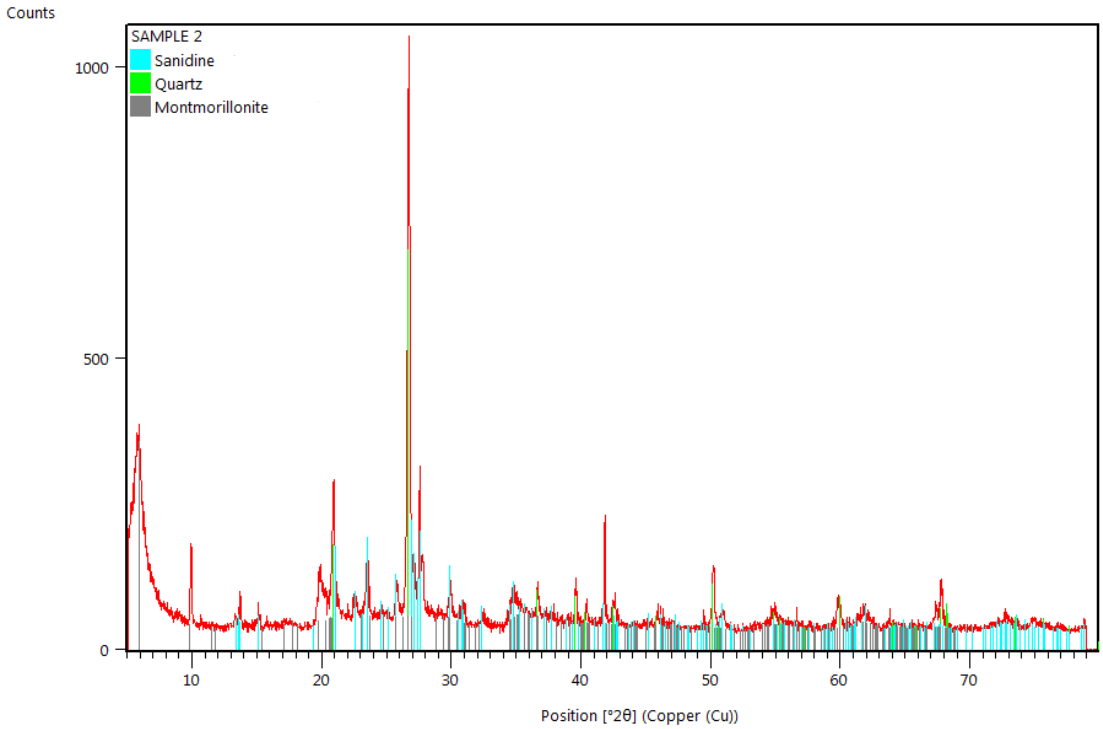

Figure 4.12 Sample two collected from the IBAS

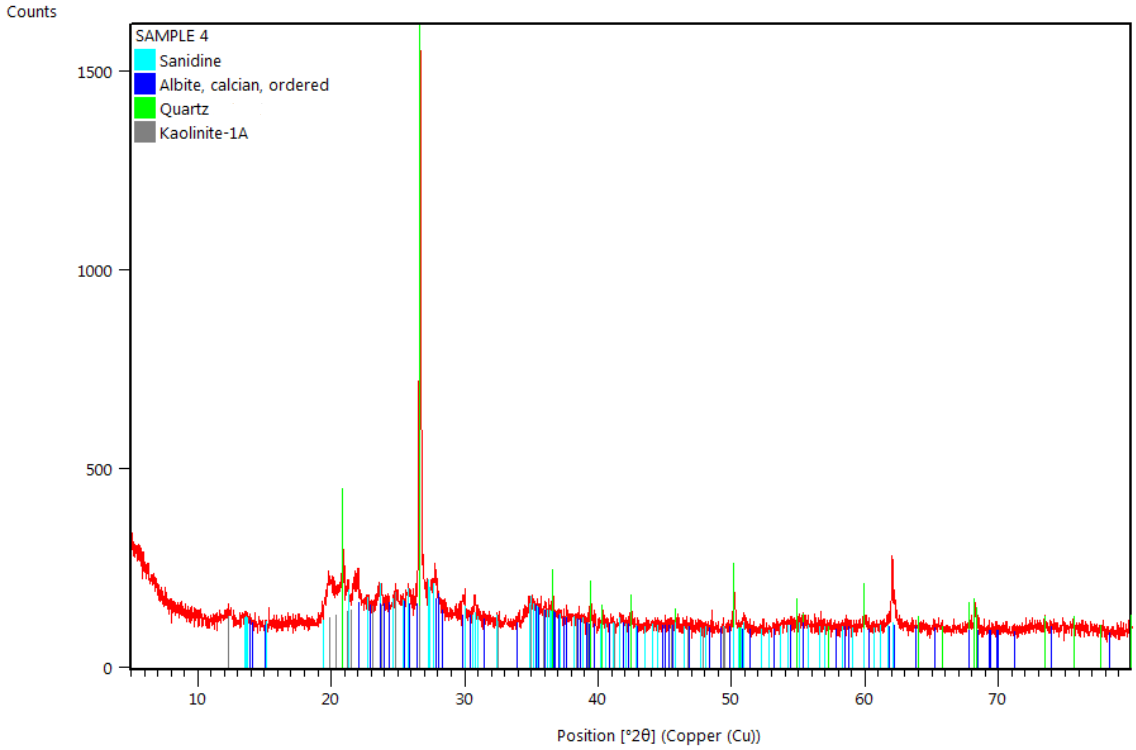

Figure 4.13 Sample four collected from the IBAS

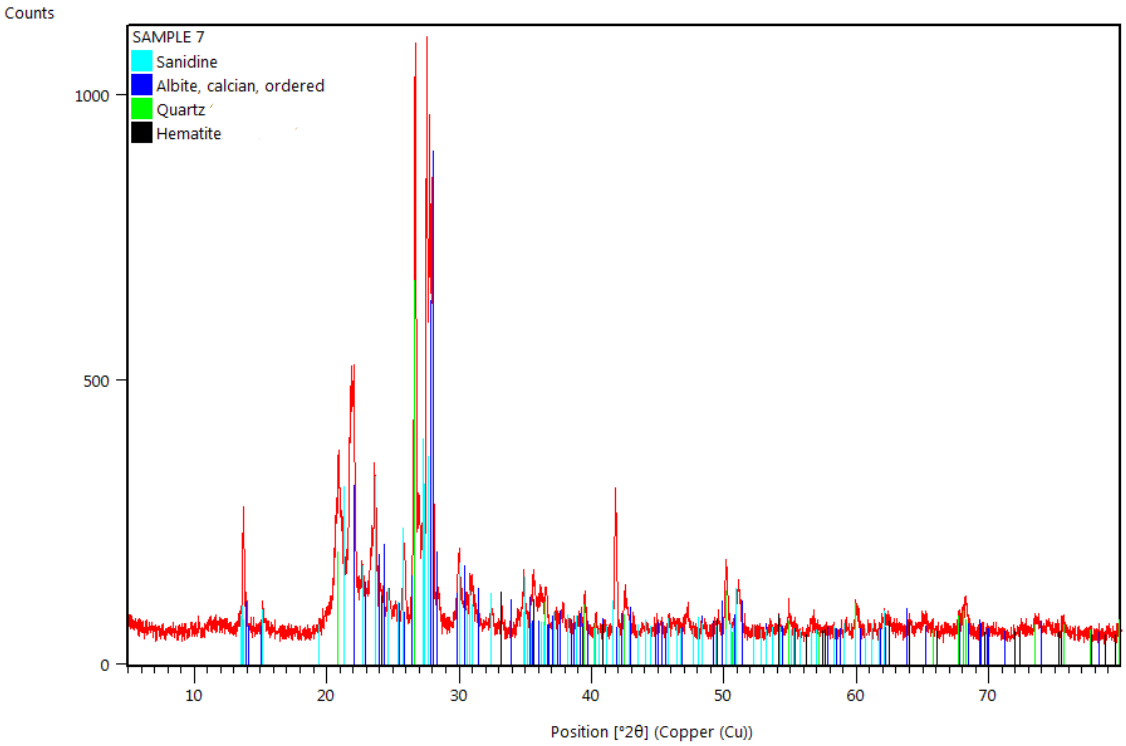

Figure 4.14 Sample seven collected from the IBAS

4.8 Petrographic Analysis Results on Thin Sections of the Drill Cuttings

Arrastres Drill Cuttings

Four thin sections were made from the Arrastres drill cuttings. The thin section from the 20 – 22 m depth displayed the presence of minerals consistent with an igneous rock of mafic to intermediate composition composed primarily of weathered olive, pyroxene, plagioclase, quartz, calcite, and apatite (Figure 4.15A and Table 4.15). The 160 – 162 m depth recovered a more felsic lava composed of plagioclase, potassium feldspar, quartz, volcanic glass, clay minerals, and zircon (Figure 4.15B and Table 4.15). The 340 – 342 m depth displayed a similar composition to the 20 – 22 m depth interval with minerals of pyroxene, amphibole, plagioclase, potassium feldspar, quartz, biotite, and clay minerals (Figure 4.15C and Table 4.15). The 440 – 442 m depth recovered a more felsic rock composition lava consisting of plagioclase, potassium feldspar, quartz, and pyroxene (Figure 4.15D and Table 4.15). The pyroxene identified in the lower most thin section of the Arrastres drill cuttings could be due to cavity collapse while drilling. Iron oxide minerals were observed in the ~440 m depth (Figure 4.15E and Table 4.15).

Table 4.15 Minerals observed in the thin sections of the Arrastres drill cuttings.

Minerals	20 – 22 m	160 – 162 m	340 – 342 m	440 – 442
Quartz	X	X	X	X
Calcite	X		X	X
Plagioclase	X	X	X	X
K-feldspar		X		X
Biotite			X	
Volcanic Glass		X		
Apatite	X		X	X
Clay Minerals	X	X	X	
Zircon		X		
Olivine	X			
Pyroxene	X		X	X
Amphibole			X	
Hematite				X

Lourdes Drill Cuttings

Five thin sections were made from the Lourdes drill cuttings. The thin sections from the Lourdes drill cuttings were examined with respect to depth and the following minerology was recorded. The 18 – 20 m depth was of sedimentary origin with rock fragments composed of plagioclase, quartz, calcite, biotite, volcanic glass, and trace amounts of apatite (Figure 4.16A and Table 4.16). The 140 – 142 m depth had a similar sedimentary origin with rock fragments composed of plagioclase, quartz, calcite, biotite, clay minerals, volcanic glass, zircon, and apatite (Figure 4.16B and Table 4.16). The 220 – 222 m depth was similar to the previously mentioned sedimentary deposits, but clasts of clay were more dominant (Figure 4.16C and Table 4.16). Aside from the clay clasts the rock fragments were composed of plagioclase, quartz, calcite, biotite, volcanic glass, clay minerals, and minor amounts of apatite. The 360 – 362 m depth was composed of mafic rock fragments containing weathered olivine, pyroxene, plagioclase, potassium feldspar, quartz, calcite, volcanic glass, and trace amounts of apatite (Figure 4.16D and Table 4.16). The 540 – 542 m depth interval of the Lourdes drill cuttings was composed of similar rock fragments as the 360 – 362 m depths (Figure 4.16E and Table 4.16). The rock fragments were composed of pyroxene, amphibole, plagioclase, potassium feldspar, quartz, calcite, and minor amounts of apatite (Figure 4.16F and Table 4.16). Iron oxides and hematite were identified under reflected light at 440 m depth in the Lourdes drill cuttings (4.15F)

Table 4.16 Minerals observed in the thin sections of the Lourdes drill cuttings.

Minerals	18 – 20 m	140 – 142 m	220 – 222 m	360 – 362 m	540 – 542 m
Quartz	X	X	X	X	X
Calcite	X	X	X	X	X
Plagioclase	X	X	X	X	X
K-feldspar	X			X	X
Biotite	X		X		X
Chlorite					X
Volcanic Glass	X	X	X	X	
Apatite	X	X	X	X	X
Clay Minerals	X	X	X	X	X
Zircon		X	X		
Olivine				X	X
Pyroxene				X	X
Amphibole					X
Hematite					X
Ilmenite					X

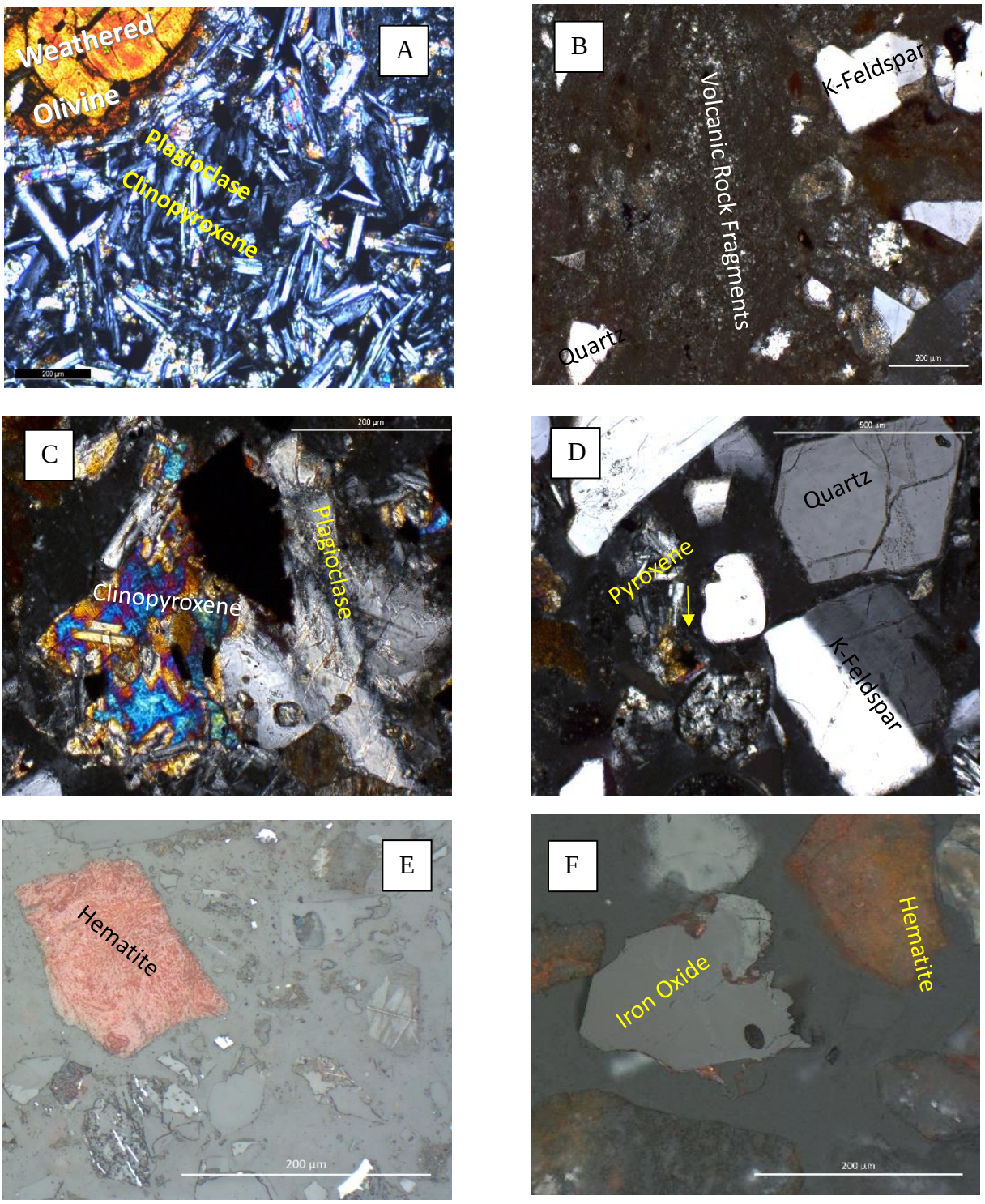

Figure 4.15 Images of the mineralogy observed in the ~20 m (A) ~160 m (B) ~340 m depth (C) and ~440 m depth (D) of the Arrastres drill cuttings Images shown in transmitted light with crossed polars. Images of the minerology observed in the ~540 m depth (E) of the Lourdes drill cuttings and the ~440 m depth (F) of the Arrastres drill cuttings shown in reflected light.

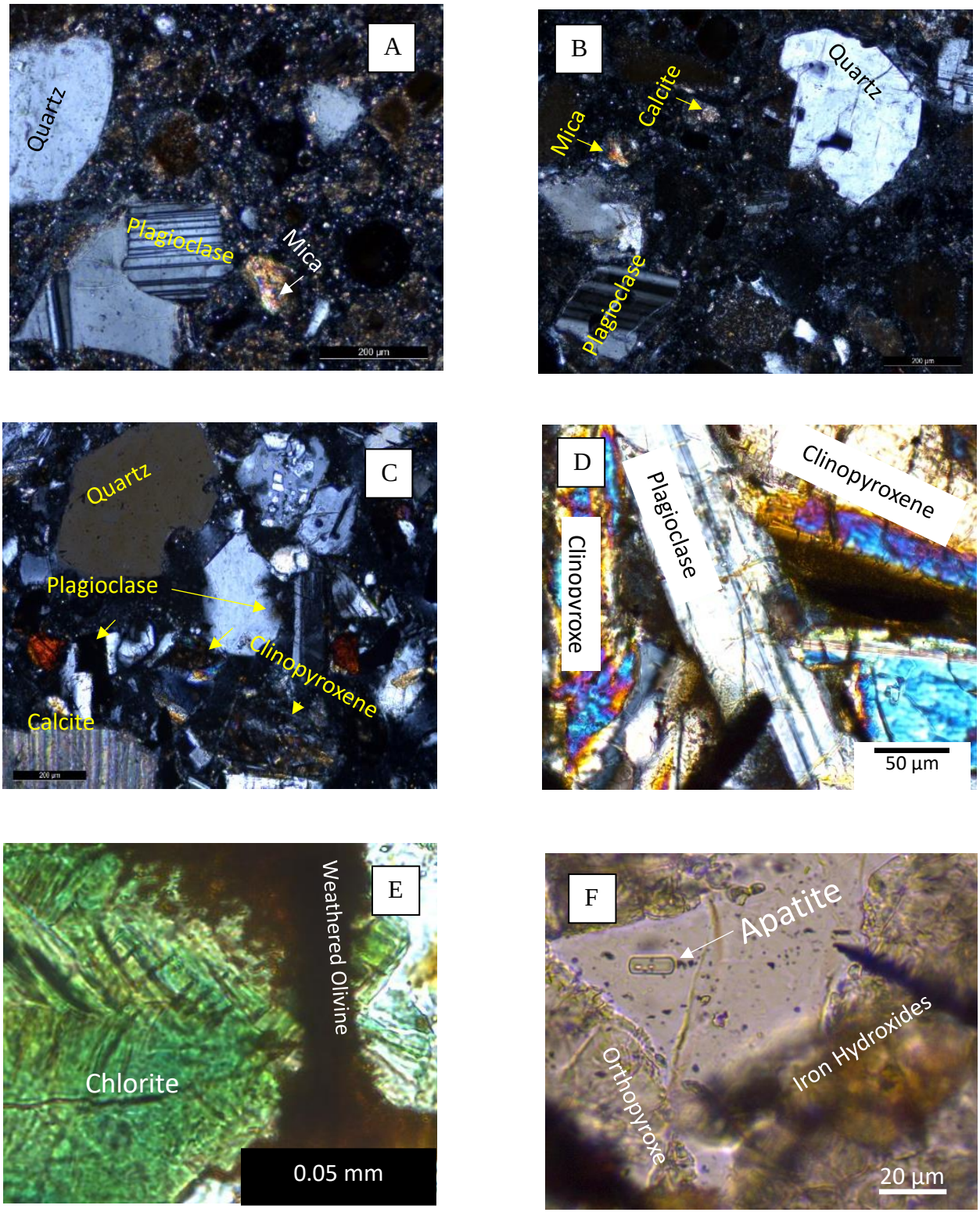

Figure 4.16 Images of the mineralogy of the Lourdes drill cuttings from images of the mineralogy observed in the ~140 m (A), ~220 m (B) ~360 m (C) depth with crossed polars, and ~540 m (D) ~540 m depth (E and F). Images shown in transmitted light.

4.9 X-ray fluorescence Results of Drill Cuttings

Arrastres Drill Cuttings:

The total elemental concentrations recovery from the XRF analysis with the Arrastres drill cuttings was on average 68% after converting the values to percent oxides. The total elemental concentrations recovery from the shale standard used was on average 92% after converting the values to percent oxides. This is the result of the instruments inability to detect Na, difficulty in determining Mg, as well as, air space between the grains attenuating the x-rays. A summary of the results can be found in Table 4.17 and Figure 4.17 and the full data set can be found in Appendix A.86 – A.88. The Arrastres drill cuttings display four distinct changes in major elemental composition as observed from 0 – 500 m (Figure 4.17). These four distinct changes occur at 0 – 40 m, 40 – 220 m, 220 – 400 m, and 400 – 500 m depth. These four sections display As concentrations which range from 2 – 5 mg/kg, 2 – 15 mg/kg, 0 – 21 mg/kg, and 8 – 27 mg/kg, respectively (Table 4.17). Potassium, Rb, and Si have similar concentration profiles with depth, comparable to As throughout the entire length of the Arrastres drill cuttings. The Ca, Fe, Mg, Sr, and Mn concentrations profile patterns are all inversely related to As for the entire length of the Arrastres drill cuttings.

Table 4.17 Range of elemental concentrations for the Arrastres Drill cuttings from 0 – 500 m. All values are reported as parts per million (mg/kg).

Element (mg/kg)	0 – 40 m	40 – 220 m	220 – 400 m	400 – 500 m
As	2 – 5	2 – 15	0 – 21	8 – 27
K	9,436 – 10,931	12,126 – 32,368	10,101 – 23,463	16,689 – 34,849
Rb	48 – 66	76 – 238	155 – 178	118 – 204
Si	179,344 – 184,334	195,070 – 284,629	164, 594 – 257,958	197,927 – 281,975
Ca	34,399 – 42,774	5,977 – 38,992	19,513 – 45,119	11,492 – 32,071
Mg	8,374 – 12,105	145 – 9,328	2,829 – 14,076	882 – 4,331
Sr	339 – 348	27 – 347	131 – 395	61 – 261
Fe	41,589 – 46,227	10,991 – 31,649	17,102 – 43,489	13,501 – 35,897
Mn	682 – 911	292 – 670	448 – 911	284 – 530

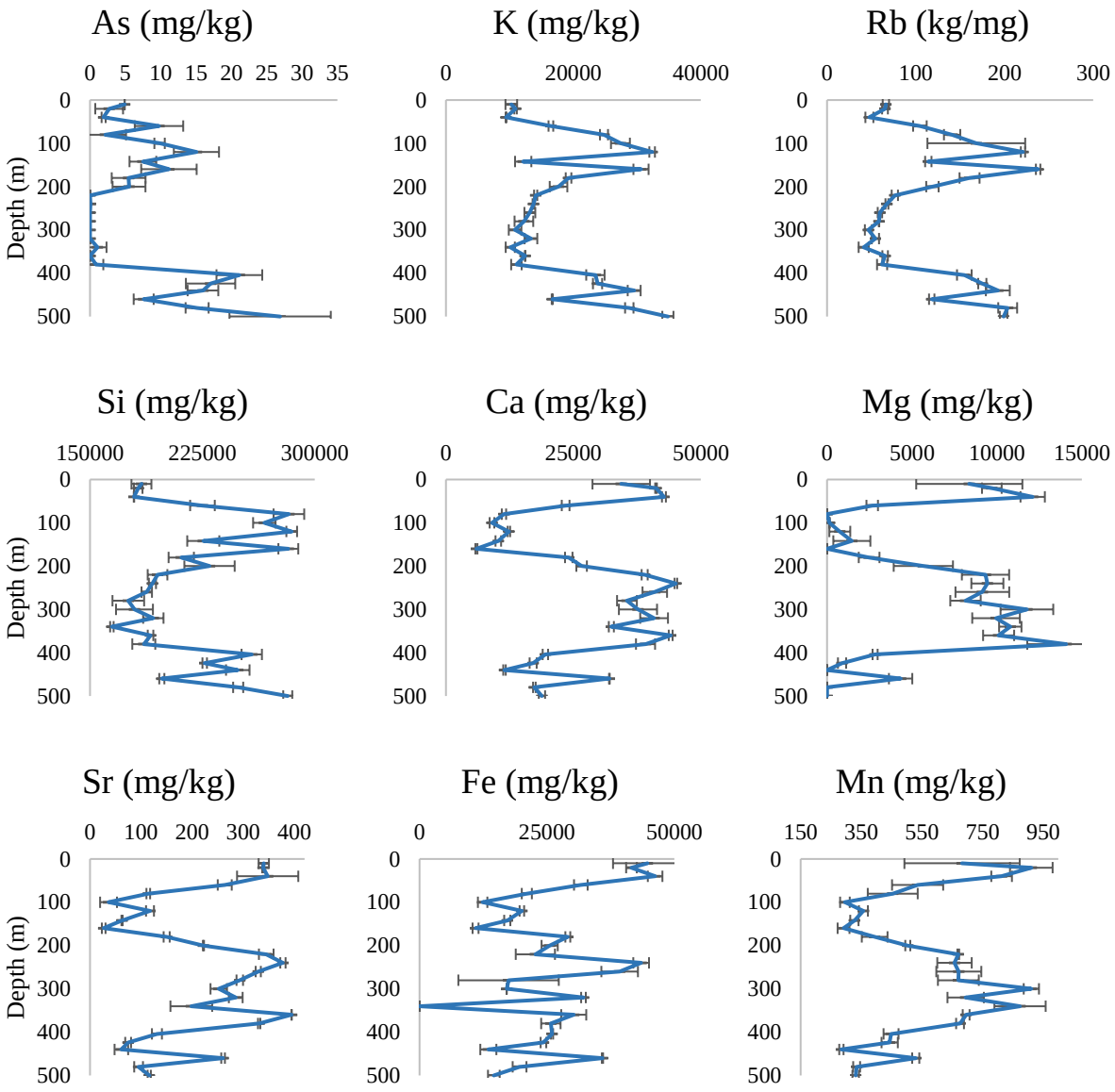

Figure 4.17 The major and trace element concentration profiles with depth for the Arrastres drill cuttings with the blue line expressing the average value and horizontal lines expressing the standard deviation calculated in Excel between the three measurements taken at each depth.

Lourdes Drill Cuttings:

The recovery from the XRF analysis with the Lourdes drill cuttings was on average 62% after converting to weight percent oxide and the recovery from the standard used was on average 89% after converting to weight percent oxide. A summary of the results can be found in Table 4.18 and Figure 4.18; the full data set can be found in Appendix A.89 – A.93. The Lourdes drill cuttings display two distinct changes in elemental composition as observed from 0 – 550 meters depth (Figure 4.20). These two distinct changes in lithology will be used to describe the changes in elemental concentration from 0 to 300 m and 300 m to 550 m. Arsenic concentrations range from 0 – 8 mg/kg in the upper 0 to 300 m and 0.5 and 4.5 mg/kg in the lower 300 to 550 m depths (Table 4.18). Potassium, Rubidium (Rb), and Silica (Si) have similar elemental concertation profiles with depth, comparable to As throughout the entire length of the Lourdes drill cuttings. The Ca elemental concentrations in the Lourdes drill cuttings displayed an inverse concertation profile to the K, Rb, and Si concentration. An increase in Ca concentrations is observed between 60 to 160 m. Fe, Mg, Sr, and Mn concentration profiles with depth are all inversely related to As for the entire length of the Lourdes drill cuttings.

Table 4.18 Range of elemental concentrations for the Lourdes Drill cuttings from 0 – 550 m. All values are reported as parts per million (mg/kg).

Element (mg/kg)	0 – 300 m	300 – 550 m
As	0 – 8	0.5 – 4.5
K	14,370 – 24,774	4,154 – 13,622
Rb	87 – 170	33 – 105
Si	183,962 – 227,452	143,885 – 179,727
Ca	13,419 – 65,293	24,876 – 45,737
Mg	1,155 – 5,084	544 – 10,735
Sr	176 – 414	305 – 455
Fe	14,643 – 37,097	17,509 – 35,567
Mn	303 – 506	429 – 724

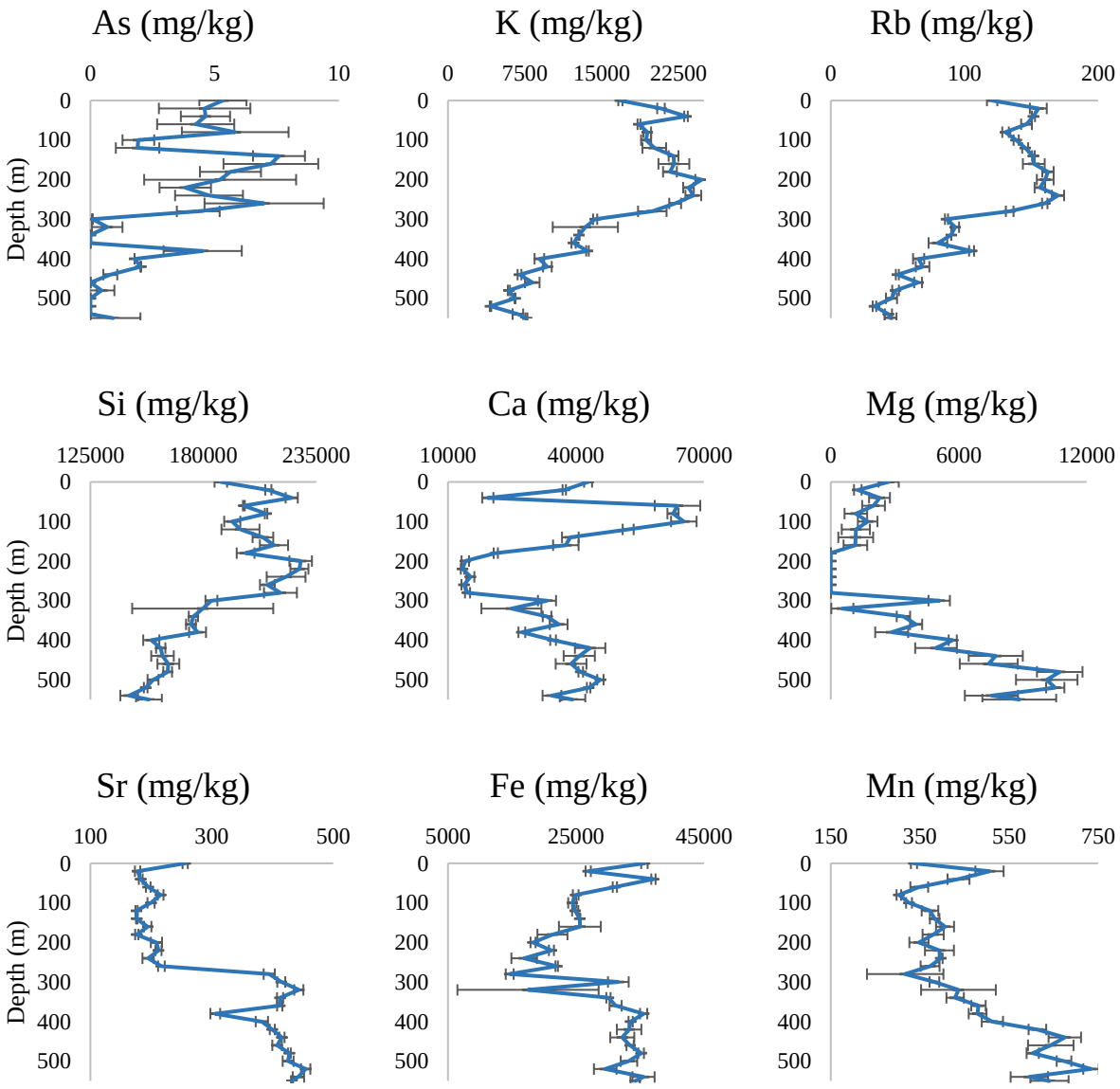

Figure 4.18 The major and trace element concentration profiles with depth for the Lourdes drill cuttings with the blue line expressing the average value and horizontal lines expressing the standard deviation calculated in Excel between the three measurements taken at each depth.

4.10 Depth Dependent Distribution of Leachable Fluoride in the Basin

Overview

All sections of the Arrastres and Lourdes cores released F to some extent (Figures 4.19A, 4.19B, 4.20A, and 4.20B). The complete dataset can be found in Appendix A.5 through A.24. The objective of this experiment is to determine which sections of the borehole drill cuttings are releasing F. Additionally, this would be an inexpensive method for determining leachable F from rocks by use of the FISE and comparing the results with measurements by IC. These leaching experiments used DI water for one set of reactors as a control. A second set of reactors used groundwater from IBAS wells which were positioned near the location of the borehole drill cuttings. A complete summary of results from this experiment can be found in the appendix. The initial water chemistry can be found in Table 4.19.

Table 4.19 Water Chemistry of the groundwater used in the leaching experiments.

Well ID	Na^+	K^+	Mg^{2+}	Ca^{2+}	Sr^{2+}	F^-	Cl^-	NO_2^-	Br^-	NO_3^-	PO_4^{3-}	SO_4^{2-}
CDW	33.74	3.43	0.66	16.02	0.33	1.18	4.76	0.28	bdl	2.11	0.37	7.87
LS-0178	132.13	2.39	bdl	5.037	0.22	15.24	24.04	bdl	0.30	3.35	0.64	44.12

Fluoride Leaching from Arrastres Drill Cutting in DI Waters:

As the Arrastres drill cuttings reacted with de-ionized water (DI) for 200 hours and generated a leached F profile (Figure 4.19A). The 0 – 40 m section leached F ranging from 1.19 – 1.28 mg/L as measured by the FISE with an average value of 1.23 mg/L. The 40 – 220 m sections leached F ranging from 0.24 – 1.09 mg/L with an average of 0.79 mg/L. The 220 – 400 m sections leached F ranging from 0.18 – 0.61 mg/L with an average of 0.39 mg/L. The 400 – 500 m sections leached F ranging from 0.33 – 0.68 mg/L with an average of 0.56 mg/L. The IC measurements display a similar leached F concentration profile, with highest values measured in the 20 – 40 m and 140 – 160 m sections (1.77 mg/L and 1.22 mg/L) with decreasing values in the central region of the drill cuttings 240 – 260 m and 360 – 380 m (0.26 mg/L and 0.53 mg/L). The 440 – 460 m sections had a higher value than the central region of the drill cuttings reaching 0.78 mg/L of F.

Fluoride Leaching from Lourdes Drill Cuttings in DI Water:

As the Lourdes drill cuttings reacted with DI water, measurements were taken with the FISE; the 0 – 300 m sections showed a decreasing trend from 0 – 20 m (2.25 mg/L) toward the 280 – 300 m (0.91 mg/L) sections (Figure 4.19B). The 300 – 550 m depths of the Lourdes drill

cuttings then showed an increasing trend from 300 – 320 m (1.34 mg/L) toward 520 – 550 m (1.5 mg/L). Between 300 – 550 meters depth higher F values were observed at 400 – 440 m and 460 – 520 m depth (2.15 – 1.86 mg/L and 2.15 – 1.99 mg/L). The IC results showed a similar trend for selected sections with relatively high values of leached F at 20 – 40 m (1.67 mg/L). A similar decreasing trend was observed in the IC results between 100 – 340 m (1.51 mg/L, 1.37 mg/L, and 1.48 mg/L). The highest F concentrations were observed in the 400 – 420 m sections (2.72 mg/L) followed by a decreased in F concertation in the 520 – 550 m (1.87 mg/L).

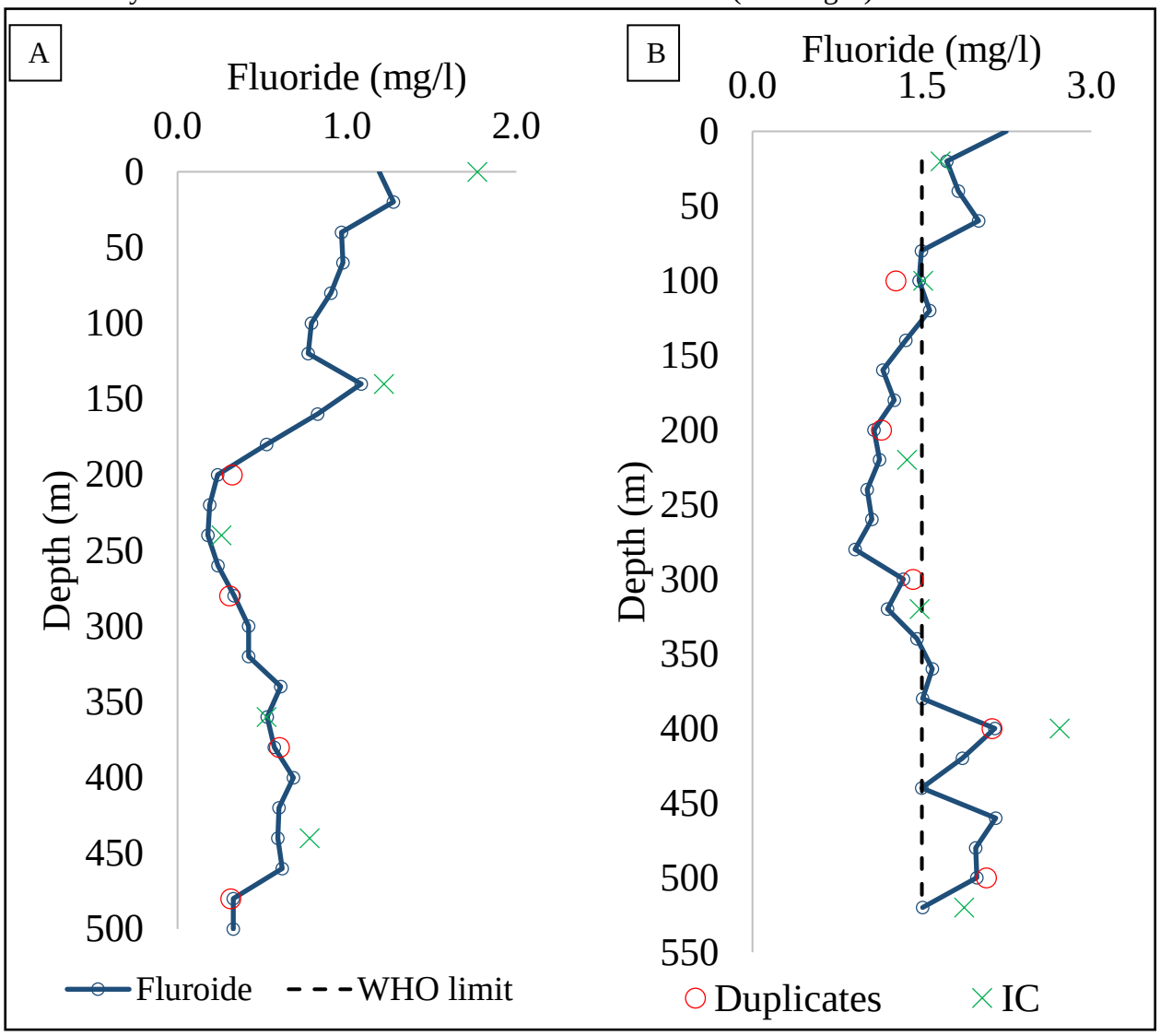

Figure 4.19 Leachable F concentrations from the Arrastres drill cuttings (A) and Lourdes drill cuttings (B). Reactors used DI water, were run alongside a set of duplicates (red circles) with measurements by IC (green X) Dashed lines represent the WHO safe drinking water limit of 1.5 mg/L for F.

Fluoride Leaching from the Arrastres Drill Cuttings in Groundwater:

The Arrastres drill cuttings was reacted with groundwater (GW) from a rural well (Well ID: CDW) from the western side of the basin (Figure 4.20A). The groundwater from this well was chosen for this experiment because it was the closest well positioned near the location of the Arrastres drill cuttings. The groundwater had an initial F concentration of 0.95 mg/L. After the rocks reacted with groundwater for 200 hours, measurements were taken with the FISE. The 0 – 40 m sections leached F ranging from 1.45 – 1.95 mg/L with an average value of 1.7 mg/L. The 40 – 220 m sections leached F ranging from 1.08 – 1.81 mg/L with an average of 1.46 mg/L. The 220 – 400 m sections leached F ranging from 0.98 – 1.36 with an average of 1.15 mg/L. The 400 – 500 m sections leached F ranging from 1.12 – 1.40 mg/L with an average of 1.28 mg/L. The IC measurements from the selected borehole sections showed a similar leached F concentration with the highest values measured in the 20 – 40 m and 140 – 160 m sections (2.04 mg/L and 1.83 mg/L) with decreasing values in the central region of the drill cuttings 240 – 260 m and 360 – 380 m (1.24 mg/L and 1.3 mg/L). The 440 – 460 m sections had a higher value than the central region of the drill cuttings reaching 1.77 mg/L of F.

Fluoride Leaching from the Lourdes Drill Cuttings in Groundwater:

The Lourdes drill cuttings reacted with groundwater from a production well (Well ID: LS-0187) from the eastern side of the basin with the highest F concentrations (Figure 4.21B). After the rocks reacted with groundwater for 200 hours, measurements were taken with the FISE. The 0 – 300 m sections showed F values that were less than the initial concentration of the groundwater used in the experiment. The F concentrations decreased from the 0 – 20 m (12.75 mg/L) to the 280 – 300 m (16 mg/L) sections. The greatest decrease in F concentrations occurred in the 40 – 60 m sections with a final concentration of 9.46 mg/L. The 300 – 550 m depths of the Lourdes drill cuttings then showed variable increases and decreases in F values from 300 – 550 m. The 300 – 320 m sections showed the highest increase in F concentrations (17.36 mg/L). At depths below these sections the lowest values of F were measured in the 360 – 380 m sections (15.52 mg/L). At the 520 – 550 m sections the F concertation was 16 mg/L. The IC results showed a similar trend for selected sections with lower than initial values of F at 0 – 20 m, 100 – 120 m, and 220 – 240 m (12.07 mg/L, 13.03 mg/L, and 15.25 mg/L). The 320 – 340 m, 400 – 420 m, and 520 – 550 m sections showed higher than initial F concentrations (17.47 mg/L, 17.25 mg/L, 16.55 mg/L). Based

on fluorite saturation index calculations completed with Geochemist Workbench Softaware with the PHREEQC thermo database. The results from the IC tested sections (20, 100, 220, 320, 400, and 520) indicate fluorite is supersaturated with repsect to the system (Appendix A.20)

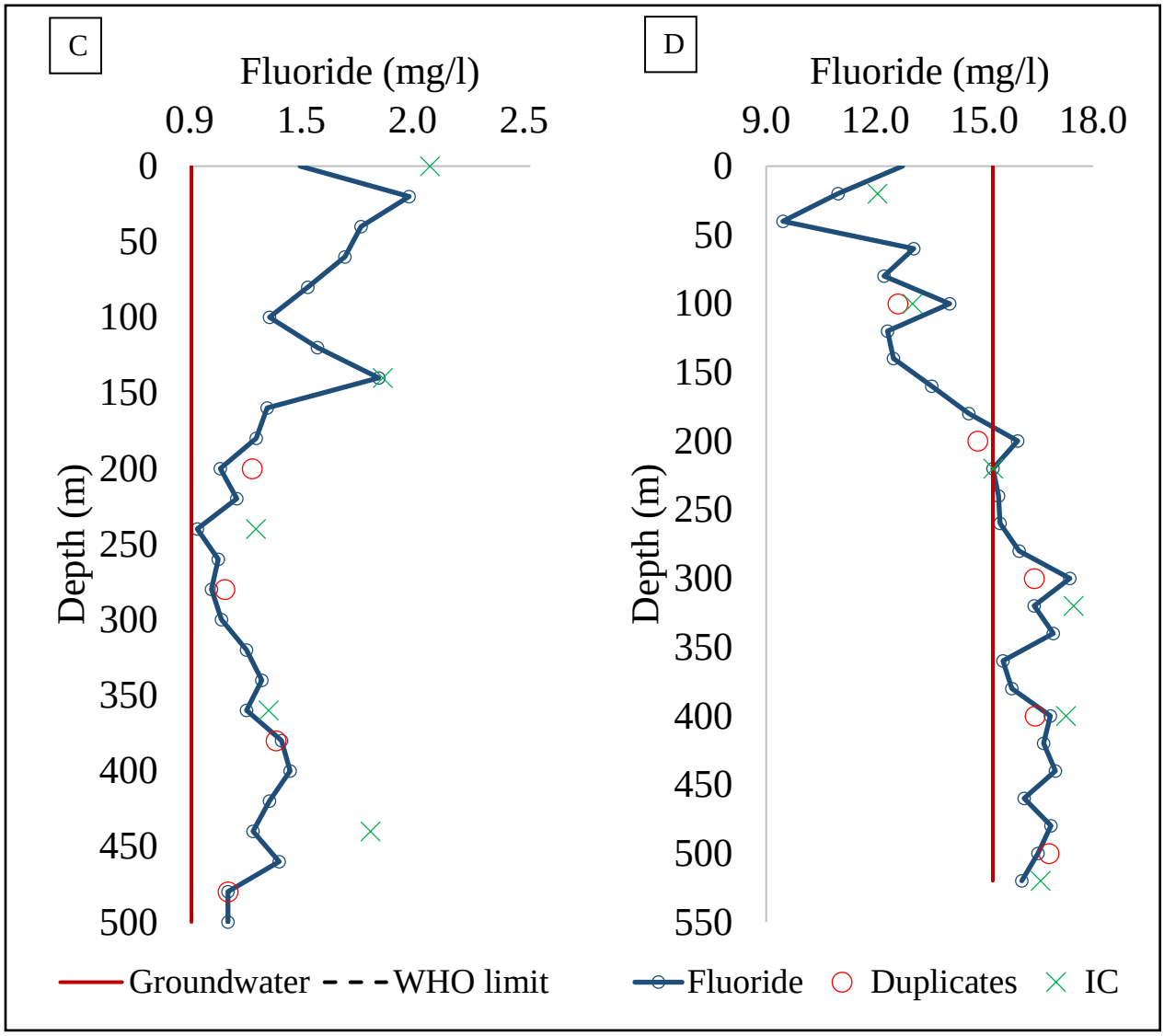

Figure 4.20 Leachable F concentration measurements for the Arrastres and Lourdes drill cuttings. Reactors used groundwater from the rural wells CDW (C) and LS-0178 (D). Red line indicates the initial F concentration of the groundwater. These reactors were run with duplicates (red circles) and IC (green X) the dashed line represents the WHO Safe Drinking Water Limit 1.5 mg/L for F.

4.11 Time and pH dependent Water-Rock Interactions

Overview

Drill cuttings from the Arrastres and Lourdes boreholes reacted with groundwater from the IBAS (Well ID: RL-2-A, Table 4.20) in laboratory scale batch reactors with adjusted pH values of ~5, ~7, and ~9. Concentration changes in the major and trace elements in the reactor are observed among the three pH values. The complete dataset can be found in Appendix A.25 and A.30. This goal of this experiment is to identify the reactions that are geochemically connected to the groundwater and rock interactions occurring in the IBAS.

Table 4.20 Water chemistry of the basin

Well ID	Na	K	Mg	Ca	Sr	F	Cl	NO_2	Br	NO_3	PO_4	SO_4
Units	mg/L	mg/L	mg/L	mg/L	mg/L	mg/L	mg/L	mg/L	mg/L	mg/L	mg/L	mg/L
RL-2-A	66.88	19.73	5.46	0.63	1.12	0.83	12.96	Bdl	0.20	10.54	Bdl	38.45

	As	B	Li	Fe
	µg/L	µg/L	µg/L	µg/L
	7.370	2891.047	98.597	9.273

Arrastres Drill Cuttings and Groundwater Interaction Experiment

The changes in average dissolved F concentrations over time vary in overall trends for each of the three pH values use in these reactors. In the reactors with groundwater at a pH of ~5, the average dissolved F concentrations are less than the initial average dissolved F concentration of the groundwater (Well ID: RL-2-A = 0.83 mg/L; 0.043 mmol/L). The average dissolved F concentrations decreased from 0.83 mg/L (0.043 mmol/L) to 0.59 mg/L (0.031 mmol/L) during the initial 50 hours followed by a decreasing trend in average dissolved F concentrations until 200 hours of reaction (Figure 4.21). In contrast, the pH ~7 reactors have fluctuating average dissolved F concentrations which vary between 0.71 mg/L (0.037 mmol/L) and 0.79 mg/L (0.042 mmol/L), which is slightly less than the initial average dissolved F concentration of 0.83 mg/L (0.043 mmol/L) (Figure 4.21). The reactors with an adjusted pH of ~9, a minor increase in average dissolved F concentrations occurs reaching 0.91 mg/L (0.048 mmol/L) after 50 hours of reaction. This increase in average dissolved F concentrations is followed by steady-state conditions with average dissolved F values fluctuating between 0.90 mg/L (0.046 mmol/L) and 0.93 mg/L (0.049 mmol/L) (Figure 4.23).

The average As concentration changes in the pH ~5, ~7 and, ~9 reactors all show continuously decreasing trends during the experiment. In the pH ~6 reactors a 1.84 µg/L (0.015 µmol/L) reduction in average As concentrations occurs during the initial 50 hours of reaction. This initial decrease in average As concentrations is followed by fluctuating values of 6.17 µg/L (0.082 µmol/L) and 5.76 µg/L (0.077 µmol/L) until 200 hours of reaction. In the pH ~7 and pH ~8 reactors the average As concentrations decrease at a similar rate and display a crossing pattern after 100 hours of reaction. The average As values in the pH ~7 reactors became slightly greater than the average concentrations observed in the pH ~9 reactors. After 200 hours of reaction, the pH ~6, ~7, and ~8 reactors have values of 5.76 µg/L (0.077 µmol/L), 6.58 µg/L (0.088 µmol/L), and 6.32 µg/L (0.084 µmol/L), respectively (Figure 4.23).

The average dissolved Ca concentrations in the pH ~5 reactors show a continuous increase in average dissolved Ca concentrations from the initial 25.44 mg/L (1.10 mmol/L) to 52.00 mg/L (2.26 mmol/L) (Figure 4.25). In the pH ~7 reactors the average dissolved Ca concentrations decrease from 25.44 mg/L (1.11 mmol/L) to 21.20 mg/L (0.92 mmol/L) after 50 hours of reaction (Figure 4.25). This initial decrease in the average dissolved Ca concentrations is followed by continuous increase in average dissolved Ca concentrations reaching 29.50 mg/L (1.28 mmol/L) at 200 hours. The average dissolved Ca concentrations in the pH ~9 reactors change from 25.44 mg/L (1.11 mmol/L) to 15.97 mg/L (0.70 mmol/L). This was followed by a slight increase in average dissolved Ca concentrations from 15.97 mg/L (0.70 mmol/L) to 20.33 mg/L (0.88 mmol/L) at 200 hours.

The average dissolved Na concentration increase from 66.88 mg/L (2.90 mmol/L) to ~101.00 mg/L (~4.40 mmol/L) in pH ~5 and ~7 reactors. The initial increase in average dissolve Na concentration was followed steady state conditions until 200 hours of reaction (Figure 4.27).

B, and Li concentrations in the pH ~5, ~7, and ~9 reactors all increased over time (Figures 4.29 and 4.31). The average dissolved boron concentrations in the pH ~5, ~7, and ~9 reactors increased from ~267.42 µmol/L to ~340 µmol/L after 200 hours of reaction. The average dissolved lithium concentrations in the pH ~5, ~7 and ~9 reactors displayed significant increases during the initial 50 hours of reaction followed by gradual increases in at all three pH values (Figure 4.28). The average dissolved Fe concentrations for all three pH values displayed steady-state conditions (Figure 4.33).

Lourdes Drill Cuttings and Groundwater Interaction Experiment

Drill cuttings from the eastern side of the basin generate increases in F concentrations are over time at pH ~5, ~7, and ~9 with peak values at 50 hours of 1.04 mg/L (0.055 mmol/L), 1.35 mg/L (0.071 mmol/L), and 1.50 mg/L (0.079 mmol/L; respectively. These peak values are followed by a continuous decrease in average dissolved F concentrations over time (Figure 4.22).

The average dissolved total arsenic concentrations in all reactors display a generally decrease over time (Figure 4.24). In the pH ~7 and ~9 reactors slight increase occurs until 50 hours of reaction to peak values of 8.04 µg/L (0.11 µmol/L) and 8.48 µg/L (0.11 µmol/L). This initial increase in total arsenic concentrations is followed a continuous decrease in concentration over time. The pH ~5 reactors displayed the most significant reduction in average dissolved total arsenic concentrations reaching minimum values 5.67 µg/L (0.08 µmol/L) after 200 hours of reaction (Figure 4.24).

The average dissolved Ca concentrations display different trends over time at the different pH values (Figure 4.26). In the pH ~5 reactors, the average dissolved Ca concentrations show a continuous increase with a maximum value of 97.43 mg/L (4.24 mmol/L) after 200 hours of reaction. In the pH ~7 reactors the average dissolved Ca concentrations decrease during the initial 50 hours of reaction from 25.44 mg/L (1.11 mmol/L) to 23.60 mg/L (1.03 mmol/L). After the initial decrease in average dissolved Ca concentrations an increase occurs with a final value of 39.40 mg/L (1.71 mmol/L) after 200 hours. In the pH ~9 reactors the Ca concentrations decrease during the initial 50 hours of reaction followed by fluctuating values between 8.99 mg/L (0.39 mmol/L) and 11.97 mg/L (0.52 mmol/L).

The average dissolved sodium and boron concentrations increased over time at all pH values (Figure 4.28 and Figure 4.30). The average dissolved lithium concentrations increased in concentration over time in pH ~5 and pH ~7 reactors. In groundwater with a pH of ~9 the average dissolved lithium concentrations display fluctuating values between 96.72 µg/L (13.94 µmol/L) and 103.44 (14.90 µmol/L) (Figure 4.32). The average dissolved Fe concentrations in the pH ~5, ~7, and ~9 reactors display a fluctuation in values with an anomalously high value of average dissolved Fe at 100 hours of reaction in the pH ~5 reactors (Figure 4.34).

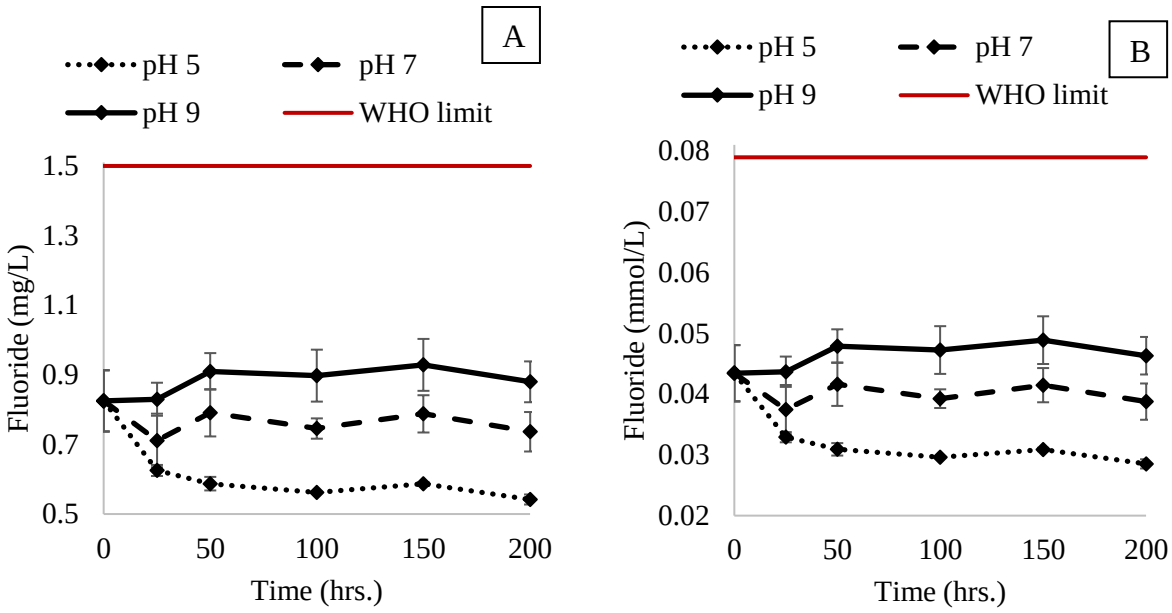

Figure 4.21 The F concentration changes from the Arrastres drill cuttings on the western side of the basin reacting with groundwater (A and B). The WHO safe drinking water limit for F 1.5 mg/L (A) and 0.79 mmol/L (B).

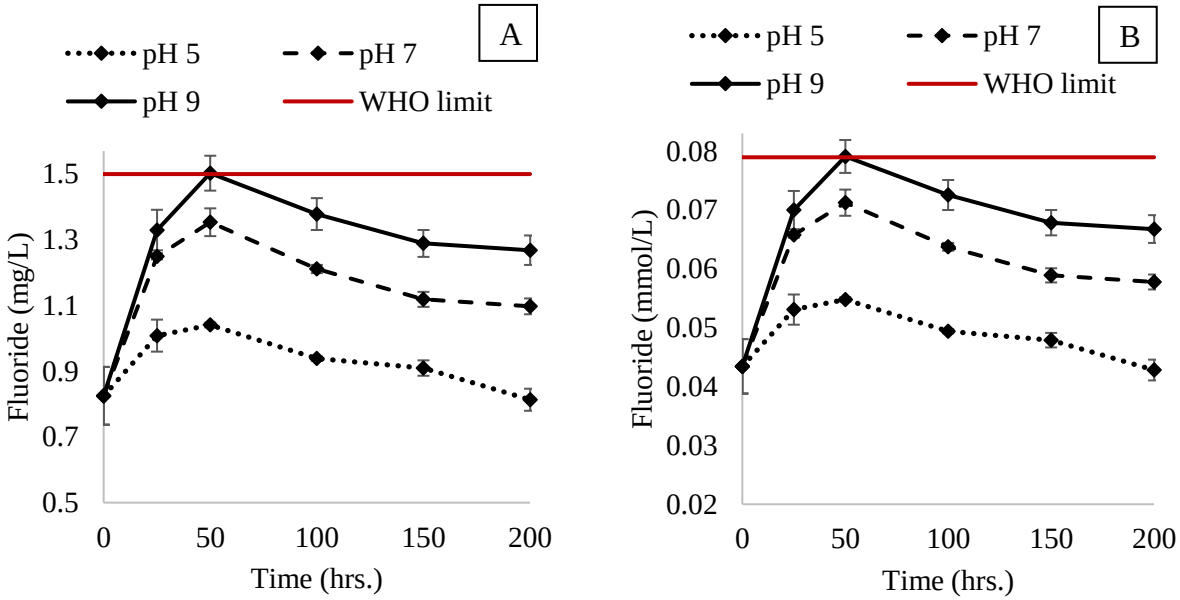

Figure 4.22 The F concentration changes from the Lourdes drill cuttings on the eastern side of the basin reacting with groundwater (C and D). The WHO safe drinking water limit for F 1.5 mg/L (A) and 0.79 mmol/L (A).

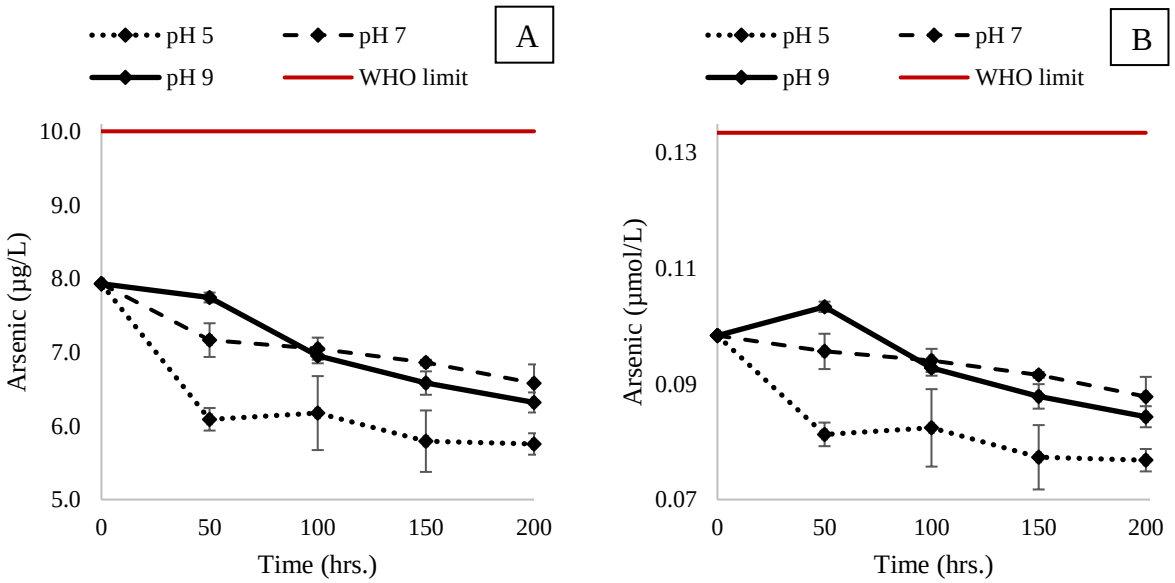

Figure 4.23 The As concentration changes from the Arrastres drill cuttings on the western side of the basin reacting with groundwater (E and F). The WHO safe drinking water limit for F 10 µg/L (A) and 0.13 µmol/L (B).

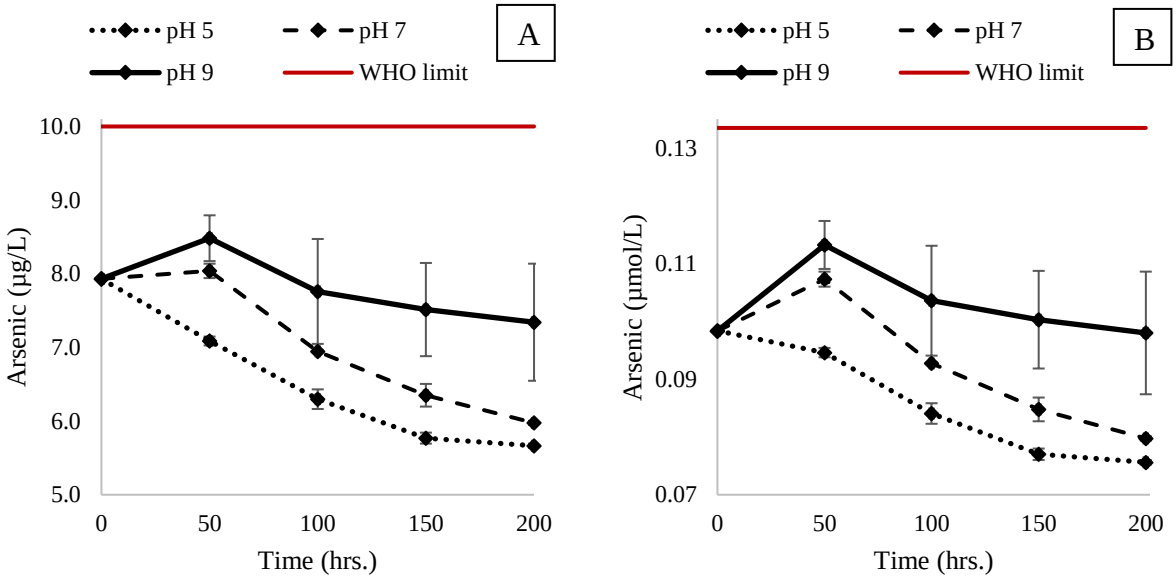

Figure 4.24 The As concentration changes from the Lourdes drill cuttings on the eastern side of the basin reacting with groundwater (E and F). The WHO safe drinking water limit for F 10 µg/L (A) and 0.13 µmol/L (B).

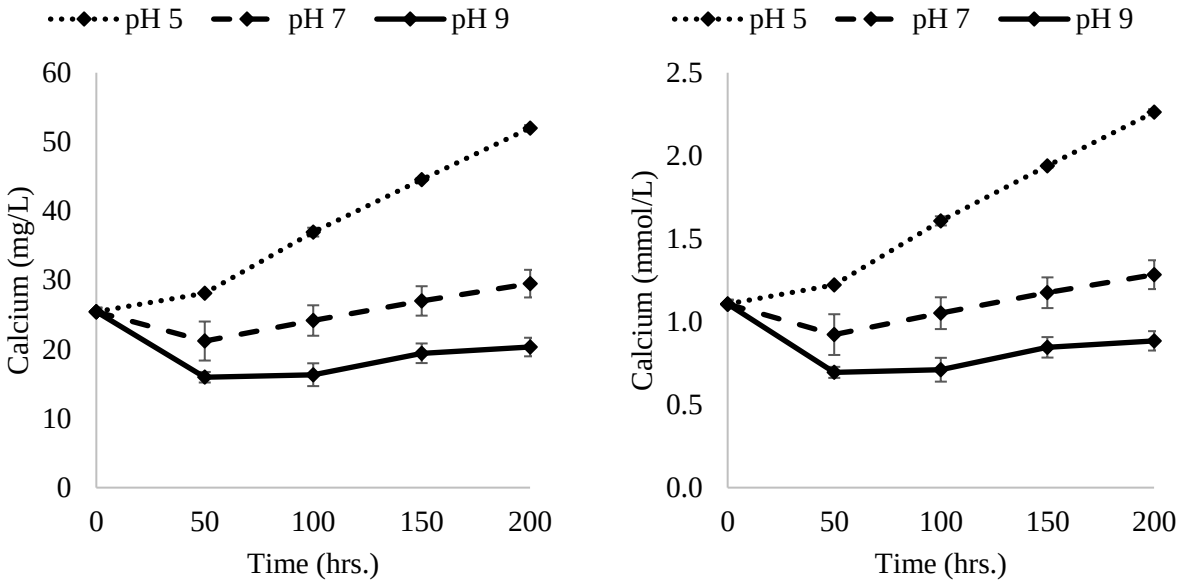

Figure 4.25 Dissolved Ca concentration changes from the Arrastres drill cuttings on the western side of the basin.

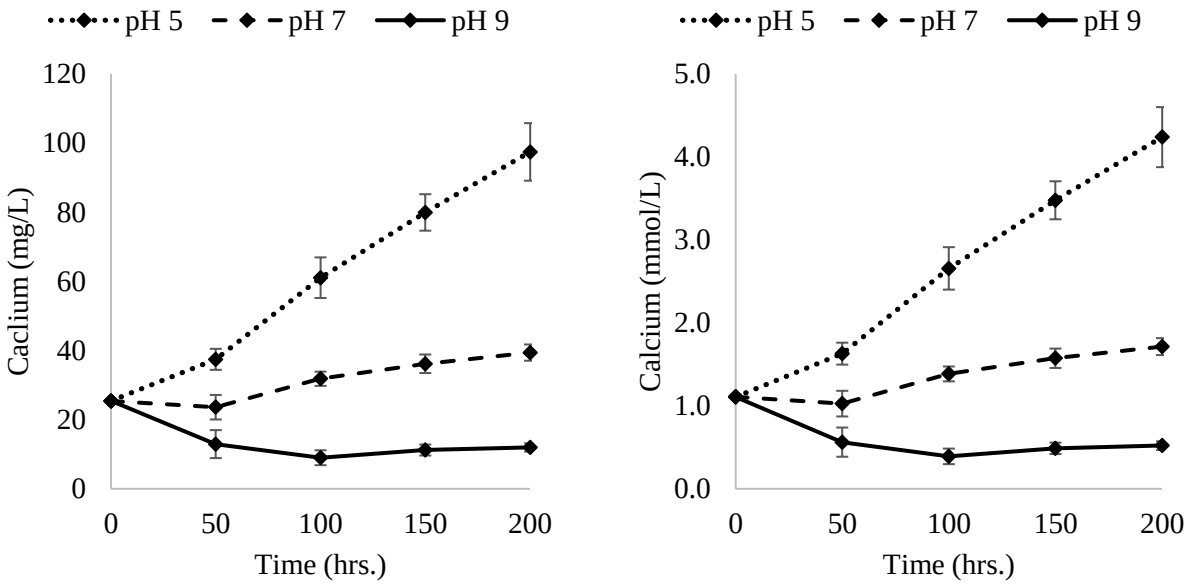

Figure 4.26 Dissolved Ca concentration changes from the Lourdes drill cuttings on the eastern side of the basin.

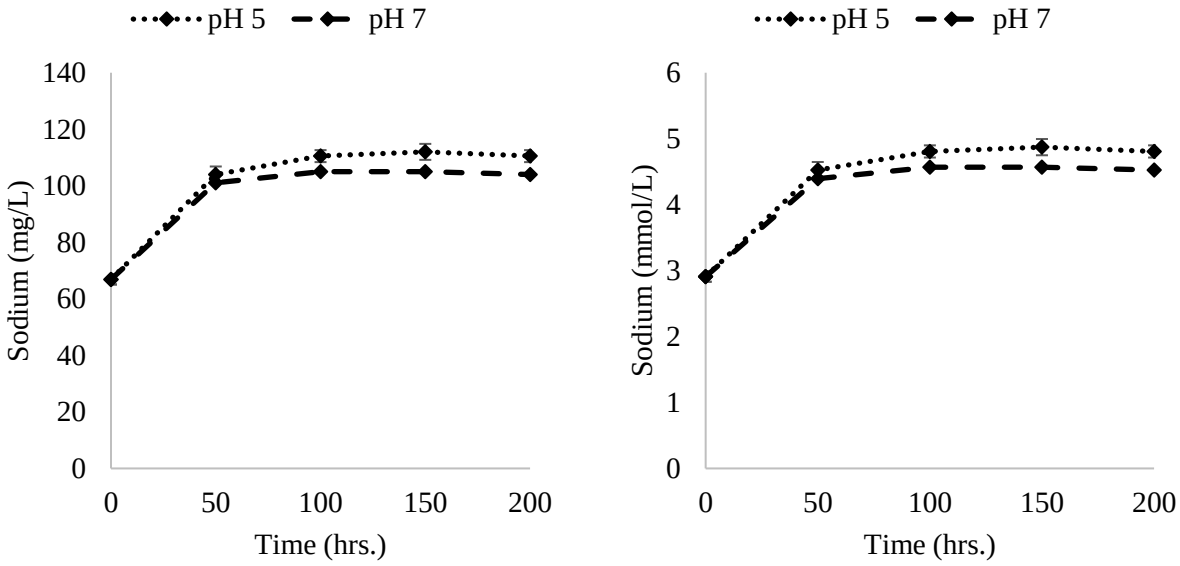

Figure 4.27 Dissolved Na concentration changes from the Arrastres drill cuttings (M) from the western side of the basin. Reactors impacted by the addition of NaOH were removed.

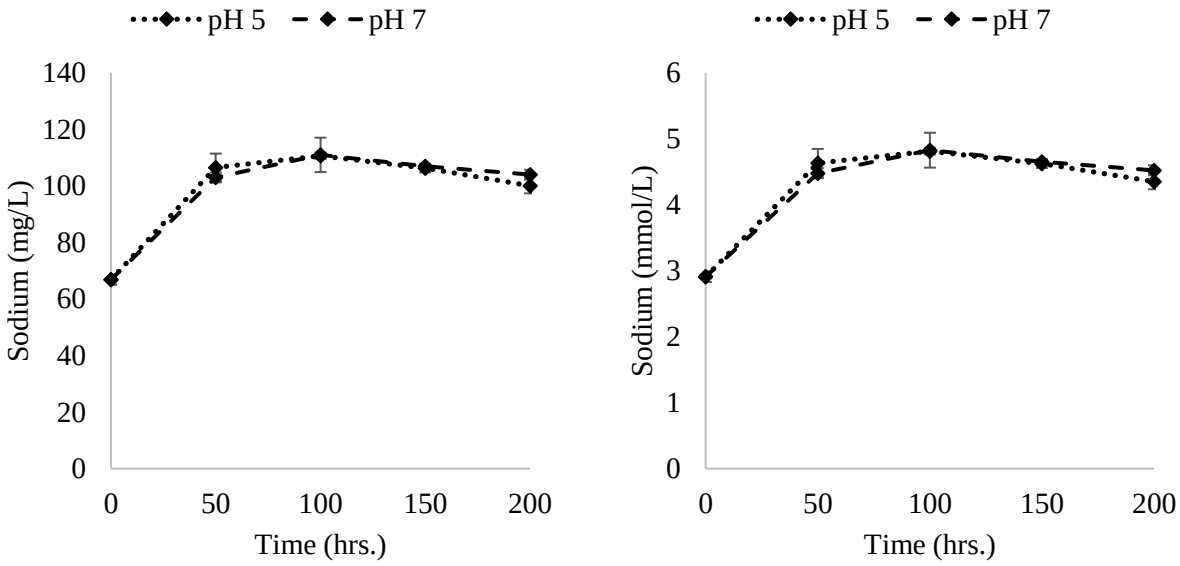

Figure 4.28 Dissolved Na concentration changes from the Lourdes drill cuttings from the eastern side of the basin. Reactors impacted by the addition of NaOH were removed.

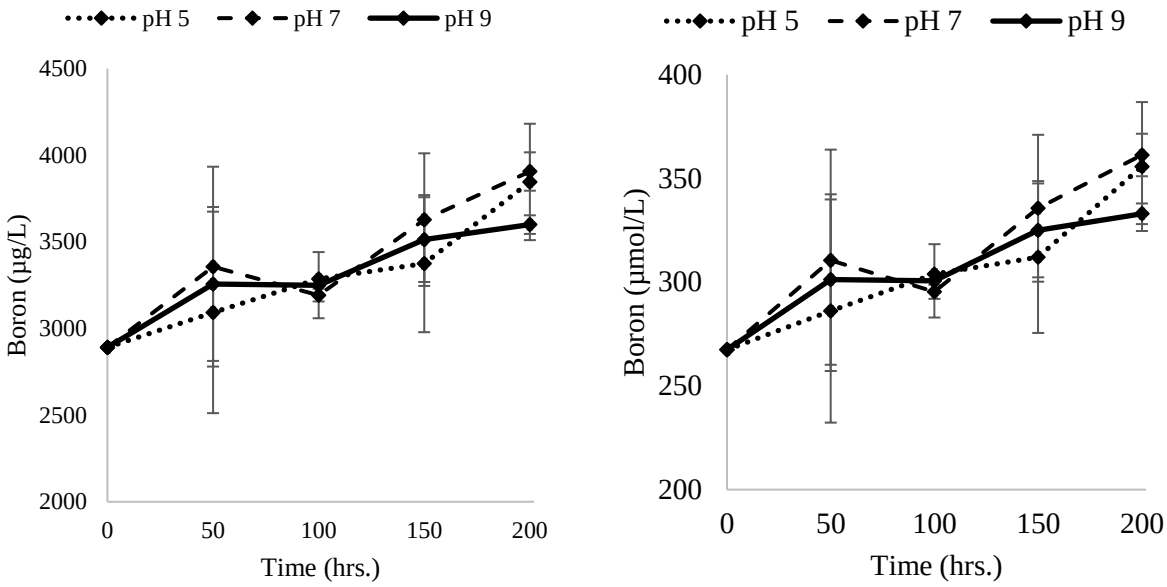

Figure 4.29 Dissolved B concentration changes from the Arrastres drill cuttings from the western side of the basin.

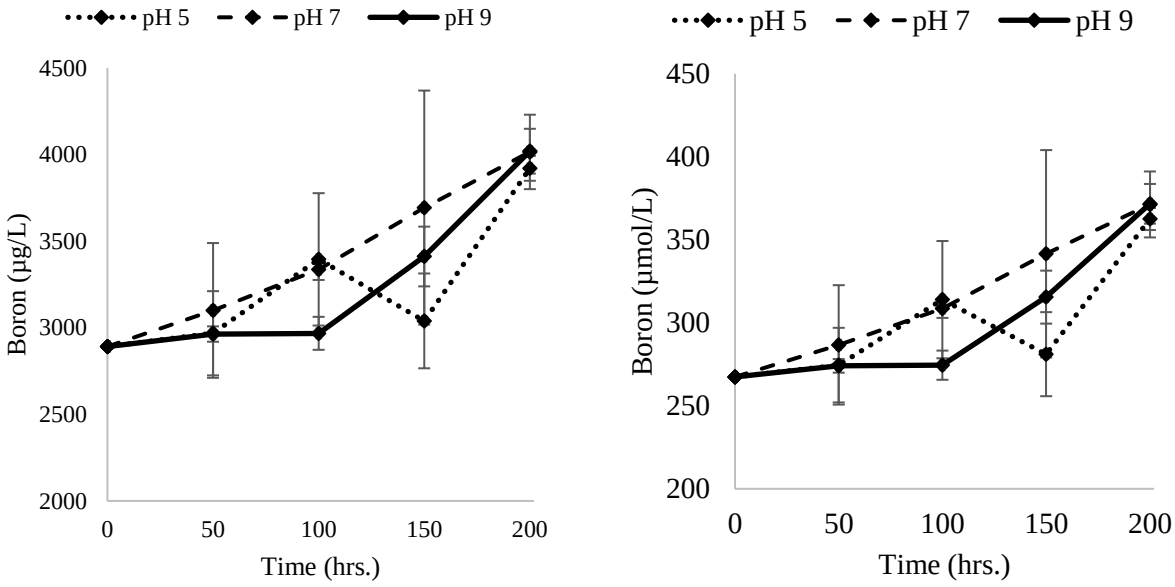

Figure 4.30 Dissolved B concentration changes from the Lourdes drill cuttings from the eastern side of the basin.

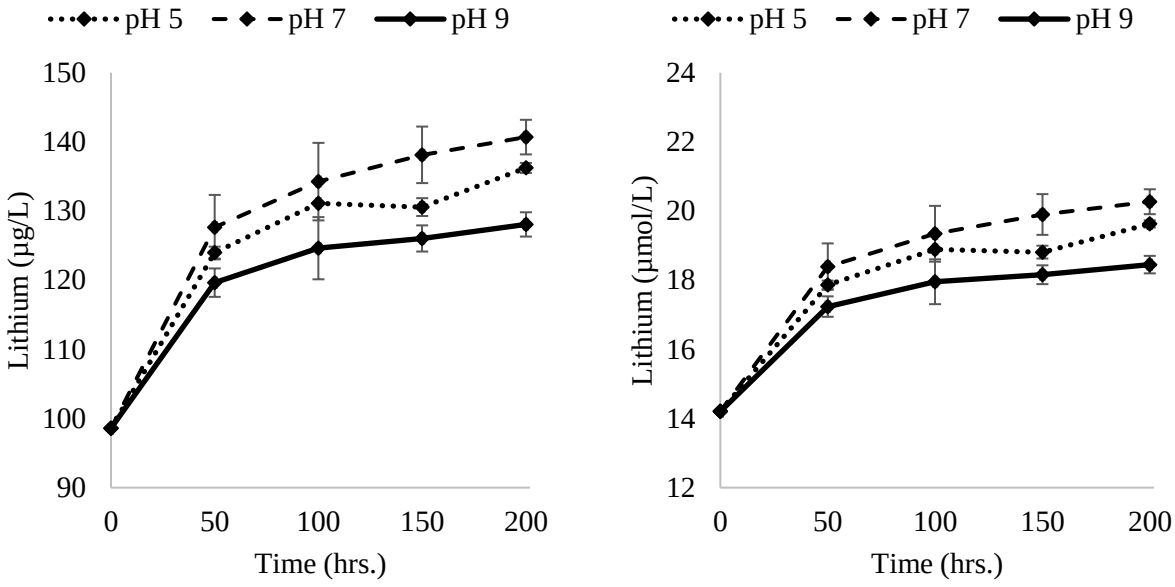

Figure 4.31 Dissolved Li concentration changes from the Arrastres drill cuttings from the western side of the basin.

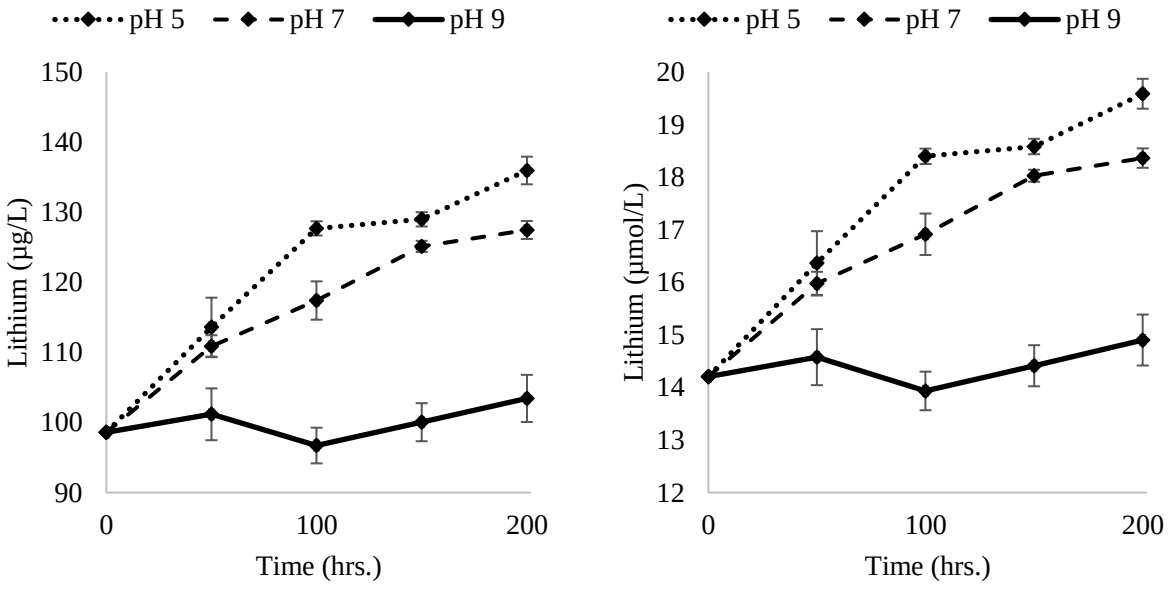

Figure 4.32 Dissolved Li concentration changes from the Lourdes drill cuttings from the eastern side of the basin.

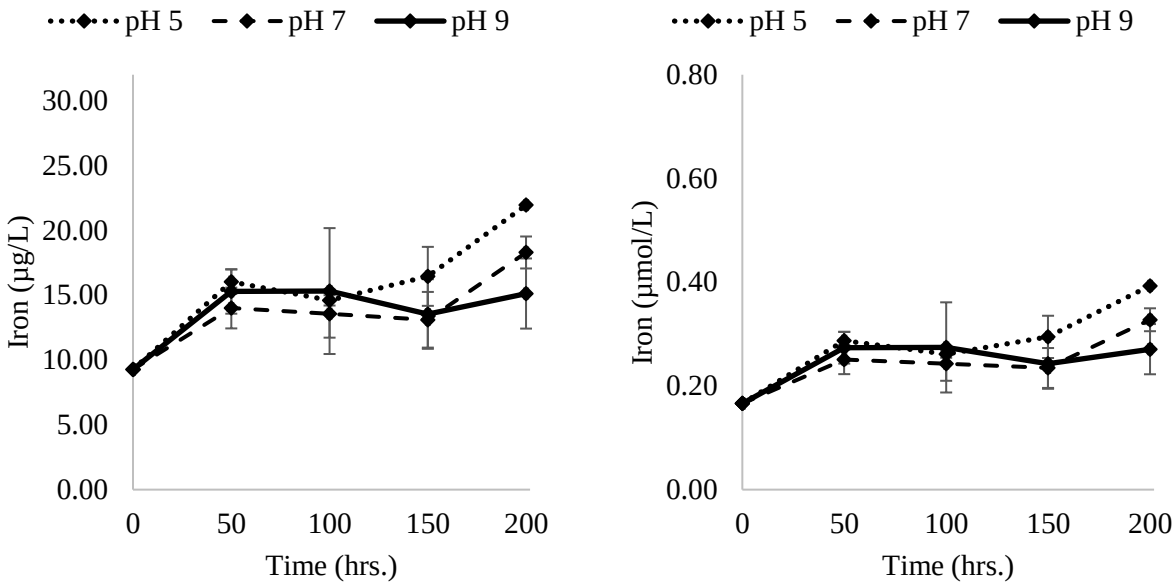

Figure 4.33 Dissolved Fe concentration changes from the Arrastres drill cuttings from the western side of the basin.

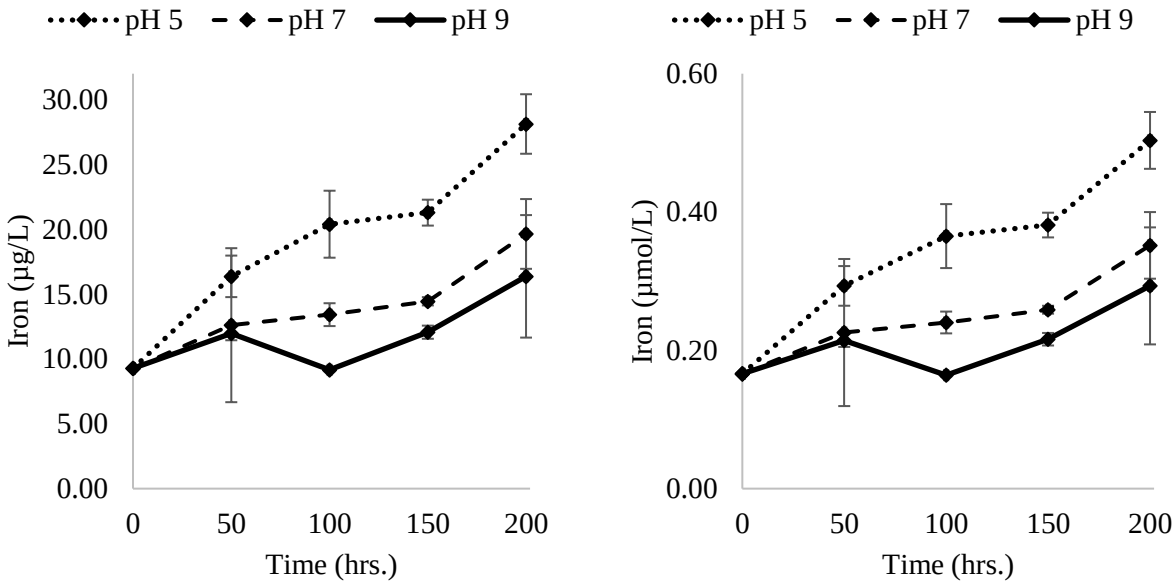

Figure 4.34 Dissolved Fe concentration changes from the Lourdes drill cuttings from the eastern side of the basin.

4.12 Rate Const ant Calculations

The results from the laboratory-controlled experiments were used to determine whether the reaction releasing F is zero, first, or second-order. A zero-order reaction results in a linear change in concertation with respect to time. A first and second-order reaction is an exponential change in concentration with time. A definitive rate order was not achieved, although the order does fall between zero and first-order. Based on the assumption that the reaction is a zero-order reaction, a linear rate of change was used to calculate the rate constant (k) (Equation 1). As the drill cuttings from the Lourdes borehole were the only water-rock interaction experiments that released F into the groundwater the rate constant for the three pH values was calculated by using the changes in average F concentrations with respect to the time (Table 4.21). These values were derived from the calculation below where C_t is the concentration of F at a specified time, C_0 is the initial concentration of F, k is the rate constant, and t is the time. This calculation was performed for the 25 hr. and 50 hr. reaction times for the changes in F concentrations and the two rate constants were averaged together to derive a single rate constant that explained the rate of release from the drill cuttings of the Lourdes borehole during the initial 50 hr. of reaction (Figure 4.35).

Equation 1

$$C_t = C_0 + kt$$

Table 4.21 Table of rate constant values

	pH ~5	pH ~7	pH ~9
k $\frac{mol}{L \cdot hr}$	3.07E-04	7.25E-04	8.41E-04

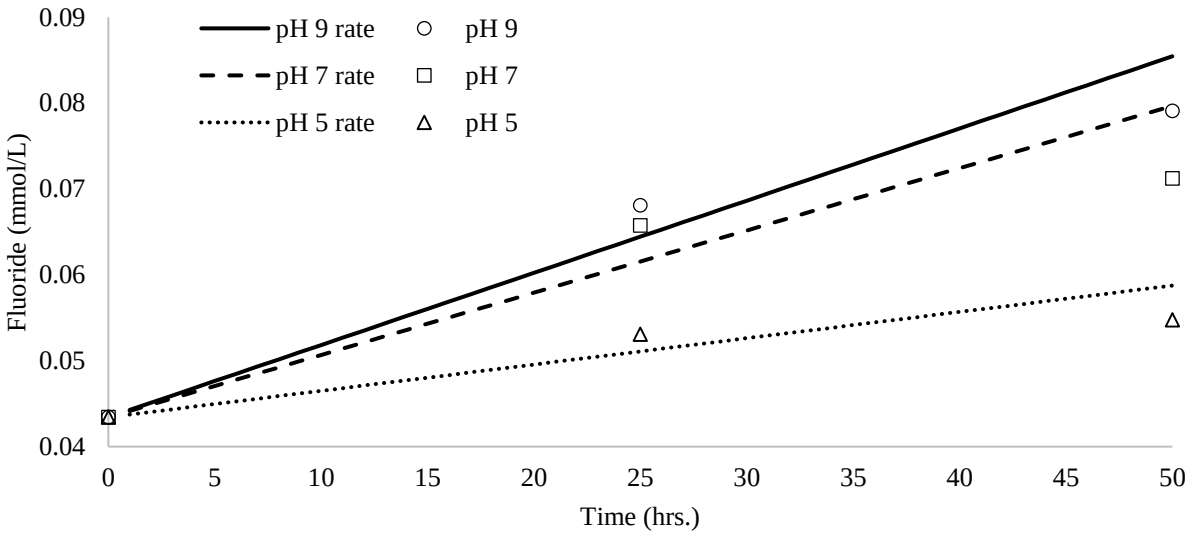

Figure 4.35 Bivariant plot representing the change in F concentrations with respect to time during the initial 50 hours of reaction.

4.13 Geochemical Modeling of Batch Reactor Results

The geochemical model developed via the Geochemist Workbench Software was used to describe the reactions with dissolved arsenate ($As(OH)_4^-$), dissolved F, and Fe oxyhydroxide minerals in groundwater with a pH of 5, 7, and 9. The Fe oxyhydroxide used in the model was goethite which was given a surface area of 600 m^2/g and 0.005 mol/mol for strong bonding sites and 0.200 mol/mol for weak bonding sites. The modeling results display a ~18% decrease in F concentrations at pH 9 (Figure 4.36A), a ~53% decrease in F concentrations at pH 7 (Figure 4.36B), and a ~98% decrease in F concentrations at pH 5 (Figure 4.36C). The modeling results for $As(OH)_4^-$ display decrease in concentration by ~7 orders of magnitude at a pH of 9 (Figure 4.37A), decrease of ~8 orders of magnitude at pH 7 (Figure 4.37B), and a decrease of ~9 orders of magnitude at pH 5 (Figure 4.37C). Comparing the experimental results with the modeling results, a discrepancy in magnitude is observed. This may be due to the model reaction dependency on mineral surface area, quantity of As and F-bearing minerals, the dimensions of the Fe oxyhydroxide mineral surfaces, and the site density on these mineral surfaces. The modeling prediction for the interactions of $As(OH)_4^-$ and F with Fe oxyhydroxides, indicate that adsorption is a possible mechanism for reducing the $As(OH)_4^-$ and F concentrations in the groundwater as F-bearing minerals undergo dissolution and release F.

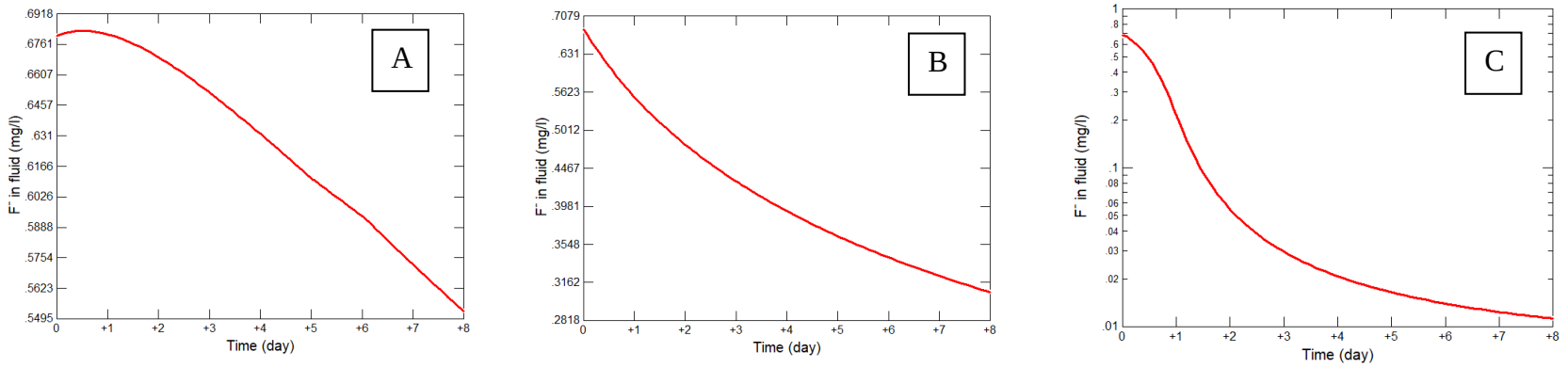

Figure 4.36 Modeling simulation output of fluorite dissolution and adsorption of F onto iron oxyhydroxide mineral surfaces (A) pH = 9, (B) pH = 7, (C) pH = 5

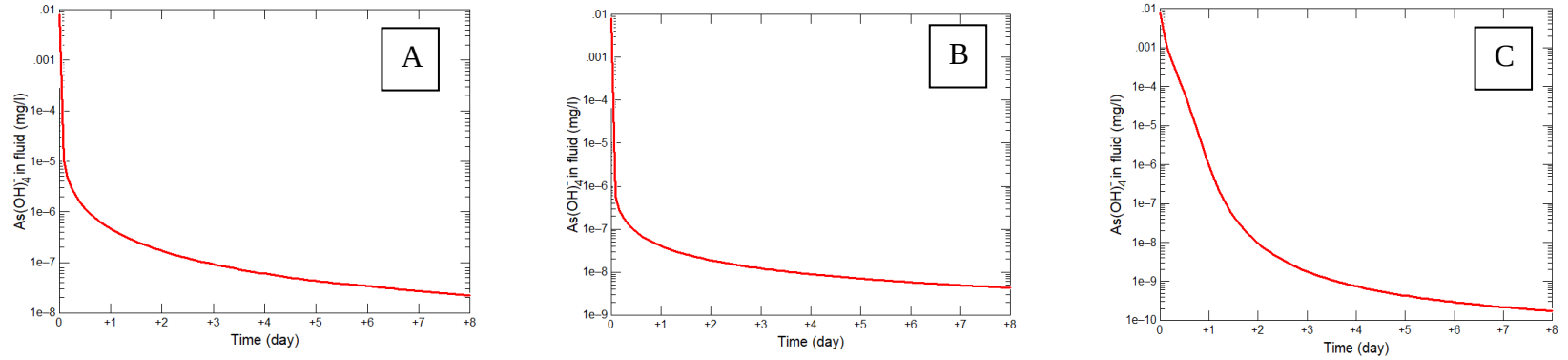

Figure 4.37 Modeling simulation output of arsenic adsorption onto iron oxyhydroxide mineral surfaces (D) pH = 9, (E) pH = 7, (F) pH = 5.

Chapter 5 - Discussion

5.1 How Water Chemistry Influences Elemental Mobilities in IBAS

The distributions of dissolved As and dissolved F in the groundwaters of the IBAS were examined by analyzing the water chemistries around five major municipalities including: San Luis de la Paz, Dolores Hidalgo, San Miguel de Allende, San Felipe, and San Diego de la Union. In this groundwater system the highest concentrations of these two contaminants were found in rural wells of the northeastern region of the IBAS near San Luis de la Paz (Figure 2.4 and Tables 4.5 and 4.9). Previous investigations also found high concentrations of As and dissolved F in this northeastern region of the basin (Mahlknecht et al., 2004; Ortega-Guerrero, 2009; Knappett et al., 2018). Arsenic and F concentrations measured in the groundwater of this area have reached levels 9 to 10 times higher than the WHO guidelines (Tables 4.5 and 4.9). In this study the correlation (R^2 = 0.82) between As and F concentrations in groundwater samples from across the basin was highly significant ($p < 0.001$) (Table 5.1). This suggests that As and F have similar geogenic source. In addition to the northeastern region of the basin a groundwater well with As and F concentrations above the WHO guidelines was located along the western side of the Taxco-San Miguel de Allende Fault System (Figure 2.4). In groundwater wells installed to a depth of ~500 meters As exceeds the WHO limit and F approaches and exceeds the WHO limit.

As well as co-varying themselves, concentrations of As and F in groundwater wells are positively correlated with elevated Li, B, and groundwater temperatures (Table 5.1 and Figure 5.1A and 5.1B). Figure 5.1A displays the relationship between As concentrations greater than 10 µg/L, B, Li, and groundwater temperatures greater than 30 ^{o}C. The groundwater wells with temperatures greater than 30 ^{o}C also show a positive correlation with elevated B, Li, and F concentrations Figure 5.1B. As reported by Webster and Nordstrom (2003) and Lopez et al. (2012) B and Li are good indicators of geothermal fluids. The occurrence of these geothermal tracers in the IBAS could indicate mixing between hydrothermal fluids and deep groundwater systems. Knappett et al. (2018) conducted a survey of production well across the IBAS found correlation between B and F. These correlations indicate a possible hydrothermal source for elevate As concentrations.

Table 5.1 R^2 Correlation matrix between physiochemical parameters and trace and major elements. Values in bold have p-values below 0.05.

Parameter	Temp.	pH	Na	HCO_3	B	Li	As	F
Temp.	1							
pH	0.01	1						
Na	0.22	**0.45**	1					
HCO_3	0.02	**0.28**	**0.6**	1				
B	**0.33**	0.06	**0.57**	**0.42**	1			
Li	**0.54**	**0.28**	**0.59**	**0.33**	**0.56**	1		
As	**0.55**	**0.3**	**0.63**	**0.38**	**0.47**	**0.68**	1	
F	**0.57**	**0.32**	**0.46**	**0.29**	**0.31**	**0.73**	**0.82**	1

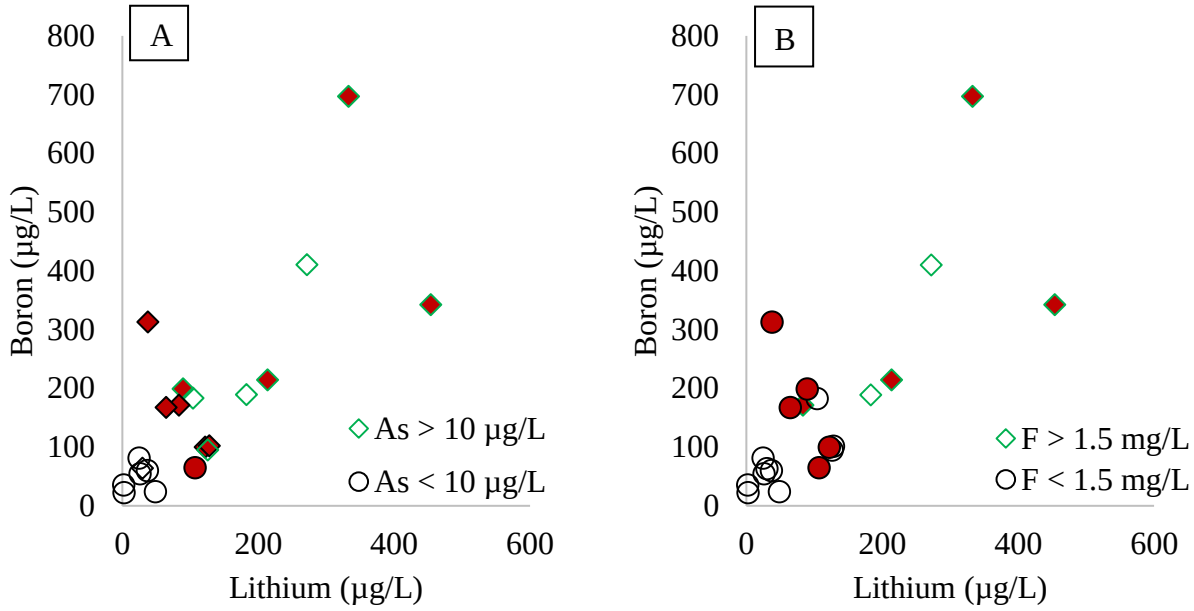

Figure 5.1 Bivariate plots which represents the relationship between boron and lithium in groundwater wells. Markers with red fill are groundwater wells with water temperatures greater than 30 C°.

Sodium and bicarbonate concentrations also correlated with elevated As and F concentrations (Table 5.1). Figure 4.1 shows that the groundwater from the rural areas of the IBAS are dominantly a Na-HCO_3 rich water. This could be owing to the alteration of albite ($NaAlSi_3O_8$) and sanidine like minerals ($(K,Na)AlSi_3O_8$) observed in the borehole drill cuttings which consume

protons thereby increasing the pH and HCO_3^- content of the groundwater as indicated by Li et al. (2013) (Equation 2 and 3).

Equation 2

$$2NaAlSi_3O_{8(albite)} + 2H^+ + 9\ H_2O \rightarrow 2\ Na^+ + 4H_4SiO_{4(aq)} + Al_2Si_2O_5(OH)_{4(kaolinite)}$$

Equation 3

$$NaAlSi_3O_{8(albite)} + H_2CO_3 + 9/2H_2O \rightarrow Na^+ + HCO_3^- + 2H_4SiO_4 + 1/2Al_2Si_2O_5(OH)_{4(kaolinite)}$$

The urban wells contain water that is predominantly of the Ca-Mg-Na-HCO_3 rich. This could be the results of weathering reactions having calcite ($CaCO_3$) in the system (Equation 4) and anorthite ($CaAl_2Si_2O_8$) (Equation 5), both of which are observed in the drill cuttings.

Equation 4

$$CaCO_{3(calcite)} + 2H^+ \leftrightarrow Ca^{2+} + H_2O + CO_2$$

Equation 5

$$2CaAl_2Si_2O_{8(anorthite)} + 6H_2O = Al_4Si_{10}O_{10}(OH)_8 + 2Ca^{2+} + 4(OH)^-$$

Additional sources of Ca could be from sodium exchange reactions which can contribute Ca to groundwater (Mahlknecht et al., 2004). These different water types are important because Ca concentration can limit F concentrations in groundwater by precipitations of fluorite (Equation 6) and apatite (Equation 7).

Equation 6

$$CaF_{2(Fluorite)} \rightarrow Ca^{2+} + F^-$$

Equation 7

$$(Ca_5(PO_4)_3(OH,F,Cl)_{(apatite)} + 3H^+ \rightarrow 5Ca^{2+} + 3HPO_4^{2-} + F^-$$

The limitation with respect to fluorite was quantified by Brown and Roberson (1977) ($K_{fluorite} = 10^{-10.6}$ at 25ºC). Theoretically, when Ca concentrations are 40.08 mg/L, then F concentrations are limited to 3.08 mg/L as stated by Hem (1985) (Figure 5.2).

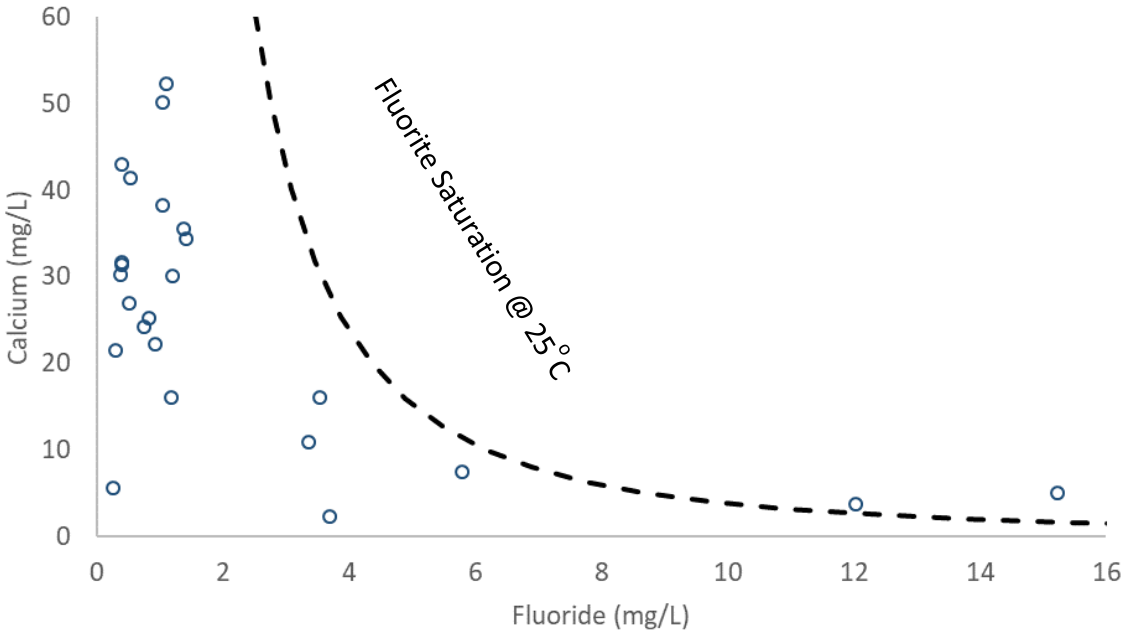

Figure 5.2 F and Ca concentration from the groundwater wells sampled in the Independence Basin with dashed line representing fluorite saturation calculated from the equilibrium constant provided by Brown and Roberson (1977).

Elevated As and F concentrations are observed in groundwater samples that also contain low Ca and high Na concentrations (Figure 5.2). These rural groundwater wells (Well ID: Terreros de la Concepciones and Well ID: LS-0178) approach and surpass the fluorite saturation point with F concentrations of 12.04 and 15.24 mg/L (Figure 5.2). The presence of high Ca concentrations in the urban wells near San Luis de la Paz will limit the solubility of fluorite through the common ion effect ensuring F concentrations in the groundwater remain low (Equations 6 and 7). The high Ca concentrations effectively decrease the solubility of Ca F-bearing minerals including fluorite and fluorapatite (Apambire et al., 1997) (Equation 6 and 7).

The physiochemical parameters of low temperature geothermal conditions, an oxic groundwater, and a high pH, as well as, elevated alkalinity, B, Li, and F indicates Fe^{2+} oxidation and desorption of As and possibly mixing of groundwater with hydrothermal waters can be attributed to the sources of As as shown by Smedley and Kinniburgh, (2002).

The O- and H-isotope ratios of the rural groundwater wells (Figure 4.6 and Figure 2.4) with the highest As and F concentrations near San Luis de la Paz have heavier isotope ratios compared to the urban wells of that major city (Knappett et al., 2018). Groundwater wells along the flow

path between San Luis de la Paz and Dolores Hidalgo are enriched in heavier isotope ratios compared to the other wells sampled in the basin (Figure 4.6). This could be the result of groundwater becoming enriched in heavier isotope ratios as subsurface groundwater flows towards the central region of the basin (Mahlknecht et al. 2006). Additionally, during the extraction of groundwater for agriculture purposes can result in enrichment in heavier isotopic ratios as the groundwater recirculates (Mahlknecht et al., 2004). This is known as irrigation return flow. The groundwater wells of Dolores Hidalgo, San Miguel de Allende, and San Diego de la Union display similar isotopic ratios on the lighter (more depleted in the heavy isotopes) end of the LMWL. The fact that As and F concentrations are particularly high in the area with heavier water isotopes (more enriched) suggests that continuous extraction and evaporation effects could be leading to rising concentrations of As (Welch et al., 2000) and F in the aquifer (Knappett et al., 2018).

5.2 How Dominant Lithologies affect the Water Chemistry and Reactions in IIBAS

The geology of the basin was examined through drill cuttings from Arrastres and Lourdes boreholes. The Arrastres borehole is located on the western side of the basin near San Felipe in the CARL aquifer and the Lourdes borehole is located on the eastern side of the basin near San Luis de la Paz in the LS aquifer. The volcanic and sedimentary rocks of the IBAS are the dominant controls on the major and trace element geochemistry of the aquifers as the groundwater flows through the fractures and pore spaces under the influence of gravity to the phreatic water table (Knappett P. personal communication). Therefore, it is important to understand the geology of the basin as these findings will help determine the sources of major and trace ion in the groundwater. The ages of the rocks of this study are not well constrained, but based on the mineralogy, hand sample examination, location of boreholes within the basin, thin section descriptions, powdered XRD, and XRF the origins of these deposits can be understood, and ages tentatively assigned.

The drill cuttings from the Arrastres borehole on the western side of the basin displayed four changes in lithology with depth. In the upper 40 m, weathered olivine, pyroxene, plagioclase, quartz, calcite, and clay minerals with trace amounts of apatite (Figure 4.8 and Table 4.15) were observed. This mineralogical composition correlates with enrichment in heavier elements of Mg, Ca, Mn, and Fe, but relatively depleted in light elements such as K, Rb, and Si. This mineral assemblage is more typical of an igneous mafic lithology (Table 4.17 and Figure 4.17). Additionally, these mafic volcanic rocks are positioned near an exposure of Quaternary basalts (personal communication Loza-Aguirre I.) (Figure 2.3). Underlying this Quaternary basalt layer at ~40 to ~220-m depth are volcanic rocks composed of felsic minerals including plagioclase, potassium feldspar, quartz, volcanic glass, clay minerals, and trace quantities of zircons (Figure 4.8 and Table 4.15). This change from mafic to felsic mineralogy is reflected in the changes in elemental composition; heavy elements of Ca, Mg, Mn, and Fe are less abundant whereas light elements such as K, Si, and Rb (Table 4.17 and Figure 4.17) occur in higher concentrations. The crystalline nature of this formation could indicate emplaced volcanic rocks during a recent pulse of extension (personal communication, Loza-Aguirre I.). Based on the geographical location of these rocks, they can be correlated with Miocene or Oligocene rhyolites or ignimbrites described by Nieto-Samaniego et al. (2007). In this region F-rich rhyolites have been observed near San

Felipe in the northwest corner of the basin and northern portion of the CARL aquifer. These F-rich rhyolites are noted to be primarily composed of quartz, sanidine, and sodic plagioclase with trace amounts of apatite, fluorite, ilmenite, and zircon (Burt et al., 1982). From ~220 to ~400-m depth, the Arrastres borehole contain pyroxene, plagioclase, quartz, calcite, biotite, clay minerals, and trace apatite; similar to the upper ~40 m of the borehole (Figure 4.8 and Table 4.15). The rocks of this section could be tentatively correlated to Oligocene andesites (Figure 2.2). Below the ~400-m depth until the termination of the borehole at ~500-m depths, felsic rocks containing plagioclase, potassium feldspar, quartz, calcite, and pyroxene are observed (Figure 4.8 and Table 4.15). The pyroxene of this section maybe the results of cavity collapse and mixing of the upper layers, due to the drilling method. The felsic nature of this section is corroborated by relatively high concentrations of light elements of K, Rb, Si alongside relatively low concentrations of heavy elements of Ca, Mg, Mn, and Fe (Table 4.17 and Figure 4.17). This section would correlate to either a lowermost section of Oligocene rhyolite (Figure 2.2).

On the eastern side of the basin, the drill cuttings from the Lourdes borehole which is ~550 m in depth displayed only two distinct changes in lithology with depth. The upper 300 m of the borehole contained rounded rock fragments composed of plagioclase, potassium feldspar, calcite, quartz, volcanic glass, biotite, muscovite, clay minerals, and trace amounts of apatite and zircon (Figure 4.9 and Table 4.16). This mineralogy is corroborated by the enrichment in K, Rb, and Si with relatively low concentrations of Mg, Mn, and Fe. The Ca concentrations in this section are anomalously high, most likely owing to the presence of limestone clasts composed of calcite ($CaCO_3$) or calcite cement (Table 4.18 and Figure 4.18). The presence of fluorite was identified by single grain XRD at 220 – 222 m of depth of the borehole drill cuttings (Appendix A.69). The Ca F-bearing minerals could represent a spatially heterogenous distributed mineral that would be a source of dissolved F. These sedimentary deposits correlated with Quaternary age sandstones and conglomerates (Figure 2.2) and overlying continental strata (Nieto-Samaniego et al. 2007). Underneath these Quaternary sedimentary deposits below ~300 m depth are basaltic rocks composed of weathered olivine, pyroxene, amphibole, plagioclase, potassium feldspar, quartz, and calcite (Figure 4.9 and Table 4.16). This mineralogy is consistent with the high concentrations of Ca, Mg, Mn, and Fe and with low concentrations of K, Rb, and Si (Table 4.18 and Figure 4.18). This section could represent Quaternary or Miocene basalts (Figure 2.2).

The occurrence of fluorite was expected as the IBAS is included in the “fluorite belt”, which includes the states of Coahuila, Zacatecas, San Luis Pototsi, Guanajuato, and Queretaro (Ortega-Guerrero, 2009). However, until this study, the presence of fluorite has only been speculated based on inverse geochemical modeling and studies in the surrounding region (Ortega-Guerrero, 2009). Knappett et al. (2018) speculated apatite as the source of F in the basin. Apatite was identified surrounded by plagioclase grain in layers of the drill cuttings, although the grains were observed only in trace amounts. No minerals of pyrite or arsenopyrite were identified in the drill cuttings of the basin by XRD or petrographic microscopy.

The minerals identified in the rocks of the basin include multiple possible sources of F including fluorite, identified by XRD analysis. Alongside this F-bearing mineral are minerals containing OH sites capable of accepting F into their lattice structure through isomorphic substitution including biotite, hornblende, and muscovite, as well as, apatite (Madhavan, 2002) which were identified in thin section.

In contrast to abundant primary mineral sources for F, no As-bearing minerals were confirmed. Although primary host minerals for As were not identified, even after an exhaustive search, As could be bonded to Fe oxyhydroxides, which is a secondary host. These were observed in the rocks.

5.3 Leaching of Major and Trace Elements from Rocks of the Arrastres and Lourdes Cores

The depth dependent release of F from the rocks of the Arrastres and Lourdes cores was examined after 200-hours of water-rock interaction. These initial experiments emphasized the spatial distribution of leachable F from the 0 - ~500 m depths of the Arrastres and Lourdes cores. Following these initial 200-hour water-rock interaction experiments, the 400 - ~500 m depths of the Arrastres and Lourdes cores were examined through water-rock interaction experiments conducted across various pH values.

The distribution of leachable F from the four dominant lithologies which comprise the rocks of the Arrastres core displayed a gradient of leachable F concentrations. The upper 140 m of the Arrastres borehole is composed of Quaternary basalts and Miocene or Oligocene rhyolites or ignimbrites which displayed the greatest release of F into the reacting DI and groundwater (Figures 4.19A and 4.20C). Compared to the upper 140 m, the Oligocene andesites of the 220 – 400 m depths and the Oligocene rhyolites or ignimbrites of the 400 – 500 m depths released significantly less F into the reacting DI and groundwater. The F concentrations in the Oligocene rhyolites and ignimbrites of the MC have been investigated by Orozco-Esquivel et al., (2002). Their study separated the Oligocene rhyolites and ignimbrites into an upper F-rich rhyolite which was underlain by rhyolites and ignimbrites with comparably less F. The leachable F concentration profile developed in this study could indicate the rhyolites or ignimbrites of the Arrastres borehole are comparable with the upper and lower rhyolite and ignimbrite lithologies of the MC described by Orozco-Esquivel et al. (2002). As these Miocene or Oligocene rhyolites or ignimbrites could be F-rich and the Quaternary basalts contain apatite (Table 4.15). Apatite's can contain F in their crystal lattice structure (Edmunds and Smedley, 2013). The dissolution from these two sources could be the reason for increased F concentrations in the upper 140 m.

The water-rock interactions involving major and trace elements from the 400 – ~500 m depths of the Arrastres core was examined using pH-controlled batch reactors with groundwater from the IBAS (Table 4.20). The pH of the groundwater used to saturate the rocks of the Arrastres core has implications for the release and sequestration of F from mineral surfaces. In the basic pH conditions (pH = ~9) the F concentrations in the IBAS groundwater increased when reacting with the rocks of the 400 - ~500 m depths of the Arrastres core (Figure 4.21). The F concentrations in

the groundwater reached steady state after 25 hours and peak concentrations were 0.88 mg/L. The F concentrations in groundwater with a pH of ~5 resulted in a decrease in F concentrations when reacting with the rocks from the 400 - ~500m depths of the Arrastres core (Figure 4.21). The decrease in F concentrations can be explained by subsequent adsorption onto Fe oxyhydroxides minerals (Jinadasa et al. 1993; Tang et al. 2010). Fe oxyhydroxides (hematite and goethite) have been observed in the drill cuttings and rocks of the basin in previous studies (Mahlknecht et al., 2006). The adsorption of F ions onto Fe oxyhydroxides is pH dependent, meaning that as the pH of the system increases towards basic conditions (pH > 7) the adsorption ability of Fe oxyhydroxides surfaces will decrease (Jinadasa et al. 1993; Tang et al., 2010). Meaning as the pH of the solution around the Fe oxyhydroxide mineral surface decreases, the hydrogen ions in solution will protonate the surface of the Fe oxyhydroxide generating a positively charged surface that will attract negatively charge anions (Mamindy-Pajany et al., 2009). These adsorption reactions are possibly through a combination of the Fe oxyhydroxide minerals present, goethite and hematite, with a zero point of charge at pH 6.9 and pH 8.1, respectively (Mamindy-Pajany et al., 2009). This point of zero charge is the pH value at which the charge on the Fe oxyhydroxide mineral surface is zero and the continued increase in pH will generate a negatively charged surface which will repel negatively charged ions (Adegoke et al., 2013). The protonation and deprotonation reactions which occur on the Fe oxyhydroxide mineral surface (S) is explained by inner-sphere complexation reactions (Equation 7 and 8) (Tang et al., 2010; Nur et al. 2014) where inner sphere complexes are difficult to dislodge.

Equation 8

$$S - OH + H^{+} \leftrightarrow S - OH^{2+}$$

Equation 9

$$S\text{-}OH^{+} + H^{+} + F^{-} \leftrightarrow S\text{-}F^{-} + H_2O$$

As apatite is the only mineral observed in the 400 - ~500 m depths of the Arrastres core that could possibly contain F in the crystal lattice structure. The changes in F concentrations observed as the pH was varied does not support the dissolution of this mineral as literature states that fluorapatite dissolution increase as pH decreases (Zhu et al., 2009). These increasing rates of fluorapatite mineral dissolution with decreasing pH would have resulted in a greater concentration of F ions released into the groundwater used in the experiment. Therefore, this studies results

support the presence of these adsorption and desorption reactions occurring as Fe oxyhydroxide minerals surfaces responding to changes in the pH.

No primary minerals containing As were observed in hand sample, thin section, or XRD analysis in this study of the 400 - ~500 m depths of the Arrastres core. Although, no primary As-bearing minerals were observed, interactions between As and Fe oxyhydroxides mineral surfaces are observed in this pH-adjusted study. The primary oxidation state of As in the groundwater used in this study is arsenate, as the conditions observed are not reducing. In studies conducted by Dixit and Hering (2003) the adsorption of arsenate onto Fe oxyhydroxide mineral surfaces is pH dependent. Similar to the previously mentioned reactions with F and Fe oxyhydroxides, as the pH of the system decreases, arsenate adsorption onto Fe oxyhydroxide mineral surfaces increases with less adsorption occurring at pH values greater than 7 (Dixit and Hering, 2003; EPA,1999; Tang et al., 2010). The data presented in Figure 4.23A displayed continuous decreasing values of As concentrations supporting the adsorption onto Fe oxyhydroxides could be possible (Equation 9).

Equation 10

$$S\text{-}OH^{+} + H^{+} + H_2AsO_4^{-} \leftrightarrows S\text{-}H_2AsO_4^{-} + H_2O$$

The pH dependence of the As adsorption could also indicate biotite, which is present in the drill cuttings from the western side of the basin, in sequestering As. Occurrence of As adsorption onto biotite was observed in studies by Chakraborty et al. (2007) when groundwater has a pH range of 6.5 – 7.5.

Interestingly, the use of B as an indicator of hydrothermal fluids influencing the chemistry of the basin (Section 5.1) may be obscured by unusually high B concentration leached from the rocks of the Arrastres core (Figure 4.29). Significant B concentrations (~1 mg/L) were leached from the drill cuttings of the Arrastres core during the experiment. The release of B from the rocks of the basin was not dependent on the pH of within the batch reactors. These elevated B concentrations from the drill cuttings from the Arrastres core could be explained by two processes hypothesized for the rocks of Guanajuato mentioned by Aranda-Gomez et al. (2003) including: the merging of boron-rich sediments accumulating in the fore-arc basin with a magma source and/or geothermal fluids mixing in a magma chamber. Lithium has also been proposed as a hydrothermal indicator in section 5.1, although Li concentration showed continuously increasing values during the experiments in all batch reactors across all three pH values. The sources of this lithium could be muscovite and biotite micas. Lithium can substitute for aluminum in micas

through isomorphic substitution (Foster, 1960). Additionally, lithium is present in rhyolites (Prodromou., 2016). The pH of the groundwater system does impact the release of Li concentrations.

The distribution of F concentrations leached from the Lourdes core on the eastern side of the basin displayed a similar distribution profile pattern as compared to the Arrastres core. During the rock and DI water interaction experiments, elevated leached F concentration were from the upper 140 m of the Quaternary sedimentary deposits and Quaternary or Miocene basaltic rocks of the 400 - ~550 m depths in the Lourdes core after 200 hours. The simplest interpretation of the leaching experiments with DI water is that these two different rock types are generating F within the aquifer from various minerals including biotite, chlorite, amphibole, and apatite, all of which are observed in the rocks of the Lourdes core. As the rocks from the Lourdes borehole reacted with groundwater containing high F concentration (Well ID: LS-0178), the upper 300 m of sedimentary rocks showed reductions in the F concentrations while the Quaternary or Miocene basaltic rocks increased the F concentrations in groundwater. Based on calculations of fluorite saturation all sections of this core are saturated with respect to fluorite (Appendix A.20). Which means the precipitation of fluorite is more favorable to remove F in the Quaternary sedimentary deposits of the basin.

The 400 - ~550 m of the Lourdes core were examined using pH-controlled batch reactors with groundwater from the IBAS to explore the migration of major and trace elements during water-rock interactions. During water-rock interactions at a pH of ~9, the F concentrations increased during the initial 50 hours of reaction with a peak value of 1.5 mg/L (Figure 4.22). In the batch reactors with a pH of ~7 and ~5 the F concentrations reached peak values after 50 hours of reaction 1.35 and 1.04 mg/L; respectively (Figure 4.22). The minerals observed in the 400 - ~550 m section of the Lourdes core which contain F were biotite, chlorite, amphibole, and apatite (Table 4.16).

The dissolution of these F-bearing minerals occurs alongside the F adsorption reaction with Fe oxyhydroxides. These reactors were selected for geochemical modeling. The modeling results indicate F concentrations are reduced during water-rock interactions with Fe oxyhydroxides (Figure 4.36). The reactor experiments display a similar process as the drill cuttings of the Lourdes core display are saturated with groundwater. The experimental data coupled with the modeling simulations could indicate that during the water-rock interaction experiments the dissolution of F-

bearing mineral releases F into the groundwater and Fe oxyhydroxide minerals are capable of adsorption of the F ion from the groundwater (Figure 4.37). Furthermore, as the pH ~5, ~7, and ~9 reactors all released F into the groundwater the rate constants were calculated to be 3.07 x 10^{-04}, 7.25 x 10^{-04}, and 8.41 x 10^{-04} mol/L·hr; respectively. These results indicate the rate of release of F from the drill cuttings of the Lourdes core decreases with decreasing pH. As precipitation of fluorite is a possibility, the water chemistries of each reactor were used to calculate saturation indexes for fluorite. The saturation index calculation indicate that fluorite is undersaturated with respect to all reactors across all three pH values of ~5, ~7, and ~9 reactors (Appendix A.31). As fluorite precipitation is not reducing the F concentrations and the dissolution of F-bearing minerals of biotite, chlorite, amphibole, and apatite increase with decreasing pH (Zhu et al., 2009; Zhang et al., 2006; Chakraborty et al. 2007; Bandstra et al., 2008) the adsorption of dissolve F onto the Fe oxyhydroxide mineral surface is the possible process resulting in decreased peak F concentrations as pH decreases.

The changes in As concentration over time in the pH ~5, ~7 and ~9 reactors with the rocks of the Lourdes core are similar to the trends observed in the reactors with the rocks of the Arrastres core (Figure 4.24). The decreasing As concentrations with could be the result of adsorption onto Fe oxyhydroxide mineral surfaces. This process is pH dependent and the rocks of the Lourdes core react with groundwater at a pH of ~5 the As concentrations are reduced from 7.93 to 5.67 µg/L (Figure 4.25). As the pH of the reactors increases the As concentrations are reduced less as the Fe oxyhydroxides mineral surfaces become protonated. Modeling simulations with Fe oxyhydroxides and groundwater, having an initial As concentration of 7.93 µg/L, display a decrease in As concentrations across all three pH values (Figure 4.37). These modeling results have a similar trend compared to the changes in As concentrations observed in the reactors across all three pH values (Figure 4.24). The leaching of B and Li concentration from the rocks of the Lourdes core in the pH ~5, ~7, and ~9 reactors displayed a similar change in concentration as the rocks of the Arrastres core (Figure 4.30). The B concentrations are independent of pH and could be attributed to the geothermally impacted rocks of the basin described by Aranda-Gomez et al. (2003). Additionally, the leaching of Li from the rocks of the Lourdes core in groundwater with a pH of ~5 and ~7 displayed a similar increasing change in concentration as the reactors with the rocks of the Arrastres core. Lithium could be present in these basalt rock and could indicate these are hydrothermally alter basalts (Dostal et al., 1996).

Chapter 6 - Conclusions

The presence of elevated As and F concentrations in the groundwaters of the Central Plateau poses a clear health-risk concern for the inhabitants of this region (Table 1.1 and 1.2) (Ortega-Guerrero, 2009; Knappett et al., 2018). Across the states of Mexico these co-occurring contaminants are present and have anthropogenic, geogenic, and geothermal sources (Reyes-Gomez et al. 2013, Table 1.1). This study focused on the IBAS of Guanajuato state in Mexico where thousands of citizens are exposed to toxic concentrations of As and F contamination in their groundwater. The rural population, who completely rely on these groundwaters for drinking water, are significantly impacted by this contamination compared to the nearby urban areas (Figure 2.4). Chemical analysis of the groundwater wells across the basin confirmed a heterogenous distribution of As and F contamination (Ortega-Guerrero, 2009). The regions primarily impacted by these two contaminants are located near the northeastern extent of the basin adjacent to San Luis de la Paz and on the western side of the Taxco-San Miguel de Allende Fault System in San Miguel de Allende (Figure 2.4). The As and F laden groundwaters in these localities display positive correlations with Li and B and physicochemical parameters such as higher groundwater temperatures and elevated pH. These findings suggest that groundwater contamination is related to hydrothermal fluids, which have undergone mixing with the Na-HCO_3^- type groundwater present in the aquifer (Table 5.1, Figures 4.1 and 5.1).

In addition to these hydrothermal fluid sources, the rocks comprising the aquifers, which are located far above geothermal activity, are speculated to be a source of As and F in the groundwaters. An examination of drill cuttings from the Arrastres core on the western side of the basin and the Lourdes core located on the eastern side of the basin revealed the presence of fluorite in Quaternary sedimentary deposits of the basin (Appendix A.69). This is the first confirmation of fluorite in the IBAS. Apatite is also confirmed for the first time in this basin, although further analysis will be needed to determine whether these is fluorapatite (Table 4.15 and 4.16). Although no primary minerals containing As have been identified, arsenic could be bound to chlorite or Fe oxyhydroxides, and possibly in the lattice structure of apatite's that are present in the borehole drill cuttings (Liu et al., 2017, Tables 4.15, 4.16 and Figures 4.15 and 4.16).

Experiments conducted with DI water and groundwater from the western side of the basin reacting with Miocene or Oligocene rhyolites and ignimbrites resulted in increased F

concentrations which approach the WHO limit of 1.5 mg/L. The F concentration leached from the Quaternary or Miocene basalts approach and exceed the WHO limit. Orozco-Esquivel et al., (2002) found that Oligocene rhyolites are enriched in F. The Quaternary or Miocene basalt contain apatite which is a possible F-bearing mineral. These could be the probable sources of the leached F from these drill cuttings. The eastern side of the basin released F primarily from the upper Quaternary sedimentary deposits and the Quaternary or Miocene basalt layers when reacting with DI water. The presence of biotite, muscovite, chlorite, apatite and amphiboles could also be sources releasing the F observed in the experiments (Tables 4.15 and 4.16, Figure 4.8, 4.9). In addition to releasing F, the Quaternary sedimentary deposits of the basin are also capable of sequestering F concentrations possibly through the precipitation of fluorite (Appendix A.20). These lithologic units can provide some spatial understanding of the distribution of leachable F within the basin.

The pH of the groundwater that interacts with the rock of the aquifer was demonstrated to have important implications for the release and sequestering of As and F. Specifically the Quaternary or Miocene basalts of the eastern side of IBAS in groundwater with a pH of ~5, ~7, and ~9. The F released from the rocks competes with possible adsorption reactions with Fe oxyhydroxides (Figures 4.22, 4.24). The Oligocene rhyolites of the western side of the basin in groundwater with an adjusted pH displayed adsorption and desorption reaction which could be linked to the surface charging of Fe oxyhydroxide minerals present in the drill cuttings (Figures 4.21, 4.23, and 4.15) Geochemical modeling simulations are consistent with the observed dissolution and adsorption reactions involving F and As with Fe oxyhydroxide mineral surfaces (Figures 4.36 and 4.37).

The arsenic and F concentrations in the groundwater of the IBAS are a cause for concern, as they create unsafe water conditions. A combination of the poor water quality due to high F concentrations and the presence of high As concentrations in groundwater will have detrimental health effects on the citizens of Guanajuato, Mexico. This study has added to the understanding of the spatial distribution of F and As, the mineralogy of the basin, as well as, the groundwater interactions controlling As and F in the IBAS.

References

Adegoke H. I., Adekola F. A., Fatoki O. S., Ximba B. J., (2013). Sorptive Interaction of Oxyanions with Iron Oxides: A Review. Pol. J. Environ. Vol. 22 p. 7-24.

Aguilar-Diaz F. C., Irigoyen-Camacho M. E., Borges-Yanez S. A., (2011). Oral-health-related quality of life in school children in an endemic fluorosis area of Mexico. Qual. Life. Res. Vol. 20. p. 1699 – 1706.

Alarcon-Herrera M. T., Bundschuh J., Nath B., Nicolli H. B., Gutierrez M., Reyes-Gomez V. M., Nunez D., Martin-Dominguez I. R., Sracek O., (2013). Co-occurrence of arsenic and fluoride in groundwater of semi-arid region Latin America: Genesis, mobility and remediation. Journal of Hazardous Materials. Vol. 262 p. 960 – 969.

Apambire W. B., Boyle D. R., Michel F. A., (1997). Geochemistry, genesis, and health implications of fluoriferous groundwater in the upper regions of Ghana. Environmental Geology. Vol. 33. p. 13 – 24

Aranda-Gomez J. J., Godchaux, M. M., Aguirre-Diaz G. J., Bonnichsen B., Martinex-Reyes J., (2003). Three Superimposed Volcanic Arcs in the Southern Cordillera-From the Early Cretaceous to the Miocene, Guanajuato, Mexico. p. 123 – 168.

Armienta M. A., Segovia N. A., (2008). Arsenic and Fluoride in the Groundwater of Mexico. Environmental Geochemistry and Health. Vol. 30 p. 345 – 353.

Baer N. S., Lewin S. Z., (1970). The Replacement of Calcite by Fluorite: A Kinetic's Study. The American Mineralogist. Vol 55. p. 466-476

Bandstra J. Z., Buss H. L., Campen R. K., Liermann L. J., Moore J., Hausrath E. M., Navarre-Sitchler N., Jang J., Brantley S. L., (2008). Appendix: Compilation of Mineral Dissolution Rates. Kinetics of water-rock interactions.

Barboza-Gudino J. R., Molina-Garza R. S., Lawton T. F., (2012). Sierra de Catorce: Remnants of the Ancient Western Equatorial Margin of Pangea in Central Mexico. The Geological Society of America Field Guide 25. p. 1–18

Betancourt-Lineares A., Irigoyen-Camacho M., Majia-Gonzalez A., Sanchez-Perez L., Zepeda-Zapeda M., (2013). Dental Fluorosis Prevalence in Mexican Localities of 27 States and the D.F.: Six Years After the Publication of the Salt Fluoridation Mexican Official Regulation. Rev. Invest. Clin. Vol. 65. p. 237 – 247.

Bia G., Borgnino L., Garcia M. G., Gaiero D., (2014) Identification of the As-bearing phases in fresh volcanic Andean ashes: Proceedings of the 5th International Congress on Arsenic in the Environment, May 11-16, 2014, Buenos Aires, Argentina. One Century of the Discovery of Arsenicosis in Latin America. p. 87 – 89.

Birkle, P., and Merkel, B., (2000). Environmental Impact by Spill of Geothermal Fluids at the Geothermal Field of Los Azufres, Michoacan, Mexico. Water Air and Soil Pollution. Vol. 124. p. 371–410.

Bissen M. and Frimmel F.H. (2003) Arsenic—A Review. Part I: Occurrence, Toxicity, Speciation, Mobility. Acta Hydrochimica et Hydrobiologica. Vol. 31 p. 9 – 18.

Borgnino L., Garcia M. G., Bia G., Stupar Y. V., Le Coustumer Ph., Depetris P. J., (2013). Mechanisms of fluoride release in sediments of Argentina's central region. Science of the Total Environment. Vol. 443 p. 245 – 255.

Brown, D. W., Roberson, C. E., (1977) Solubility of natural fluorite at 25°C. U.S. Geological Survey Journal of Research, Vol. 5 p. 506 – 517.

Burt D. M., Sheridan M. F., Bikun J. V., Christiansen E. H., (1982). Topaz Rhyolites-Distribution, Origin, and Significance for Exploration. Economic Geology. Vol. 77. p. 1818 – 1836

Camprubi A., (2013). Tectonic and Metallogenic History of Mexico. Special Publication Vol. 17. p. 201 – 243.

Carrizales L., Razo I., Tellez-Hernandez J. I., Torres-Nerio R., Torres A., Batres L. E., Cubillas A. C., Diaz-Barriga F., (2006). Exposure to Arsenic and Lead of Children Living Near a Copper-smelter in San Luis Potosi, Mexico: Importance of Soil Contamination for Exposure of Children. Environmental Research. Vol. 101. p. 1 – 10.

Castro de Esparza M. L., (2006). Presencia de arsenic en el aqua de bebida en America Latina y su efecto en la salud publica. Natural Arsenic in Groundwaters of Latin America. June 20 – 24 2005.

Centeno-Garcia E., Guerrero-Suastegui M., Talavera-Mendoza O., (2008). The Guerrero Composite Terrane of western Mexico: Collision and subsequent rifting in a supra-subduction zone E. The Geological Society of America Special Paper 436 p. 279 – 308.

Chae G., Yun S., Kwon M., Kim Y., Mayer B., (2006). Batch dissolution of granite and biotite in water: Implication for fluorine geochemistry in groundwater. Geochemical Journal. Vol. 40 p. 95 - 102.

Chakraborty S., Wolthers M., Chatterjee D., Charlet L. (2007). Adsorption of Arsenite and Arsenate onto Muscovite and Biotite Mica. Journal of Colloid and Interface Science. Vol. 309 p. 392 – 401.

Chouhan S., Flora S., (2010) Arsenic and fluoride: two major ground water pollutants. Indian Journal of Experimental Biology Vol. 48 p. 666 – 678.

Cortes A., Durazo J., Farvolden R. N., (1989) Isotopes studies of precipitation and groundwater in the sierra de las cruses, Mexico. Journal of Hydrology Vol. 107 p. 147-153

Craig, H., (1961). Isotopic Variations in Meteoric Waters. Science. Vol. 133. p. 1702 – 1703

Dixit S. and Hering J. G., (2003). Comparison of Arsenic(V) and Arsenic(III) Sorption onto Iron Oxide Minerals: Implications for Arsenic Mobility. Environ. Sci. Technol. Vol. 37. p.4182 – 4189.

Dostal J., Dupuy C., Dudoignon P., (1996). Distribution of boron, lithium, and beryllium in ocean island basalts from French Polynesia: implications for the B/Be and Li/Be ratios as tracers of subducted components. Mineraological Magazine. Vol. 60 p. 563 – 580.

Dozal S. R., Alarcon-Herrera M. T., Cifuentes E., Chihuahua L. H. S., Loyola-Rodrigues J. P., Barraza A., (2005). Dental Fluorosis in Rural Communities of Chihuahua, Mexico. Fluoride. Vol. 38 p. 143 – 150.

Dzombak D.A., Morel D. A., Morel F. F. M., 1990. Surface Complexation Modeling, Hydrous Ferric Oxide.

Ecosystem Sciences Foundation., (2006). Well water quality San Miguel de Allende. Phase 1: results and conclusions. p. 1 – 35.

Edmunds M. W., Smedley P. L., (2013). Fluoride in Natural Waters. In: Essentials of Medical Geology, Second Edition. Eds. Selinus O., Alloway B., Ceneno J. A., Finkelman R. B., Fuge R., Lindh U., and Smedley P. L., p. 311-336.

Ferrari L., Orozco-Esquivel T. O., Manea V., Manea M., (2012). The dynamic history of the Trans-Mexican Volcanic Belt and the Mexico subduction zone. Tectonophysics. Vol. 522 – 523. p. 522 – 523.

Ferrari, L., Valencia-Moreno, M., and Bryan, S., (2007). Magmatism and tectonics of the Sierra Madre Occidental and its relation with the evolution of the western margin of North America. Geological Society of America Special Paper 422, p. 1 – 39.

Flores-Armenta M., Gutierrez-Negrin L. C. A., (2011). Geothermal Activity and Development in Mexico. Proceedings: Short Course on Geothermal Drilling, Resource Development and Power Plants, January 16-22

Foster M. D., (1960). Interpretation of the Composition of Lithium Micas. Geological Survey Professional Papers 354 – E

Freydier C., Lapierre H., Ruiz J., Tardy M., Martinez-R J., Coulon C., (2000). The Early Cretaceous Arperos Basin: an Oceanic Domain Dividing the Guerrero Arc from Nuclear Mexico Evidenced by the Geochemistry of the Lavas and Sediments. Journal of South American Earth Sciences. Vol. 13. p. 325 – 336.

Gaciri S. J. and Davies T. C., (1993). The occurrence and geochemistry of fluoride in some natural waters of Kenya. Journal of Hydrology. Vol. 143. p. 395-412.

Gago C., Romar A., Fernandez-Marcos M. L., Alvarez-Rodriguez E., (2014). Fluoride sorption and desorption on soils located in the surroundings of an aluminum smelter in Galica (NW Spain). Environmental Earth Sciences. Vol. 10. p. 4105 – 4114.

Garcia M. G., Borgnino L., (2015). Fluoride in the Context of the Environment. Florine: Chemistry, Analysis, Function and Effects. p. 3-21.

Garcia M. G., Borgnino L., Bia G., Depetris P.J., (2007). Mechanisms of arsenic and fluoride release from Chacopampean sediments (Argentina). International Journal of Environment and Health. Vol. 7. p. 41 – 57.

Gonzalez Davila O., (2011). Water Arsenic and Fluoride Contamination in Zacatecas Mexico: an Exploratory Study.

Gonzalez-Horta C., Ballinas-Casarrubias L., Sanchez-Ramirez B., Ishida M. C., Barrera-Hernandez A., Gutierrez-Torres D., Zacarias O. L., Saunders R. J., Drobna Z., Mendez M. A., Garcia-Vargas G., Loomis D., Styblo M., Del Razo L. M. (2015). A concurrent exposure to arsenic and fluoride from drinking water in Chihuahua, Mexico. International Journal of Environmental Research and Public Health Vol. 12. p. 4587 – 4601.

Harrington L. F., Cooper E. M., Vasudevan D., (2003), Fluoride sorption and association aluminum release in variable charge soils. Journal of Colloid and Interface Science. Vol. 267 p. 302-313

Hem, J. D. (1985). Study and interpretation of the chemical characteristics of natural water. Third edition, U.S. Geological Survey Water-Supply Paper 2254

Hernandez-Montoya V., Bueno-Lopez J., Sanchez-Rules A., Garcia J., Trajo-Vazquez R., Bonilla-Petriciolet A., Algara C. M., (2003). Fourosis y caries dental en ninos de 9 – 11 anos del estado de Aguascalientes, Mexico. Revista Internacional de Contaminacion Ambiental. Vol. 19. p. 197 – 204.

Hinkle S. R., Polette D. J. (1999). Arsenic in Ground Water of the Willamette Basin, Oregon. U.S.G.S. Water-Resources Investigations Report 98–4205

Horst A., Mahlknecht J., Merkel B. J., (2007). Estimating Groundwater Mixing and Origin in an Overexploited aquifer in Guanajuato, Mexico, Using Stable Isotopes (strontium-87, carbon-13, deuterium and oxygen-18). Isotopes in Environmental and Health Studies. Vol. 43 p. 323 – 338.

Hurtado-Jimenez M., and Gardea-Torresdey J., (2004). Estimacion de la exposicion a fluoruros en Los Altos de Jalisco, Mexico. Salud Publica de Mexico. Vol. 47. p. 58 – 63.

Hurtado-Jimenez R., and Gardea-Torresdey J. L., (2006). Arsenic in Drinking water in the Los Altos de Jalisco Region of Mexico. Rev Panam Salud Publica. Vol. 20 p. 236 – 247.

Hurtado-Jimenez R., Gardea-Torresdey J., (2005). Estimacion de la Exposicion a Fluoruros en Los Altos de Jalisco, Mexico. Salud Publica Mex. Vol. 47 p. 58 – 63

Instituto Nacional de Estadística y Geografía, 2015. CARTA USO DEL SUELO Y VEGETACIÓN 1:250000 SERIE V GUANAJUATO F14-7.

Jarquin-Yanez L., Mejia-Saavedra J., Molina-Frechero N., Gaona E., Rocha-Amador D., Lopez-Guzman O., Bologna-Molina R., (2015). Association between Urine Fluoride and Dental Fluorosis as a Toxicity Factor in Rural Community in the State of San Luis Potosi. The Scientific World Journal. Vol. 2015. p. 1-5

Jinadasa K. B. P. N., Dissanayake C. B., Weerasooriya S. V. R., Senaratne A. (1993). Adsorption of Fluoride on Goethite Surfaces-Implications on Dental Epidemiology. Environmental Geology. Vol. 21 p. 251 – 255.

Kapaj S., Peterson H., Liber K., Bhattacharya P., (2006). Human Health Effects from Chronic Arsenic Poisoning – A Review. Journal of Environemntal Science and Health Part A. Vol. 41 p. 2399-2428.

Knappett P. S. K., Li Y., Hernandez H., Rodriguez R., Aviles M., Deng C., Pina V., Giardino R., Mahlknecht J., Datta S., (2018). Changing Recharge Pathways within an Intensively Pumped Aquifer with High Fluoride Concentrations in Central Mexico. Science of the Total Environment. Vol. 622-623. p. 1029 – 1045.

Kohler S. J., Harouiya N., Chairat C., Oelkers E. H., (2005). Experimental studies of REE fractionation during water-mineral interactions: REE release rates during apatite dissolution from pH 2.8 to 9.2. Vol. 222 p. 168 – 182

Kumar M., Das A., Das N. Goswami R., Singh U. K. (2016). Co-occurrence Perspective of Arsenic and Fluoride in the Groundwater of Diphu, Assam, Northeastern India. Vol. 150 p. 227 – 238.

Lennon M.A., Whelton H., O'Mullane D., Ekstrand J., (2004). Fluoride. World Health Organization

Li L., Wang Y., Wu Y., Li J., (2013). Major Geochemical Controls on Fluoride Enrichment in Groundwater: A case study at Datong Basin, Northern China. Journal of Earth Science. Vol. 24. p. 976 – 986.

Liu W., Mei Y., Etschmann B., Brugger J., Pearce M., Ryan C. G., Borg S., Wykes J., Kappen P., Paterson D., Boesenberg U., Garrevoet. (2017). Arsenic in hydrothermal apatite: Oxidation state, mechanism of uptake, and comparison between experiments in nature. 2017. Chechimica et Cosmochimica Acta. Vol. 196 p., 144 – 159.

Lopez D. I., Bundschuh J., Birkle P., Armienta M. A., Cumbal L., Sracek O., Cornejo L., Ormachea M., (2012). Arsenic in Volcanic Geothermal Fluids of Latin America. Science of the Total Environment. Vol. 429 p. 57 – 75

Loza-Aguirre I., 2018. Personnal Communication.

Madhavan N., Subramanian V., (2002). Fluoride in fractionated soil samples of Ajmer district, Rajasthan Journal of Environmental Monitoring. Vol 4. p. 821-822

Mahlknecht J. Steinich B. Navarro de Leon I., (2004). Groundwater chemistry and mass transfers in the Independence Basin, central Mexico, by using multivariate statistics and mass-balance models. Environmental Geology. Vol. 45. p. 781 – 795

Mahlknecht J., (2003). Estimation of recharge in the Independence Basin, central Mexico, by combining geochemical and groundwater flow models. PhD Thesis, Institute of Applied Geology, University of Agricultural and Life Sciences.

Mahlknecht J., Garfias-Solis J., Aracena R., Tesch R., (2006). Geochemical and Isotopic Incestigations on Groundwater Residence Time and Flow in the Independence Basin, Mexico. Journal of Hydrology. Vol. 324. p. 283 – 300

Mahlknecht J., Horst A., Hernandez-Limon G., Aravena R., (2008). Groundwater Geochemistry of the Chihuahua City region in the Rio Conchos Basin (northern Mexico) and implication for water resources management. Hydrological Processes. Vol. 22 p. 2736 – 4751.

Mahlknecht J., Schneider J. F., Merkel B. J., Navarro de Leon I., Bernasconi S. M., (2004). Groundwater recharge in a sedimentary basin in semi-arid Mexico. Hydrogeology Journal. Vol. 12. p. 511 – 530

Mamindy-Pajany Y., Hurel C., Marmier N., Romeo M., (2009). Arsenic Adsorption onto Hematite and Goethite. C. R. Chimie Vol. 12 p 876 – 881

Martinez-Prado M. A., Perez-Lopez M. E., Villanueva-Fierro I., Gonzalez-Nevarez C. C., (2013) Behavior of Arsenic and Fluoride concentration in Guadiana Valley Aquifer of Durango, Mexico. Journal of Environmental Protection. Vol. 4 p. 14 – 20.

Masuda H., Shinoda K., Okudaira T., Takahashi Y., Noguchi N., (2012). Chlorite-sources of arsenic groundwater pollution in the Holocene aquifer of Bangladesh. Geochemical Journal. Vol. 46. P. 381 – 391.

Mazziotti-Tagliani S. Angelone M., Armiento G., Pacifico R., Cremisini C., Gianfagna A., (2012). Arsenic and fluorine in the etnean volcanics from Biancavilla Sicily, Italy: environmental implications. Environ Earth Sci. Vol. 66 p. 561 – 572.

McBride M. B., (1994). Environmental chemistry of soils, Oxford press.

Mendez M. A., Gonzalez-Horta C., Sanchez-Ramirez B., Ballinas-Casarrubias L., Ceron R. H., Morales D. V., Tarrazas F. A. B., Ishida M. C., Gutierrez-Torres D. S., Saunders R. J., Drobna Z., Fry R. C., Buse J. B., Lomis D., Garcia-Vargas G. G., Del Razo L. M., Styblo M., (2016). Chronic Exposure to Arsenic and Markers of Cardiometabolic Risk: A Cross-Sectional Study in Chihuahua, Mexico. Environmental Health Perspective. Vol. 124. p. 104 – 111.

Mendoza L. A., Del Razo L. A., Barbier O., Saldana M. C. M., Gonzalez F. J. A., Juarez F. J., Sanchez J. L. R., (2011). Potable Water Pollution with Heavy Metals, Arsenic, and Fluordies and Chronic Kidney Disease in Infant Population of Aquascalientes. Water Resouces in Mexico. Vol. 7. p. 231 – 238.

Muehlberger W. R., (1985 – 1990), Written Communications

Navarro de Leon I., Garfias-Soliz J., Mahlknecht J., (2005). Groundwater flow regime under natural conditions as inferred from past evidence and contemporary field observations in a semi-arid basin: Cuenca de la Independencia, Guanjuato, Mexico. Journal of Arid Environments. Vol 63. p. 756 – 771

Navarro O., Gonzalez J., Junez-Ferreira H. E., Bautista C-Fa., Cardona A., (2017) Correlation of Arsenic and Fluoride in the groundwater for human consumption in a semiarid region of Mexico. Procedia Engineering. Vol. 186 p. 333 – 340.

Nieto-Samaniego A. F., Alaniz-Alvarez S. A., Camprubi A., (2007). Mesa Central of Mexico: Stratigraphy, Structure, and Cenozoic tectonic evolution. Geological Society of America Special Paper 422. p. 40 – 70

Nieto-Samaniego A. F., Ferrari L., Alaniz-Alvarez S. A., Labarthe-Hernandez G., Rosas-Elguera J., (1999). Variation of Cenozoic extension and volcanism across the southern Sierra Madre Occidental volcanic province, Mexico. GSA Bulletin. Vol. 111 p. 347 – 363.

Nordstrom D.K. and Jenne E.A., (1977). Fluoride solubility equilibria in selected geothermal waters. Geochim. Cosmochim. Acta. Vol. 41. p. 175-188.

Nur T. Loganathan P., Nguyen T. C., Vigneswaran S., Singh G., Kandasamy J., (2014). Batch and Column Adsorption and Desorption of fluoride using Hydrous Ferric Oxide: Solution Chemistry and Modeling.

Orozco-Esquivel M. T., Nieto-Samaniego A. F., Alaniz-Alvarez S. A., (2002). Origin of Rhyolitic Lavas in the Mesa Central, Mexico, by Crustal Melting Related to Extension. Journal of Volcanology and Geothermal Research, Vol. 118 p. 37 – 56.

Ortega-Guerrero M. A., (2009). Presencia, distribución, hidrogeoquímica y origen de arsénico, fluoruro y otros elementos traza disueltos en agua subterránea, a escala de Cuenca hidrológica tributaria de Lerma-Chapala, México. Revista Mexicana de Ciencias Geológicas. Vol. 26. p. 143 – 161

Ortega-Guerrero, M.A., Castellanos, J.Z., Aguilar G.R., Vázquez-Alarcón, A., Alanis-R., E., Vargas-C., C., Urrutia-E., F., (2002). A conceptual model for increases of sodium, sar, alkalinity and pH at the Independence Basin in Guanajuato, Mexico: TERRA Latinoamericana. Vol. 20. p. 199 – 207

Ortega-Gutierrez, F., Ruiz J., Centeno-Garcia, E., (1995). Oaxaquia, a Proterozoic microcontinent accrected to North America during the late Paleozoic. Geology Vol. 23 p. 1127 – 1130.

Ortega-Gutierrez, F., (1992). Carta Geologica de la Repulica Mexicana (5th edition): Consejo de Resursos Minerales y en el instituto de Geologica de la Universidad Nacional Autonoma de Mexico, scale 1:2,000,000

Ortiz-Hernandez L. E., Acevedo-Sandoval O. A., Flores-Castro K., (2003). Early Cretaceous Intraplate Seamounts from Guanajuato Central Mexico: Geochemical and Mineralogical Data. Revista Mexicana de Ciencias Geologicas. Vol. 20 p. 27 – 40

Pablo-Galan L. D., Chavez-Garcia M. L., Cruz-Sanchez M., (1996). Sedimentary Zeolites in the Sierra Madre Del Sur and Sierra Madre Occidental, Mexico. Revista Mexicana de Ciencias Geologicas. Vol. 12. p. 188 – 200.

Palacios-Garcia N. B. Martini M., (2014). From back-arc rifting to arc accretion: the Late Jurrassic-Early Cretaceous evolution of Guerrero terrane recorded by a major provenance change in sandstones from the Sierra de Cuarzos area, central Mexico. International Geology Review.

Padilla y Sanchez R. J., Martinez Serrano R. G., Rodiroguez V. R., and 7 collaborators (1994). Estados Unidos Mexicanos, Carta Tectnoica: Universidad Nacional Autonoma de Mexico, scale 1:2,000,000.

Pinon-Miramontes M., Bautista-Margulis R. G., Perez-Hernandez A., (2003). Removal of Arsenic and Fluoride from Drinking Water with Cake Alum and a Polymeric Anionic Flocculent. Fluoride. Vol. 36. p. 122 – 128.

Planer-Friedrich B., Armienta M. A., Merkel B. J., 2001. Origin of arsenic in the groundwater of the Rioverde basin, Mexico. Environmental Geology. Vol. 40 p. 1290 – 1298

Pontigo-Loyola A. P., Islas-Marquez A., Loyola-Rodriguez J. P., Maupome G., Marquez-Corona M. L., Medina-Solis C. E., (2008). Dental Fluorosis in 12- and 15-year-old at high altitudes in above-optimal fluroidated communities in Mexico. Journal of Public Health Dentistry. Vol. 68. p. 163 – 166.

Prodromou K. P., (2016). Lithium Adsorption on Amorphous Aluminum Hydroxides and gibbsite. Eurasian Journal of Soil Science. Vol. 5 p.13 – 16.

Razo I., Carrizales L., Castro J., Diaz-Barriga F., Monroy M., (2004). Arsenic and Heavy Metal Pollution of Soil, Water and Sediments in a Semi-Arid Climate Mining Area in Mexico. Water Air and Soil Pollution. Vol. 152. p. 129 – 152.

Reimann C., Matschullat J., Birke M., Salminen R., (2009). Arsenic distribution in the environment: The effects of scale. Applied Geochemistry. Vol. 24 p. 1147 – 1167.

Reyes-Gomez V. M., Alarcon-Herrera M. T., Gutierrez M., Nunez D., (2013). Fluoride and Arsenic in an Alluvial Aquifer System in Chichuahua, Mexico: Contaminant Levels, Potential Sources, and Co-occurrence. Water Air and Soil Pollution. Vol. 224. p. 1-15.

Rowe H., Hughes N., Robinson K., (2012). The quantification and application of handheld energy-dispervice x-ray fluorescence (ED-XRF) in mudrock chemostrtigraphy and geochemistry. Chemical Geology Vol. 324 – 325. p. 122 – 131.

Simons F. S. and Mapes-Vazquez E. (1956). Geology and ore deposits of the Zimapan mining district, State of Hidalgo, Mexico. US Geological Survey Professional Paper 284.

Sivasankar V., Darchen A., Omine K., Sakthivel R., (2016). Fluoride: A World Ubiquitous Compound, Its Chemistry, and Ways of Contamination.

Smedley P.L., Nicolli H.B., Macdonald D.M.J., Kinniburgh D.G., (2008). Arsenic in groundwater and sediments from La Pampa Province, Argentina. Natural arsenic in groundwaters of Latin America (Arsenic in the environment). p. 35-45.

Smedley, P. L. and Kinniburgh, D. G. (2002). A review of the source, behavior and distribution of arsenic in natural waters. Applied Geochemistry. Vol. 17. p. 517-568

Stollenwerk K. G., Breit G. N., Welch A. H., Yount J. C., Whitney J. W., Foster A. L., Uddin M. N., Majumder R. K., Ahmed N., (2007). Arsenic Attenuation by oxidized aquifer sediments in Bangladesh. Science of the Total Environment. Vol. 379 p. 133 – 150.

Tang Y., Wang J., Gao N., (2010). Characteristics and Model Studies for Fluoride and Arsenic Adsorption on Geothite. Journal of Environmental Sciences. Vol. 22 p. 1689 – 1694.

Torres R. M., Hernandez A. E. M., Gallage-Solorzano J. C., Santiago-Garcia E. J., Hernandez I., (2009). Arsenic in Mexico Children Exposed to Contaminated Well Water. Ecology of Food and Nutrition. Vol. 48. p. 59 – 75.

Ure A., Berrow M., (1982). Chapter 3. The elemental constituents of soils. Environmental Chemistry. p. 94 – 203.

USGS, Geologic Map of North America: https://ngmdb.usgs.gov/gmna

Viero A. P., Roisenberg C., Roisenberg A., Vigo A., (2008). The origin of fluoride in the granitic aquifer of Porto Alegre, Southern Brazil. Environmental Geology. Vol. 56. p. 1707-1719.

Webster J. G., Nordstrom D. K., (2003). Geothermal arsenic: The Source, Transport and Fate of Arsenic in Geothermal Systems. Arsenic in Ground Water. p. 101 – 125.

Welch A. H., Westjohn D. B., Helsel D. R., Wanty R. B., (2000). Arsenic in Groundwater of the United States: Occurrence and Geochemistry. Vol. 4. p. 589 – 604

Westerhoff P., Esparza-Soto M., Caballero Mata P., Parry W. T., Johnson W. P., (2004). Drinking water quality in the US–Mexico Border Region. p. 72.

World Health Organization, (2003) Toxicology profile for Fluorides, Hydrogen Fluoride, and Fluorine.

World Health Organization, (2004). Fluoride in Drinking-water

Wyatt C. J., Quiroga V. L., Acosta R. T. O., Mendez R., (1998) Excretion of Arsenic (As) in Urine of Children, 7-11 years, Exposed to Elevated Levels of As in the city Water Supply in Hermosillo, Sonora, Mexico. Environmental Research. Vol. 78. p. 19-24.

Yanmei L., (2018) Personal Communication.

Yinian Z., Stober I., Bucher K., (2003). Gneiss-water interaction and water evolution during the early stages of dissolution experiments at room temperature. Chinese journal of geochemistry. Vol. 22. p. 302 - 312

Zhang R., Hu S. and Zhang X. (2006) Experimental study of dissolution rates of fluorite in HCl–H2O solutions. Aqueous Chemistry, Vol. 12 p. 123–159.

Zhu Y., Zhang X., Chen Y., Xie Q., Lan J., Qian M., He N., (2009). A comparative study on the dissolution and solubility of hydroxylapatite and fluoapatite at 25ºC and 45ºC. Chemical Geology. Vol. 268 p. 89 – 96.

Appendix A - Supplementary Data

Table A.1 Field measurement collected in the IBAS. (Bdl) indicates below detection limit. (nm) indicates no measurement.

Well Sampled	F	F (tracer)	As (ppb)	Mn (mg/L)	NO2-N	Fe	Fe	SO4	PO4	Cl	NH4
Rural											
Lourdes	0.826	1.8	20	0	Bdl	<0.2	nm	71	0	nm	Bdl
LS-331-P	4.37	nm	50	0	Bdl	<0.2	nm	63.9	0.04	Over	0
LS-012-L	3.19	nm	35	0	Bdl	nm	0	57	0.08	nm	0.128
LS-0178	9.37	nm	80	0	Bdl	nm	0	70	2	nm	0.092
Terreros de la Concepciones	8.53	nm	75	0	Bdl	nm	0	60	0.08	nm	Bdl
RL-2-A	1.23	2.7	10	0	Bdl	<0.2	nm	58	0	nm	Bdl
CARL-453-P	0.753	nm	20	0	Bdl	<0.2	nm	58	6	nm	Bdl
CARL-506-P	3.45	nm	25	0	Bdl	<0.2	nm	59.5	0	Over	0
CR7	0.772	nm	10	0	Bdl	<0.2	nm	20	0	nm	0.4
CARL-145-P	0.88	nm	<10	0	Bdl	<0.2	nm	<20	0	Over	0
CDW	0.925	nm	<10	0	Bdl	<0.2	nm	<20	0.04	Over	0
Urban											
Pozo 9	0.937	nm	<10	0	Bdl	0.281	nm	<20	0	nm	Bdl
LS-531-P	1.04	1.1	<10	0	Bdl	<0.2	nm	53.4	0.08	nm	0.043
LS-529-P	1.5	1.5	<10	0	Bdl	<0.2	nm	63.3	0.04	nm	0.192
CARL-228	0.826	nm	<10	0	Bdl	<0.2	nm	<20	0.04	Over	0
Pozo 4	0.538	nm	<10	0	Bdl	<0.2	nm	<20	0.04	18.07	0
CARL-238-P	0.434	nm	0	0	Bdl	<0.2	nm	<20	0.04	31.07	0
CARL-234-P	0.421	nm	<10	0	Bdl	<0.2	nm	<20	0.02	3.593	0
Ejido de Tirado	3	4	25	0	Bdl	<0.2	nm	19	0.04	nm	Bdl
Insurgentes 2	0.293	0.6	0	0	Bdl	<0.2	nm	<20	0	nm	0.045
SMA:171:P	0.351	0.6	0	0	Bdl	<0.2	nm	27	0.2	nm	Bdl
Waste Water Treatment Plant											
Planta San Pablo	0.714	nm	<10	0	Bdl	0.231	nm	<20	12	Over	0
Hand Dug Well											
CARL-157-N-HD	0.291	0.8	0	0	Bdl	<0.2	nm	16	0	nm	Bdl
Pozo Sergio	0.325	nm	0	0	Bdl	0.201	nm	<20	0.08	0.334	0
LS-27-P (No Sample)	0.915	nm	15	0	nm	nm	0	57	0.04	nm	0.109
LS-817-NS (No Sample)	0.493	nm	<10	0	nm	nm	0	45	0.08	nm	1.093

Table A.2 Field measurements continued. (nm) indicates no measurement.

Alkalinity (HACH) (ppm)	Alkalinity (Chemetrics) (ppm)	S (ppm)	Br (ppm)	SiO_2 (ppm)
163.9	nm	0	0.5	100
313.9	nm	0	0	80
nm	210	0	0.9	80
nm	250	0	0	120
nm	360	0	0	100
169.8	nm	0	0.25	120
113.9	210	0	0.7	140
331.8	nm	0	0	160
193.4	nm	0	0	180
165.5	210	0	0.25	120
147.1	nm	0	0	120
298.9	nm	0	0	160
236.1	nm	0	0	180
152.5	nm	0	nm	160
142.2	nm	0	0	40
53.7	nm	0	0	120
126.6	nm	0	0.2	140
133.7	nm	0	0	100
<50	nm	0	0	180
127.6	nm	0	0	160
182	nm	0	0	160
394.1	nm	0	0	160
<50	nm	0	0	80
111.6	nm	0	0	160
nm	208	0	1.4	Nm
nm	225	0	1.4	nm

Table A.3 Trace elements for the groundwater samples collected from the IBAS. The (n.a.) symbol indicates vales are not available.

Well Sampled	Ag	As	B	Ba	Be	Bi	Ce	Co	Cd	Cr	Cs	Cu
	µg/L	µg/L	µg/L	µg/L	µg/L	µg/L	µg/L	µg/L	µg/L	µg/L	µg/L	µg/L
Rural												
Lourdes	0.199	32.100	199	74.9	n.a.	0.055	0.375	n.a.	0.038	3.06	0.791	8.99
LS-331-P	0.173	35.600	189	8.59	0.119	n.a.	0.273	n.a.	0.04	1.37	6.81	n.a.
LS-012-L	0.021	38.100	214	10.1	0.013	n.a.	0.04	n.a.	0.021	1.31	7.33	n.a.
LS-0178	0.035	69.500	342	11	0.129	n.a.	0.038	n.a.	0.061	1.33	13.8	n.a.
Terreros de la Concepciones	n.a.	93.500	410	11.3	n.a.	n.a.	0.04	n.a.	0.063	5.38	0.912	0.78
RL-2-A	0.083	7.930	65.1	97.9	n.a.	0.017	0.358	n.a.	0.028	1.82	1.15	2.63
CARL-453-P	0.007	13.121	167.5	127.1	0.009	n.a.		0.073	0.026	3.003		0.263
CARL-506-P	0.024	28.300	183	97.6	n.a.	n.a.	0.034	n.a.	0.024	3.3	0.543	n.a.
CR7	n.a.	40.300	697	54.6	0.025	n.a.	0.086	n.a.	0.03	0.89	1.91	n.a.
CARL-145-P	0.079	11.300	313	31.5	0.035	0.05	0.31	n.a.	0.056	1.29	4.31	0.54
CDW	0.023	19.300	99.7	23.4	0.112	n.a.	0.034	n.a.	0.013	0.47	6.45	n.a.
Urban												
Pozo 9	0.010	6.369	60.322	48.913	0.009	n.a.	n.a.	0.256	0.006	0.627	n.a.	2.237
LS-531-P	n.a.	7.040	81.6	49.1	n.a.	n.a.	0.065	0.141	n.a.	0.69	1.27	2.02
LS-529-P	0.010	11.333	95.088	42.139	0.009	n.a.	n.a.	0.465	0.014	1.320	n.a.	0.649
CARL-228	0.022	15.214	101.806	111.227	0.008	n.a.	n.a.	0.054	0.006	2.001	n.a.	0.251
Pozo 4	0.022	10.813	63.663	92.821	0.016	n.a.	n.a.	0.092	0.018	1.277	n.a.	4.926
CARL-238-P	0.011	6.345	54.562	102.003	0.037	n.a.	n.a.	0.065	0.009	0.819	n.a.	4.864
CARL-234-P	0.011	8.780	35.779	121.681	0.009	n.a.	n.a.	0.062	0.004	0.488	n.a.	0.383
Ejido de Tirado	0.047	25.500	171	19.2	n.a.	0.056	0.345	n.a.	0.036	1.69	1.52	n.a.
Insurgentes 2	n.a.	3.010	24.2	90.9	n.a.	n.a.	0.044	n.a.	0.018	1.69	8.1	0.88
SMA:171:P	0.007	3.668	22.883	83.267	0.009	n.a.	n.a.	0.097	0.007	1.256	n.a.	0.407
Waste Water Treatment Plant												
Planta San Pablo	n.a.	8.260	161	96.4	n.a.	0.03	0.044	0.565		1.77	0.73	0.79
Hand Dug Well												
CARL-157-N-HD	0.042	5.154	9.673	79.322	0.141	n.a.	n.a.	0.173	0.026	0.169	n.a.	0.639
Pozo Sergio	n.a.	1.370	12.7	56.7	n.a.	0.018	0.134	0.186	n.a.	n.a.	0.07	n.a.

Well Sampled	Dy	Er	Eu	Fe	Fe	Ga	Gd	Ge	Hf	Hg	Ho	In	La	Li	Lu
	µg/L	µg/L	µg/L	µg/L	mg/L	µg/L	µg/L	µg/L	µg/L	µg/L	µg/L	µg/L	µg/L	µg/L	µg/L
Rural															
Lourdes	0.02	0.004	n.a.	58	n.a.	n.a.	0.056	0.888	0.017	n.a.	n.a.	n.a.	n.a.	89.7	n.a.
LS-331-P	n.a.	n.a.	n.a.	11	0.04	0.429	n.a.	2.18	n.a.	n.a.	7E-04	n.a.	n.a.	183	0.007
LS-012-L	n.a.	1E-03	n.a.	n.a.	n.a.	0.513	0.005	2.04	n.a.	n.a.	3E-04	n.a.	n.a.	214	0.001
LS-0178	n.a.	n.a.	n.a.	n.a.	n.a.	1.13	0.003	3.52	n.a.	n.a.	2E-04	n.a.	n.a.	454	0.002
Terreros de la Concepciones	n.a.	7E-04	n.a.	n.a.	n.a.	0.049	n.a.	3.05	n.a.	n.a.	n.a.	n.a.	14.614	272	9E-04
RL-2-A	0.005	0.011	n.a.	n.a.	n.a.	n.a.	n.a.	0.958	0.0343	0.68	4E-04	n.a.	n.a.	107.2	n.a.
CARL-453-P	n.a.	n.a.	n.a.	8.336	0.04	n.a.	n.a.	n.a.	n.a.	n.a.	n.a.	n.a.	n.a.	64.5	0.001
CARL-506-P	n.a.	0.002	6E-04	n.a.	n.a.	n.a.	0.003	0.82	0.00149	n.a.	2E-04	n.a.	n.a.	104	0.002
CR7	n.a.	0.005	n.a.	138	0.12	0.021	n.a.	3.21	n.a.	n.a.	0.001	n.a.	n.a.	333	6E-04
CARL-145-P	n.a.	0.004	n.a.	28	0.04	n.a.	n.a.	2.03	n.a.	n.a.	n.a.	n.a.	0.015	38	0.001
CDW	n.a.	n.a.	n.a.	n.a.	n.a.	0.057	n.a.	1.52	n.a.	n.a.	n.a.	n.a.	n.a.	122	0.001
Urban															
Pozo 9	n.a.	n.a.	n.a.	41.439	n.a.	n.a.	n.a.	n.a.	n.a.	n.a.	n.a.	n.a.	n.a.	36.659	n.a.
LS-531-P	0.008	0.005	6E-04	36	n.a.	n.a.	0.012	0.272	n.a.	n.a.	6E-04	n.a.	n.a.	24.361	n.a.
LS-529-P	n.a.	n.a.	n.a.	22.325	n.a.	n.a.	n.a.	n.a.	n.a.	n.a.	n.a.	n.a.	n.a.	126	0.003
CARL-228	n.a.	n.a.	n.a.	9.421	n.a.	n.a.	n.a.	n.a.	n.a.	n.a.	n.a.	n.a.	n.a.	128	0.012
Pozo 4	n.a.	n.a.	n.a.	7.629	n.a.	n.a.	n.a.	n.a.	n.a.	n.a.	n.a.	n.a.	n.a.	29.9	0.001
CARL-238-P	n.a.	n.a.	n.a.	12.141	n.a.	n.a.	n.a.	n.a.	n.a.	n.a.	n.a.	n.a.	n.a.	25.6	n.a.
CARL-234-P	n.a.	n.a.	n.a.	7.884	0.12	n.a.	n.a.	n.a.	n.a.	n.a.	n.a.	n.a.	0.069	1.75	0.004
Ejido de Tirado	n.a.	0.011	n.a.	20	n.a.	n.a.	n.a.	0.567	0.0346	0.5	n.a.	n.a.	n.a.	83.4	0.005
Insurgentes 2	n.a.	1E-03	n.a.	n.a.	n.a.	n.a.	n.a.	0.551	n.a.	n.a.	n.a.	n.a.	n.a.	48.27	n.a.
SMA:171:P	n.a.	n.a.	n.a.	8.519	n.a.	n.a.	n.a.	n.a.	n.a.	n.a.	n.a.	n.a.	n.a.	2.252	n.a.
Water Treatment															
Planta San Pablo	n.a.	0.002	n.a.	48	n.a.	n.a.	0.009	0.098	0.00227	n.a.	4E-04	n.a.	n.a.	60.030	n.a.
Hand Dug Well															
CARL-157-N-HD	n.a.	n.a.	n.a.	196.88	n.a.	n.a.	n.a.	n.a.	n.a.	n.a.	n.a.	n.a.	n.a.	27.330	n.a.
Pozo Sergio	0.02	0.016	n.a.	127	n.a.	n.a.	0.028	0.016	n.a.	n.a.	0.006	n.a.	n.a.	1.898	n.a.

Well Sampled	Mn	Mn	Mo	Nb	Nd	Ni	Pb	Pr	Rb	Re	Sb	Sc	Se	Sm
	µg/L	mg/L	µg/L	µg/L	µg/L	µg/L	µg/L	µg/L	µg/L	µg/L	µg/L	µg/L	µg/L	µg/L
Rural														
Lourdes	1.28	n.a.	6.89	n.a.	n.a.	n.a.	6.64	0.00508	41.5	0.004	0.076	n.a.	n.a.	n.a.
LS-331-P	n.a.	n.a.	4.17	n.a.	n.a.	n.a.	6.8	0.00274	4.46	0.0035	0.249	n.a.	n.a.	n.a.
LS-012-L	n.a.	n.a.	4.39	n.a.	n.a.	2.03	0.226	0.00162	4.82	0.0027	0.295	n.a.	n.a.	n.a.
LS-0178	n.a.	n.a.	17.2	n.a.	n.a.	1.91	0.15	0.00167	8.27	0.0036	1.02	n.a.	n.a.	n.a.
Terreros de la Concepciones	n.a.	n.a.	23.3	n.a.	n.a.	2.05	0.205	n.a.	8.89	0.0027	0.205	n.a.	n.a.	n.a.
RL-2-A	5.688	n.a.	7.310	n.a.	n.a.	1.447	0.043	n.a.	n.a.	n.a.	0.174	n.a.	1.133	n.a.
CARL-453-P	36.2	0.03	0.91	0.0019	n.a.	14.9	5.89	0.00184	39.9	0.0017	0.367	n.a.	n.a.	n.a.
CARL-506-P	n.a.	n.a.	6.98	n.a.	n.a.	2.53	0.147	0.00165	24.6	0.004	0.162	n.a.	n.a.	n.a.
CR7	21.8	0.02	8.45	n.a.	0.0045	1.63	0.183	0.00266	25.1	0.0023	0.137	n.a.	n.a.	n.a.
CARL-145-P	9	n.a.	1.64	n.a.	0.0081	2.43	0.256	0.00409	19.2	0.0156	0.06	n.a.	n.a.	n.a.
CDW	1.15	n.a.	0.763	n.a.	n.a.	2.92	0.239	0.00062	14	n.a.	0.32	n.a.	n.a.	n.a.
Urban														
Pozo 9	6.443	n.a.	1.433	n.a.	n.a.	1.314	0.356	n.a.	n.a.	n.a.	0.180	n.a.	0.334	n.a.
LS-531-P	6.237	n.a.	3.712	n.a.	n.a.	1.515	0.016	n.a.	n.a.	n.a.	0.051	n.a.	9.119	n.a.
LS-529-P	0.63	n.a.	3.35	n.a.	n.a.	n.a.	6.78	0.00711	32.9	n.a.	0.04	n.a.	n.a.	n.a.
CARL-228	0.7	n.a.	1.31	n.a.	n.a.	n.a.	6.04	0.00279	17.6	n.a.	0.267	n.a.	n.a.	n.a.
Pozo 4	n.a.	n.a.	1.45	n.a.	n.a.	1.7	0.171	0.00085	23.8	0.0022	0.124	n.a.	n.a.	n.a.
CARL-238-P	7.224	n.a.	1.005	n.a.	n.a.	1.307	0.156	n.a.	n.a.	n.a.	0.154	n.a.	0.201	n.a.
CARL-234-P	159	0.14	0.576	n.a.	0.117	2.44	0.165	0.0247	13.4	n.a.	0.146	n.a.	n.a.	0.0243
Ejido de Tirado	0.68	n.a.	1.28	n.a.	n.a.	n.a.	6.31	0.00179	11.6	0.0062	0.494	n.a.	n.a.	0.0078
Insurgentes 2	3.759	n.a.	1.686	n.a.	n.a.	1.513	0.027	n.a.	n.a.	n.a.	0.129	n.a.	0.862	n.a.
SMA:171:P	9.867	n.a.	1.368	n.a.	n.a.	0.513	0.341	n.a.	n.a.	n.a.	0.421	n.a.	0.195	n.a.
Water Treatment														
Planta San Pablo	5.339	n.a.	1.651	n.a.	n.a.	1.055	0.036	n.a.	n.a.	n.a.	0.177	n.a.	0.447	n.a.
Hand Dug Well														
CARL-157-N-HD	8.198	n.a.	1.565	n.a.	n.a.	2.140	0.072	n.a.	n.a.	n.a.	0.049	n.a.	7.850	n.a.
Pozo Sergio	0.542	n.a.	1.968	n.a.	n.a.	1.482	0.380	n.a.	n.a.	n.a.	0.535	n.a.	0.459	n.a.

Well Sampled	Sn	Ta	Tb	Te	Th	Ti	Tl	Tm	U	V	W	Y	Yb	Zn	Zr	Al
	µg/L	µg/L	µg/L	µg/L	µg/L	µg/L	µg/L	µg/L	µg/L	µg/L	µg/L	µg/L	µg/L	µg/L	µg/L	mg/L
Rural																
Lourdes	15.3	n.a.	n.a.	n.a.	n.a.	3.33	n.a.	n.a.	3.98	28.6	0.828	0.021	0.00528	6.2	0.499	n.a.
LS-331-P	15	n.a.	n.a.	n.a.	n.a.	1.48	0.0099	n.a.	8.84	5.38	3.85	n.a.	0.00488	n.a.	0.503	n.a.
LS-012-L	n.a.	n.a.	n.a.	n.a.	0.00193	0.3	0.0028	n.a.	8.61	5.94	3.52	0.0091	0.00071	5.1	n.a.	n.a.
LS-0178	n.a.	n.a.	n.a.	n.a.	0.00758	0.59	0.0068	n.a.	1.97	5.31	11.3	0.0058	n.a.	14.7	0.02	n.a.
Terreros de la Concepciones	n.a.	n.a.	n.a.	0.018	0.00591	0.26	0.0119	n.a.	1.41	20.5	19	0.0054	n.a.	n.a.	0.023	n.a.
RL-2-A	0.003	n.a.	n.a.	n.a.	0.011	n.a.	0.003	n.a.	3.451	14.883	n.a.	n.a.	n.a.	5.996	n.a.	0.010
CARL-453-P	n.a.	n.a.	n.a.	0.019	0.00035	1.15	0.0013	n.a.	0.516	5.78	0.01	0.0115	0.00252	27.8	0.116	n.a.
CARL-506-P	44.8	n.a.	n.a.	n.a.	0.00038	0.19	0.0036	n.a.	4.5	27.9	0.323	0.0135	0.00124	n.a.	n.a.	n.a.
CR7	0.37	n.a.	n.a.	0.017	0.00258	0.27	0.0524	n.a.	2.71	18.9	2.31	0.0397	0.002	11.1	0.026	n.a.
CARL-145-P	n.a.	n.a.	n.a.	n.a.	0.00176	0.19	0.0151	n.a.	4.99	53.7	0.087	0.0471	0.00289	6.9	n.a.	n.a.
CDW	n.a.	n.a.	n.a.	n.a.	0.00079	1.28	0.0116	n.a.	1.55	2.95	2.45	n.a.	n.a.	n.a.	n.a.	n.a.
Urban																
Pozo 9	0.013	n.a.	n.a.	n.a.	0.046	n.a.	0.013	n.a.	0.843	8.007	n.a.	n.a.	n.a.	50.499	n.a.	0.013
LS-531-P	0.002	n.a.	n.a.	n.a.	0.026	n.a.	0.016	n.a.	5.202	47.651	n.a.	n.a.	n.a.	3.753	n.a.	0.012
LS-529-P	15.1	n.a.	n.a.	n.a.	n.a.	2.6	0.0067	n.a.	3.57	23.2	0.396	n.a.	0.00361	25	0.386	n.a.
CARL-228	15.5	n.a.	n.a.	0.488	n.a.	1.84	0.0074	n.a.	1.59	13.7	0.575	n.a.	n.a.	n.a.	0.474	n.a.
Pozo 4	n.a.	n.a.	n.a.	n.a.	0.00198	0.24	0.0063	n.a.	2.38	47.9	0.17	0.0091	n.a.	n.a.	n.a.	n.a.
CARL-238-P	n.a.	n.a.	n.a.	n.a.	0.002	n.a.	0.001	n.a.	0.956	5.648	n.a.	n.a.	n.a.	4.388	n.a.	0.012
CARL-234-P	n.a.	n.a.	0.0022	n.a.	0.00768	0.26	0.0203	0.0024	0.147	0.975	0.016	0.166	0.0189	n.a.	0.096	n.a.
Ejido de Tirado	14.7	n.a.	n.a.	n.a.	n.a.	2.52	0.0056	n.a.	1.47	20.8	1.23	n.a.	0.00897	52.3	0.557	n.a.
Insurgentes 2	2.669	n.a.	n.a.	n.a.	0.058	n.a.	0.114	n.a.	4.946	2.791	n.a.	n.a.	n.a.	19.870	n.a.	0.012
SMA:171:P	0.058	n.a.	n.a.	n.a.	0.140	n.a.	0.152	n.a.	0.119	1.241	n.a.	n.a.	n.a.	11.603	n.a.	0.594
Water Treatment																
Planta San Pablo	0.000	n.a.	n.a.	n.a.	0.009	n.a.	0.001	n.a.	1.172	14.814	n.a.	n.a.	n.a.	4.423	n.a.	0.012
Hand Dug Well																
CARL-157-N-HD	0.005	n.a.	n.a.	n.a.	0.034	n.a.	0.014	n.a.	5.372	35.042	n.a.	n.a.	n.a.	9.766	n.a.	0.010
Pozo Sergio	1.123	n.a.	n.a.	n.a.	0.416	n.a.	0.355	n.a.	0.558	0.900	n.a.	n.a.	n.a.	24.870	n.a.	0.020

Table A.4 Dissolved organic carbon values for all wells in the IBAS. The values without highlighting are DOC values for samples that were acidified with 10.2 M HCl in the field. The values highlighted yellow are from samples not acidified in the field.

Well Sampled	City	DOC mg/L	DOC mg/L
Rural			
Lourdes	San Luis de La Paz	0.9558	70.16
LS - 331 – P	San Luis de La Paz	1.061	94.31
LS - 012 – L	San Luis de La Paz	1.481	57.64
LS-0178	San Luis de La Paz	1.271	58.96
Terreros de la Concepciones	San Luis de La Paz	1.363	89.62
CARL - 453 – P	Dolores Hidalgo	0.6504	64.83
CARL - 506 – P	Dolores Hidalgo	1.461	69.64
CR7	Dolores Hidalgo	0.8835	107.6
CDW	Dolores Hidalgo	1.925	33.45
CARL - 145 – P	Dolores Hidalgo	1.36	56.12
RL-2-A	San Diego de La Union	0.4749	61.07
Urban			
Pozo 9	San Luis de La Paz	1.648	64.87
LS-531-P	San Luis de La Paz	1.592	73.62
LS-529-P	San Luis de La Paz	1.623	73
CARL-228	Dolores Hidalgo	0.7483	46.59
Pozo 4	Dolores Hidalgo	0.388	43.39
CARL-238-P	Dolores Hidalgo	1.475	45.58
CARL-234-P	Dolores Hidalgo	0.5739	42.34
Ejido de Terredos	San Miguel de Allende (W of fault)	1.32	47.32
Insurgentes 2	San Miguel de Allende (E of fault)	0.8327	64.39
SMA:171:P	San Miguel de Allende (E of fault)	0.6089	65.39
Water Treatment			
Planta San Pablo	Dolores Hidalgo	16.18	62.34
Hand Dug Wells			
CARL - 157 - P - HD	San Felipe	5.093	33.82
Pozo Sergio	San Felipe	2.961	13.27

Table A.5 Arrastres rock drill cuttings: data collected from the target batch reactor for F using DI water.

Drill cuttings Sections m	EC µs/cm	SC µs/cm	pH	F mg/L	F mg/L	F average mg/L	T °C
0 - 20	331	370	7.48	1.200	1.180	1.19	19.5
20 - 40	222	248	7.59	1.270	1.280	1.275	19.5
40 - 60	167.9	188	7.54	0.947	0.988	0.968	19.5
60 - 80	136.1	152	7.7	0.963	0.989	0.976	19.5
80 - 100	185.8	208	7.6	0.922	0.888	0.905	19.5
100 - 120	106.9	119	7.65	0.893	0.687	0.79	19.6
120 - 140	151.8	169	7.34	0.708	0.835	0.772	19.7
140 - 160	146.5	163	7.62	1.070	1.100	1.085	19.6
160 - 180	121.7	136	7.54	0.841	0.811	0.826	19.6
180 - 200	123.9	138	7.53	0.526	0.525	0.526	19.5
200 - 200	198	220	8.34	0.252	0.220	0.236	19.8
220 - 240	176.4	196	8.48	0.202	0.177	0.190	19.7
240 - 260	167.7	187	8.24	0.190	0.168	0.179	19.7
260 - 280	153	170	8.37	0.246	0.230	0.238	19.7
280 - 300	169.9	190	8.23	0.381	0.288	0.335	19.5
300 - 320	210.2	234	8.09	0.346	0.493	0.420	19.6
320 - 340	181	201	8.03	0.393	0.447	0.42	19.7
340 - 360	194.2	216	8.23	0.601	0.617	0.609	19.7
360 - 380	241	269	8.18	0.518	0.540	0.529	19.5
380 - 400	185.7	207	7.96	0.527	0.615	0.571	19.6
400 - 420	158.4	177	7.99	0.667	0.700	0.684	19.5
420 - 440	177.2	198	8.04	0.506	0.690	0.598	19.5
440 - 460	222	248	8.01	0.527	0.658	0.593	19.6
460 - 480	219	245	7.89	0.521	0.716	0.619	19.5
480 - 504	243	272	7.71	0.319	0.338	0.329	19.5

Table A.6 Arrastres Drill cuttings: Ion chromatography anion results from the DI batch reactors.

Drill cuttings Sections m	Water type	F mg/L	Cl mg/L	NO_2 mg/L	Br mg/L	NO_3 mg/L	PO_4 mg/L	SO_4 mg/L	Fluorite Saturation Index Log (Q/K)
0 - 20	DI	1.7705	4.7695	n.a.	0.0129	n.a.	n.a.	32.6276	-1.188
140 – 160	DI	1.2193	3.7481	n.a.	n.a.	n.a.	n.a.	7.6648	-1.687
240 – 260	DI	0.2595	2.3216	n.a.	n.a.	n.a.	n.a.	2.6983	-3.687
360 – 380	DI	0.5259	3.3364	n.a.	n.a.	n.a.	n.a.	8.3704	-2.798
440 – 460	DI	0.7799	5.7507	0.5075	n.a.	6.6815	n.a.	15.8193	-2.555

Table A.7 Arrastres Drill cuttings: Ion chromatography cation results from the DI batch reactors.

Drill cuttings Sections m	Water type	Na mg/L	NH_4 mg/L	K mg/L	Mg mg/L	Ca mg/L	Sr mg/L
0 - 20	DI	47.0299	1.2549	14.0534	n.a.	9.7598	0.1543
140 – 160	DI	27.0209	0.4796	8.0435	0.7785	5.8577	n.a.
240 – 260	DI	43.8652	0.3772	3.0653	n.a.	1.2673	n.a.
360 – 380	DI	66.1152	0.7066	5.5586	0.0945	2.5379	n.a.
440 – 460	DI	59.9266	0.6848	0.8616	n.a.	2.0474	n.a.

Table A.8 Arrastres Drill cuttings: Duplicates using DI water batch reactor.

Drill cuttings Sections m	Water type	EC µs/cm	SC µs/cm	pH	F mg/L	F mg/L	F average mg/L	T °C
200 - 220	DI	208	227	9.35	0.312	0.333	0.323	20.7
280 - 300	DI	166.8	180	8.81	0.292	0.320	0.306	21.1
380 - 400	DI	155.4	165	8.04	0.566	0.634	0.600	22.1
480 - 504	DI	219.1	232	8.2	0.297	0.329	0.313	22

Table A.9 Arrastres rock drill cuttings: The F values from batch reactor using groundwater from the rural well (CDW).

Drill cuttings Sections m	EC µs/cm	SC µs/cm	pH	F mg/L	F mg/L	F average mg/L	T °C
0 – 20	475	525	7.12	1.6	1.29	1.445	20
20 - 40	354	381	7.63	1.99	1.9	1.945	21.3
40 - 60	315	337	7.74	1.82	1.63	1.725	21.6
60 - 80	281	302	7.81	1.66	1.64	1.65	21.3
80 - 100	318	344	7.49	1.51	1.45	1.48	21.1
100 - 120	247	265	7.43	1.32	1.29	1.305	21.4
120 - 140	303	327	6.86	1.55	1.5	1.525	21.1
140 - 160	289	312	7.29	1.85	1.76	1.805	21.2
160 - 180	282	303	7.32	1.32	1.27	1.295	21.3
180 - 200	272	293	7.51	1.25	1.24	1.245	21.2
200 - 220	331	357	8.19	1.09	1.07	1.08	21.2
220 - 240	320	346	8.41	1.15	1.16	1.155	21.1
240 - 260	293	315	8.36	0.963	0.986	0.975	21.3
260 - 280	283	305	8.31	1.06	1.08	1.07	21.2
280 - 300	310	334	7.86	1.08	1	1.04	21.2
300 - 320	333	359	8.22	1.11	1.06	1.085	21.2
320 - 340	319	344	8.17	1.21	1.19	1.2	21.2
340 - 360	304	328	8.38	1.28	1.26	1.27	21.1
360 - 380	327	353	8.36	1.33	1.07	1.2	21.1
380 - 400	280	301	8.33	1.38	1.34	1.36	21.4
400 - 420	296	320	8.13	1.42	1.38	1.4	21.1
420 - 440	307	332	8.21	1.3	1.31	1.305	21.1
440 - 460	352	376	8.1	1.23	1.23	1.23	21.6
460 - 480	369	400	8.08	1.3	1.4	1.35	21
480 - 504	336	363	7.95	1.14	1.09	1.115	21.1

Table A.10 Arrastres Drill cuttings: Ion chromatography anion results from the GW batch reactors.

Drill cuttings Sections m	Water type	F mg/L	Cl mg/L	NO_2 mg/L	Br mg/L	NO_3 mg/L	PO_4 mg/L	SO_4 mg/L	Fluorite Saturation Index Log(Q/K)
0 - 20	GW	2.0399	5.9985	n.a.	0.0262	n.a.	n.a.	39.7173	-0.9855
140 - 160	GW	1.8245	5.7072	n.a.	n.a.	0.0745	n.a.	15.8051	-1.016
240 – 260	GW	1.2431	4.1909	n.a.	0.0192	n.a.	n.a.	9.9566	-20.98
360 – 380	GW	1.3013	4.6945	n.a.	n.a.	8.2874	n.a.	16.2888	-1.754
440 - 460	GW	1.7683	9.3605	n.a.	n.a.	8.2841	n.a.	23.1449	-1.59

Table A.11Arrastres Drill cuttings: Ion chromatography cation results from the GW batch reactors.

Drill cuttings Sections m	Water type	Na mg/L	NH_4 mg/L	K mg/L	Mg mg/L	Ca mg/L	Sr mg/L
0 - 20	GW	92.6809	1.9764	15.7694	2.8293	13.0854	0.3547
140 – 160	GW	58.8051	0.649	13.6929	2.413	14.4701	0.2618
240 – 260	GW	86.077	0.9637	6.5176	0.163	2.4822	n.a.
360 – 380	GW	93.9932	1.1446	7.3787	0.7722	5.1971	n.a.
440 – 460	GW	99.9095	1.3195	1.2353	0.0751	4.2173	n.a.

Table A.12 Arrastres Drill cuttings: Duplicates using groundwater from CDW.

Drill cuttings Sections m	Water type	EC µs/cm	SC µs/cm	pH	F mg/L	F mg/L	F average mg/L	Temp °C
200 - 220	GW	324	349	9.18	1.260	1.190	1.225	21.2
280 – 300	GW	294	317	8.5	1.120	1.080	1.100	21.2
380 - 400	GW	290	317	7.87	1.34	1.33	1.335	20.6
480 - 504	GW	308	322	7.94	1.12	1.11	1.115	22.8

Table A.13 The initial measurements of the waters in the F targeting batch reactor.

Water type	EC µs/cm	SC µs/cm	pH	F mg/L	Temp °C	DO mg/L	ORP mV
GW – CDW	207.9	226	7.16	0.948	20.9	10	525.4
DI Water	5.33	6	7.22	BDL	22.1	3	457.5

Table A.14 Controls used for the experiment after 200 hours.

Water type	EC µs/cm	SC µs/cm	pH	F mg/L	F mg/L	F average mg/L	Temp °C
GW – CDW	196.2	214	7.46	1.07	1.01	1.040	20.7
DI Water	8.34	9	7.81	0.0533	0.0561	0.055	20.7

Table A.15 Lourdes rock drill cuttings: data collected from the target batch reactor for F using DI water.

Drill cuttings Sections m	Avg. EC µs/cm	Avg. SC µs/cm	Avg. pH	Avg. ORP mV	Avg. Ag/AgCl mV	Average F mg/L	Avg. Temp °C
0 - 20	471	508	8.7	120	319	2.247	21.2
20 - 40	363	393	8.5	121	320	1.721	21
40 - 60	318	345	8.4	128	327	1.822	20.9
60 - 80	264	287	8.5	127	326	2.003	20.7
80 - 100	286	312	8.6	127	326	1.495	20.7
100 - 120	n.a.	n.a.	8.5	127	326	1.475	20.6
120 - 140	261	285	8.5	129	328	1.569	20.6
140 - 160	240	262	8.5	127	326	1.359	20.6
160 - 180	229	250	8.5	129	328	1.153	20.6
180 - 200	234	254	8.8	126	325	1.257	20.8
200 - 220	218	237	8.7	127	326	1.077	20.7
220 - 240	237	257	8.7	130	329	1.127	20.9
240 - 260	251	272	8.7	131	330	1.017	20.9
260 - 280	286	310	8.7	132	331	1.057	20.9
280 - 300	234	253	8.7	133	332	0.908	21
300 - 320	218	236	8.6	139	338	1.337	21
320 - 340	211	228	8.9	134	333	1.197	21
340 - 360	233	252	8.9	134	333	1.457	21
360 - 380	271	294	8.9	135	334	1.593	20.9
380 - 400	280	304	8.9	134	333	1.507	20.9
400 - 420	245	267	8.8	137	336	2.147	20.7
420 - 440	259	283	8.9	138	337	1.860	20.6
440 - 460	212	231	9.1	132	331	1.500	20.6
460 - 480	240	262	9.0	133	332	2.153	20.6
480 – 500	245	267	9.1	133	332	1.977	20.7
500 – 520	257	276	9.0	99	298	1.987	21.4
520 - 540	264	283	8.8	110	309	1.507	21.5

Table A.16 Lourdes Drill cuttings: Ion chromatography anion results from the DI batch reactors.

Drill cuttings Sections m	Water type	F mg/L	Cl mg/L	NO_2 mg/L	Br mg/L	NO_3 mg/L	PO_4 mg/L	SO_4 mg/L	Fluorite Saturation Index Log(Q/K)
20 - 40	DI	1.67	7.68	n.a.	0.13	0.15	n.a.	62.68	-1.630
100 – 120	DI	1.51	5.20	n.a.	0.09	0.19	n.a.	15.51	-1.721
220 – 240	DI	1.37	5.32	n.a.	0.09	0.18	n.a.	18.42	-1.999
320 – 340	DI	1.48	4.51	n.a.	n.a.	0.18	n.a.	11.22	-1.915
400 – 420	DI	2.72	5.18	n.a.	n.a.	0.34	n.a.	12.71	-1.390
520 - 550	DI	1.87	4.53	n.a.	n.a.	0.17	n.a.	15.85	-1.842

Table A.17 Lourdes Drill cuttings: Ion chromatography cation results from the DI batch reactors.

Drill cuttings Sections m	Water type -	Na mg/L	NH_4 mg/L	K mg/L	Mg mg/L	Ca mg/L	Sr mg/L
20 - 40	DI	81.6292	n.a.	12.9962	0.4805	4.539	0.6433
100 – 120	DI	55.4251	0.6536	13.3073	0.6429	3.8857	0.3943
220 – 240	DI	56.217	n.a.	6.4972	0.5562	2.482	0.3549
320 – 340	DI	46.5553	n.a.	6.4012	0.9597	2.5245	0.352
400 – 420	DI	59.4654	n.a.	6.5663	1.2081	2.5743	n.a.
520 - 550	DI	66.8043	n.a.	4.611	0.6637	1.9705	n.a.

Table A.18 Lourdes Drill cuttings: Duplicates for DI water batch reactor

Drill cuttings Sections m	Avg. EC µs/cm	Avg. SC µs/cm	Avg. pH	Avg. ORP mV	Avg. Ag/AgCl mV	Average F mg/L	Avg. Temp °C
100 – 120	323	348	8.3	105	304	1.27	21.3
200 – 220	223	240	8.6	98	297	1.14	21.2
300 – 320	219	236	8.7	96	295	1.42	21.2
400 – 420	247	267	8.8	104	303	2.12	21.2
500 – 520	253	271	9.1	104	303	2.06	21.5

Table A.19 Lourdes rock drill cuttings: data collected from the target batch reactor for F using groundwater.

Drill cuttings Sections m	Avg. EC µs/cm	Avg. SC µs/cm	Avg. pH	Avg. ORP mV	Avg. Ag/AgCl mV	Average F mg/L	Avg. Temp °C
0 – 20	832	905	8.5	143	342	12.750	20.8
20 – 40	697	758	8.4	152	351	10.980	20.8
40 – 60	629	687	8.4	153	352	9.460	20.6
60 – 80	635	693	8.4	157	356	13.060	20.6
80 – 100	641	699	8.4	158	357	12.240	20.7
100 - 120	604	657	8.4	157	356	14.050	20.8
120 - 140	581	630	8.4	167	366	12.340	20.9
140 - 160	615	667	8.5	163	362	12.500	20.9
160 - 180	603	654	8.4	169	368	13.560	20.9
180 - 200	598	648	8.4	167	366	14.580	21.0
200 - 220	596	644	8.4	167	366	15.920	21.1
220 - 240	632	685	8.4	170	369	15.240	21.0
240 - 260	637	692	8.4	168	367	15.400	20.8
260 - 280	664	730	8.4	167	366	15.440	20.3
280 - 300	634	689	8.5	164	363	15.960	20.9
300 - 320	609	660	8.5	163	362	17.360	21.0
320 - 340	608	658	8.6	164	363	16.380	21.0
340 - 360	621	672	8.5	166	365	16.900	21.0
360 - 380	633	685	8.6	165	364	15.520	21.0
380 - 400	638	692	8.5	166	365	15.760	21.0
400 - 420	623	674	8.6	167	366	16.820	21.0
420 - 440	638	692	8.6	165	364	16.640	20.9
440 - 460	615	672	8.6	165	364	16.960	20.5
460 - 480	621	678	8.7	163	362	16.100	20.6
480 – 500	624	679	8.6	163	362	16.840	20.7
500 – 520	617	667	8.6	161	360	16.480	21.0
520 - 540	625	675	8.6	163	362	16.040	21.1

Table A.20 Lourdes Drill cuttings: Ion chromatography anion results from the GW batch reactors

Drill cuttings Sections m	Water type	F mg/L	Cl mg/L	NO_2 mg/L	Br mg/L	NO_3 mg/L	PO_4 mg/L	SO_4 mg/L	Fluorite Saturation Index Log(Q/K)
20 - 40	GW	12.07	33.07	n.a.	0.46	0.34	n.a.	110.24	0.3636
100 – 120	GW	13.03	30.11	n.a.	0.42	0.29	n.a.	66.73	0.5121
220 – 240	GW	15.25	29.97	n.a.	0.41	2.76	n.a.	66.89	0.5451
320 – 340	GW	17.47	29.32	n.a.	0.40	2.50	n.a.	62.06	0.6079
400 – 420	GW	17.25	30.04	0.16	0.39	2.89	n.a.	62.87	0.5559
520 – 550	GW	16.55	29.30	n.a.	0.40	2.95	n.a.	66.62	0.5071

Table A.21 Lourdes Drill Cuttings: Ion chromatography cation results from the GW batch reactors

Drill cuttings Sections m	Water type -	Na mg/L	NH_4 mg/L	K mg/L	Mg mg/L	Ca mg/L	Sr mg/L
20 – 40	GW	166.3652	1.4716	20.9352	0.9008	10.184	n.a.
100 – 120	GW	135.3372	0.9388	23.0936	1.5852	11.3948	0.0136
220 – 240	GW	149.3268	1.114	13.8424	1.1848	9.0688	1.8792
320 – 340	GW	151.4204	1.414	14.1016	1.5656	7.9524	n.a.
400 – 420	GW	150.9564	1.4156	12.5176	1.618	7.2344	n.a.
520 – 550	GW	165.6016	1.5072	9.828	1.3308	7.1316	n.a.

Table A.22 Lourdes Drill Cuttings: Ion chromatography cation results from the DI batch reactors

Drill cuttings Sections m	Water type -	Na mg/L	NH_4 mg/L	K mg/L	Mg mg/L	Ca mg/L	Sr mg/L
20 – 40	DI	81.9248	0.6454	13.5204	0.451	5.5134	0.0662
100 – 120	DI	54.305	0.5526	13.2766	0.5882	4.4122	n.a.
220 – 240	DI	57.335	0.383	7.012	0.4972	3.0786	n.a.
320 – 340	DI	59.6578	0.5074	8.7048	1.1496	5.6434	10.024
400 – 420	DI	59.3044	0.4968	6.9194	1.1486	3.0384	n.a.
520 – 550	DI	68.5538	0.4578	5.0876	0.5634	2.0952	0.3614

Table A.23 Lourdes Drill cuttings: Duplicates for GW batch reactor

Drill cuttings Sections m	Avg. EC µs/cm	Avg. SC µs/cm	Avg. pH	Avg. ORP mV	Avg. Ag/AgCl mV	Average F mg/L	Avg. Temp °C
100 – 120	617	667	8.4	165	364	12.62	21.1
200 – 220	601	650	8.5	164	363	14.82	21.1
300 – 320	606	653	8.5	167	366	16.38	21.2
400 – 420	619	666	8.6	166	365	16.4	21.3
500 – 520	615	662	8.6	164	363	16.78	21.3

Table A.24 Lourdes Drill Cuttings physicochemical parameters.

Water type	EC µs/cm	SC µs/cm	pH	F mg/L	Temp °C	DO mg/L
GW – LS-0178	207.9	541	8.0	16	20.9	9
DI Water	5.33	2	7.2	BDL	22.1	7

Table A.25 Major anion analysis of pH adjusted batch reactor.

Sample ID	F (mg/L)	Cl (mg/L)	NO_2 (mg/L)	Br (mg/L)	NO_3 (mg/L)	PO_4 (mg/L)	SO_4 (mg/L)
1-1A 25 hr	0.6139	145.7596	0.206	0.1547	42.442	n.a.	35.1889
1-2A 25 hr	0.6364	142.1002	0.2207	0.1565	39.4142	n.a.	35.4943
2-1A 25 hr	0.6425	55.4794	0.1395	0.168	170.782	n.a.	36.7295
2-2A 25 hr	0.6971	60.4003	0.1879	0.1675	78.1201	n.a.	36.9207
2-3A 25 hr	0.7945	38.2694	0.2168	0.1686	72.6672	n.a.	36.5252
3-1A 25 hr	0.8535	13.5671	0.3161	0.162	34.6179	n.a.	36.6031
3-2A 25 hr	0.7752	20.6343	0.3439	0.1609	30.7748	0.3795	33.5822
3-3A 25 hr	0.8607	14.6738	0.3754	0.1667	27.6535	0.3822	36.5683
1-1L 25 hr	1.0415	172.2539	0.3726	0.2196	44.8887	0.0687	41.3525
1-2L 25 hr	0.9523	147.6919	0.6601	0.2104	166.6316	0.4139	41.2488
1-3L 25 hr	1.031	171.3386	0.4622	0.2104	62.6586	0.2813	41.524
2-1L 25 hr	1.2519	40.1354	0.4189	0.2242	70.1554	0.1492	43.6492
2-2L 25 hr	1.2393	30.6328	0.4202	0.221	164.4638	0.2802	43.804
2-3L 25 hr	1.2579	56.5722	0.3286	0.2187	55.4987	0.064	43.4075
3-1L 25 hr	1.2976	14.5483	0.2607	0.2142	34.3148	0.0485	42.9743
3-2L 25 hr	1.2905	14.4839	0.2498	0.2191	47.7181	0.0067	43.2229
3-3L 25 hr	1.4007	14.9868	0.428	0.2279	149.8969	0.2915	44.6109
1-1A 50 hr	0.5735	186.1752	0.5198	0.1572	41.2893	n.a.	35.1369
1-2A 50 hr	0.601	190.0187	0.4829	0.1625	47.1814	n.a.	35.9829
2-1A 50 hr	0.7229	59.6758	0.3507	0.1661	175.372	n.a.	38.4759
2-2A 50 hr	0.791	66.5363	1.0874	0.168	82.5021	n.a.	38.8394
2-3A 50 hr	0.8586	49.0755	0.8062	0.1667	76.4221	n.a.	37.5888
3-1A 50 hr	0.9504	14.8168	1.0686	0.177	42.9806	n.a.	37.6901
3-2A 50 hr	0.8507	23.2274	1.0395	0.1643	46.462	n.a.	36.192
3-3A 50 hr	0.9287	16.7079	1.0502	0.1664	35.4514	n.a.	37.3183
1-1L 50 hr	1.0417	259.0082	0.7286	0.2215	45.6043	n.a.	43.2586
1-2L 50 hr	1.033	222.5084	1.0791	0.226	184.9259	0.0201	43.4788
1-3L 50 hr	1.0472	257.0842	0.5369	0.2225	64.9396	n.a.	43.2501
2-1L 50 hr	1.3635	62.2539	1.0752	0.2421	71.7976	n.a.	46.2408
2-2L 50 hr	1.307	47.5739	1.9922	0.2374	180.0734	n.a.	46.246

2-3L 50 hr	1.3897	75.643	0.813	0.2223	55.7681	n.a.	44.4399
3-1L 50 hr	1.4656	13.5998	1.0339	0.1885	30.3856	n.a.	39.5872
3-2L 50 hr	1.5635	14.3934	1.8796	0.189	47.4563	n.a.	39.7717
3-3L 50 hr	1.4789	14.5277	1.1501	0.192	145.4974	n.a.	39.8626
1-1A 100 hr	0.5607	n.a.	0.4694	0.177	43.6768	0.1821	33.4835
1-2A 100 hr	0.5636	n.a.	0.6053	0.1782	49.5603	0.1811	34.0439
2-1A 100 hr	0.7121	58.9669	0.3385	0.1892	150.6909	0.2149	36.442
2-2A 100 hr	0.7593	64.593	0.965	0.1825	69.3883	0.1979	37.0481
2-3A 100 hr	0.7655	58.2145	0.8596	0.181	69.7957	0.2305	36.1672
3-1A 100 hr	0.9502	15.519	2.5109	0.1824	46.5103	0.1776	34.8904
3-2A 100 hr	0.8122	20.3503	1.8579	0.1829	52.7258	0.3052	33.9806
3-3A 100 hr	0.9304	17.9582	2.1979	0.1862	43.0273	0.5841	35.7416
1-1L 100 hr	0.945	n.a.	3.2083	0.1802	24.2442	0.1621	36.2456
1-2L 100 hr	0.9315	n.a.	1.0018	0.1766	152.249	0.2196	36.4152
1-3L 100 hr	0.9386	n.a.	1.1582	0.1842	49.0587	0.2116	36.4063
2-1L 100 hr	1.1999	69.3951	2.898	0.1977	49.8412	0.2031	39.002
2-2L 100 hr	1.2246	49.2866	1.4324	0.1902	151.7663	0.1835	39.3511
2-3L 100 hr	1.2085	76.8113	1.9776	0.1862	42.0326	n.a.	38.5315
3-1L 100 hr	1.3698	13.7982	3.8033	0.1865	12.9736	n.a.	38.2077
3-2L 100 hr	1.4304	14.0664	3.0199	0.1792	41.1741	0.1799	36.705
3-3L 100 hr	1.3345	13.9855	11.3766	0.1702	95.0803	0.1945	35.9089
1-1A 150 hr	0.5831	n.a.	1.4184	0.1831	41.5228	0.2339	35.2881
1-2A 150 hr	0.5905	n.a.	2.738	0.1806	45.1108	n.a.	35.5258
2-1A 150 hr	0.7294	73.0253	0.281	0.1994	147.6854	n.a.	38.686
2-2A 150 hr	0.7996	77.446	0.4712	0.1844	64.1359	n.a.	38.8056
2-3A 150 hr	0.8344	72.6793	0.8337	0.2009	66.3563	n.a.	38.52
3-1A 150 hr	0.9947	16.7767	3.6963	0.198	47.1439	n.a.	36.4156
3-2A 150 hr	0.8477	20.9152	2.4563	0.1924	57.9963	n.a.	35.558
3-3A 150 hr	0.9431	19.4618	3.4315	0.1902	42.5421	n.a.	36.6614
1-1L 150 hr	0.9019	n.a.	0.8512	0.1792	12.9855	n.a.	36.2891
1-2L 150 hr	0.9359	n.a.	2.5003	0.1778	129.8672	n.a.	36.8693
1-3L 150 hr	0.8909	n.a.	2.4299	0.1836	34.3713	n.a.	36.176

2-1L 150 hr	1.096	75.425	6.151	0.1626	22.479	n.a.	36.8266
2-2L 150 hr	1.1417	58.0642	1.0872	0.1732	120.734	n.a.	37.5304
2-3L 150 hr	1.1185	83.0928	5.1905	0.169	23.4481	0.1488	37.1395
3-1L 150 hr	1.2654	13.6174	2.0667	0.167	6.032	0.1735	36.1695
3-2L 150 hr	1.3361	13.3824	2.6479	0.1616	23.1199	0.1685	34.9573
3-3L 150 hr	1.2651	14.2358	26.249	0.1406	5.7101	n.a.	33.787
1-1A 200 hr	0.5316	n.a.	3.6006	0.16	28.9406	n.a.	33.5019
1-2A 200 hr	0.552	n.a.	7.9485	0.1557	25.7025	n.a.	33.7421
2-1A 200 hr	0.6763	72.169	0.2758	0.2056	112.1993	0.2719	36.3636
2-2A 200 hr	0.789	78.8768	0.4144	0.1637	51.3172	n.a.	37.1351
2-3A 200 hr	0.7438	75.1334	0.8086	0.1912	53.3469	0.3367	36.4288
3-1A 200 hr	0.9233	15.388	4.6383	0.1751	38.7123	n.a.	34.2256
3-2A 200 hr	0.8131	19.2622	2.7691	0.1826	51.155	n.a.	34.2953
3-3A 200 hr	0.9031	18.7707	5.1795	0.1678	36.2299	n.a.	35.3063
1-1L 200 hr	0.7888	n.a.	1.0978	0.1574	2.4583	n.a.	33.8113
1-2L 200 hr	0.8514	n.a.	1.4593	0.1625	95.1257	0.154	34.5627
1-3L 200 hr	0.7992	n.a.	7.2703	0.1559	9.7597	n.a.	34.181
2-1L 200 hr	1.1046	91.1417	2.1272	0.1723	7.6703	n.a.	37.7188
2-2L 200 hr	1.117	68.5989	3.7955	0.1781	86.1326	n.a.	37.7055
2-3L 200 hr	1.0705	95.3401	4.5036	0.1682	4.027	n.a.	36.5631
3-1L 200 hr	1.2229	13.8486	0.8667	0.1705	2.4139	n.a.	36.4108
3-2L 200 hr	1.3126	13.636	4.3922	0.1597	6.7054	n.a.	35.2418
3-3L 200 hr	1.2693	14.9566	0.3704	0.1639	1.9507	n.a.	34.2645

Table A.26 Major cation result from pH adjusted batch reactor

Sample ID	Na (mg/L)	NH_4 (mg/L)	K (mg/L)	Mg (mg/L)	Ca (mg/L)	Sr (mg/L)
1-1A 50 hr	116.5184	n.a.	4.1889	3.1723	29.3892	n.a.
1-2A 50 hr	119.75	n.a.	4.0292	2.9979	28.6848	n.a.
2-1A 50 hr	126.0316	n.a.	4.1231	2.9221	24.1012	n.a.
2-2A 50 hr	120.0392	n.a.	3.9239	2.6907	21.604	n.a.
2-3A 50 hr	113.3044	n.a.	3.714	2.3546	17.9147	n.a.
3-1A 50 hr	118.5868	n.a.	3.3786	1.9504	15.3267	n.a.
3-2A 50 hr	120.9276	n.a.	3.6407	2.0056	16.4574	n.a.
3-3A 50 hr	121.4524	n.a.	3.4782	1.9066	15.246	n.a.
1-1L 50 hr	118.188	n.a.	18.411	1.9078	35.78	n.a.
1-2L 50 hr	121.4724	n.a.	19.7969	7.5298	47.4384	n.a.
1-3L 50 hr	121.794	n.a.	19.7016	6.8676	38.2096	n.a.
2-1L 50 hr	118.0952	n.a.	15.9404	4.0253	22.4736	n.a.
2-2L 50 hr	116.9828	n.a.	17.7379	4.7561	27.8876	n.a.
2-3L 50 hr	118.3644	n.a.	16.5155	3.9676	21.8216	n.a.
3-1L 50 hr	115.6864	n.a.	13.3227	1.9838	10.0303	n.a.
3-2L 50 hr	123.2712	n.a.	14.1992	2.0824	10.6931	n.a.
3-3L 50 hr	137.7048	n.a.	16.2991	3.3544	18.1036	n.a.
1-1A 100 hr	121.566	n.a.	4.6574	3.6638	36.3228	n.a.
1-2A 100 hr	125.8552	1.2122	4.5842	3.5239	36.6644	n.a.
2-1A 100 hr	138.7288	n.a.	4.267	2.9689	31.4632	n.a.
2-2A 100 hr	121.3164	n.a.	4.0956	2.7807	24.0844	n.a.
2-3A 100 hr	117.4512	n.a.	3.7683	2.4586	21.8156	n.a.
3-1A 100 hr	120.7365	n.a.	3.754	1.7755	15.0032	n.a.
3-2A 100 hr	129.3248	n.a.	3.8055	2.0832	16.7699	n.a.
3-3A 100 hr	125.488	n.a.	3.7031	1.9281	17.9862	n.a.
1-1L 100 hr	125.0356	n.a.	21.81	9.525	53.3428	0.8748
1-2L 100 hr	124.1976	n.a.	23.1162	11.4292	64.6268	n.a.
1-3L 100 hr	128.4856	n.a.	23.0506	10.8251	61.6732	0.9203
2-1L 100 hr	123.8216	n.a.	18.4002	5.3547	30.45	n.a.

2-2L 100 hr	120.632	n.a.	19.3811	6.0367	33.1792	n.a.
2-3L 100 hr	121.3812	n.a.	18.8624	5.2819	29.1292	n.a.
3-1L 100 hr	123.1844	n.a.	13.1766	2.0675	10.5785	n.a.
3-2L 100 hr	137.58	n.a.	12.4136	1.4432	6.3694	n.a.
3-3L 100 hr	154.48	1.6064	14.4894	2.2166	9.5011	n.a.
1-1A 150 hr	122.2676	n.a.	4.3147	4.1954	45.5148	n.a.
1-2A 150 hr	128.8876	n.a.	4.8609	4.1134	46.664	n.a.
2-1A 150 hr	129.3012	n.a.	4.3674	3.0955	30.1256	n.a.
2-2A 150 hr	122.1408	n.a.	4.3035	3.0233	28.074	n.a.
2-3A 150 hr	119.1072	n.a.	4.1186	2.8823	24.8088	n.a.
3-1A 150 hr	129.1484	n.a.	4.1155	2.082	18.5792	n.a.
3-2A 150 hr	128.9744	n.a.	3.9971	2.3231	19.8476	n.a.
3-3A 150 hr	131.0076	n.a.	4.1093	2.2365	20.0132	n.a.
1-1L 150 hr	120.4644	n.a.	22.8344	11.7895	72.6816	n.a.
1-2L 150 hr	117.9248	n.a.	23.555	13.2387	82.8312	n.a.
1-3L 150 hr	116.7248	n.a.	23.567	12.4488	74.6616	2.5841
2-1L 150 hr	118.716	n.a.	18.8923	6.448	34.0796	1.452
2-2L 150 hr	118.9052	n.a.	19.147	6.8493	37.0568	1.5527
2-3L 150 hr	120.3984	n.a.	18.7222	6.0894	32.2124	1.4193
3-1L 150 hr	127.3068	n.a.	13.6084	2.2806	11.4487	n.a.
3-2L 150 hr	133.1756	n.a.	13.2014	1.9247	9.3042	n.a.
3-3L 150 hr	149.2608	n.a.	14.8617	2.5442	12.181	n.a.
1-1A 200 hr	108.1876	n.a.	4.9155	4.6746	51.2724	n.a.
1-2A 200 hr	123.32	n.a.	4.8941	4.5187	50.7796	n.a.
2-1A 200 hr	122.7536	n.a.	4.3342	3.4115	30.0036	n.a.
2-2A 200 hr	113.9428	n.a.	4.2702	3.3424	27.12	n.a.
2-3A 200 hr	114.7852	n.a.	3.912	3.1883	27.026	n.a.
3-1A 200 hr	130.4328	n.a.	3.9103	2.3364	18.6528	n.a.
3-2A 200 hr	131.632	n.a.	4.0347	2.6324	18.6388	n.a.
3-3A 200 hr	133.8476	n.a.	4.1785	2.5527	21.2308	n.a.
1-1L 200 hr	113.9168	n.a.	23.4635	14.075	89.3756	3.0827
1-2L 200 hr	112.5972	n.a.	18.7891	16.2991	103.2812	n.a.

1-3L 200 hr	111.2936	n.a.	23.5449	14.3809	90.1916	2.6287
2-1L 200 hr	113.1856	n.a.	18.4986	6.8678	36.3856	1.47
2-2L 200 hr	113.0208	n.a.	19.3539	7.4865	39.9664	n.a.
2-3L 200 hr	115.7492	n.a.	19.2673	6.9136	35.744	1.5243
3-1L 200 hr	128.1132	n.a.	13.5769	2.6111	12.3624	0.8198
3-2L 200 hr	135.7832	n.a.	12.9326	2.1782	9.8523	n.a.
3-3L 200 hr	143.9084	n.a.	13.836	2.5093	11.6304	n.a.

Table A.27 Major and trace results from pH-adjusted batch reactor

Sample ID	Al (mg/L)	B (mg/L)	Ba (mg/L)	Be (mg/L)	Ca (mg/L)	Cr (mg/L)	Cu (mg/L)	Fe (mg/L)	K (mg/L)	Mg (mg/L)	Mn (mg/L)	Mo (mg/L)	Na (mg/L)
1-1A-50hr	0.232	2.66	0.004	<0.0001	28.1	<0.005	0.019	0.009	4.06	3.42	0.207	0.019	102
1-1A-100hr	0.282	3.15	0.004	0.0001	36.5	<0.005	0.009	0.007	4.32	3.98	0.302	0.017	109
1-1A-150hr	0.276	3.02	0.005	0.0001	44.4	<0.005	0.009	0.007	4.81	4.64	0.398	0.016	110
1-1A-200hr	0.254	3.18	0.005	<0.0001	51.7	<0.005	0.008	0.029	4.97	5.11	0.493	0.014	109
1-2A-50hr	0.321	3.52	0.003	<0.0001	28.1	<0.005	0.019	0.011	3.92	3.22	0.196	0.02	106
1-2A-100hr	0.301	3.32	0.003	<0.0002	37.4	<0.010	0.015	0.012	4.32	4.03	0.297	0.02	112
1-2A-150hr	0.26	3.56	0.003	<0.0001	44.7	<0.005	0.01	0.011	4.79	4.5	0.386	0.017	114
1-2A-200hr	0.692	3.62	0.004	0.0001	52.3	<0.005	0.009	0.01	5.03	5.26	0.491	0.016	112
2-1A-50hr	0.349	3.74	0.003	<0.0001	23.8	<0.005	0.018	0.01	3.94	3.16	0.127	0.021	111
2-1A-100hr	0.307	3.16	0.003	<0.0002	26.4	<0.010	0.013	0.015	3.98	3.34	0.148	0.022	112
2-1A-150hr	1.09	3.22	0.003	<0.0001	29.3	<0.005	0.018	0.017	4.26	3.58	0.184	0.021	117
2-1A-200hr	0.275	3.33	0.003	<0.0001	31.7	<0.005	0.019	0.011	4.31	3.89	0.197	0.018	114
2-2A-50hr	0.561	3.65	0.004	<0.0001	21.6	<0.005	0.021	0.105	3.77	2.93	0.142	0.022	106
2-2A-100hr	0.249	2.95	0.002	<0.0001	24.1	<0.005	0.013	0.007	3.8	3.15	0.159	0.02	106
2-2A-150hr	0.324	3.72	0.003	<0.0001	26.6	<0.005	0.018	0.007	4.11	3.51	0.172	0.018	107
2-2A-200hr	0.342	3.53	0.003	<0.0001	29	<0.005	0.018	0.01	4.12	3.81	0.187	0.017	106
2-3A-50 hr	0.236	2.76	0.002	<0.0001	18.2	<0.005	0.019	0.008	3.61	2.5	0.103	0.022	101
2-3A-100 hr	0.293	3.11	0.003	<0.0001	22	<0.005	0.016	0.01	3.65	2.86	0.128	0.021	105
2-3A-150 hr	0.304	3.26	0.003	<0.0001	25.1	<0.005	0.014	0.007	3.95	3.25	0.147	0.018	105
2-3A-200 hr	0.314	3.42	0.003	<0.0001	27.8	<0.005	0.014	0.012	3.94	3.54	0.168	0.017	104
3-1A-50 hr	0.276	2.86	0.002	<0.0001	15.8	<0.005	0.011	0.009	3.38	2.11	0.018	0.022	106
3-1A-100 hr	0.317	3.13	0.002	<0.0001	14.5	<0.005	0.012	0.018	3.55	2.01	0.02	0.019	112
3-1A-150 hr	0.324	3.28	0.003	<0.0002	17.9	<0.010	<0.010	0.008	3.84	2.39	0.031	0.019	114
3-1A-200 hr	0.302	3.12	0.002	<0.0001	18.8	<0.005	0.007	0.007	3.89	2.61	0.032	0.016	117

Sample ID	Al (mg/L)	B (mg/L)	Ba (mg/L)	Be (mg/L)	Ca (mg/L)	Cr (mg/L)	Cu (mg/L)	Fe (mg/L)	K (mg/L)	Mg (mg/L)	Mn (mg/L)	Mo (mg/L)	Na (mg/L)
3-2A-50 hr	0.322	3.66	0.003	<0.0001	16.8	<0.005	0.015	0.013	3.46	2.1	0.017	0.02	109
3-2A-100 hr	0.265	2.95	0.003	<0.0001	16.8	<0.005	0.007	0.01	3.77	2.46	0.023	0.015	112
3-2A-150 hr	0.304	3.14	0.003	<0.0002	20.7	<0.010	0.014	0.017	3.87	2.95	0.032	0.014	111
3-2A-200 hr	0.294	3.19	0.002	<0.0001	20.9	<0.005	0.009	0.008	3.97	2.94	0.032	0.012	116
3-3A-50 hr	0.344	3.36	0.002	<0.0001	15.3	<0.005	0.015	0.012	3.27	1.96	0.016	0.022	106
3-3A-100 hr	0.351	3.31	0.003	<0.0001	17.7	<0.005	0.012	0.011	3.52	2.21	0.025	0.02	113
3-3A-150 hr	0.304	3.61	0.003	<0.0001	19.7	<0.005	0.009	0.008	3.9	2.53	0.032	0.018	117
3-3A-200 hr	1.05	3.33	0.003	<0.0001	21.3	<0.005	0.011	0.014	4.11	2.82	0.042	0.015	119
1-1L-50 hr	0.279	2.71	0.057	0.0001	35.3	<0.005	<0.005	0.007	18.8	7.02	0.077	0.013	103
1-1L-100 hr	0.307	3.19	0.076	<0.0001	54.9	<0.005	<0.005	0.009	21.6	10.5	0.098	0.013	110
1-1L-150 hr	0.282	3.14	0.098	<0.0001	75.9	<0.005	<0.005	0.007	23.5	14.1	0.14	0.012	108
1-1L-200 hr	0.317	3.53	0.115	<0.0001	91.9	<0.005	<0.005	0.009	24.2	16.9	0.186	0.012	103
1-2L-100 hr	0.286	3.01	0.088	<0.0001	66.6	<0.005	0.006	0.029	22.9	12.6	0.135	0.013	110
1-2L-150 hr	0.201	2.67	0.104	<0.0001	85.9	<0.005	0.006	0.008	24.2	15.8	0.171	0.012	105
1-2L-200 hr	0.306	3.6	0.121	<0.0002	107	<0.010	<0.010	0.011	24.7	19.4	0.214	0.01	99.2
1-3L-50 hr	0.292	3.1	0.06	<0.0001	39.6	<0.005	<0.005	0.01	20.4	7.79	0.083	0.013	110
1-3L-100 hr	0.288	3.72	0.083	<0.0001	61.7	<0.005	<0.005	0.012	22.8	11.9	0.121	0.013	112
1-3L-150 hr	0.28	3.12	0.098	<0.0001	78	<0.005	<0.005	0.009	24	14.6	0.16	0.011	106
1-3L-200 hr	0.306	3.47	0.11	<0.0002	93.4	<0.010	<0.010	0.009	23.9	17.2	0.2	0.01	97.9
2-1L-50 hr	0.828	3.21	0.037	<0.0001	21.7	<0.005	0.01	0.017	16.6	4.45	0.034	0.015	104
2-1L-100 hr	0.331	3.25	0.044	<0.0001	29.5	<0.005	0.008	0.008	18.4	5.93	0.035	0.014	108
2-1L-150 hr	0.332	3.37	0.05	<0.0001	35.2	<0.005	0.008	0.008	19.2	7	0.044	0.013	107
2-1L-200 hr	0.372	3.69	0.053	<0.0001	38.2	<0.005	0.006	0.009	19.3	7.88	0.05	0.012	103

Sample ID	Al (mg/L)	B (mg/L)	Ba (mg/L)	Be (mg/L)	Ca (mg/L)	Cr (mg/L)	Cu (mg/L)	Fe (mg/L)	K (mg/L)	Mg (mg/L)	Mn (mg/L)	Mo (mg/L)	Na (mg/L)
2-2L-50 hr	<0.001	2.56	0.053	<0.0001	27.7	<0.005	0.012	<0.001	18	5.19	0.059	0.016	101
2-2L-100 hr	0.31	3.18	0.053	<0.0001	33.4	<0.005	0.008	0.008	19	6.63	0.048	0.014	107
2-2L-150 hr	0.324	2.99	0.056	<0.0001	39.2	<0.005	0.008	0.007	20	7.76	0.056	0.014	107
2-2L-200 hr	0.466	3.35	0.058	<0.0001	42.1	<0.005	<0.005	0.009	20.1	8.54	0.062	0.013	103
2-3L-50 hr	1.2	3.12	0.038	<0.0001	21.4	<0.005	0.005	0.012	16.9	4.34	0.037	0.014	104
2-3L-100 hr	0.35	3.65	0.05	<0.0001	32.6	<0.005	0.007	0.009	19.8	6.24	0.043	0.014	118
2-3L-150 hr	0.357	4	0.05	<0.0002	34.1	<0.010	<0.010	0.008	19.2	6.93	0.04	0.014	107
2-3L-200 hr	0.362	3.66	0.054	<0.0001	37.9	<0.005	0.006	0.008	19.8	7.8	0.05	0.013	106
3-1L-50 hr	3.04	2.79	0.019	<0.0001	10.5	<0.005	0.013	0.024	13.3	2.31	0.036	0.015	104
3-1L-100 hr	0.257	2.74	0.018	<0.0001	10.7	<0.005	0.009	0.006	13.1	2.35	0.01	0.015	110
3-1L-150 hr	0.349	3.05	0.019	<0.0001	11.7	<0.005	0.011	0.008	13.5	2.55	0.01	0.013	113
3-1L-200 hr	0.297	3.41	0.021	<0.0001	12.8	<0.005	0.01	0.013	13.7	2.87	0.01	0.012	115
3-2L-50 hr	0.25	2.8	0.018	<0.0001	10.7	<0.005	0.009	0.01	13.5	2.34	0.007	0.017	105
3-2L-100 hr	0.266	2.84	0.012	<0.0001	6.57	<0.005	0.006	0.007	12.1	1.66	0.005	0.016	119
3-2L-150 hr	0.317	2.84	0.017	<0.0001	9.45	<0.005	<0.005	0.1	12.7	2.11	0.009	0.014	117
3-2L-200 hr	0.362	3.58	0.018	<0.0001	10.6	<0.005	0.01	0.019	13.1	2.35	0.009	0.014	122
3-3L-50 hr	0.308	2.92	0.028	<0.0001	17.6	<0.005	0.008	0.009	15.8	3.68	0.017	0.014	119
3-3L-100 hr	0.32	2.93	0.017	<0.0001	9.7	<0.005	0.015	0.008	14	2.53	0.008	0.012	138
3-3L-150 hr	0.31	3.24	0.021	<0.0001	12.5	<0.005	0.012	0.008	14.6	2.9	0.011	0.012	136
3-3L-200 hr	0.639	3.39	0.019	<0.0001	12.5	<0.005	0.013	0.009	14.3	2.83	0.014	0.011	133

Sample ID	Ni (mg/L)	P (mg/L)	S (mg/L)	Si (mg/L)	Sr (mg/L)	V (mg/L)	Zn (mg/L)
1-1A-50hr	0.003	0.39	11.9	50.8	0.032	0.006	0.048
1-1A-100hr	0.003	0.45	11.6	51	0.031	<0.005	0.05
1-1A-150hr	0.005	0.46	11.7	50.7	0.036	<0.005	0.064
1-1A-200hr	0.006	0.47	11.6	50.8	0.039	<0.005	0.064
1-2A-50hr	0.002	0.42	11.9	50.3	0.0292	0.006	0.064
1-2A-100hr	0.006	0.49	12.2	50.1	0.0318	<0.010	0.08
1-2A-150hr	0.005	0.49	11.8	50	0.0359	<0.005	0.102
1-2A-200hr	0.005	0.49	11.6	51.7	0.0395	<0.005	0.106
2-1A-50hr	0.002	0.23	12.5	51.4	0.0278	0.01	0.026
2-1A-100hr	<0.004	0.29	13	50.2	0.0246	<0.010	0.021
2-1A-150hr	0.003	0.21	12.8	51	0.0242	0.009	0.028
2-1A-200hr	0.003	0.28	12.8	51	0.0267	0.01	0.033
2-2A-50hr	0.003	0.31	12.5	51.8	0.0252	0.011	0.017
2-2A-100hr	0.004	0.3	12.4	50.2	0.0221	0.01	0.027
2-2A-150hr	0.004	0.32	12.6	51.4	0.0243	0.01	0.021
2-2A-200hr	0.004	0.34	12.8	52	0.0256	0.011	0.02
2-3A-50 hr	<0.002	0.3	12.6	50.3	0.0213	0.012	0.012
2-3A-100 hr	<0.002	0.34	12.4	50.3	0.021	0.011	0.034
2-3A-150 hr	0.002	0.37	12.6	51.3	0.0231	0.01	0.024
2-3A-200 hr	0.003	0.36	12.5	51.1	0.0241	0.01	0.026
3-1A-50 hr	<0.002	0.85	12.6	48.8	0.0187	0.016	0.004
3-1A-100 hr	0.005	1.24	11.9	46.7	0.0157	0.015	0.011
3-1A-150 hr	<0.004	1.41	12.4	48.2	0.0192	0.015	0.012
3-1A-200 hr	0.002	1.5	11.7	48.3	0.0193	0.015	0.012

Sample ID	Ni (mg/L)	P (mg/L)	S (mg/L)	Si (mg/L)	Sr (mg/L)	V (mg/L)	Zn (mg/L)
3-2A-50 hr	<0.002	1.16	12.2	47.9	0.018	0.016	0.018
3-2A-100 hr	0.005	1.7	11.9	48.5	0.0191	0.016	0.021
3-2A-150 hr	<0.004	1.83	11.7	48.6	0.0233	0.015	0.033
3-2A-200 hr	0.003	2.04	11.5	49.8	0.0207	0.014	0.01
3-3A-50 hr	<0.002	1.04	12.3	47.7	0.0176	0.017	0.004
3-3A-100 hr	<0.002	1.54	12.3	47.3	0.0177	0.015	0.02
3-3A-150 hr	0.003	1.7	11.9	47.5	0.0201	0.014	0.017
3-3A-200 hr	<0.002	1.83	11.9	48.5	0.0223	0.014	0.02
1-1L-50 hr	<0.002	0.38	12.2	47.7	0.253	0.019	0.024
1-1L-100 hr	<0.002	0.38	12.2	48.7	0.379	0.017	0.022
1-1L-150 hr	<0.002	0.39	11.8	49.3	0.507	0.014	0.027
1-1L-200 hr	0.005	0.37	11.5	50.3	0.597	0.012	0.027
1-2L-100 hr	<0.002	0.64	12.3	51	0.447	0.015	0.019
1-2L-150 hr	<0.002	0.57	11.8	50.5	0.561	0.013	0.017
1-2L-200 hr	<0.004	0.56	11.6	51.8	0.673	0.011	0.017
1-3L-50 hr	<0.002	0.44	12.5	48.3	0.281	0.019	0.018
1-3L-100 hr	0.003	0.49	12.3	49.2	0.423	0.016	0.039
1-3L-150 hr	0.002	0.45	11.7	49.7	0.52	0.012	0.041
1-3L-200 hr	<0.004	0.44	11.8	50.3	0.595	0.011	0.033
2-1L-50 hr	<0.002	0.34	13	47.9	0.163	0.03	0.007
2-1L-100 hr	<0.002	0.43	13.1	46.9	0.219	0.03	0.009
2-1L-150 hr	0.002	0.4	12.9	47.3	0.257	0.028	0.011
2-1L-200 hr	0.002	0.41	12.6	48.7	0.28	0.026	0.014

Sample ID	Ni (mg/L)	P (mg/L)	S (mg/L)	Si (mg/L)	Sr (mg/L)	V (mg/L)	Zn (mg/L)
2-2L-50 hr	<0.002	0.33	13	49.1	0.192	0.028	0.015
2-2L-100 hr	0.003	0.46	13	48.3	0.241	0.028	0.036
2-2L-150 hr	0.017	0.44	13	48.7	0.283	0.028	0.016
2-2L-200 hr	<0.002	0.44	12.7	49.5	0.303	0.026	0.015
2-3L-50 hr	<0.002	0.29	12.9	46.6	0.16	0.029	0.004
2-3L-100 hr	<0.002	0.39	14.3	50.8	0.234	0.033	0.027
2-3L-150 hr	<0.004	0.4	12.9	47.9	0.252	0.03	0.017
2-3L-200 hr	<0.002	0.41	12.7	48.5	0.276	0.027	0.013
3-1L-50 hr	<0.002	0.24	12.9	44.5	0.0822	0.041	0.006
3-1L-100 hr	<0.002	0.37	12.9	42	0.0848	0.046	0.011
3-1L-150 hr	<0.002	0.36	12.5	41.9	0.0925	0.047	0.011
3-1L-200 hr	0.004	0.35	12.1	42.3	0.102	0.047	0.017
3-2L-50 hr	<0.002	0.3	12.9	43.4	0.0848	0.043	0.003
3-2L-100 hr	0.002	0.35	12.4	40.6	0.0572	0.052	0.026
3-2L-150 hr	<0.002	0.35	11.9	40.2	0.0769	0.05	0.014
3-2L-200 hr	0.002	0.35	12.1	41.8	0.0841	0.051	0.009
3-3L-50 hr	<0.002	0.4	12.7	43.3	0.137	0.034	<0.002
3-3L-100 hr	0.004	0.46	11.9	40.4	0.084	0.041	0.016
3-3L-150 hr	<0.002	0.48	12	41.2	0.1	0.043	0.023
3-3L-200 hr	0.009	0.41	11.8	41.1	0.0961	0.047	0.02

Table A.28 Trace element data for the pH adjusted batch reactors.

Sample ID	Li µg/L	Be µg/L	B µg/L	Al µg/L	Mn µg/L	Co µg/L	Ni µg/L	Cu µg/L	Zn µg/L	Sr µg/L	Mo µg/L	Ag µg/L	Cd µg/L
1-1A-50hr	123.373	0.106	2681.777	208.833	177.530	1.015	3.121	17.018	42.872	32.378	18.398	0.009	0.207
1-2A-50hr	124.596	0.092	3504.122	286.256	169.908	1.207	3.174	19.488	58.272	29.961	20.367	0.007	0.206
2-1A-50hr	129.130	0.020	3651.011	310.654	110.463	0.484	2.869	17.126	25.388	28.546	22.100	0.014	0.136
2-2A-50hr	131.423	0.038	3727.935	474.728	125.819	0.643	2.416	17.991	17.847	26.390	21.873	0.020	0.131
2-3A-50 hr	122.449	0.016	2692.739	210.749	88.503	0.382	1.665	17.095	12.941	21.949	21.324	0.009	0.117
3-1A-50 hr	117.897	0.007	2761.425	243.269	15.851	0.085	0.973	11.982	6.631	19.322	21.703	0.015	0.075
3-2A-50 hr	119.121	0.005	3619.026	283.142	15.311	0.088	1.096	14.039	18.387	18.881	19.306	0.032	0.073
3-3A-50 hr	121.909	0.007	3390.861	300.794	14.552	0.087	0.988	12.583	6.429	18.528	22.062	0.022	0.071
1-1L-50 hr	108.786	0.022	2691.928	270.038	69.949	0.360	2.005	7.821	24.337	260.268	13.633	0.016	0.061
1-2L-50 hr	116.482	0.030	3150.087	321.530	100.937	0.500	2.442	8.954	33.083	318.605	13.048	0.024	0.070
1-3L-50 hr	115.579	0.016	3061.653	280.392	73.516	0.332	1.904	5.979	18.137	289.425	13.160	0.013	0.060
2-1L-50 hr	109.099	0.004	3299.520	337.143	24.905	0.133	1.014	10.996	8.103	168.061	14.946	0.016	0.051
2-2L-50 hr	111.569	0.004	2651.482	1.661	54.490	0.223	1.249	16.069	25.553	207.686	14.542	0.006	0.059
2-3L-50 hr	112.007	0.006	3348.083	359.702	25.671	0.110	1.020	9.053	6.464	170.923	15.309	0.009	0.052
3-1L-50 hr	99.585	0.004	2972.525	467.923	7.436	0.050	0.850	12.428	7.774	87.797	15.371	0.009	0.040
3-2L-50 hr	98.547	0.002	2914.928	237.452	6.465	0.065	0.827	11.063	5.611	90.145	16.867	0.011	0.054
3-3L-50 hr	105.412	0.006	3002.271	295.387	15.436	0.085	0.776	11.501	3.899	145.186	14.129	0.010	0.044
1-1A-100hr	131.095	0.075	3285.132	273.800	265.836	1.160	4.596	10.615	48.837	34.400	17.591	0.008	0.274
1-2A-100hr	131.175	0.077	3286.107	280.673	252.039	1.608	5.891	12.042	71.789	33.621	18.635	0.008	0.255
2-1A-100hr	137.565	0.016	3215.396	293.964	128.938	0.537	3.221	15.325	21.932	26.594	20.942	0.007	0.110
2-2A-100hr	137.411	0.019	3212.641	239.470	138.972	0.536	2.892	16.721	27.626	24.863	20.391	0.039	0.115
2-3A-100 hr	127.782	0.010	3150.587	279.859	112.783	0.429	2.264	15.689	33.285	23.445	19.736	0.028	0.115
3-1A-100 hr	128.769	0.005	3373.630	310.285	19.005	0.134	4.337	11.552	11.544	17.930	19.653	0.025	0.057
3-2A-100 hr	119.840	0.002	3030.145	254.693	19.652	0.095	4.194	11.601	18.881	21.192	14.922	0.022	0.050
3-3A-100 hr	125.254	0.006	3346.999	322.330	22.608	0.104	1.128	12.582	20.949	19.571	19.867	0.023	0.054
1-1L-100 hr	126.536	0.014	3311.509	311.848	88.271	0.363	2.859	4.458	22.626	421.311	13.360	0.037	0.045
1-2L-100 hr	128.260	0.009	3060.801	294.483	118.798	0.477	3.082	6.910	20.096	494.422	12.972	0.027	0.054
1-3L-100 hr	128.333	0.014	3811.043	291.681	106.702	0.419	4.840	5.917	37.962	468.304	12.653	0.019	0.054

2-1L-100 hr	117.065	0.003	3314.569	312.650	31.337	0.137	1.649	9.667	11.224	241.905	14.228	0.061	0.038
2-2L-100 hr	120.312	0.003	3288.980	304.735	43.929	0.162	4.205	9.288	35.685	268.739	14.731	0.040	0.042
2-3L-100 hr	114.874	0.002	3403.524	326.993	35.219	0.137	1.832	9.247	26.077	237.597	14.483	0.074	0.042
3-1L-100 hr	98.874	0.002	2863.644	246.709	8.936	0.052	1.458	12.160	12.116	92.862	15.068	0.024	0.044
3-2L-100 hr	93.906	0.002	2988.188	253.661	4.516	0.038	1.453	9.658	24.748	62.547	15.759	0.035	0.041
3-3L-100 hr	97.384	0.001	3050.510	311.980	7.145	0.050	3.004	11.613	15.497	92.108	13.078	0.012	0.038
1-1A-150hr	129.658	0.086	3094.628	268.113	343.007	1.330	5.351	8.606	58.844	39.583	15.664	0.014	0.373
1-2A-150hr	131.482	0.045	3654.150	252.038	331.903	1.991	5.945	9.845	93.362	39.562	16.820	0.013	0.348
2-1A-150hr	141.564	0.012	3405.198	365.668	153.953	0.676	3.846	15.885	26.852	26.958	19.956	0.011	0.133
2-2A-150hr	139.206	0.010	4070.513	309.860	151.588	0.524	2.938	15.829	21.547	27.388	17.989	0.014	0.101
2-3A-150 hr	133.605	0.017	3409.977	294.788	128.775	0.406	2.532	13.865	22.476	25.855	17.736	0.016	0.127
3-1A-150 hr	127.280	0.010	3402.602	306.930	27.559	0.117	1.469	11.042	13.159	21.020	17.553	0.009	0.046
3-2A-150 hr	123.857	0.003	3343.342	298.253	27.584	0.131	1.582	10.970	18.321	22.723	13.573	0.008	0.039
3-3A-150 hr	126.963	0.016	3793.577	290.112	29.346	0.246	2.798	11.732	18.811	22.772	18.433	0.075	0.120
1-1L-150 hr	128.240	0.009	3216.962	286.077	124.193	0.540	3.344	4.244	27.396	564.428	12.470	0.026	0.062
1-2L-150 hr	130.165	0.014	2724.101	220.277	152.460	0.556	3.700	5.533	16.995	624.590	11.860	0.012	0.058
1-3L-150 hr	128.608	0.014	3176.802	295.224	140.608	0.662	4.435	4.478	39.295	573.605	11.231	0.010	0.052
2-1L-150 hr	124.384	0.002	3542.456	321.474	39.802	0.158	2.629	8.449	12.846	286.436	13.250	0.014	0.045
2-2L-150 hr	125.962	0.010	3105.554	319.031	49.917	0.214	15.891	8.361	16.732	311.301	13.484	0.010	0.082
2-3L-150 hr	125.079	n.a.	4431.183	324.109	35.895	0.193	1.644	7.369	17.957	248.249	14.266	0.035	0.053
3-1L-150 hr	102.269	n.a.	3426.162	312.454	9.109	0.063	0.921	10.300	12.299	93.089	14.151	0.018	0.049
3-2L-150 hr	97.021	n.a.	3231.238	285.083	7.613	0.062	1.062	8.394	14.664	77.918	15.207	0.025	0.047
3-3L-150 hr	100.849	n.a.	3575.235	276.260	9.322	0.062	1.241	10.872	21.783	99.443	12.283	0.030	0.037
1-1A-200hr	135.722	0.076	3608.455	238.110	420.229	1.518	6.446	8.248	58.339	40.750	14.232	0.019	0.476
1-2A-200hr	136.746	0.091	4083.576	435.291	423.805	2.563	6.522	9.251	94.337	41.591	15.873	0.012	0.482
2-1A-200hr	143.223	0.011	3778.961	248.089	172.473	2.420	3.841	16.895	30.184	28.127	17.811	0.014	0.138
2-2A-200hr	138.220	0.004	3958.185	304.225	160.574	0.532	2.952	16.307	19.384	26.750	16.337	0.011	0.108
2-3A-200 hr	140.627	0.000	3981.289	283.721	145.111	0.430	2.803	12.841	24.529	25.473	15.992	0.017	0.122
3-1A-200 hr	129.155	n.a.	3542.105	276.816	28.351	0.119	2.155	10.895	13.105	20.710	15.566	0.012	0.062
3-2A-200 hr	126.035	n.a.	3608.467	268.813	28.897	0.148	2.803	10.133	11.206	21.792	12.124	0.003	0.048
3-3A-200 hr	128.996	n.a.	3648.653	541.864	33.023	0.151	2.545	11.895	19.990	23.065	15.566	0.013	0.060
1-1L-200 hr	138.126	0.002	4000.551	318.894	164.835	0.654	7.209	4.239	25.164	617.269	11.308	0.020	0.056

1-2L-200 hr	134.252	0.001	3894.851	316.587	190.254	0.648	5.091	4.581	17.522	702.584	10.581	0.102	0.056
1-3L-200 hr	135.540	0.002	3863.723	305.205	177.166	0.714	4.645	3.757	29.278	624.731	10.420	0.009	0.061
2-1L-200 hr	127.107	0.012	4175.458	334.168	44.627	0.341	2.641	9.239	15.541	299.471	13.310	0.093	0.137
2-2L-200 hr	128.907	0.000	3770.678	418.429	54.187	0.246	2.572	7.778	15.241	319.832	12.847	0.021	0.071
2-3L-200 hr	126.420	n.a.	4097.623	332.335	44.216	0.204	2.354	6.702	13.811	299.136	13.191	0.015	0.053
3-1L-200 hr	107.246	n.a.	4065.874	270.719	9.262	0.068	3.002	8.514	16.981	106.663	13.003	0.017	0.040
3-2L-200 hr	102.243	n.a.	4118.015	320.828	7.547	0.113	1.475	8.222	10.129	88.404	13.992	0.028	0.041
3-3L-200 hr	100.842	n.a.	3872.563	388.501	10.657	0.068	8.507	12.692	19.739	99.291	11.401	0.111	0.038

Table A.29 Trace elements results from the pH adjusted batch reactors.

Sample ID	Sn µg/L	Sb µg/L	Ba µg/L	Tl µg/L	Pb µg/L	Th µg/L	U µg/L	Cr µg/L	Fe µg/L	Ni µg/L	Se µg/L	As µg/L	V µg/L
1-1A-50hr	1.332	0.152	3.256	0.052	0.175	0.017	0.186	1.567	15.375	3.146	1.237	5.990	9.785
1-2A-50hr	0.895	0.134	2.810	0.052	0.214	0.013	0.189	1.667	16.708	3.043	1.192	5.560	8.984
2-1A-50hr	3.340	0.135	2.927	0.051	0.170	0.015	3.893	1.301	15.120	2.889	1.110	6.614	13.401
2-2A-50hr	6.644	0.142	3.883	0.053	0.663	0.075	4.853	1.462	92.950	2.290	1.180	6.960	13.789
2-3A-50 hr	2.341	0.155	2.165	0.044	0.155	0.014	5.039	1.820	12.896	1.661	1.158	7.210	14.754
3-1A-50 hr	9.571	0.135	2.046	0.042	0.214	0.020	6.324	2.441	13.738	0.940	1.064	7.756	17.822
3-2A-50 hr	15.392	0.198	2.353	0.041	0.226	0.021	6.032	2.643	17.125	1.059	1.093	7.545	17.661
3-3A-50 hr	5.455	0.161	2.309	0.038	0.167	0.021	6.459	2.590	14.985	0.974	1.064	7.710	17.613
1-1L-50 hr	2.703	0.240	55.574	0.045	0.121	0.025	0.493	1.553	14.922	2.052	1.061	7.140	19.775
1-2L-50 hr	7.062	0.254	65.953	0.060	0.188	0.026	0.689	1.928	18.088	2.394	1.219	6.774	17.772
1-3L-50 hr	3.079	0.226	55.779	0.049	0.117	0.017	0.522	1.776	16.102	1.845	1.117	6.768	18.341
2-1L-50 hr	21.711	0.241	34.681	0.185	0.139	0.012	4.835	2.182	18.748	0.975	1.116	7.769	26.694
2-2L-50 hr	2.701	0.311	50.340	0.089	0.032	0.013	3.893	1.421	6.893	1.224	1.185	7.737	24.404
2-3L-50 hr	23.085	0.241	37.124	0.063	0.138	0.019	4.968	2.111	12.175	0.974	1.064	7.748	26.961
3-1L-50 hr	43.996	0.257	18.561	0.041	0.167	0.012	5.469	2.390	11.479	0.772	1.143	8.368	34.663
3-2L-50 hr	3.506	0.274	17.293	0.035	0.139	0.010	5.476	2.301	11.905	0.752	1.088	7.897	35.903
3-3L-50 hr	34.883	0.252	27.139	0.038	0.114	0.023	5.548	2.157	12.536	0.741	1.039	8.692	29.983
1-1A-100hr	1.418	0.140	3.685	0.063	0.130	0.019	0.319	1.097	14.316	4.071	1.073	6.254	6.205
1-2A-100hr	1.164	0.143	2.802	0.059	0.141	0.016	0.231	1.283	14.876	5.320	1.117	5.683	5.976

2-1A-100hr	4.837	0.182	2.576	0.056	0.160	0.010	4.867	1.128	15.284	2.962	1.023	6.816	10.498
2-2A-100hr	8.122	0.164	2.283	0.056	0.829	0.009	5.671	1.095	11.606	2.613	1.112	6.917	10.414
2-3A-100 hr	2.858	0.168	2.472	0.049	0.163	0.012	5.274	1.311	13.831	1.992	1.133	6.852	10.967
3-1A-100 hr	4.722	0.164	2.230	0.046	0.251	0.016	6.598	2.359	20.761	3.899	0.973	6.794	14.330
3-2A-100 hr	6.833	0.178	2.056	0.047	0.172	0.009	5.816	2.324	11.442	3.746	1.045	6.759	14.718
3-3A-100 hr	3.089	0.196	2.309	0.042	0.146	0.020	6.638	2.350	13.744	1.072	1.045	6.812	14.208
1-1L-100 hr	2.790	0.252	71.339	0.052	0.179	0.015	1.230	1.207	18.567	2.557	1.050	6.350	15.104
1-2L-100 hr	8.643	0.256	81.223	0.055	0.144	0.012	0.975	1.524	38.293	2.780	1.106	6.049	13.479
1-3L-100 hr	3.763	0.251	75.822	0.051	0.216	0.014	1.291	1.563	22.220	4.323	0.962	5.939	13.547
2-1L-100 hr	19.852	0.295	40.655	0.035	0.099	0.008	4.889	1.398	12.533	1.435	1.109	6.667	23.900
2-2L-100 hr	17.223	0.281	49.490	0.043	0.123	0.010	4.945	1.217	14.295	3.789	1.117	6.691	22.519
2-3L-100 hr	16.540	0.296	42.301	0.037	0.117	0.010	4.982	1.651	13.423	1.687	0.946	6.650	23.781
3-1L-100 hr	20.714	0.319	17.380	0.024	0.132	0.029	5.662	2.169	9.076	1.266	1.072	7.309	35.469
3-2L-100 hr	4.464	0.313	11.227	0.022	0.130	0.017	5.426	2.301	9.139	1.240	1.060	7.140	38.118
3-3L-100 hr	30.113	0.292	16.097	0.027	0.159	0.013	5.551	1.982	9.274	2.638	0.884	8.352	31.314
1-1A-150hr	0.836	0.169	4.546	0.061	0.138	0.016	0.241	1.000	14.840	4.822	0.995	5.977	5.308
1-2A-150hr	1.027	0.155	2.999	0.058	0.210	0.013	0.203	1.378	18.057	5.375	1.039	5.482	5.233
2-1A-150hr	4.676	0.174	2.488	0.054	2.043	0.014	5.270	1.244	15.580	3.417	1.107	6.581	9.291
2-2A-150hr	9.034	0.146	2.433	0.052	0.171	0.007	5.817	1.286	11.891	2.601	1.001	6.802	9.856
2-3A-150 hr	2.986	0.178	2.324	0.055	0.306	0.037	5.432	1.234	11.831	2.208	0.954	6.533	10.045
3-1A-150 hr	2.224	0.165	2.199	0.045	0.194	0.022	6.361	2.206	10.930	1.285	0.953	6.347	12.868
3-2A-150 hr	5.372	0.189	2.210	0.046	0.164	0.014	5.888	2.289	13.412	1.446	0.995	6.302	13.220
3-3A-150 hr	2.266	0.295	2.959	0.120	0.338	0.016	6.555	2.489	16.294	2.575	1.137	6.664	12.843
1-1L-150 hr	7.626	0.259	89.767	0.072	0.171	0.018	1.975	1.050	20.209	3.065	1.052	5.538	12.140
1-2L-150 hr	4.796	0.287	96.356	0.059	0.138	0.017	1.338	1.152	22.182	3.249	0.963	5.610	11.456
1-3L-150 hr	3.372	0.248	89.982	0.054	0.123	0.016	1.237	1.248	21.465	3.904	0.949	5.438	10.861
2-1L-150 hr	16.272	0.304	46.095	0.039	0.130	0.013	5.597	1.333	14.352	2.334	1.065	6.074	21.604
2-2L-150 hr	13.125	0.326	52.237	0.048	0.143	0.048	5.070	1.337	14.187	13.848	1.057	6.132	21.036
2-3L-150 hr	11.225	0.279	46.536	0.041	0.158	0.086	4.994	1.971	14.805	1.656	1.397	6.870	30.905
3-1L-150 hr	14.712	0.320	17.909	0.024	0.124	0.035	5.632	2.232	11.707	0.955	1.276	7.869	47.692
3-2L-150 hr	3.275	0.340	15.843	0.023	0.117	0.032	5.377	2.424	99.409	1.123	1.248	8.629	50.122
3-3L-150 hr	21.209	0.324	18.754	0.025	0.178	0.025	5.675	2.018	12.423	1.313	1.147	9.515	42.993

1-1A-200hr	1.386	0.171	4.700	0.063	0.282	0.027	0.280	1.660	38.708	6.866	1.280	7.058	6.989
1-2A-200hr	1.215	0.141	3.275	0.065	0.236	0.024	0.235	1.261	21.945	6.897	1.427	6.806	6.504
2-1A-200hr	3.544	0.165	2.530	0.054	0.180	0.023	5.097	1.550	18.136	3.969	1.234	8.059	12.095
2-2A-200hr	8.691	0.142	2.469	0.050	0.173	0.022	5.473	1.565	17.144	3.137	1.427	8.604	13.001
2-3A-200 hr	2.463	0.162	2.594	0.050	0.233	0.021	5.167	1.533	19.595	3.021	1.343	7.970	12.893
3-1A-200 hr	1.471	0.190	2.222	0.055	0.167	0.055	5.941	2.418	12.838	2.243	1.295	7.951	16.372
3-2A-200 hr	4.778	0.209	2.149	0.047	0.141	0.033	5.576	2.473	14.426	3.023	1.255	7.957	16.716
3-3A-200 hr	1.991	0.326	2.536	0.045	0.217	0.027	6.007	2.697	18.109	2.672	1.284	8.201	16.502
1-1L-200 hr	1.645	0.221	104.383	0.054	0.128	0.033	1.509	1.154	26.848	6.967	1.192	6.394	14.487
1-2L-200 hr	3.629	0.236	109.480	0.055	0.141	0.032	2.086	1.250	30.771	4.868	1.011	6.200	13.874
1-3L-200 hr	2.405	0.202	99.601	0.052	0.155	0.025	1.190	1.334	26.745	4.615	1.134	6.307	12.574
2-1L-200 hr	14.790	0.355	48.783	0.131	0.415	0.021	5.380	1.850	22.086	2.787	1.421	7.471	25.675
2-2L-200 hr	11.609	0.283	52.232	0.068	0.189	0.019	5.008	1.581	20.081	2.675	1.258	7.344	25.250
2-3L-200 hr	10.078	0.270	49.221	0.046	0.146	0.019	5.218	1.758	16.760	2.419	1.328	7.377	26.000
3-1L-200 hr	13.261	0.301	19.175	0.025	0.179	0.018	5.723	2.010	15.401	3.031	1.278	8.236	41.362
3-2L-200 hr	2.857	0.319	16.377	0.023	0.142	0.020	5.622	2.273	21.506	1.525	1.291	9.650	45.298
3-3L-200 hr	14.542	0.328	17.008	0.025	0.211	0.019	5.928	1.523	12.209	8.831	1.131	10.562	41.323

Table A.30 Control De-ionized water and groundwater used in the pH adjusted reactor.

Sample ID	Li µg/L	Be µg/L	B µg/L	Al µg/L	Mn µg/L	Co µg/L	Ni µg/L	Cu µg/L	Zn µg/L	Sr µg/L	Mo µg/L	Ag µg/L	Cd µg/L	Cd µg/L
DI	0.565	0.003	99.486	2.290	0.053	0.000	0.000	0.001	0.002	0.004	0.001	0.000	0.000	-0.045
RL-2A	98.597	0.004	2891.047	251.243	0.214	0.059	1.169	3.265	16.106	191.625	3.791	0.005	0.026	0.018
	Sn µg/L	Sb µg/L	Ba µg/L	Tl µg/L	Pb µg/L	Pb µg/L	Mn µg/L	Al µg/L	Al µg/L	Cr µg/L	Fe µg/L	Fe µg/L	Ni µg/L	Ni µg/L
DI	0.000	0.000	0.000	0.000	0.000	0.000	0.060	2.327	2.194	0.001	0.001	0.000	0.000	0.000
RL-2A	0.629	0.056	87.957	0.007	0.168	0.170	0.261	249.913	254.615	2.562	9.273	13.467	1.230	0.455
	Se µg/L	Se µg/L	As µg/L	V µg/L										
DI	0.000	0.000	0.001	0.000										
RL-2A	1.017	1.173	7.370	21.827										

Table A.31 Fluorite saturation index calculation for the pH-adjusted batch reactors

Sample ID	Fluorite Saturation Index log(Q/K)	Sample ID	Fluorite Saturation Index log(Q/K)	Sample ID	Fluorite Saturation Index log(Q/K)	Sample ID	Fluorite Saturation Index log(Q/K)
1-1A 25 hr	-1.91009	2-3A 150 hr	-1.58203	3-2L 50 hr	-1.37893	3-3L 200 hr	-1.52244
1-2A 25 hr	-1.89585	3-1A 150 hr	-1.53611	3-3L 50 hr	-1.22468		
2-1A 25 hr	-1.89177	3-2A 150 hr	-1.64936	1-1L 100 hr	-1.17659		
2-2A 25 hr	-1.84466	3-3A 150 hr	-1.55269	1-2L 100 hr	-1.13001		
2-3A 25 hr	-1.78755	1-1A 200 hr	-1.66979	1-3L 100 hr	-1.132		
3-1A 25 hr	-1.74715	1-2A 200 hr	-1.64589	2-1L 100 hr	-1.19031		
3-2A 25 hr	-1.86967	2-1A 200 hr	-1.69208	2-2L 100 hr	-1.14497		
3-3A 25 hr	-1.74836	2-2A 200 hr	-1.59176	2-3L 100 hr	-1.20204		
1-1A 50 hr	-1.86519	2-3A 200 hr	-1.6434	3-1L 100 hr	-1.49174		
1-2A 50 hr	-1.83714	3-1A 200 hr	-1.59757	3-2L 100 hr	-1.67819		
2-1A 50 hr	-1.73025	3-2A 200 hr	-1.71153	3-3L 100 hr	-1.58319		
2-2A 50 hr	-1.68677	3-3A 200 hr	-1.56591	1-1L 150 hr	-1.09892		
2-3A 50 hr	-1.6855	1-1L 25 hr	-1.3781	1-2L 150 hr	-1.03054		
3-1A 50 hr	-1.6515	1-2L 25 hr	-1.40263	1-3L 150 hr	-1.1027		
3-2A 50 hr	-1.72011	1-3L 25 hr	-1.38648	2-1L 150 hr	-1.2217		
3-3A 50 hr	-1.67387	2-1L 25 hr	-1.3362	2-2L 150 hr	-1.15958		
1-1A 100 hr	-1.76422	2-2L 25 hr	-1.28988	2-3L 150 hr	-1.22805		
1-2A 100 hr	-1.7587	2-3L 25 hr	-1.36825	3-1L 150 hr	-1.52739		
2-1A 100 hr	-1.63302	3-1L 25 hr	-1.53047	3-2L 150 hr	-1.57089		
2-2A 100 hr	-1.67469	3-2L 25 hr	-1.46445	3-3L 150 hr	-1.51244		
2-3A 100 hr	-1.70465	3-3L 25 hr	-1.34037	1-1L 200 hr	-1.13888		
3-1A 100 hr	-1.66055	1-1L 50 hr	-1.28216	1-2L 200 hr	-1.03012		
3-2A 100 hr	-1.75548	1-2L 50 hr	-1.19382	1-3L 200 hr	-1.12563		
3-3A 100 hr	-1.6066	1-3L 50 hr	-1.58203	2-1L 200 hr	-1.18842		
1-1A 150 hr	-1.64226	2-1L 50 hr	-1.20558	2-2L 200 hr	-1.1463		
1-2A 150 hr	-1.62415	2-2L 50 hr	-1.16266	2-3L 200 hr	-1.22395		
2-1A 150 hr	-1.63097	2-3L 50 hr	-1.20052	3-1L 200 hr	-1.52476		
2-2A 150 hr	-1.56992	3-1L 50 hr	-1.45544	3-2L 200 hr	-1.56098		

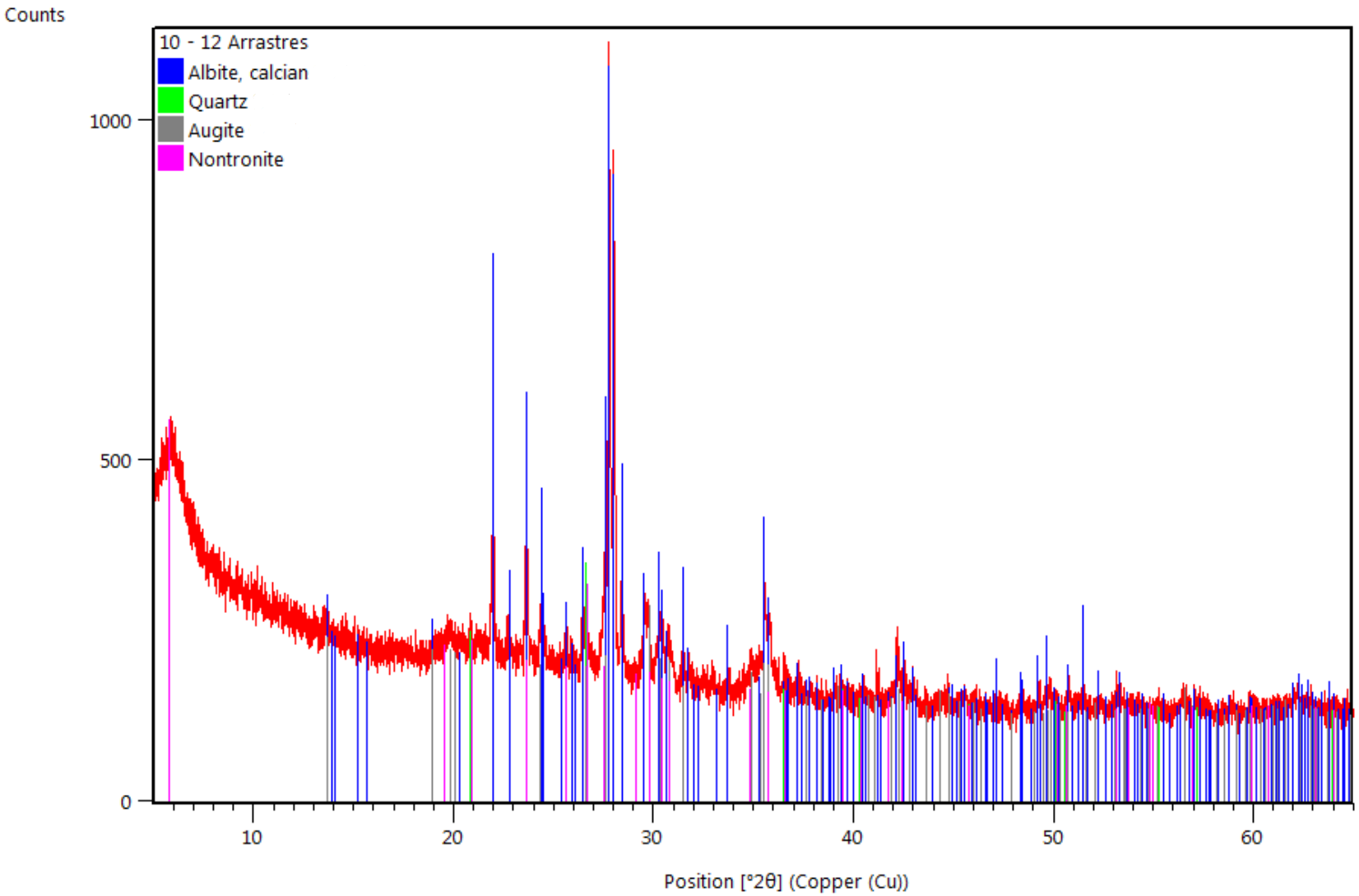

Figure A.32 X-ray diffraction pattern for Arrastres drill cuttings.

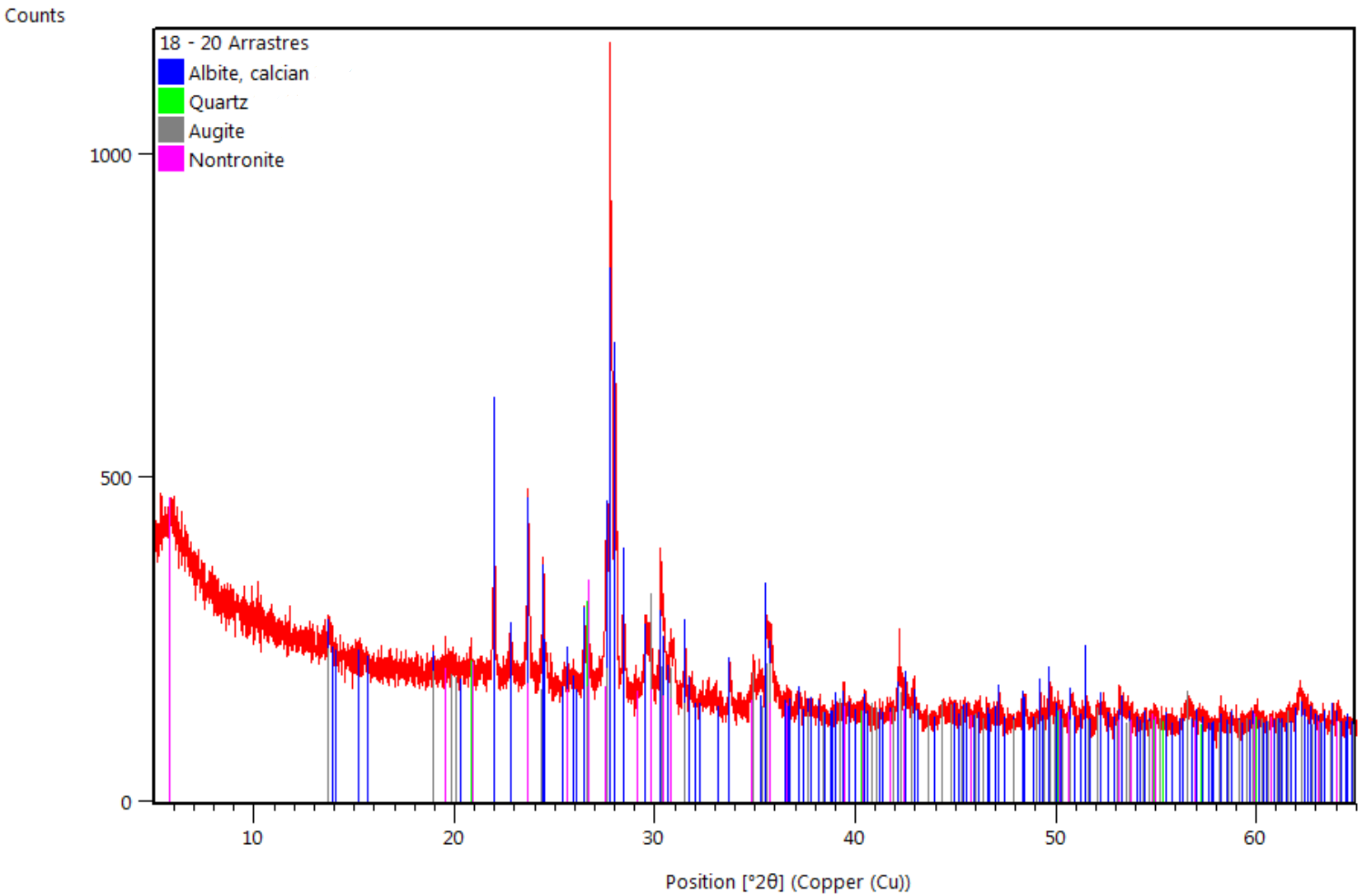

Figure A.33 X-ray diffraction pattern for Arrastres drill cuttings

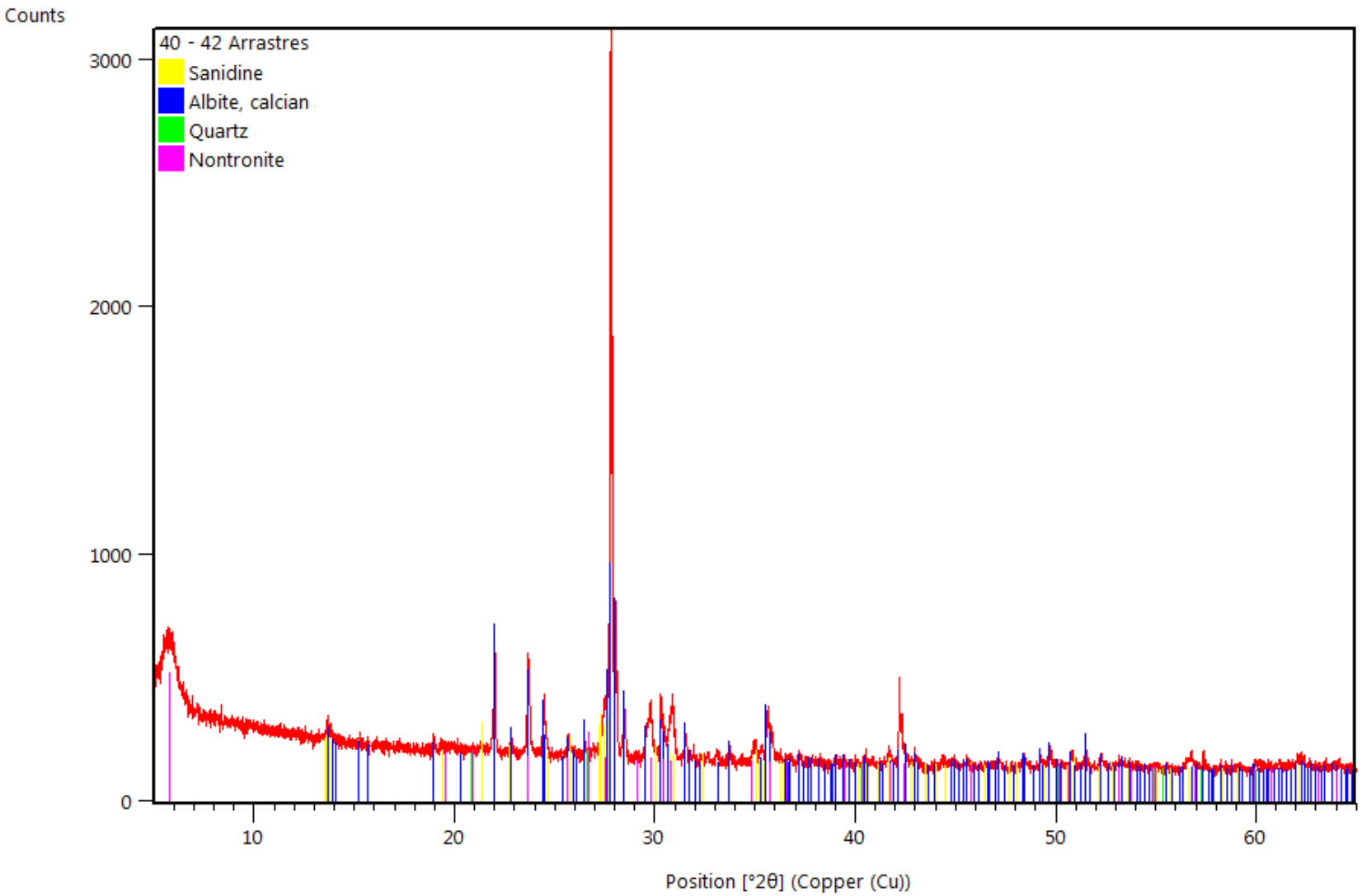

Figure A.34 X-ray diffraction pattern for Arrastres drill cuttings

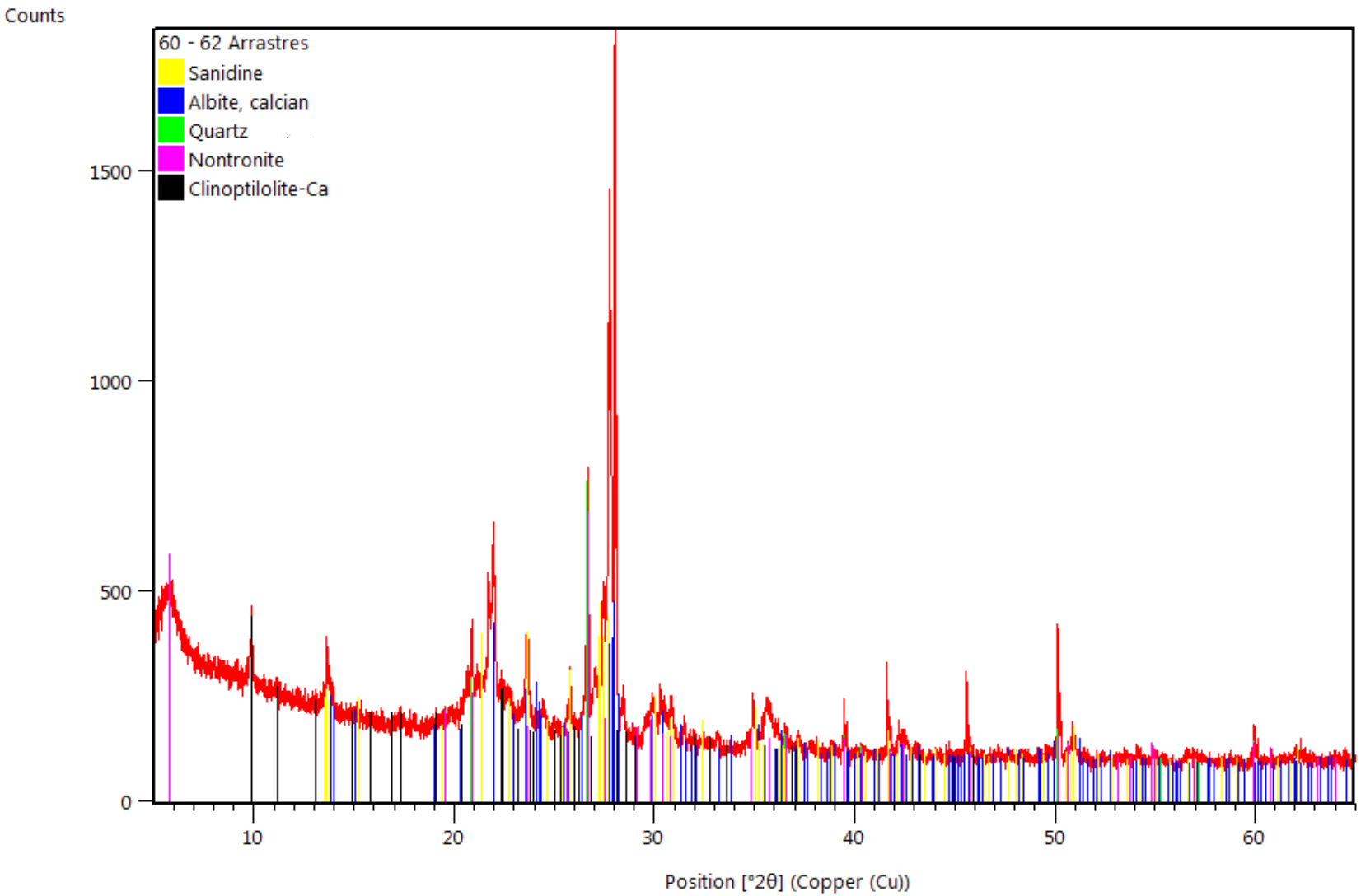

Figure A.35 X-ray diffraction pattern for Arrastres drill cuttings

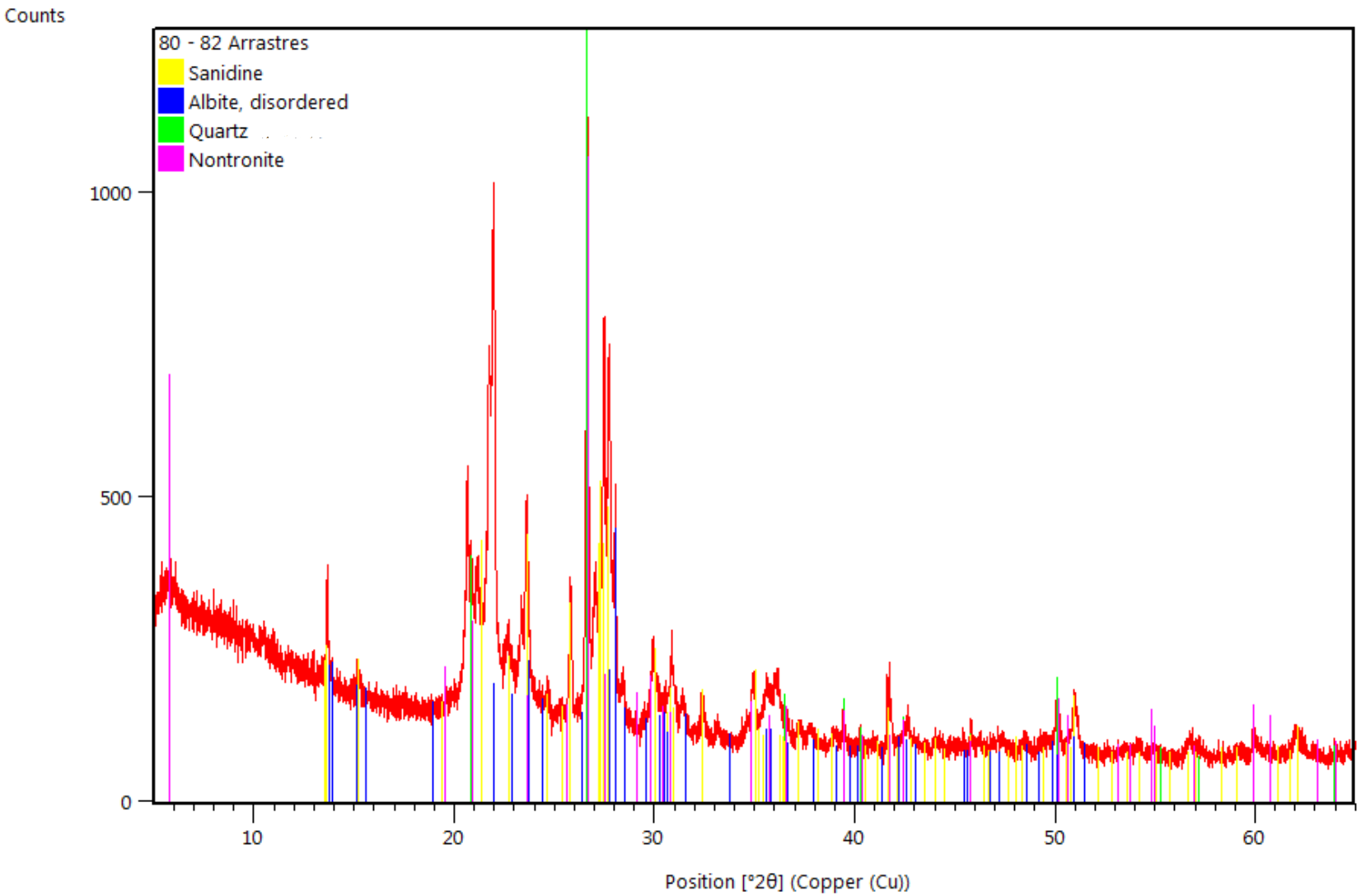

Figure A.36 X-ray diffraction pattern for Arrastres drill cuttings

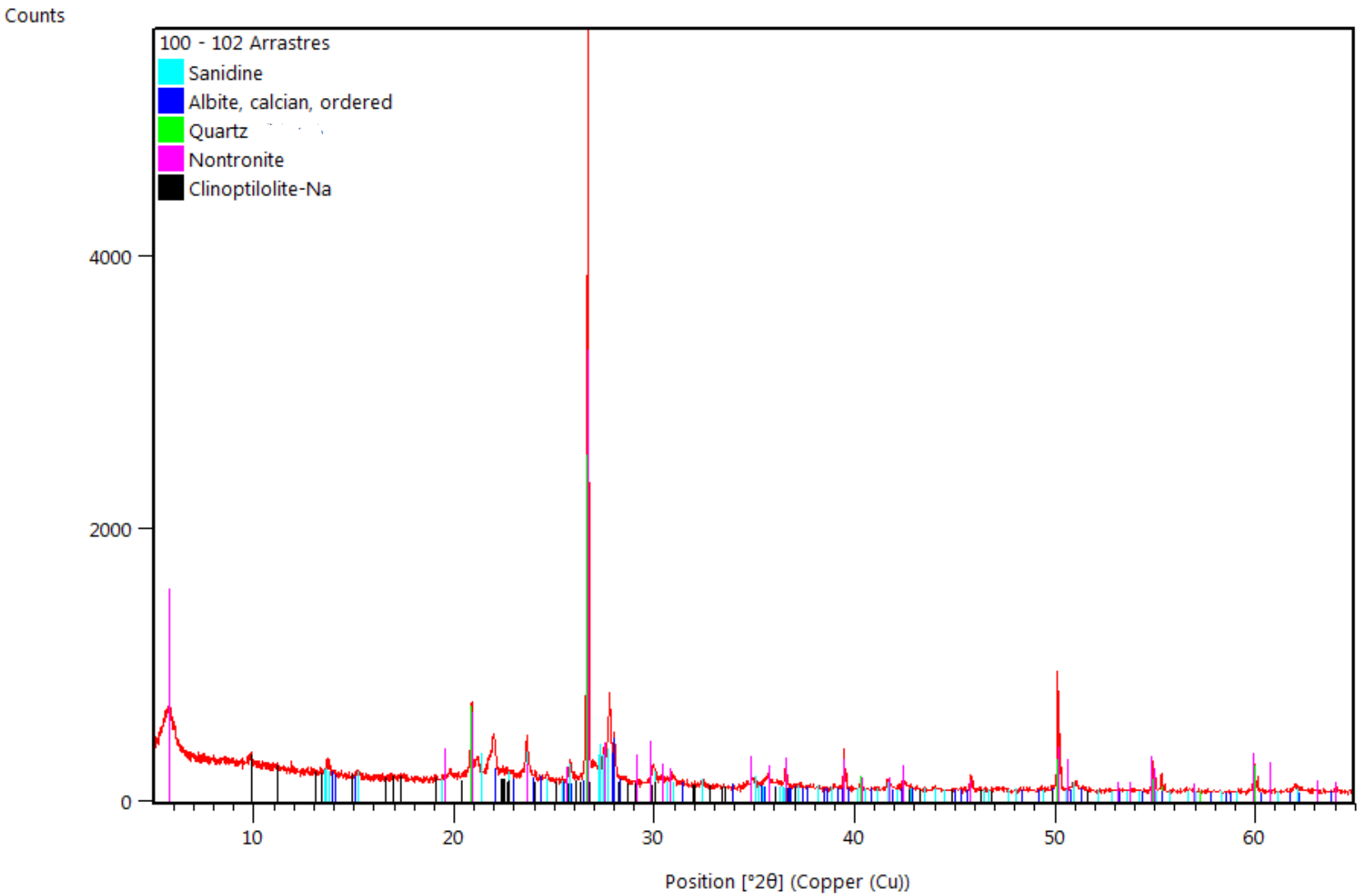

Figure A.37 X-ray diffraction pattern for Arrastres drill cuttings

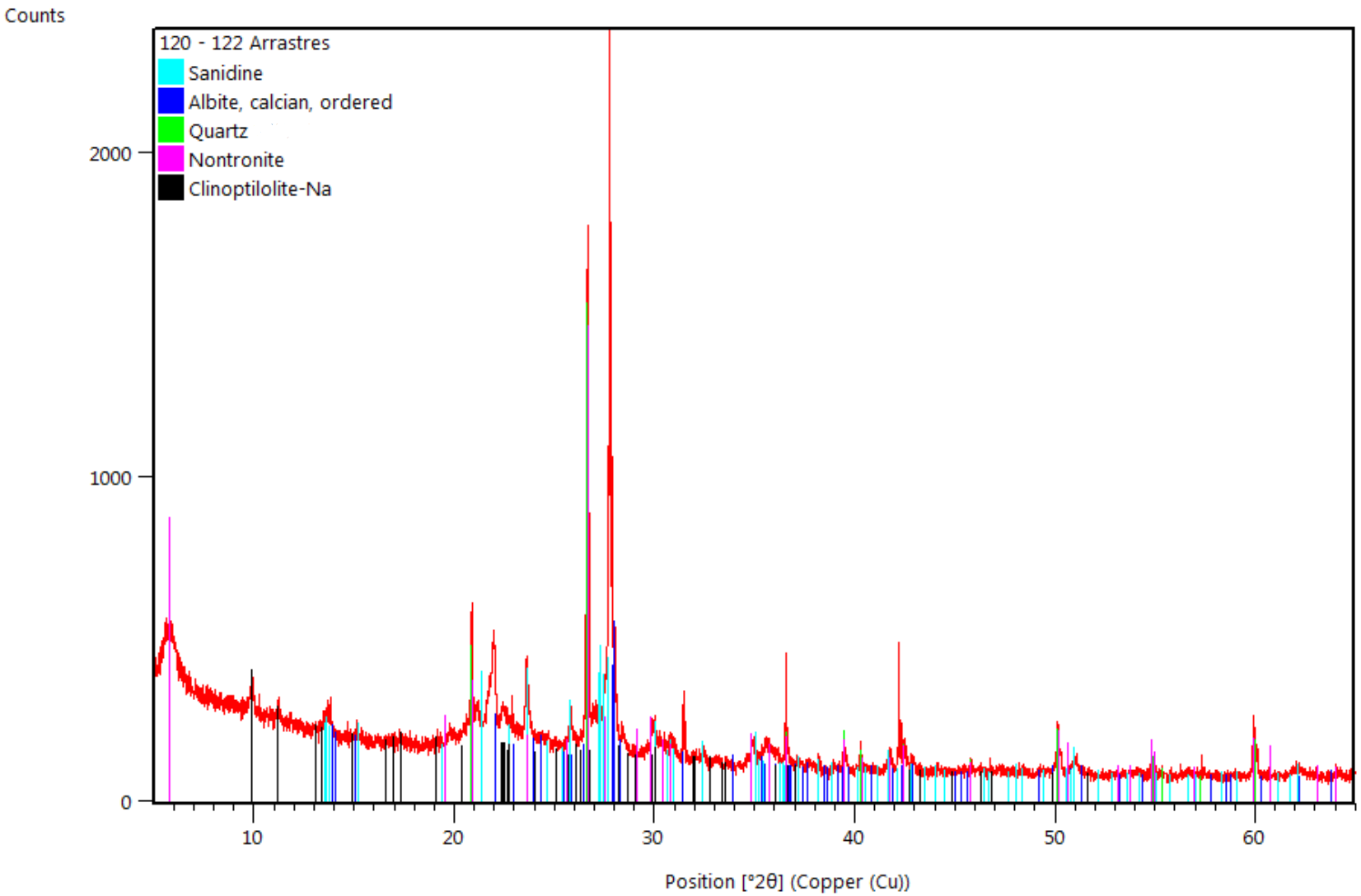

Figure A.38 X-ray diffraction pattern for Arrastres drill cuttings

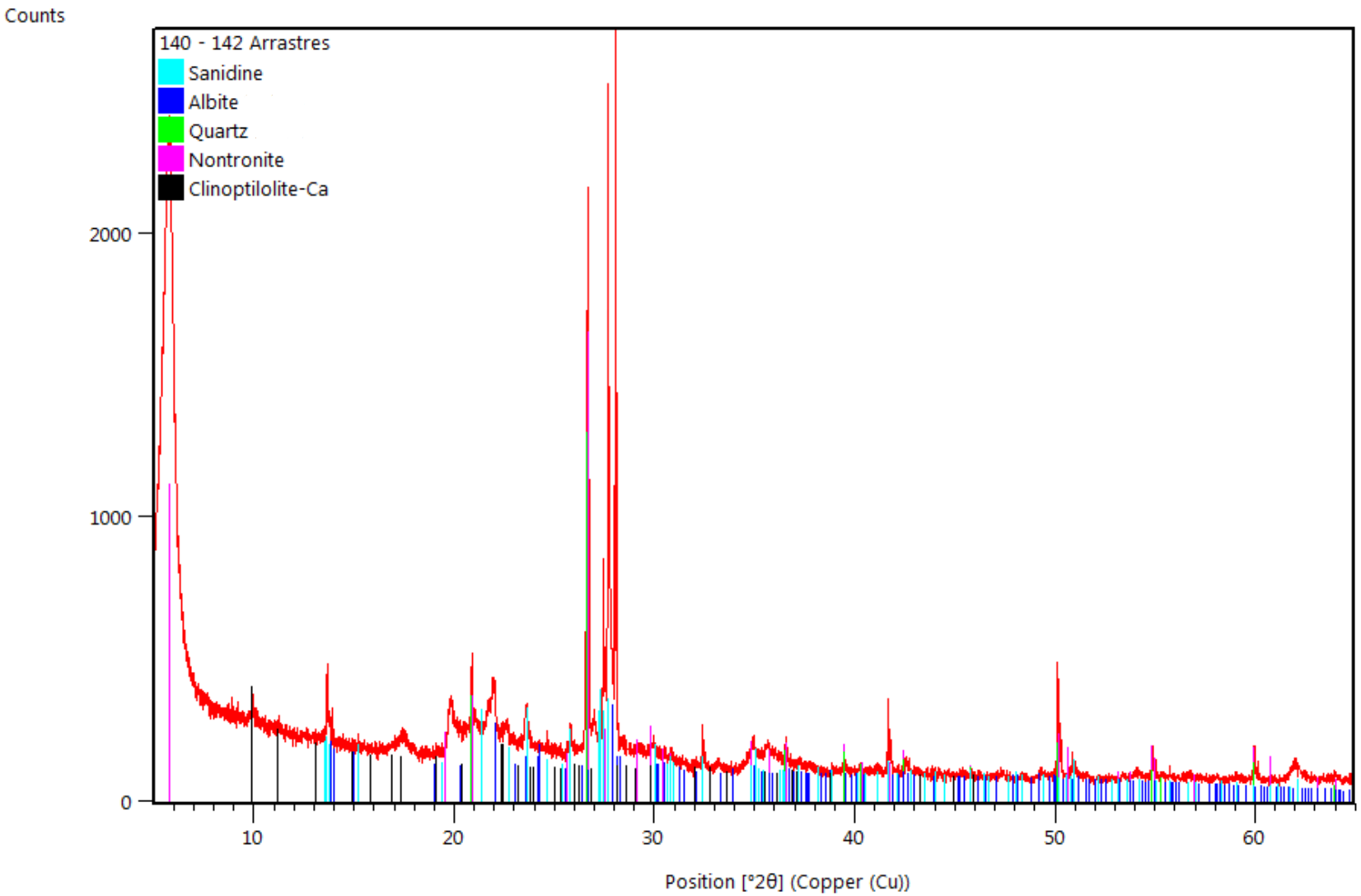

Figure A.39 X-ray diffraction pattern for Arrastres drill cuttings

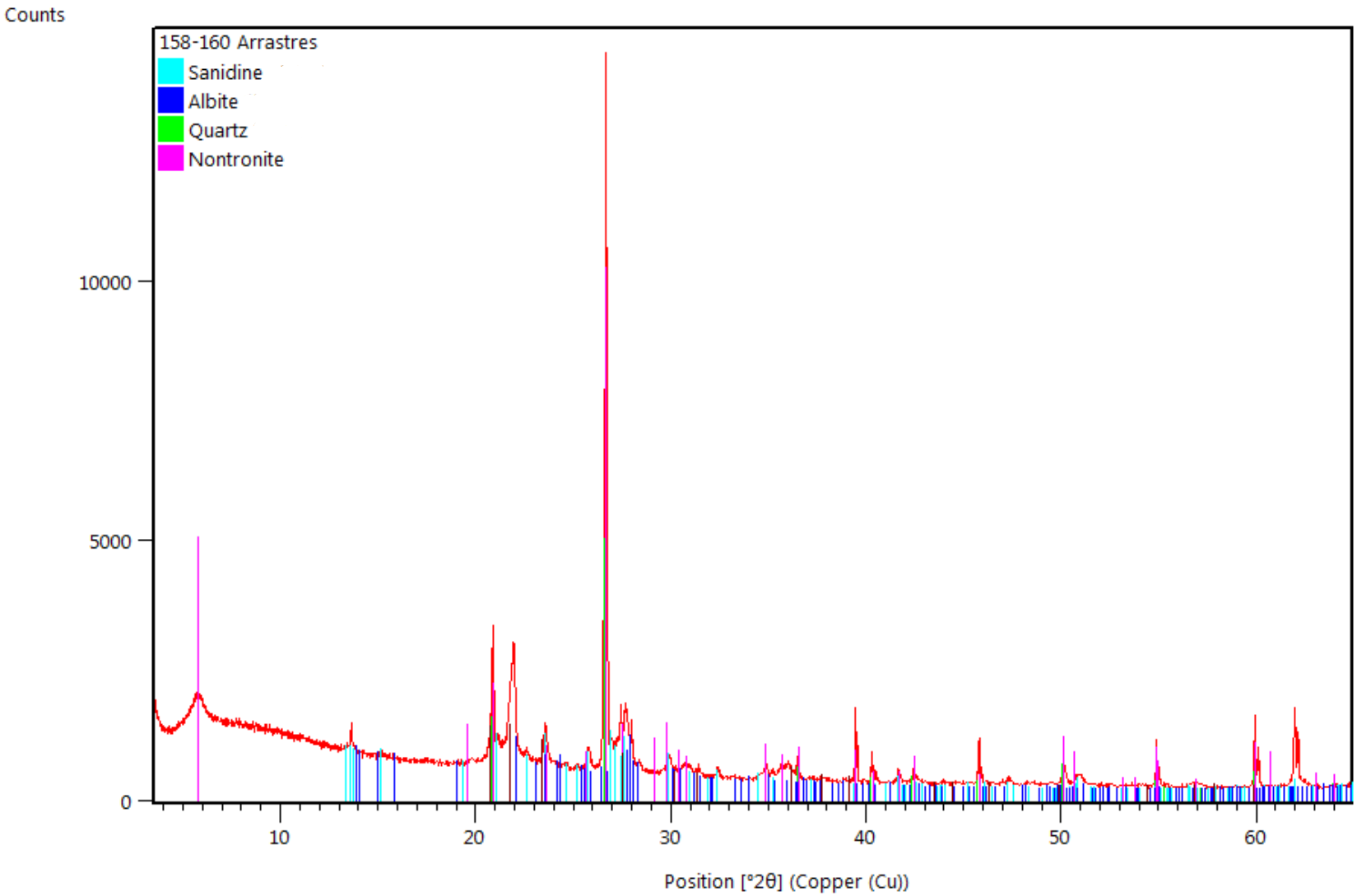

Figure A.40 X-ray diffraction pattern for Arrastres drill cuttings

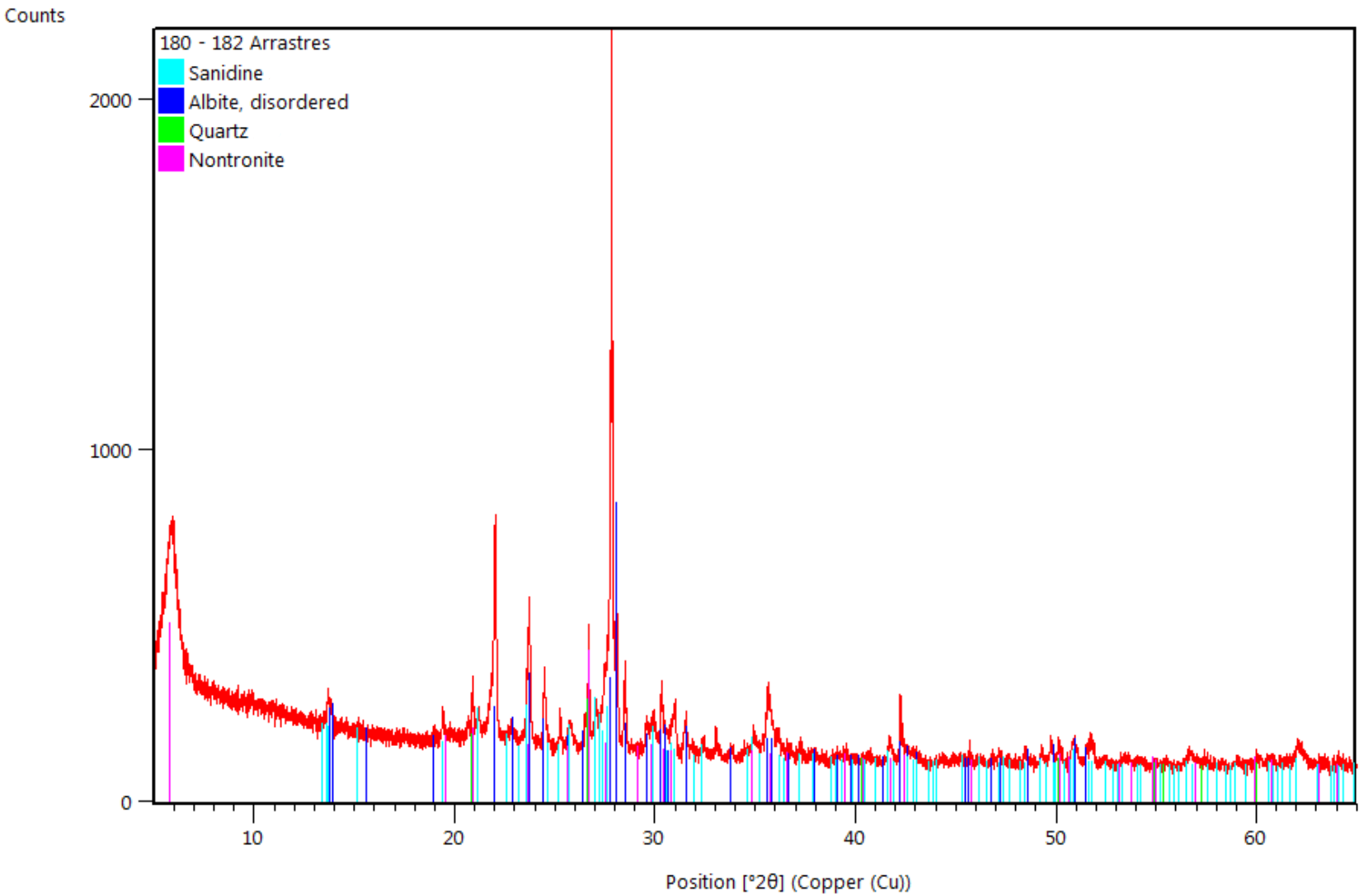

Figure A.41 X-ray diffraction pattern for Arrastres drill cuttings

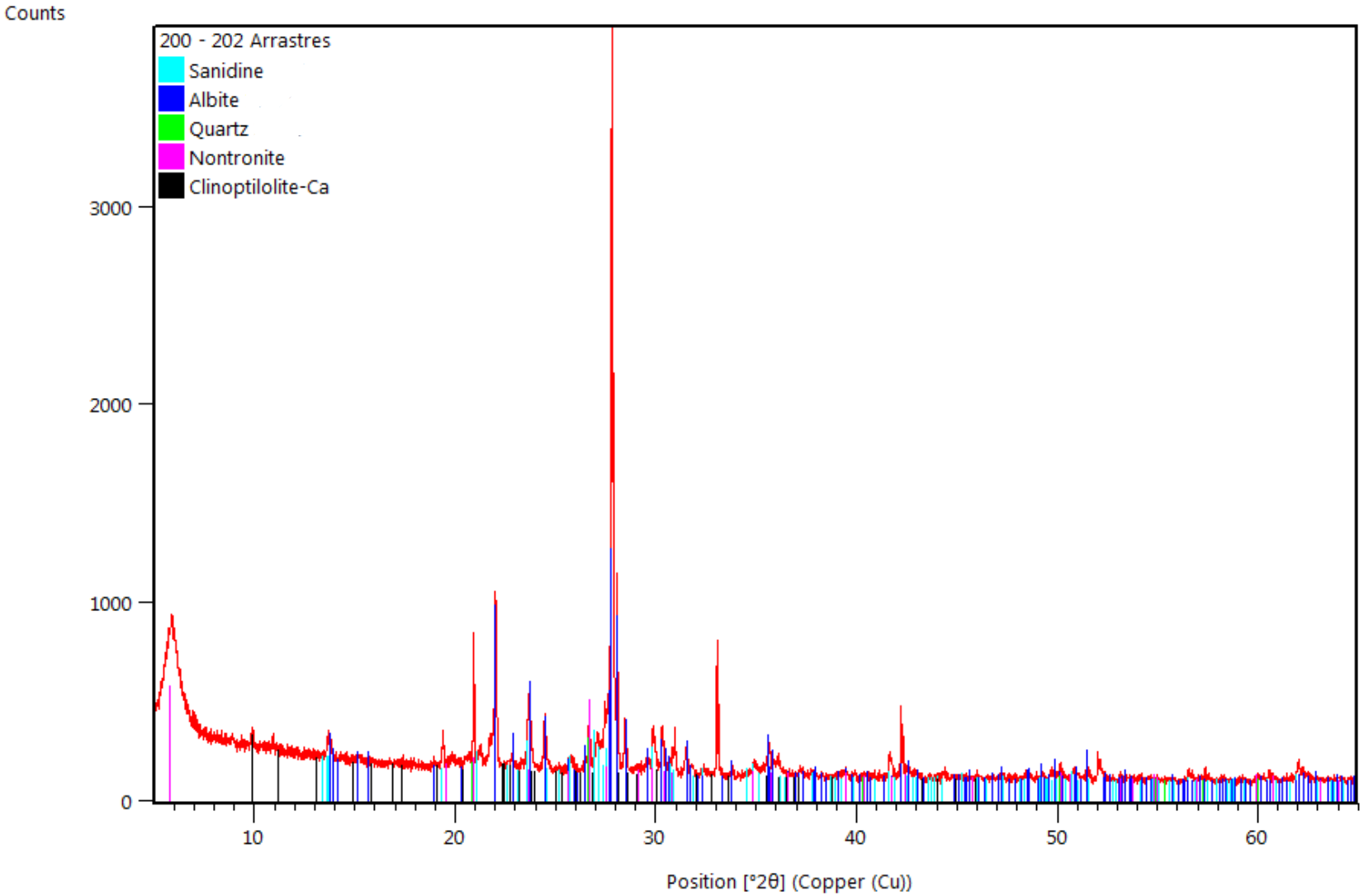

Figure A.42 X-ray diffraction pattern for Arrastres drill cuttings

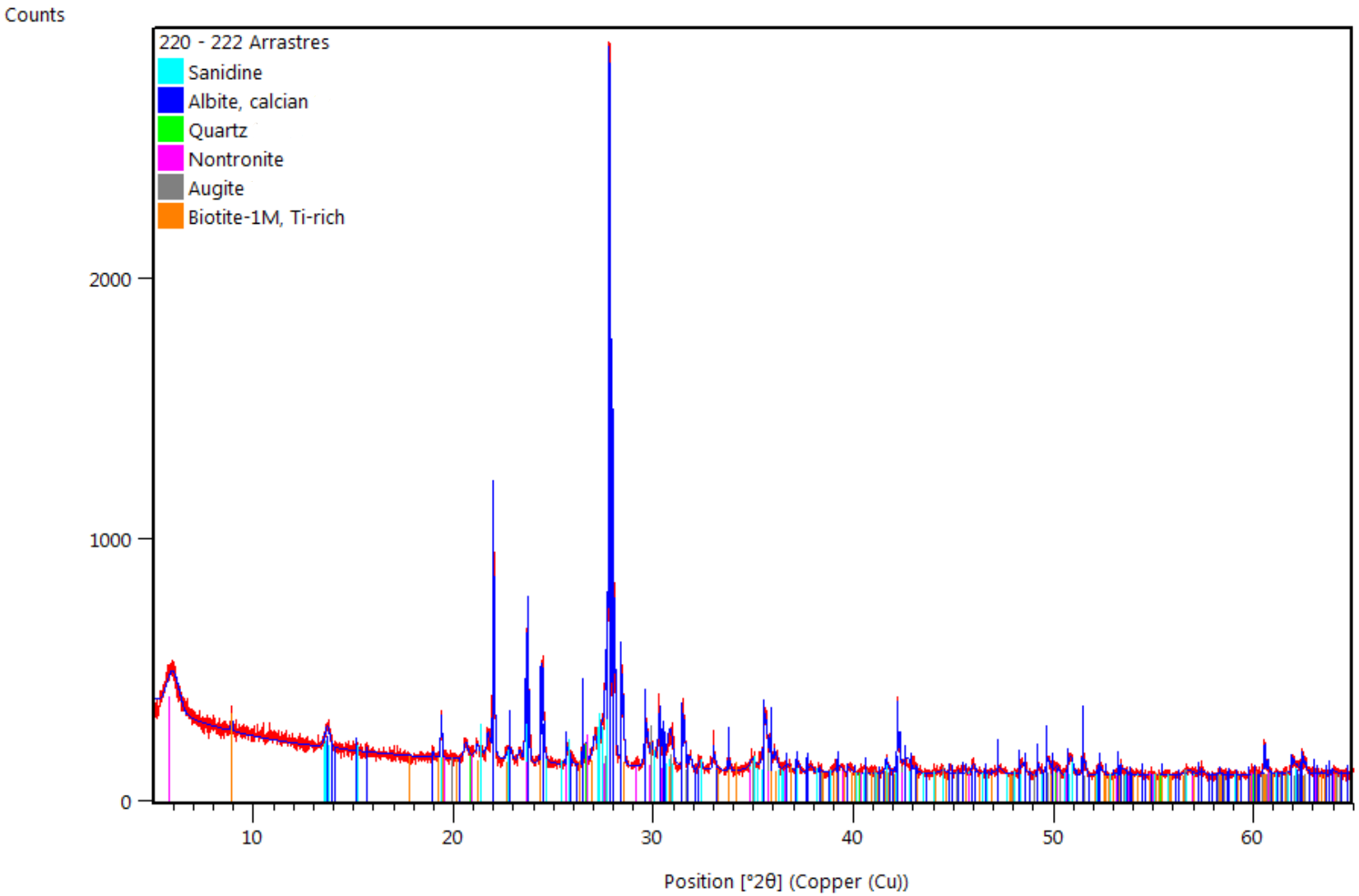

Figure A.43 X-ray diffraction pattern for Arrastres drill cuttings

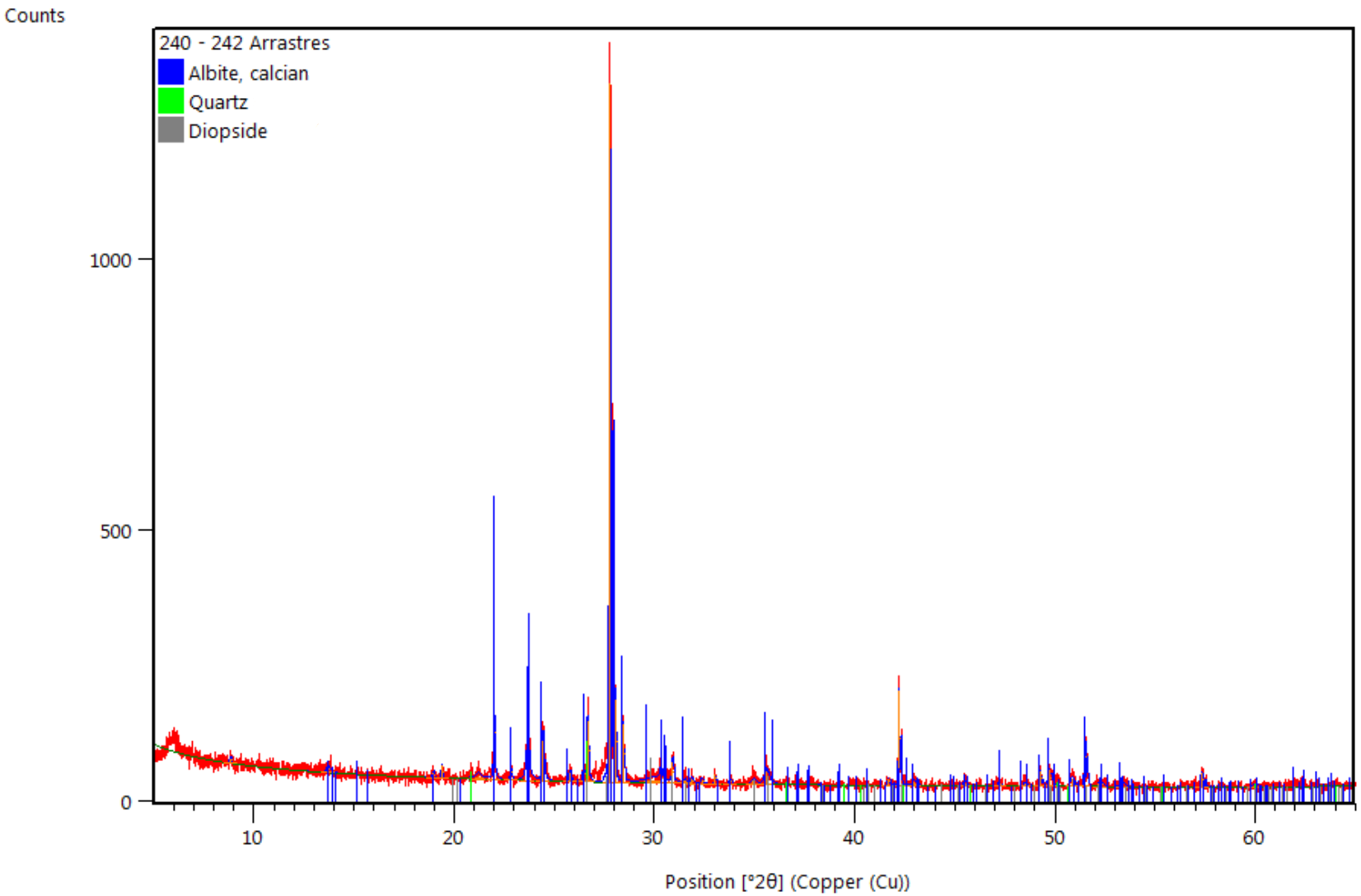

Figure A.44 X-ray diffraction pattern for Arrastres drill cuttings

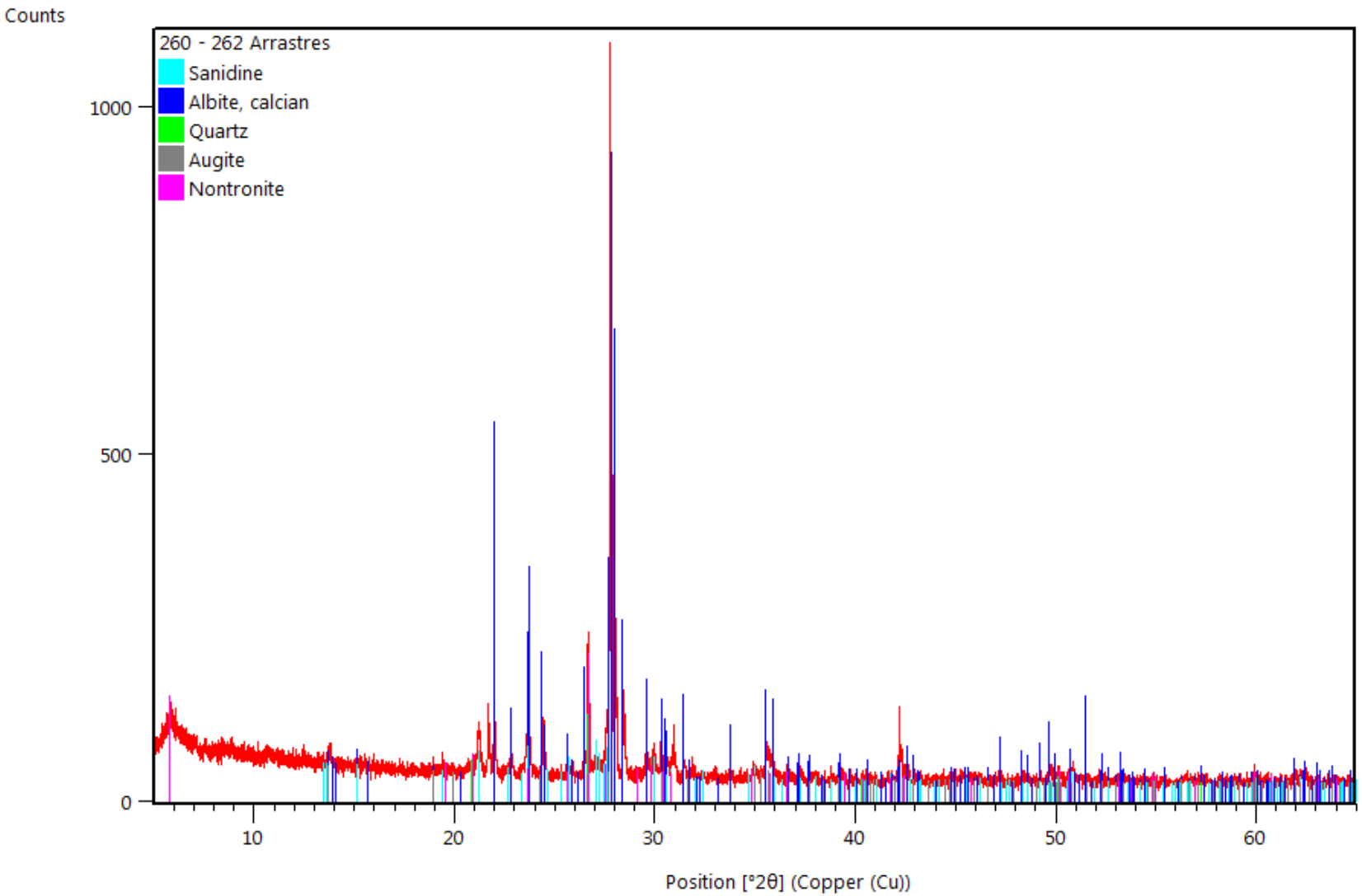

Figure A.45 X-ray diffraction pattern for Arrastres drill cuttings

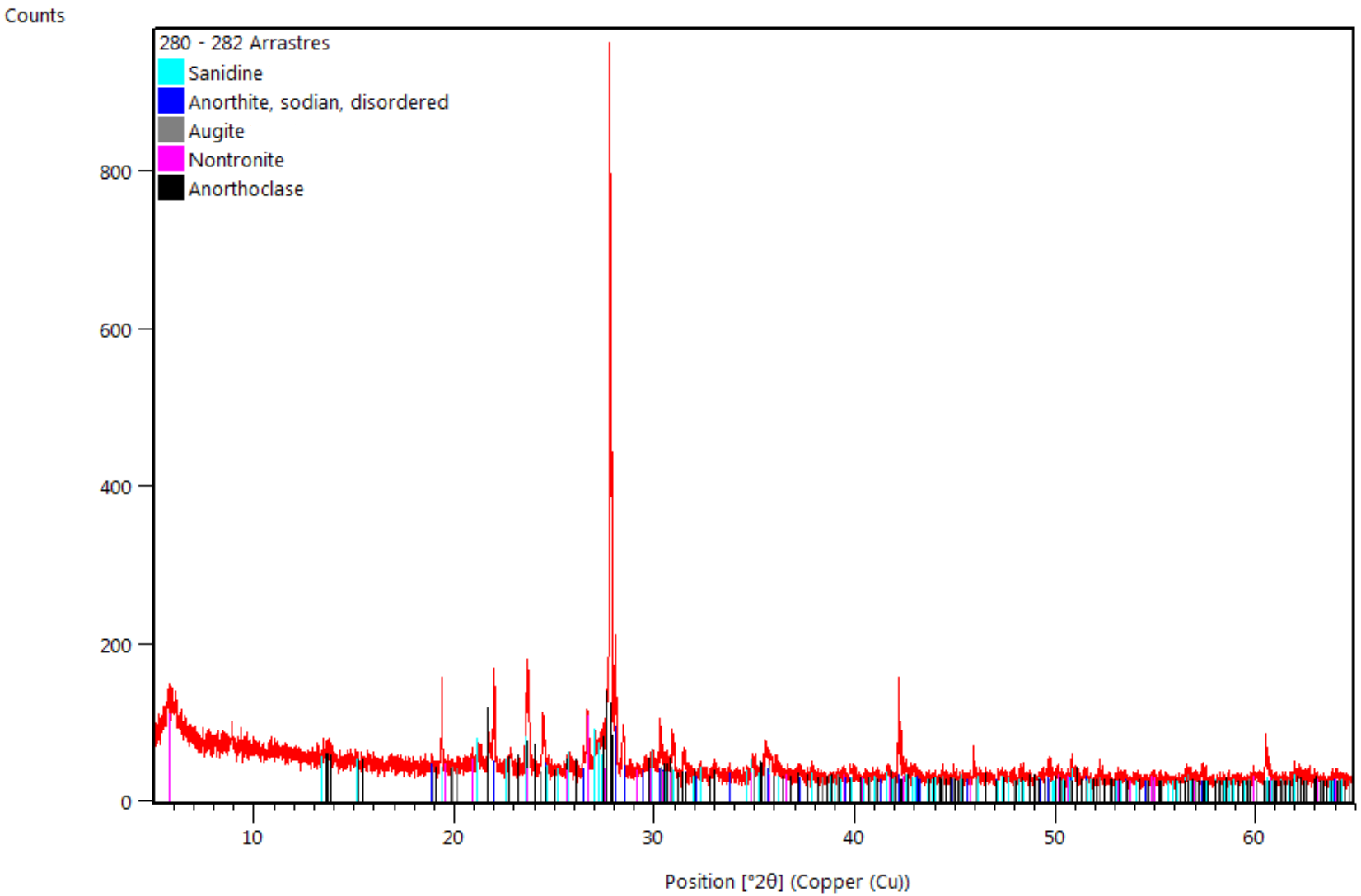

Figure A.46 X-ray diffraction pattern for Arrastres drill cuttings

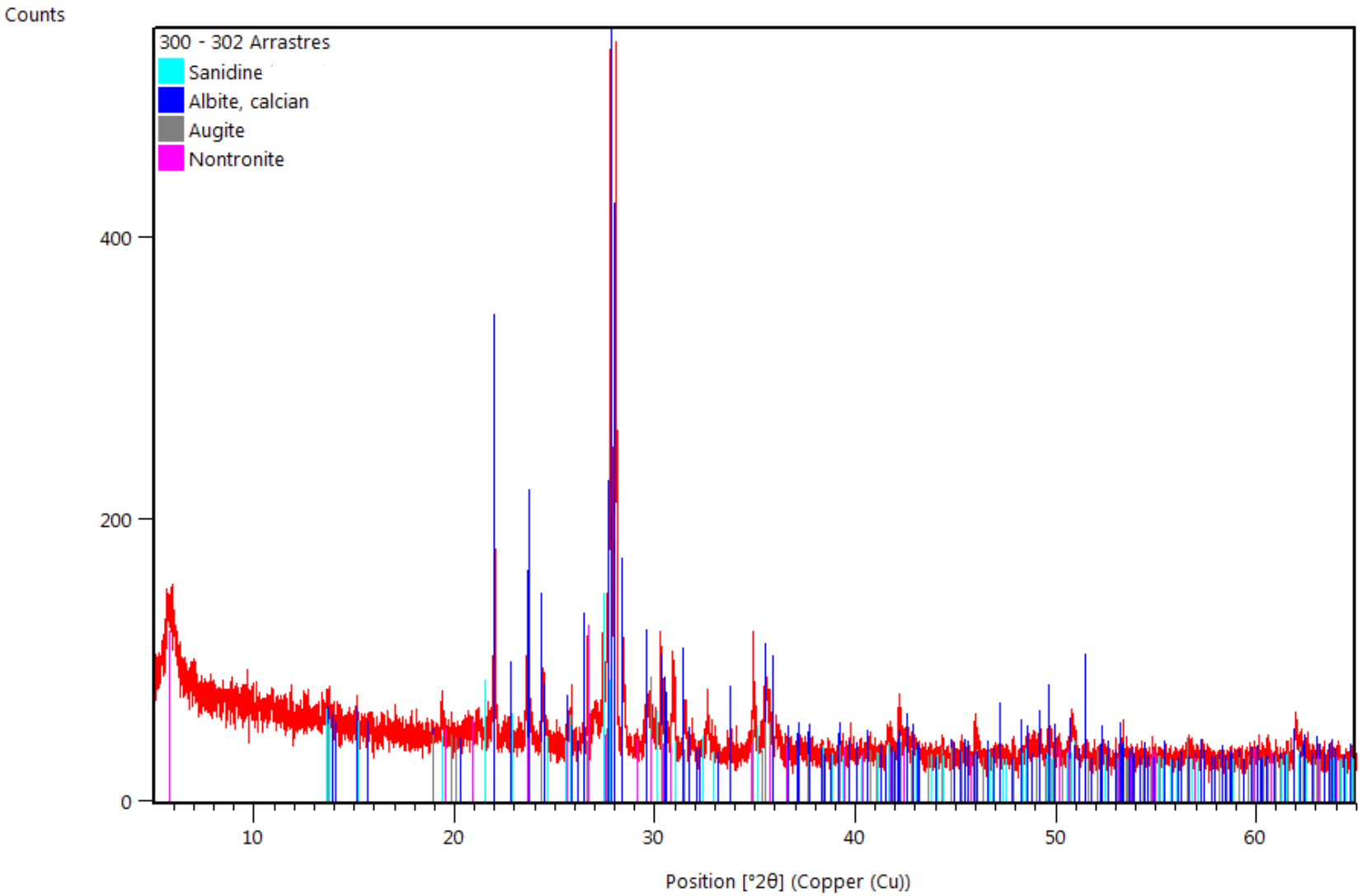

Figure A.47 X-ray diffraction pattern for Arrastres drill cuttings

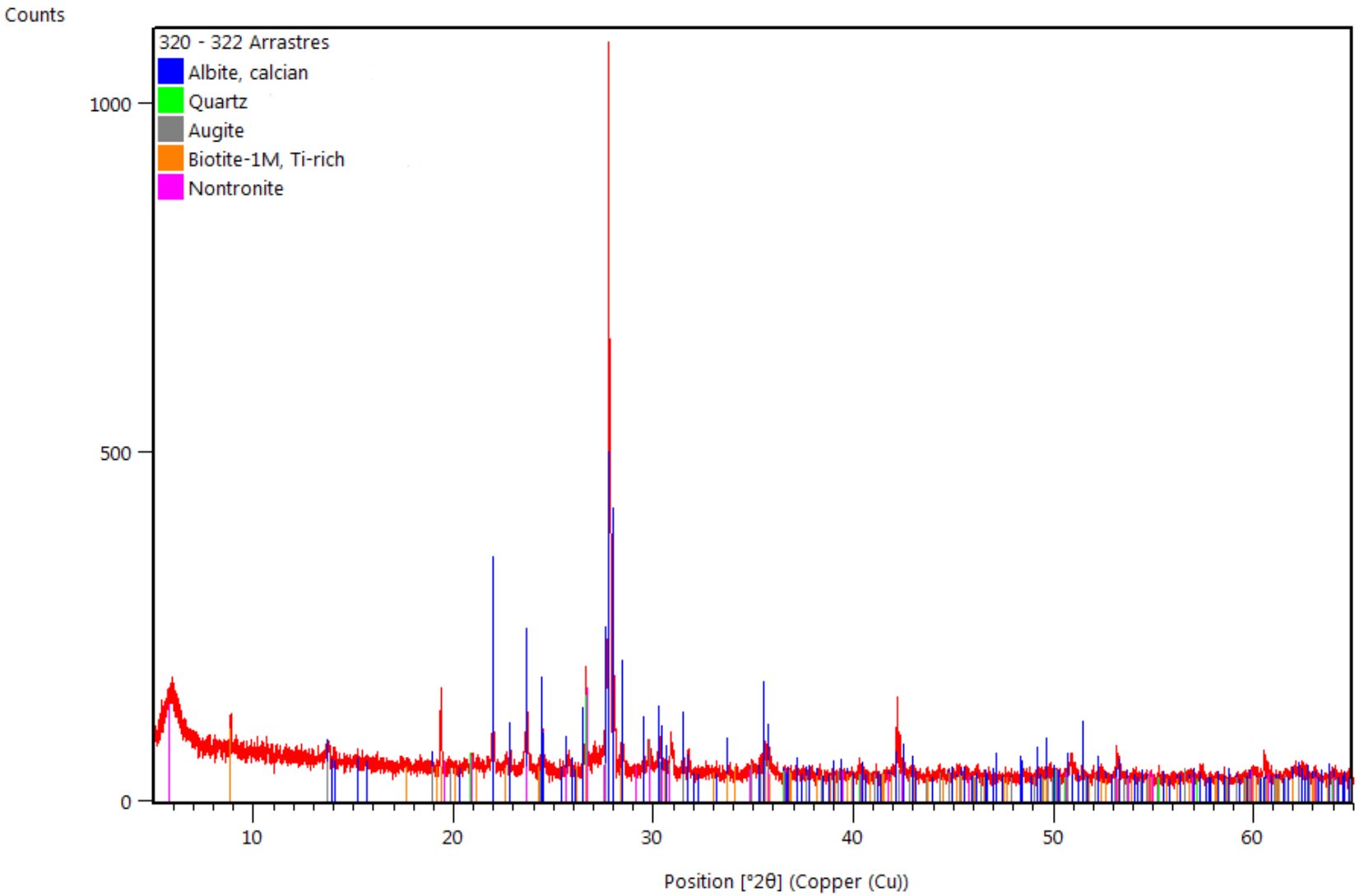

Figure A.48 X-ray diffraction pattern for Arrastres drill cuttings

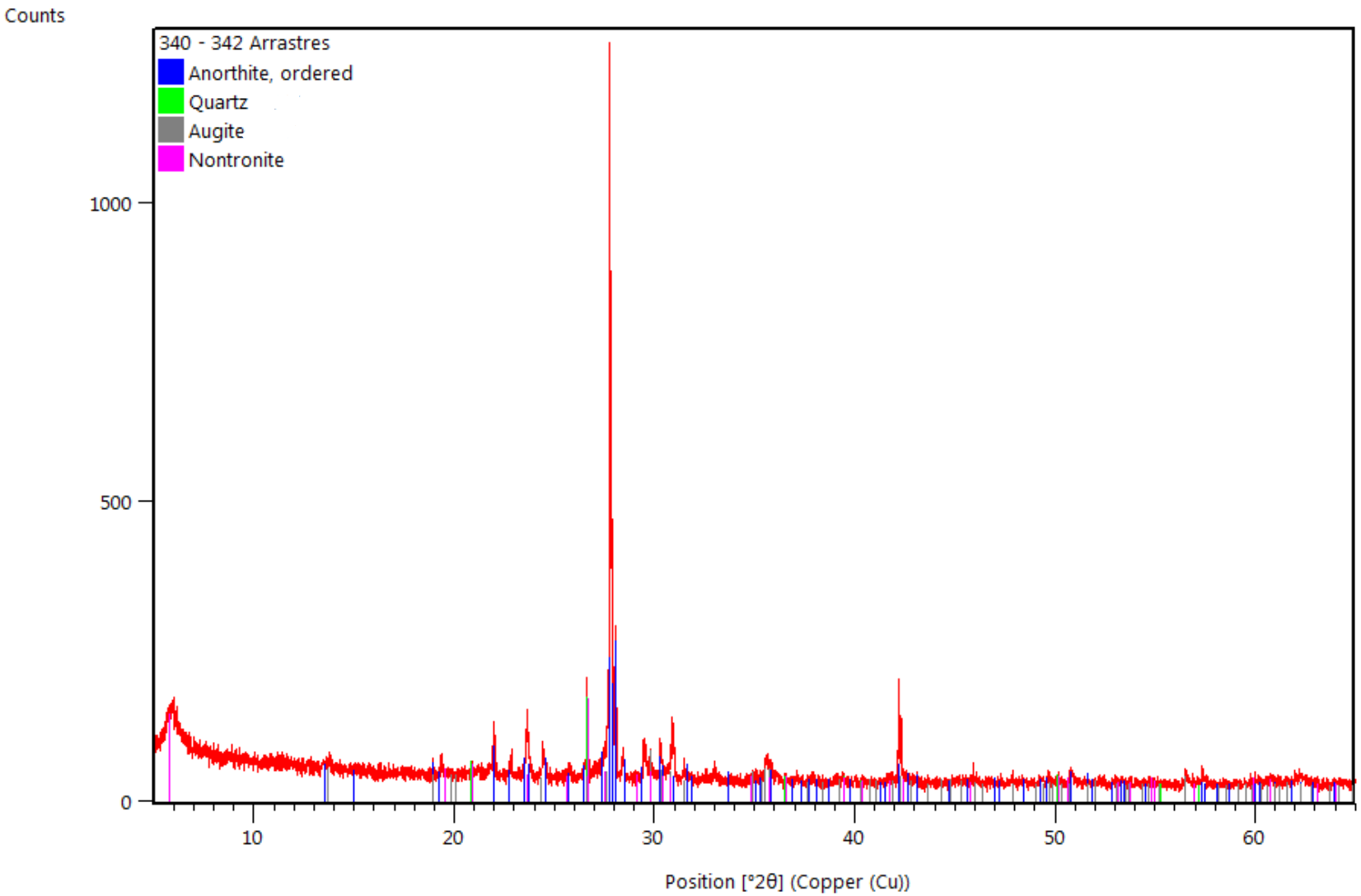

Figure A.49 X-ray diffraction pattern for Arrastres drill cuttings

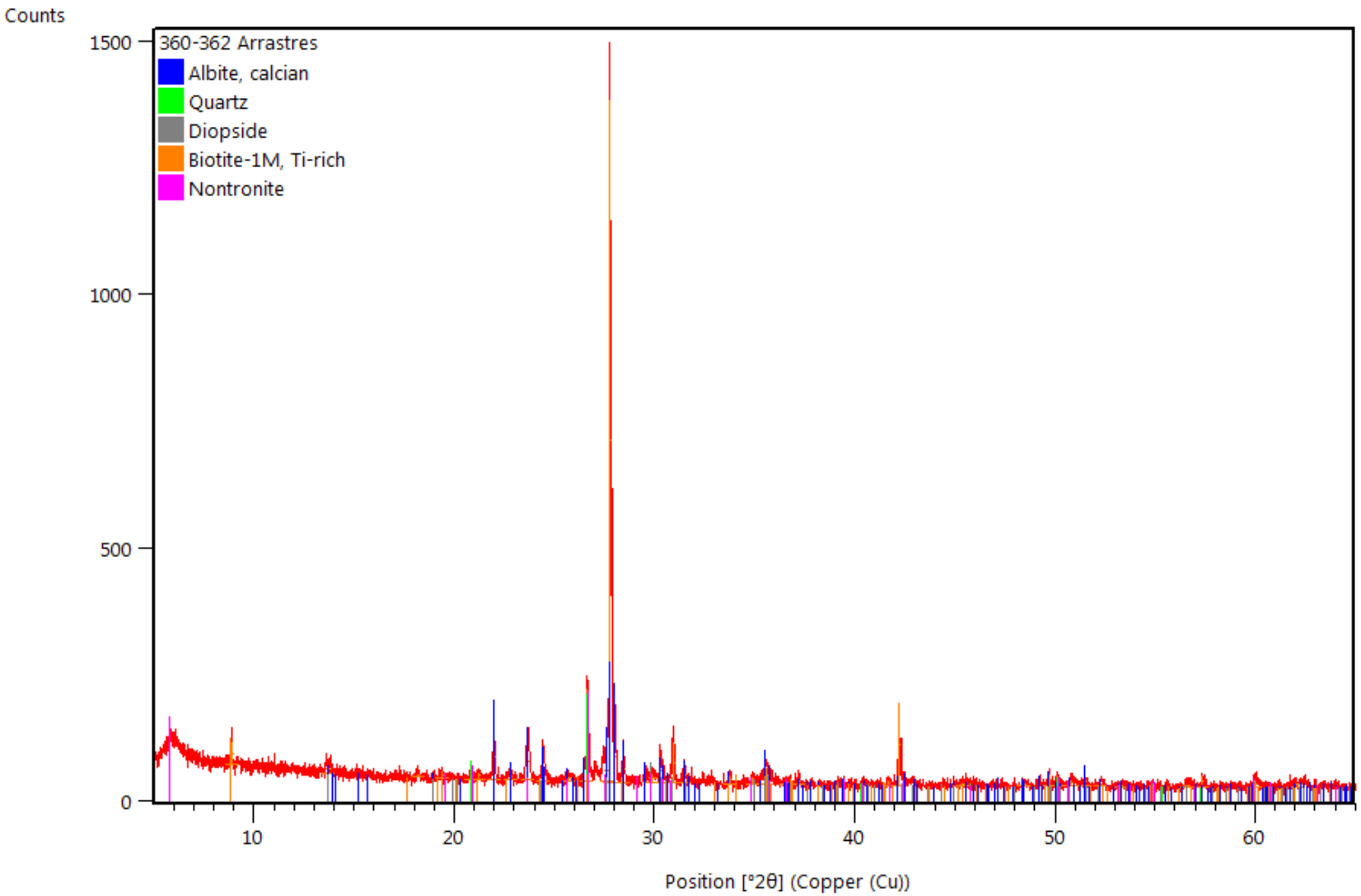

Figure A.50 X-ray diffraction pattern for Arrastres drill cuttings

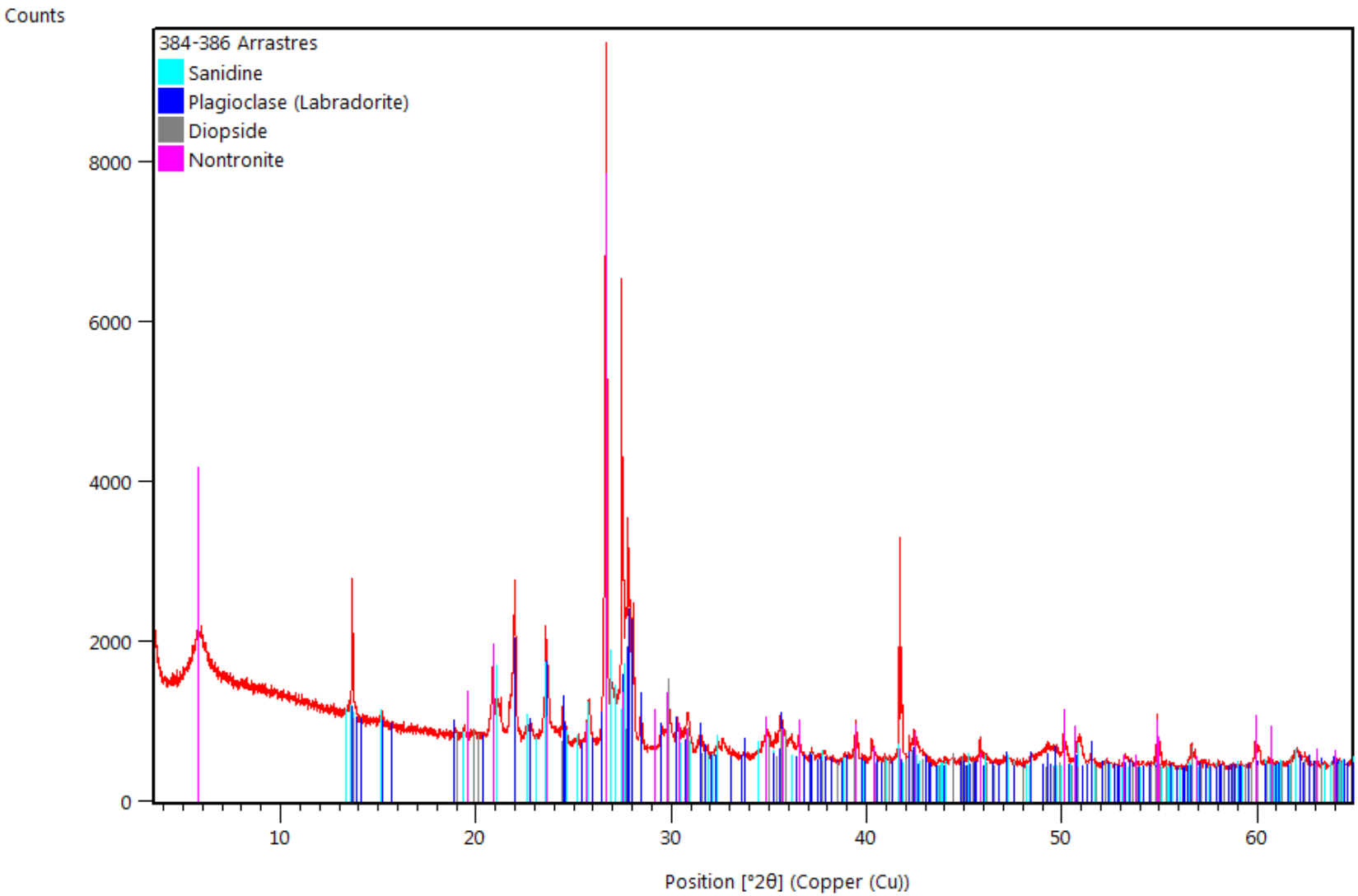

Figure A.51 X-ray diffraction pattern for Arrastres drill cuttings

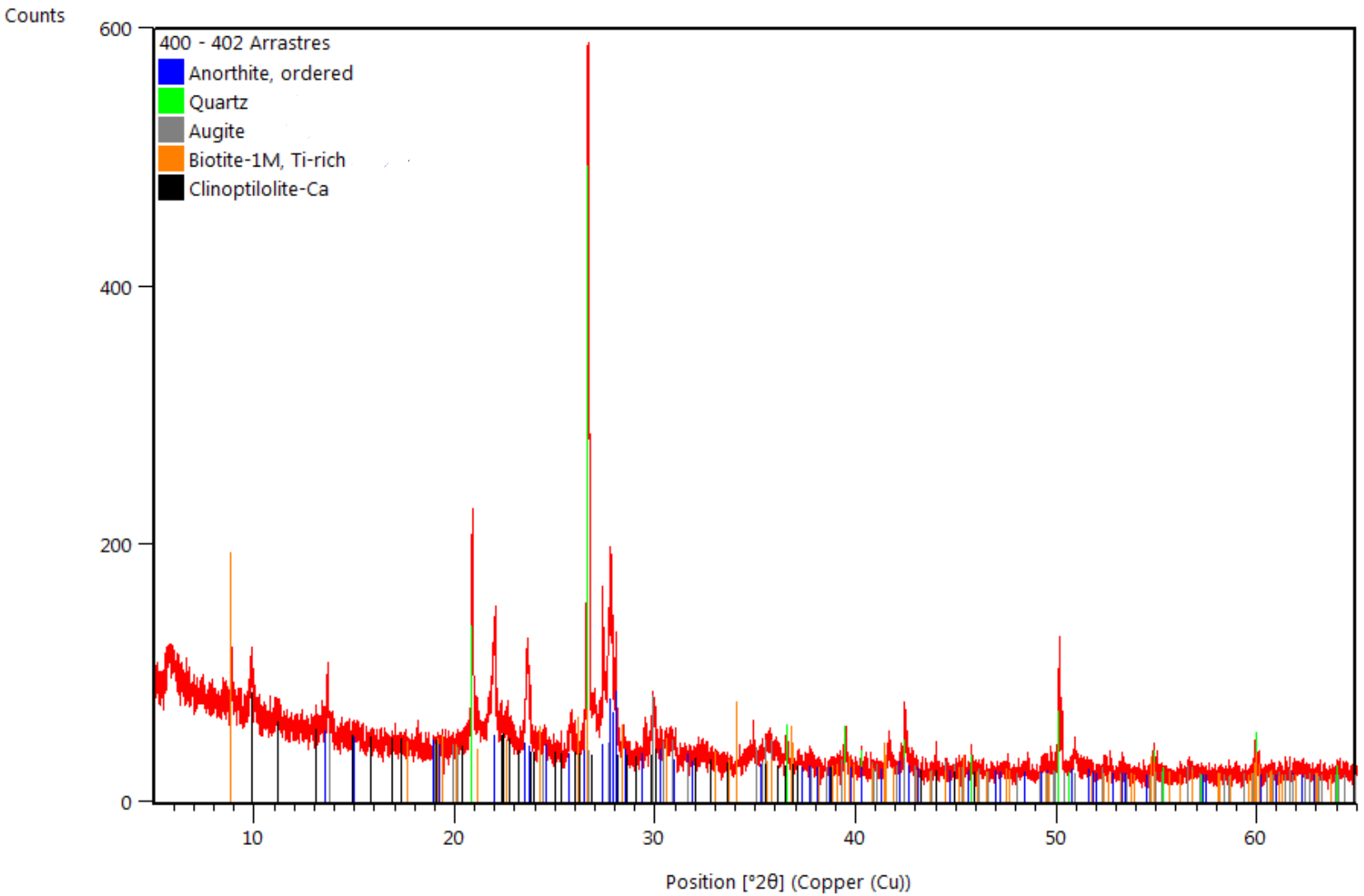

Figure A.52 X-ray diffraction pattern for Arrastres drill cuttings

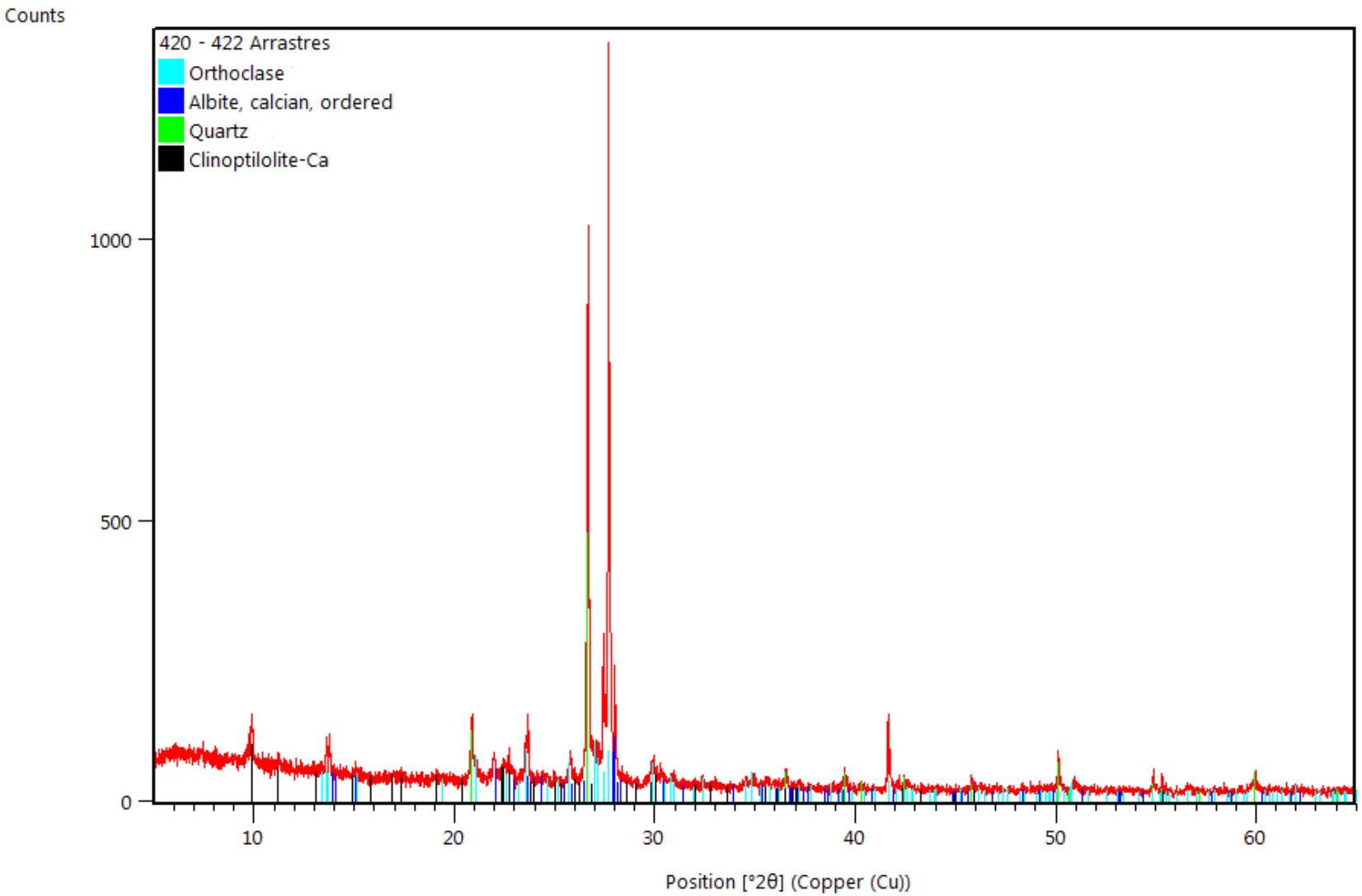

Figure A.53 X-ray diffraction pattern for Arrastres drill cuttings

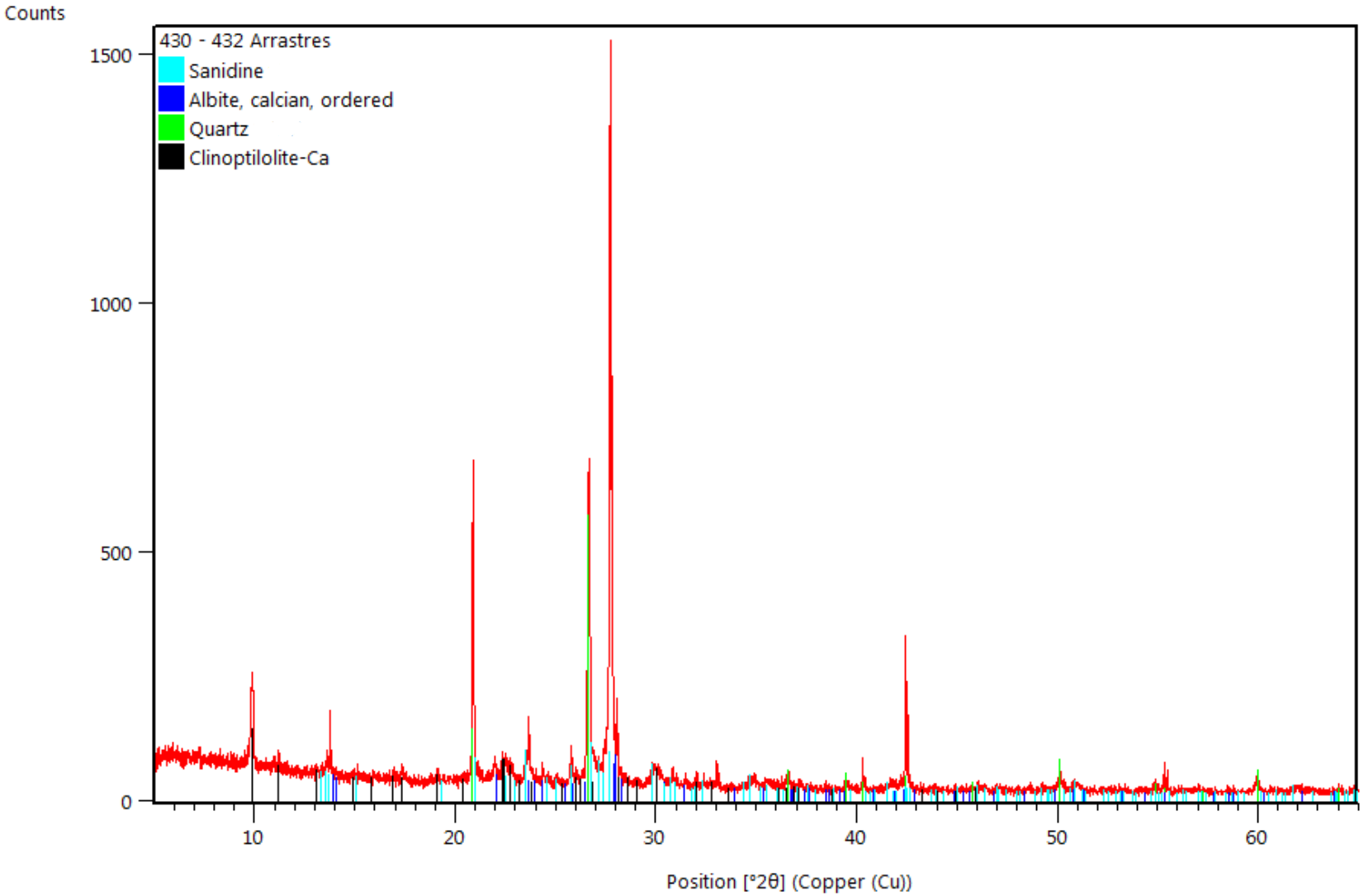

Figure A.54 X-ray diffraction pattern for Arrastres drill cuttings

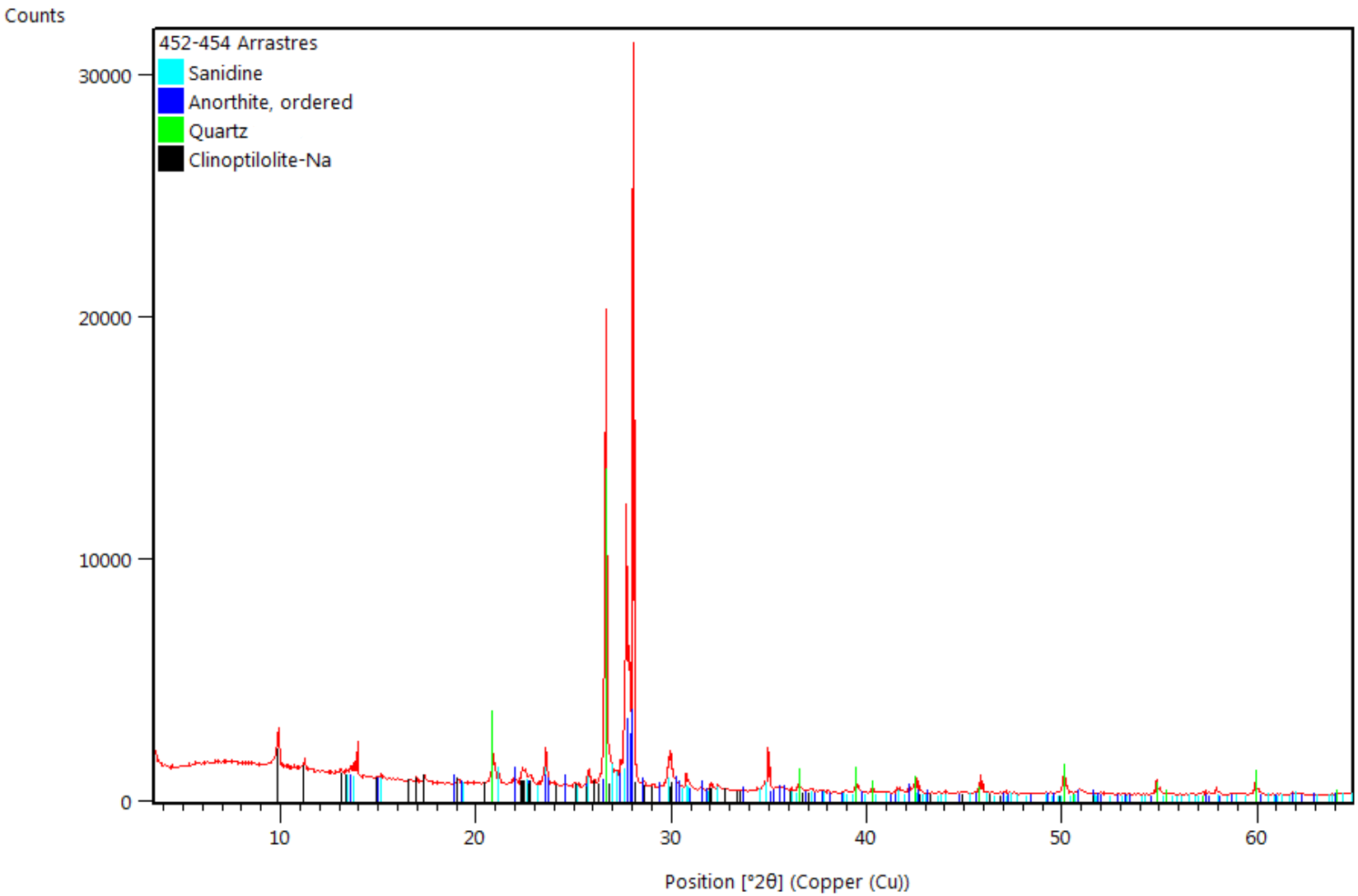

Figure A.55 X-ray diffraction pattern for Arrastres drill cuttings

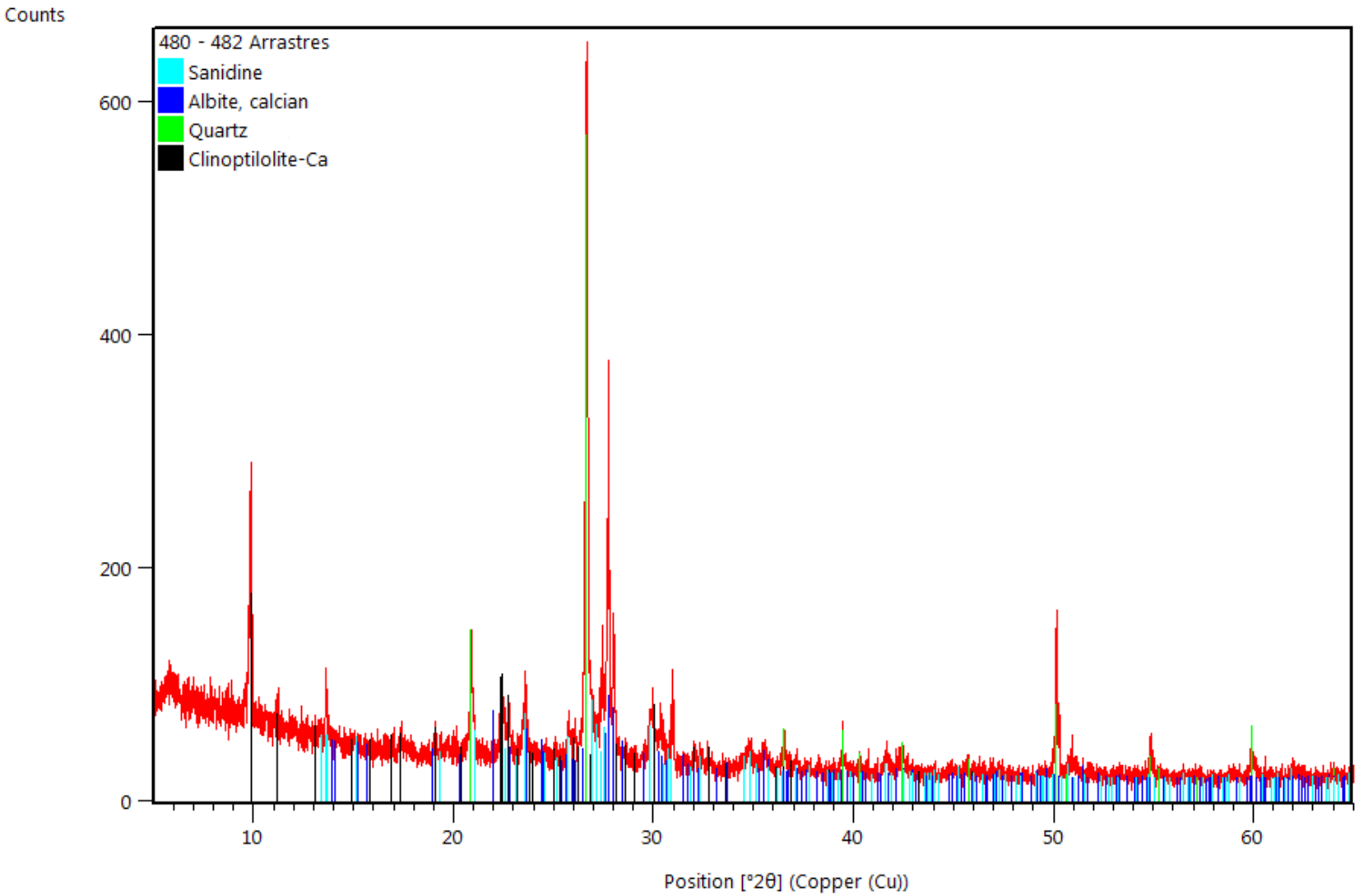

Figure A.56 X-ray diffraction pattern for Arrastres drill cuttings

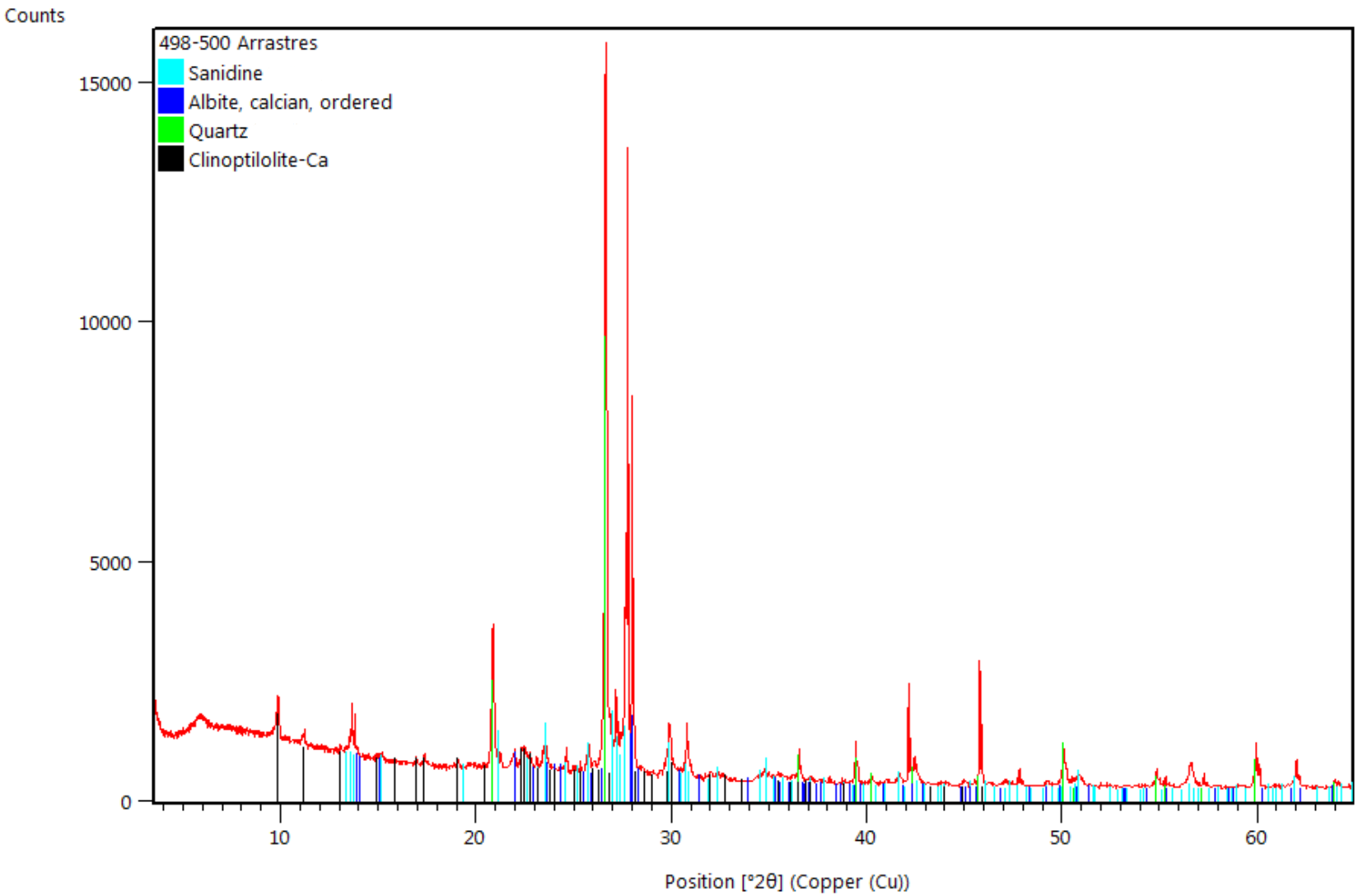

Figure A.57 X-ray diffraction pattern for Arrastres drill cuttings

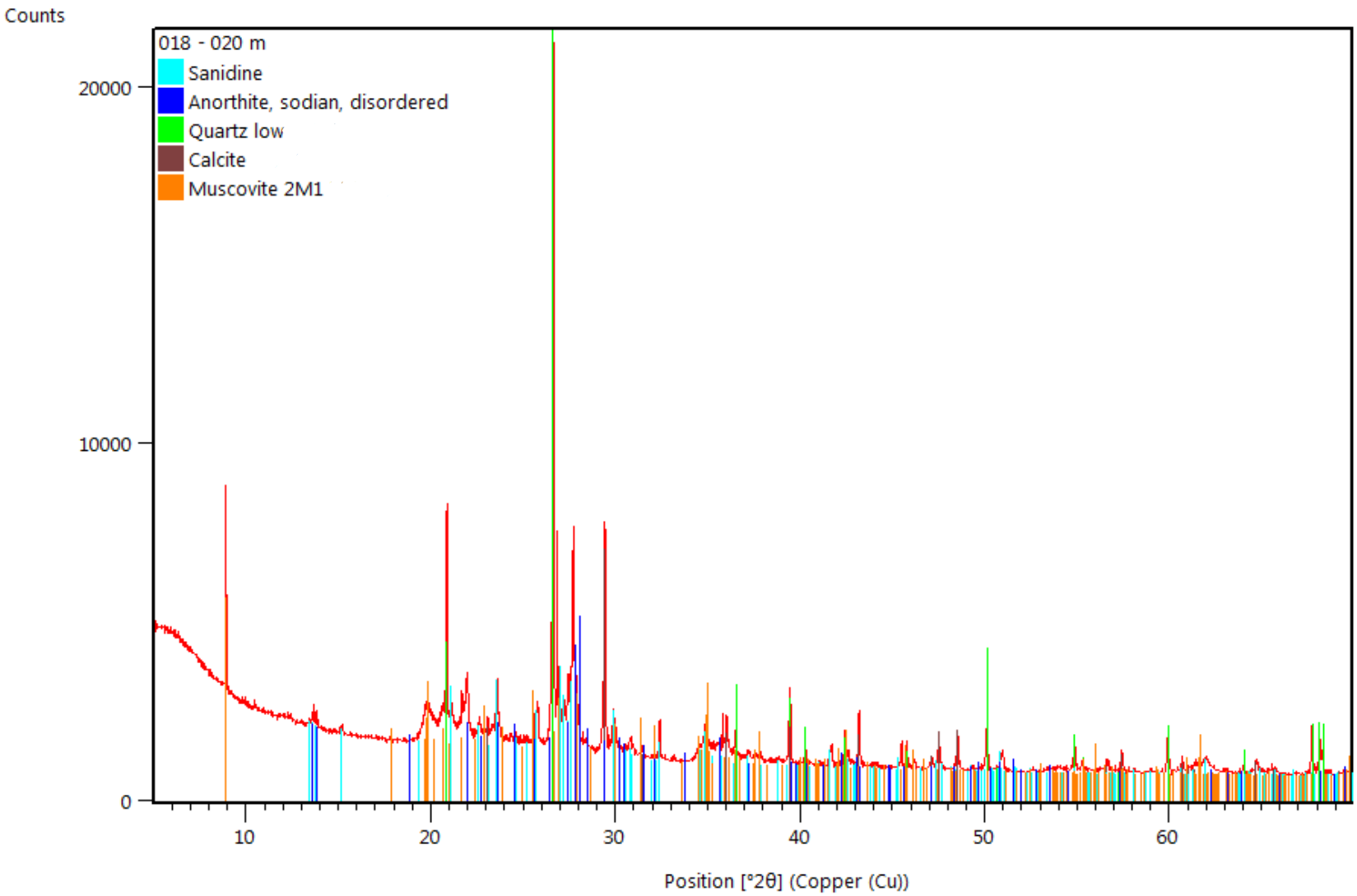

Figure A.58 X-ray diffraction pattern for Lourdes drill cuttings

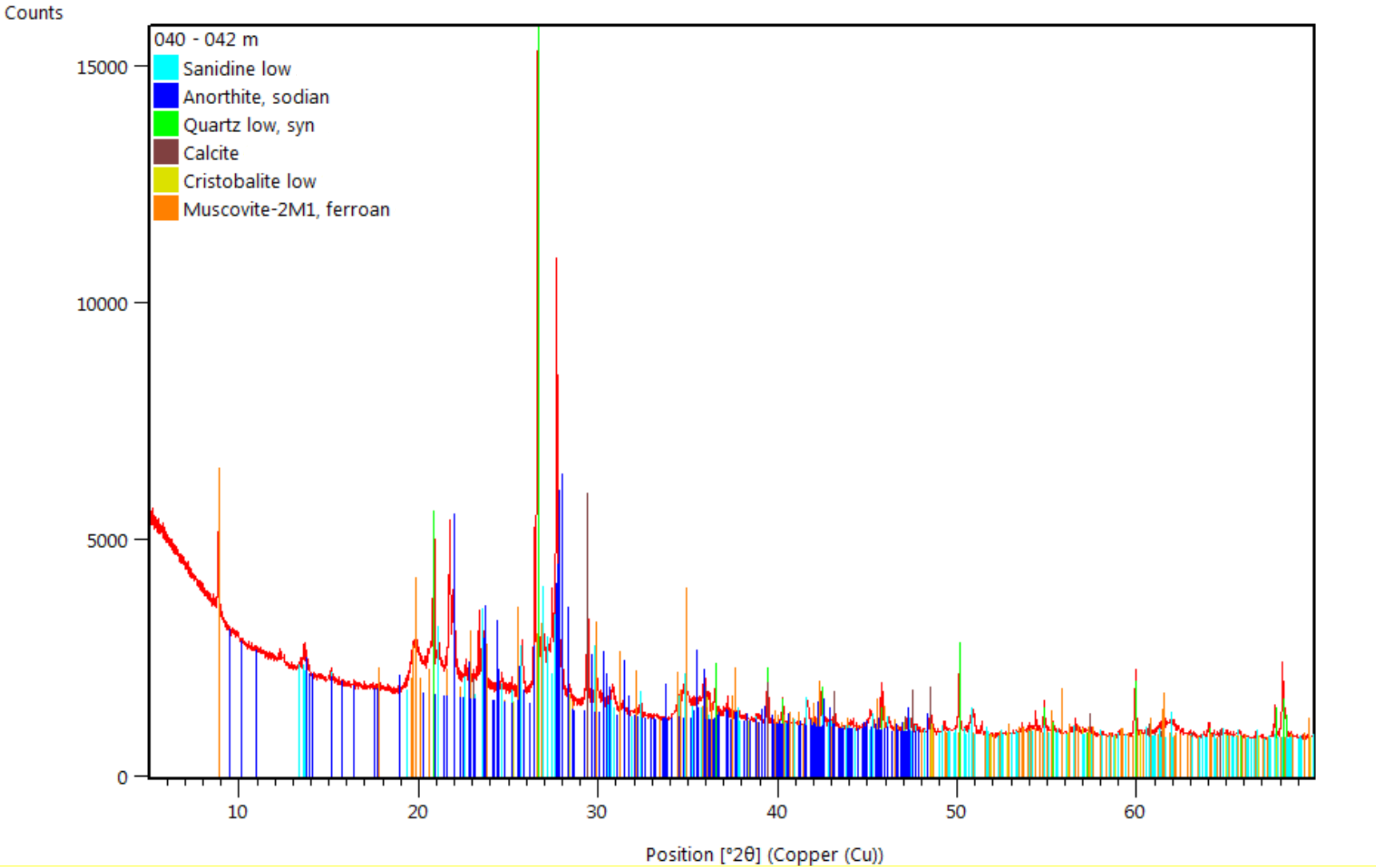

Figure A.59 X-ray diffraction pattern for Lourdes drill cuttings

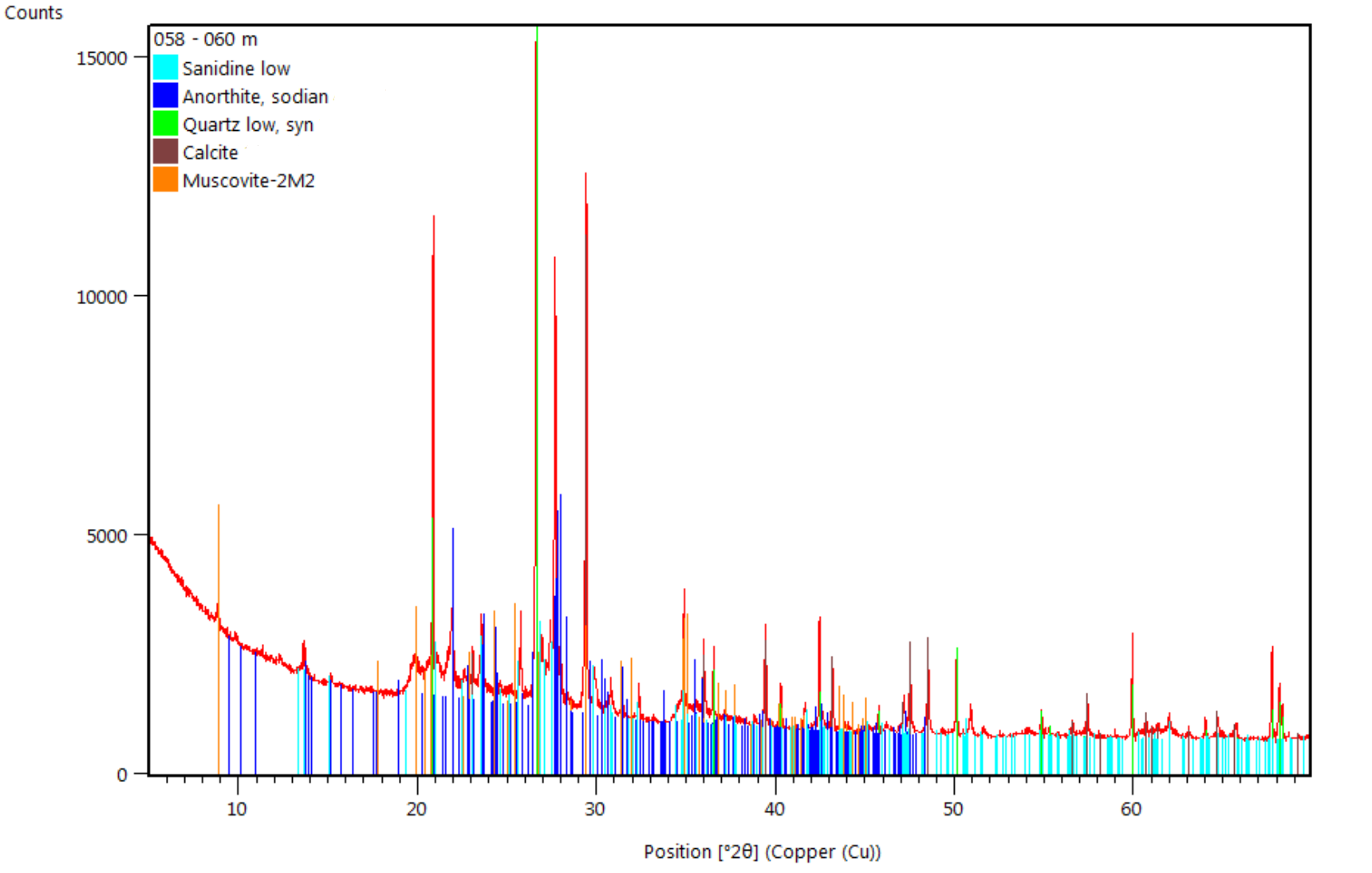

Figure A.60 X-ray diffraction pattern for Lourdes drill cuttings

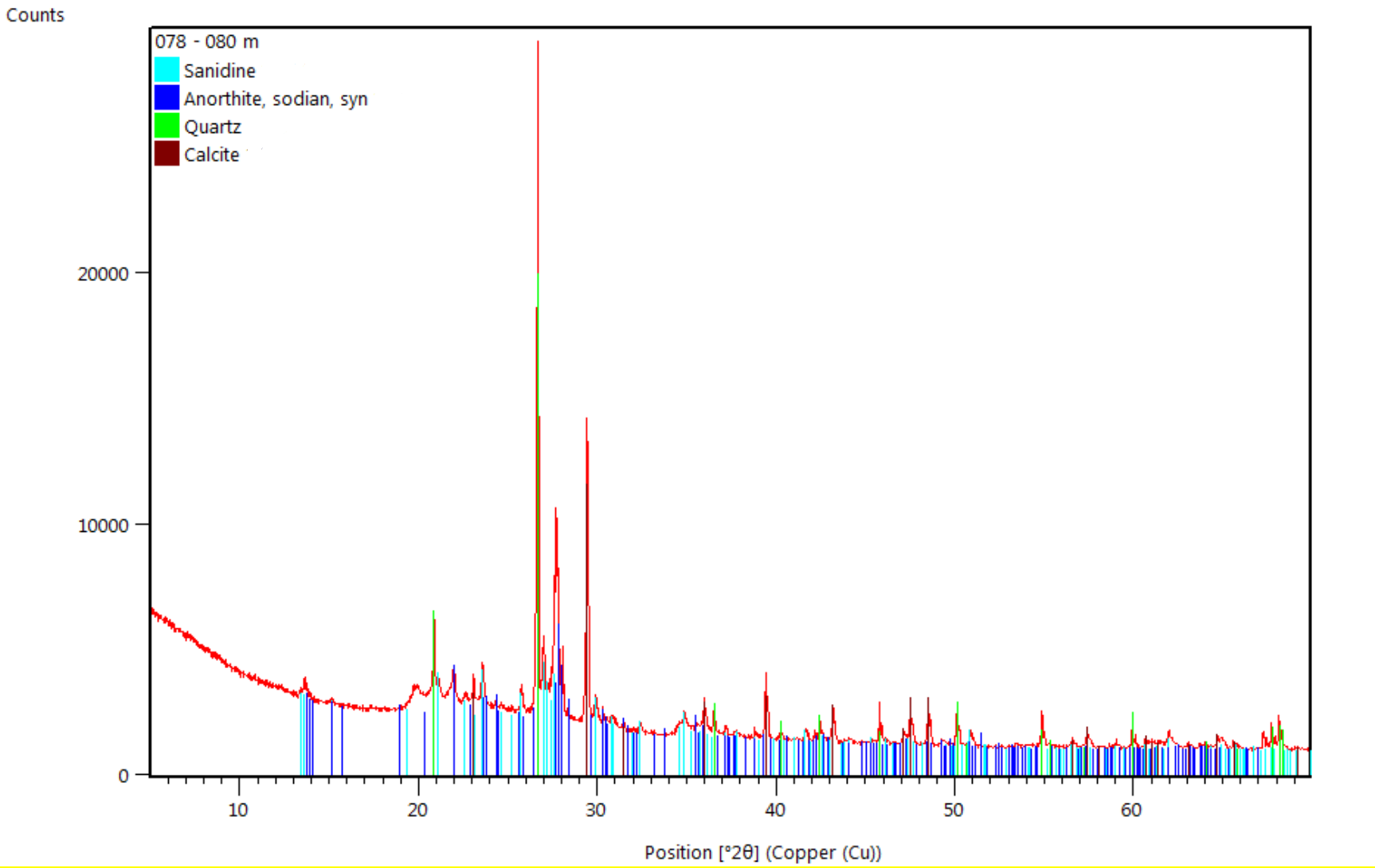

Figure A.61 X-ray diffraction pattern for Lourdes drill cuttings

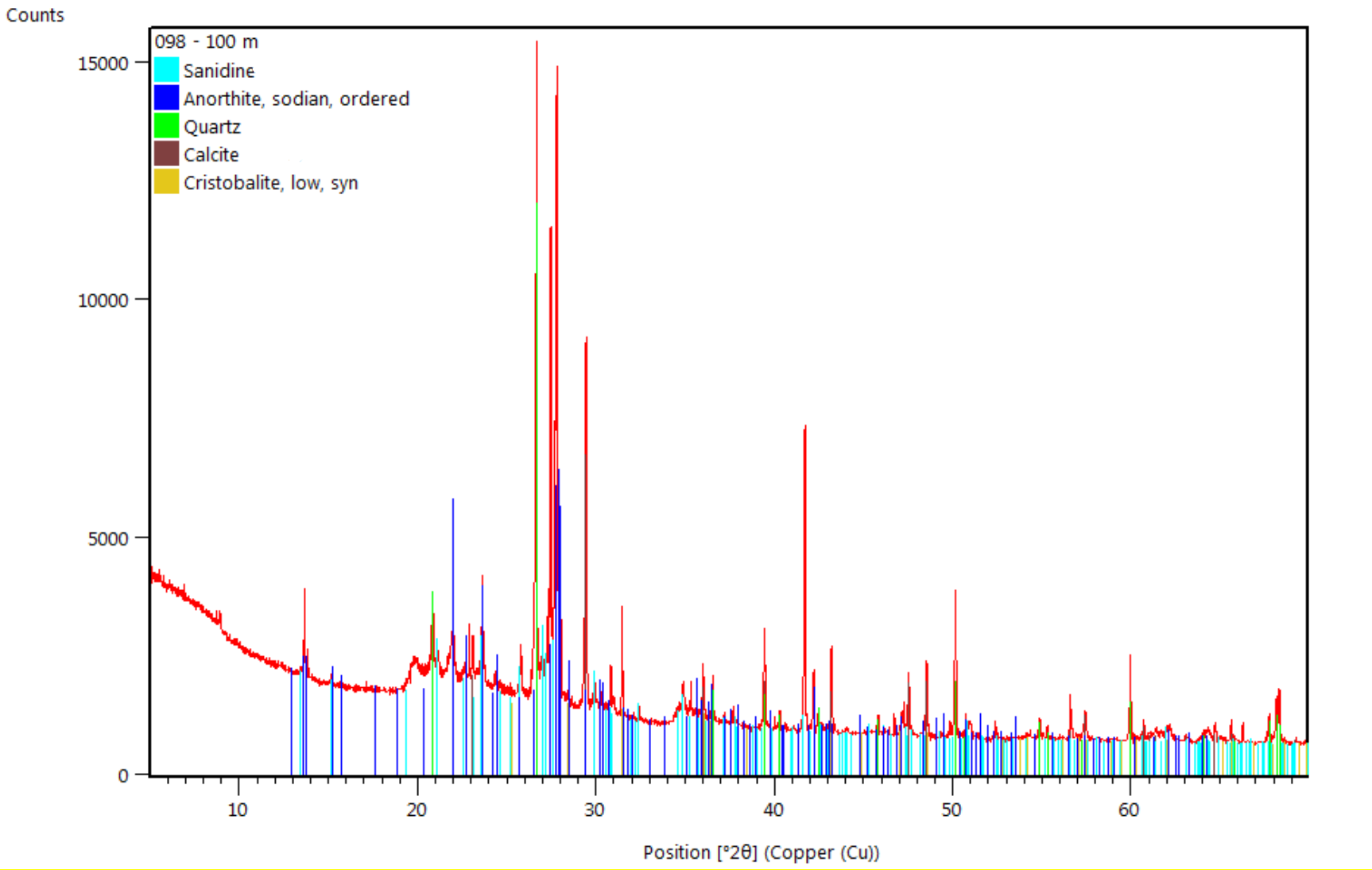

Figure A.62 X-ray diffraction pattern for Lourdes drill cuttings

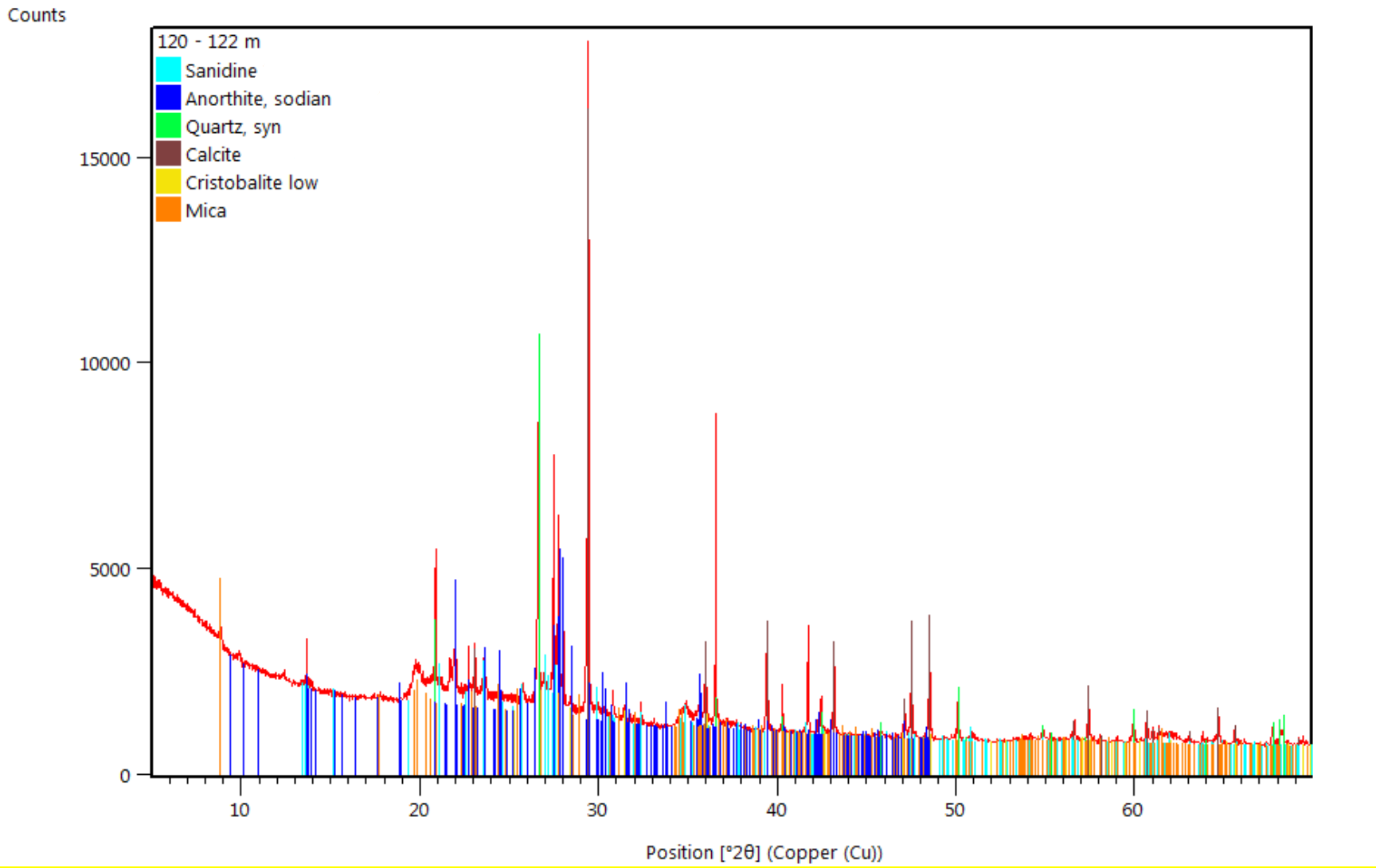

Figure A.63 X-ray diffraction pattern for Lourdes drill cuttings

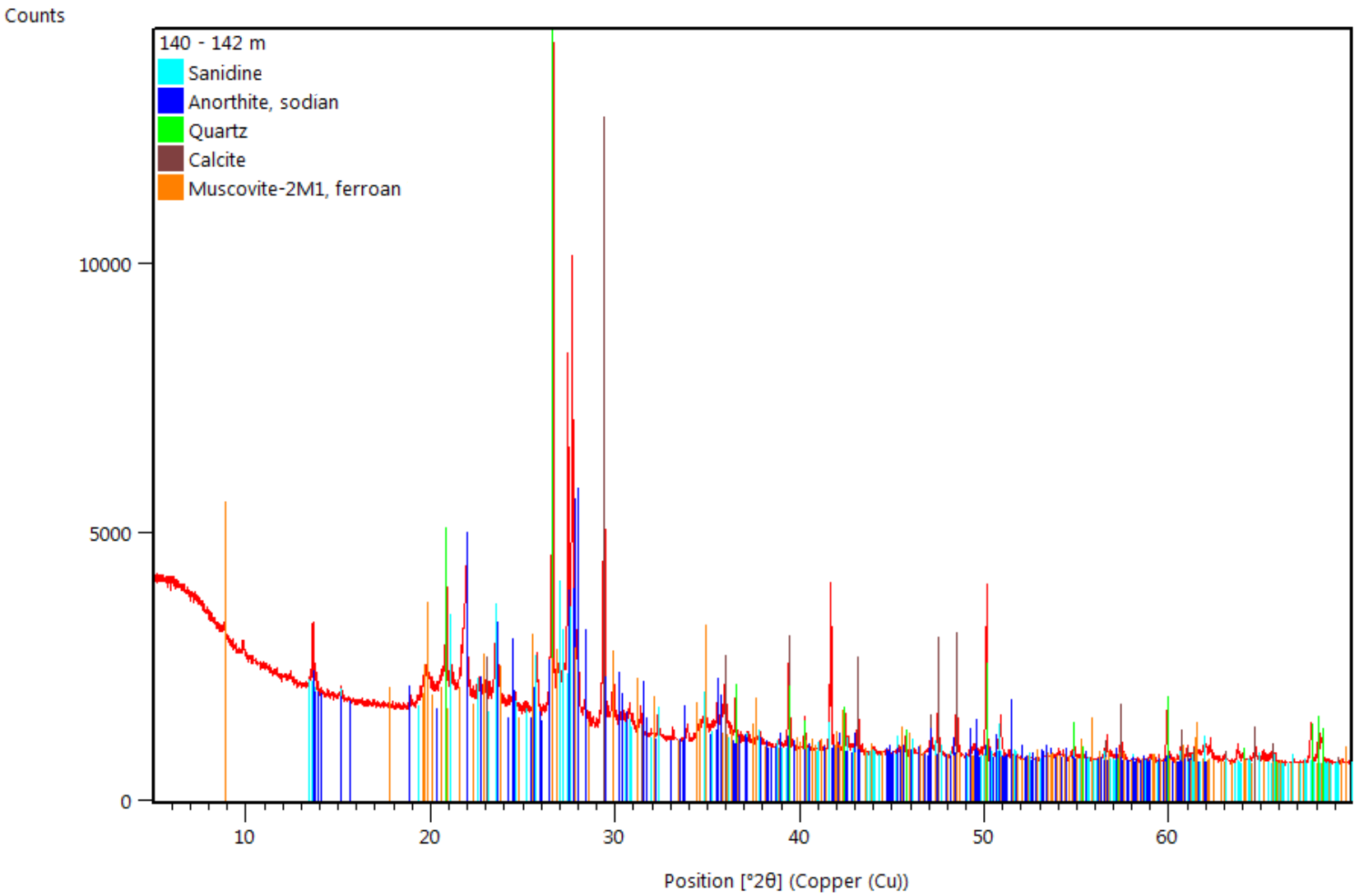

Figure A.64 X-ray diffraction pattern for Lourdes drill cuttings

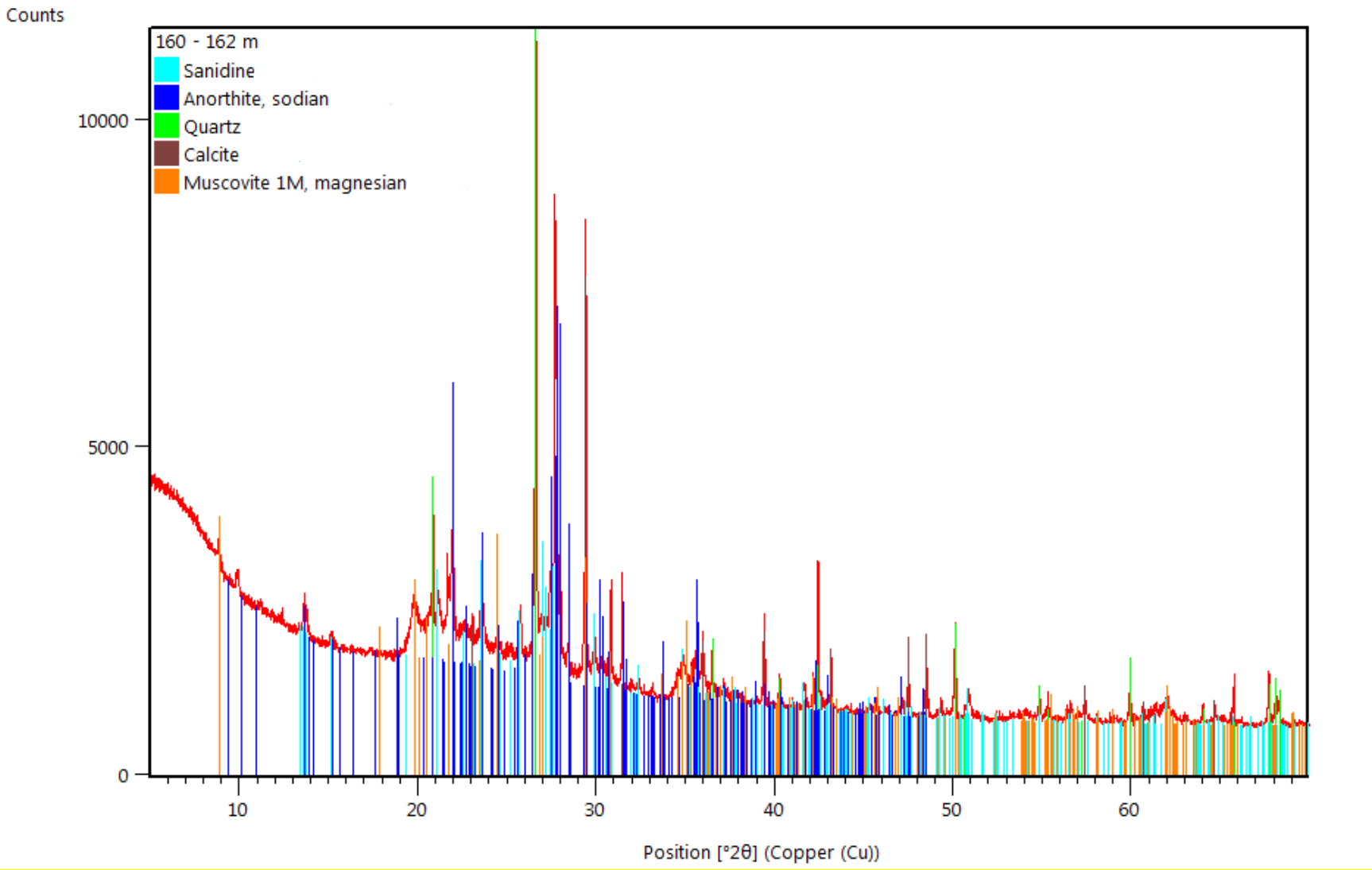

Figure A.65 X-ray diffraction pattern for Lourdes drill cuttings

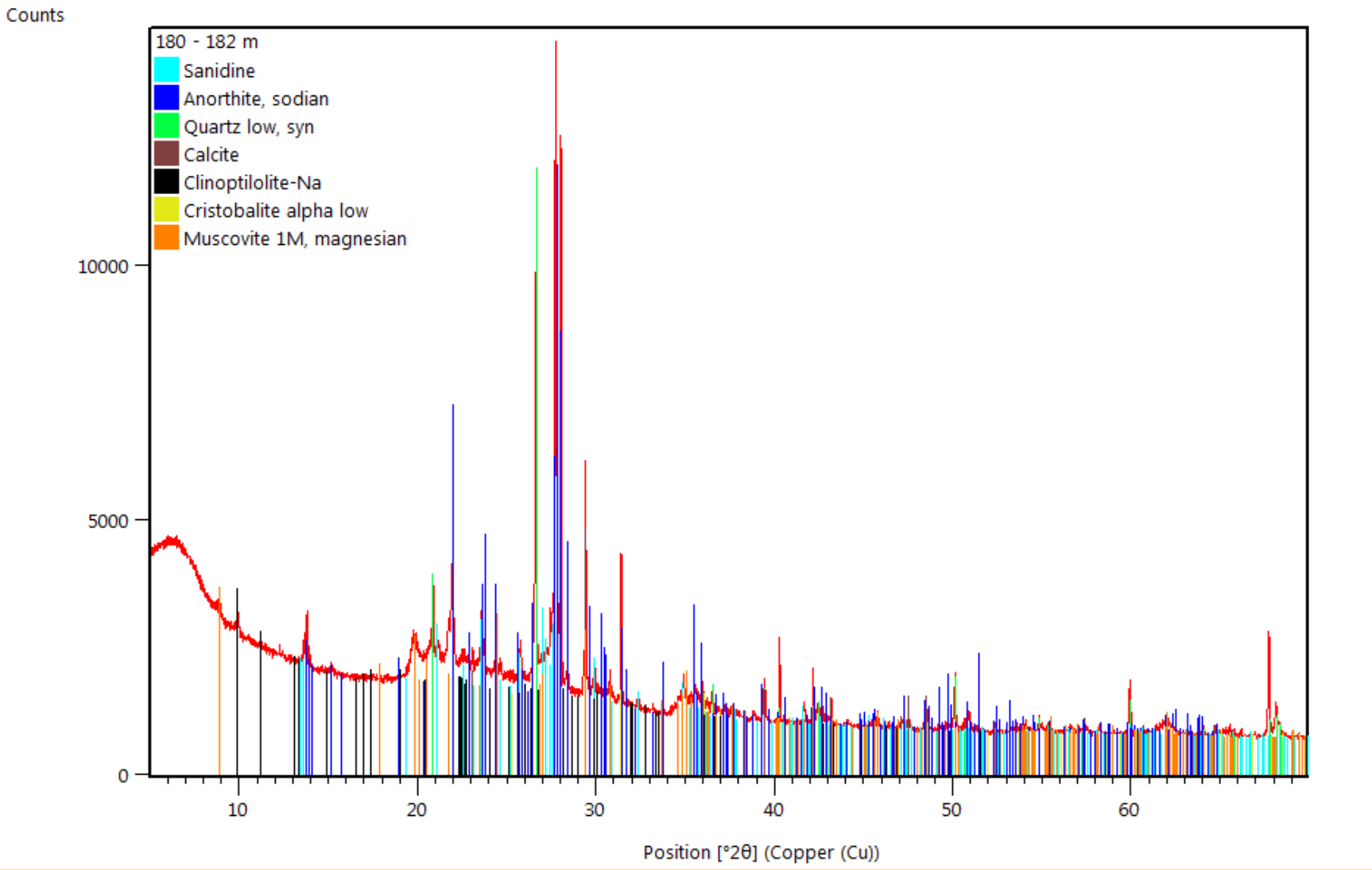

Figure A.67 X-ray diffraction pattern for Lourdes drill cuttings

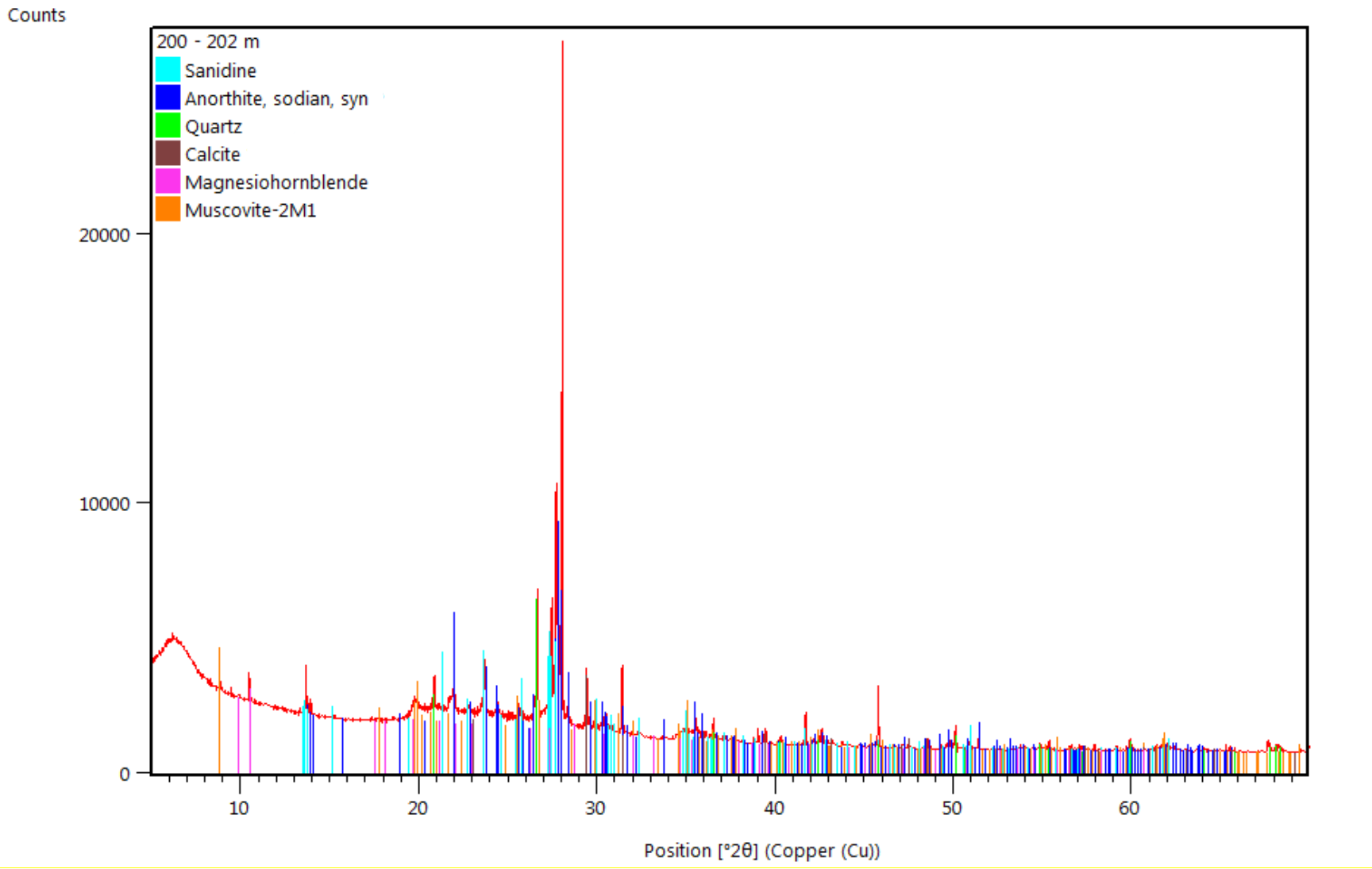

Figure A.68 X-ray diffraction pattern for Lourdes drill cuttings

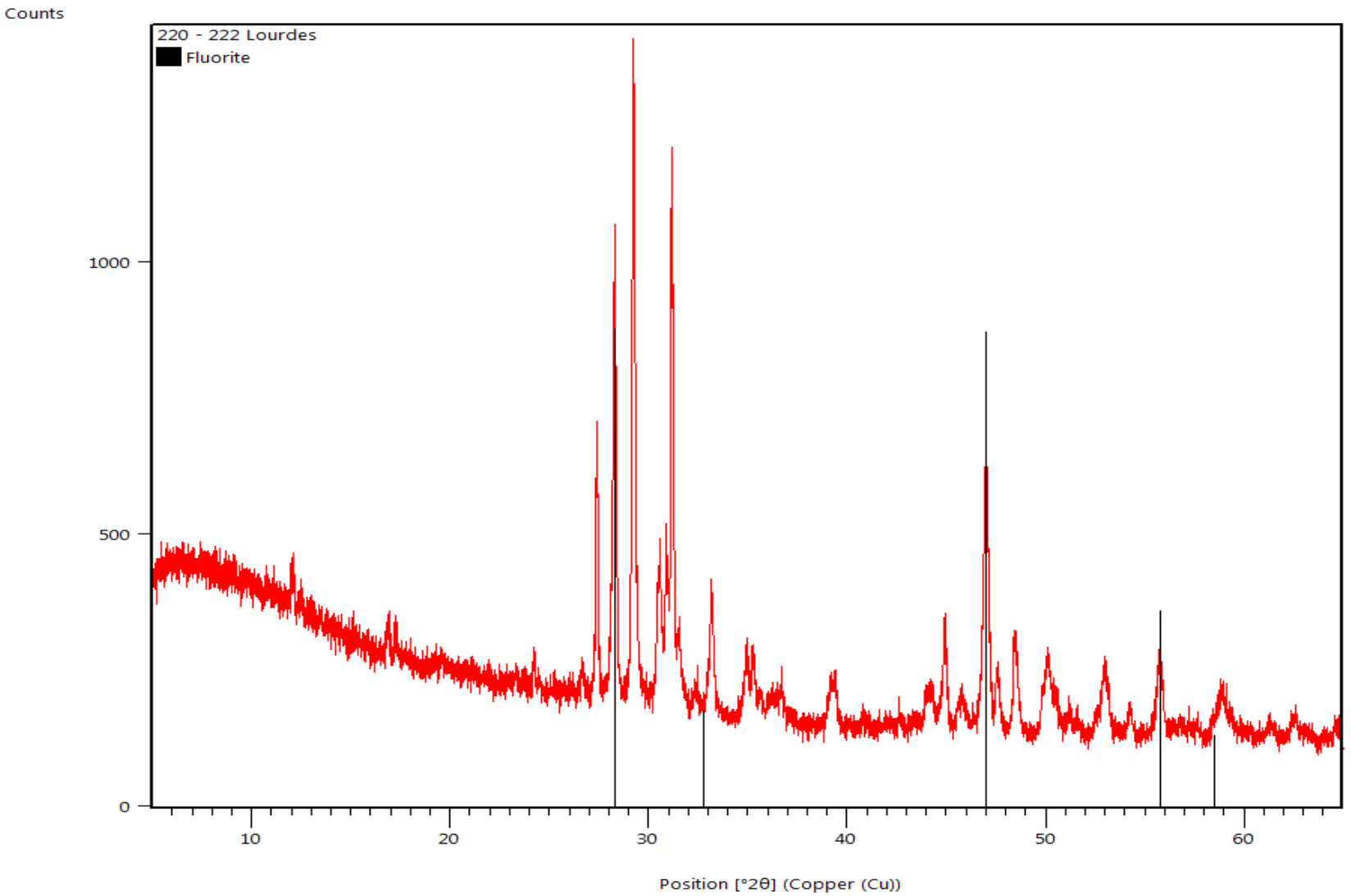

Figure A.69 X-ray diffraction pattern for Lourdes drill cuttings

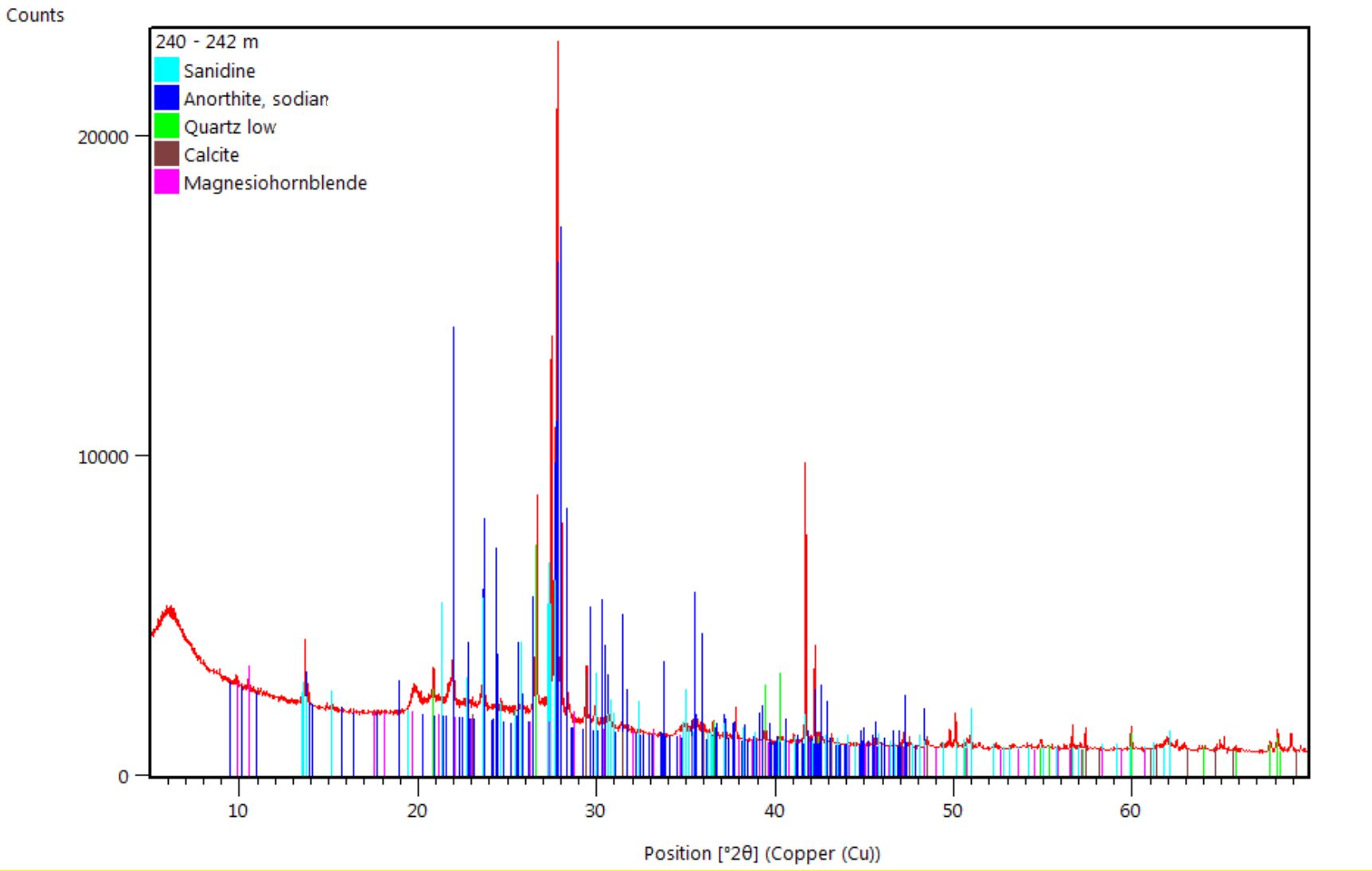

Figure A.70 X-ray diffraction pattern for Lourdes drill cuttings

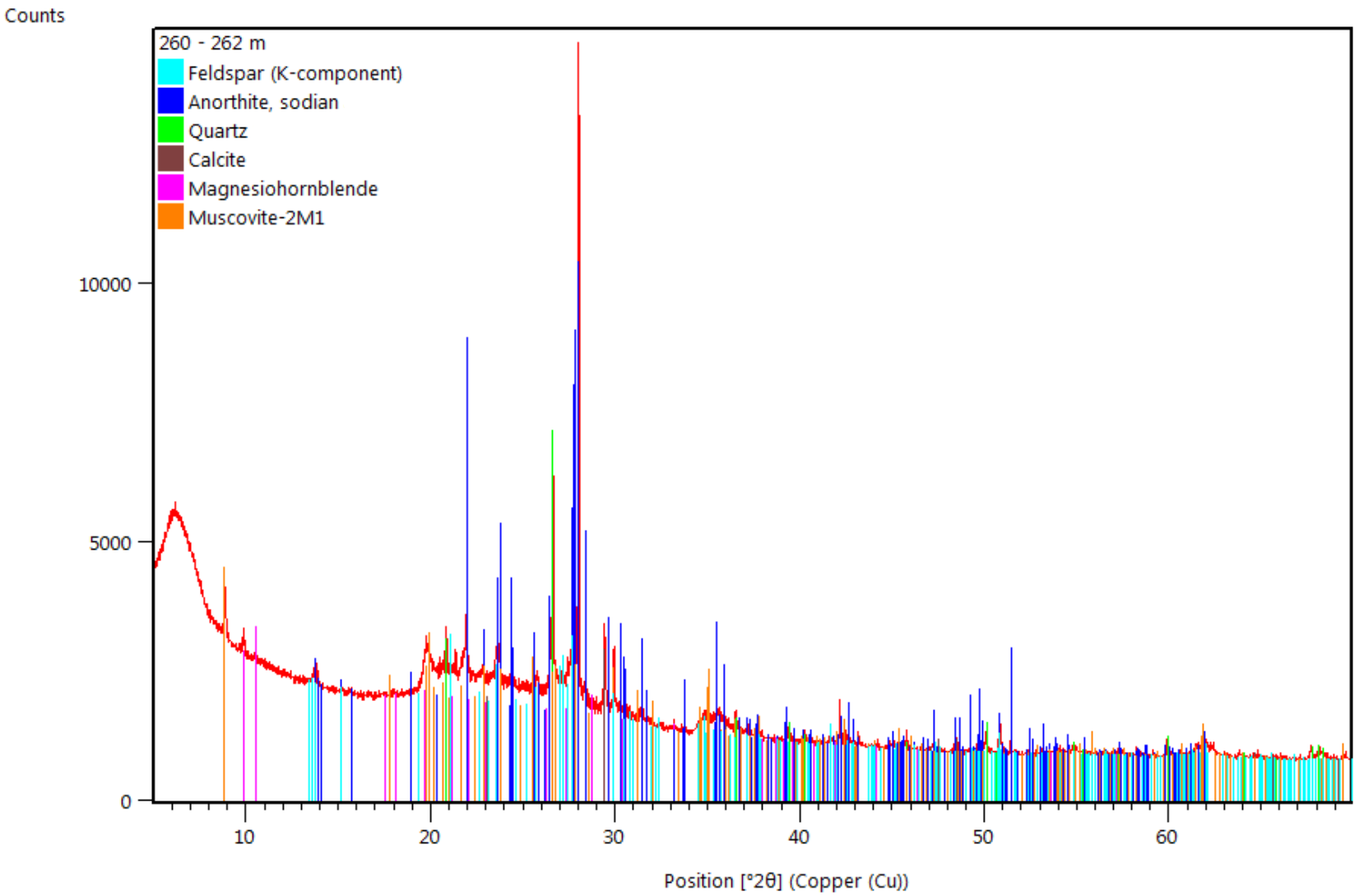

Figure A.71 X-ray diffraction pattern for Lourdes drill cuttings

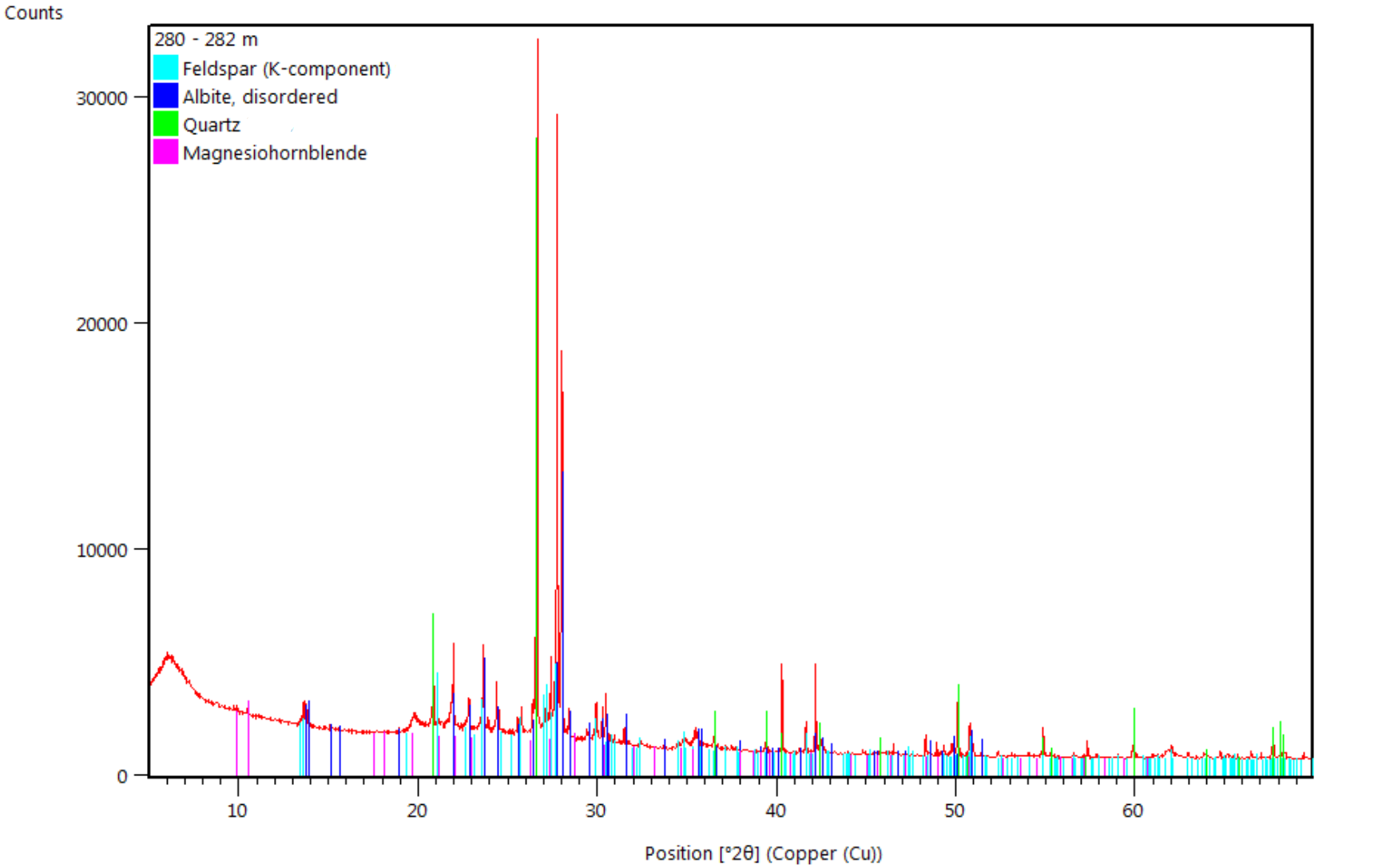

Figure A.72 X-ray diffraction pattern for Lourdes drill cuttings

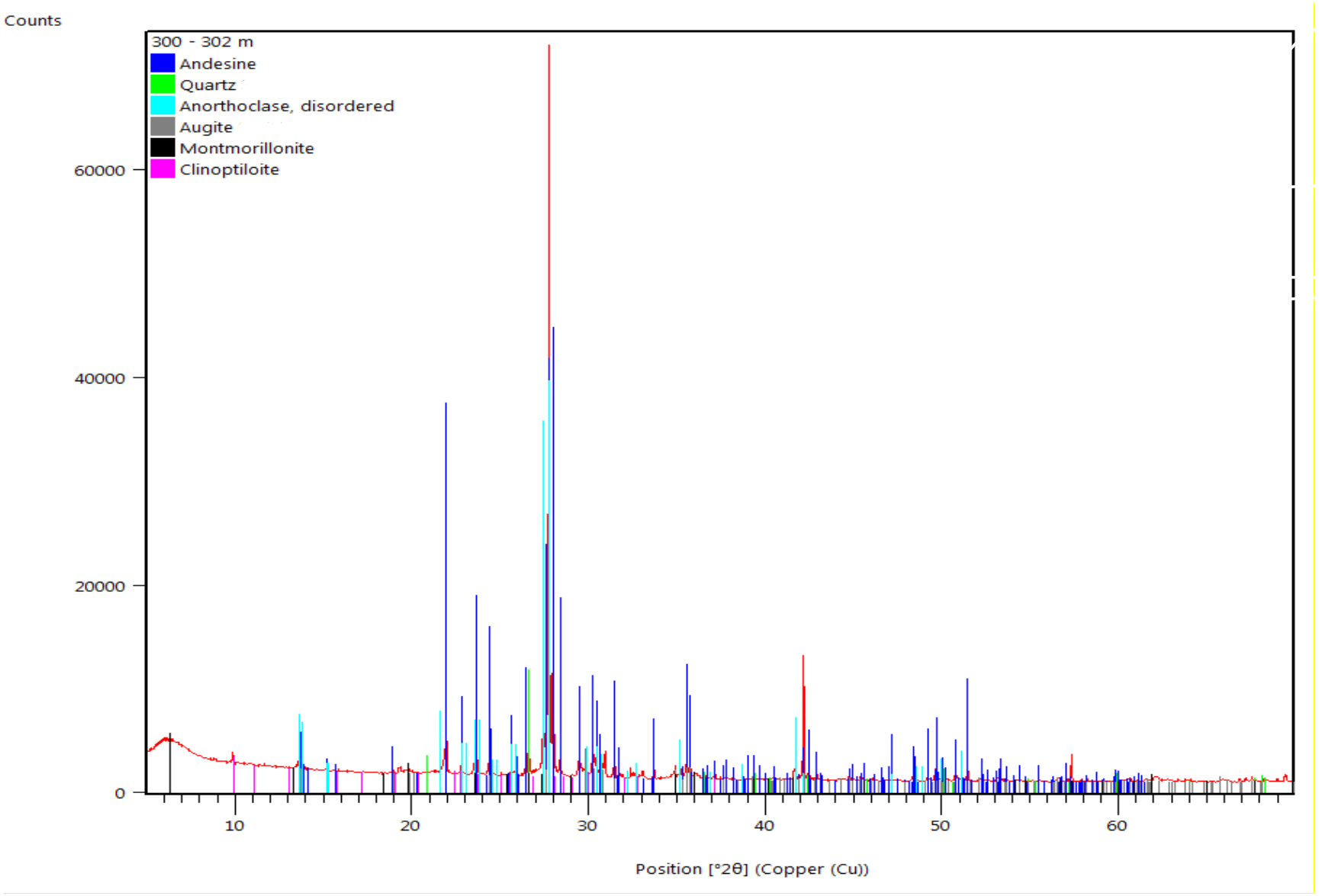

Figure A.73 X-ray diffraction pattern for Lourdes drill cuttings

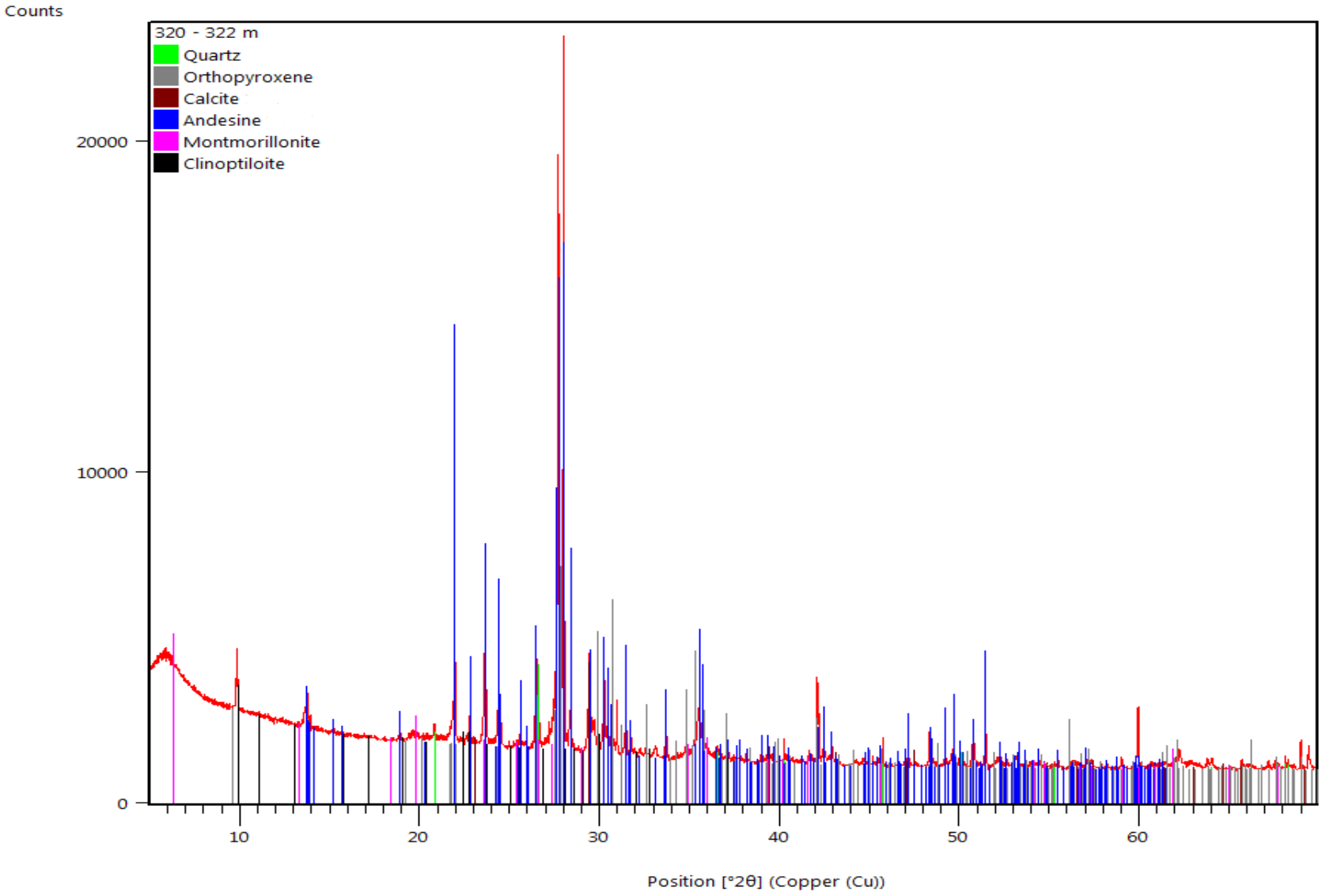

Figure A.74 X-ray diffraction pattern for Lourdes drill cuttings

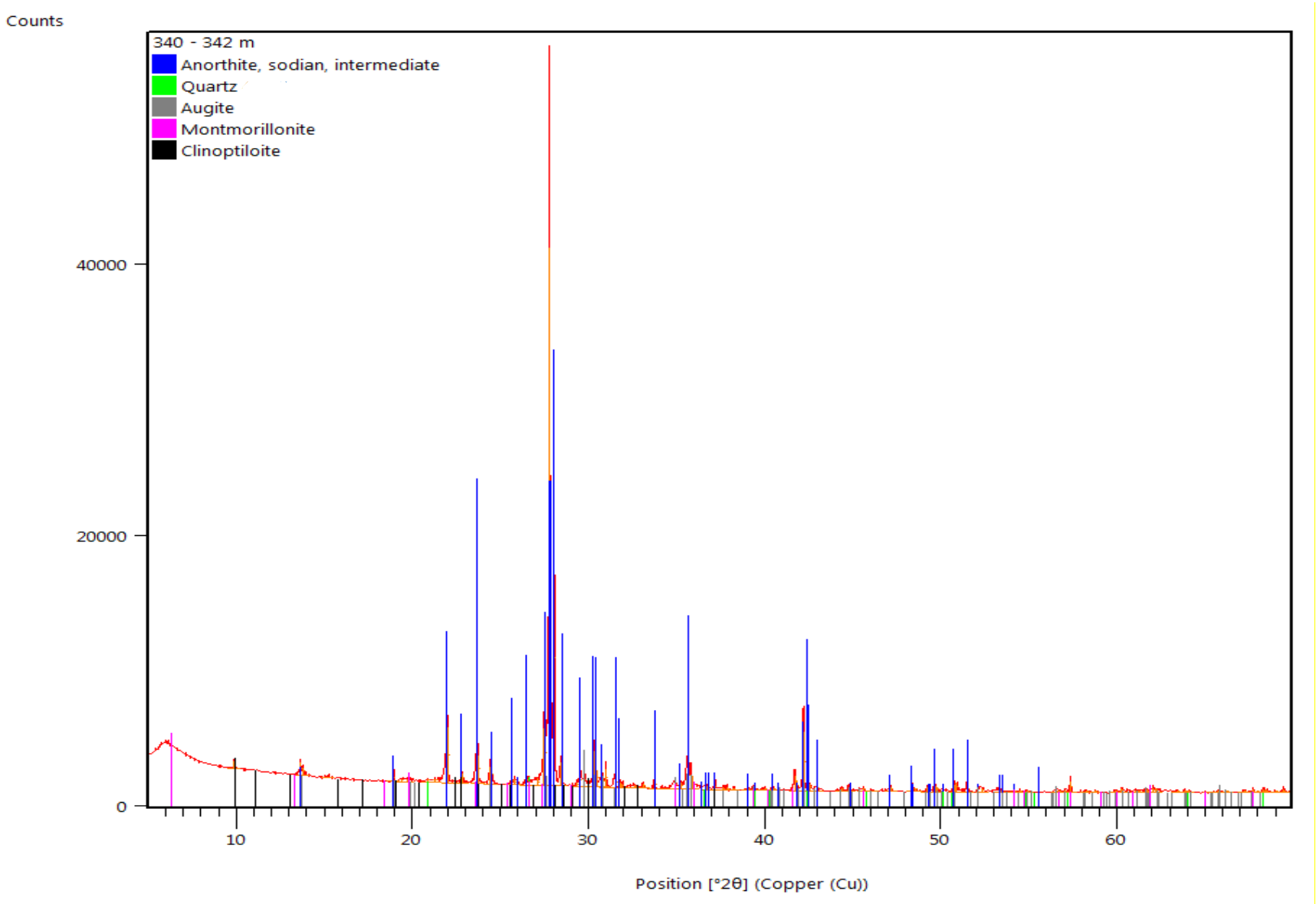

Figure A.75 X-ray diffraction pattern for Lourdes drill cuttings

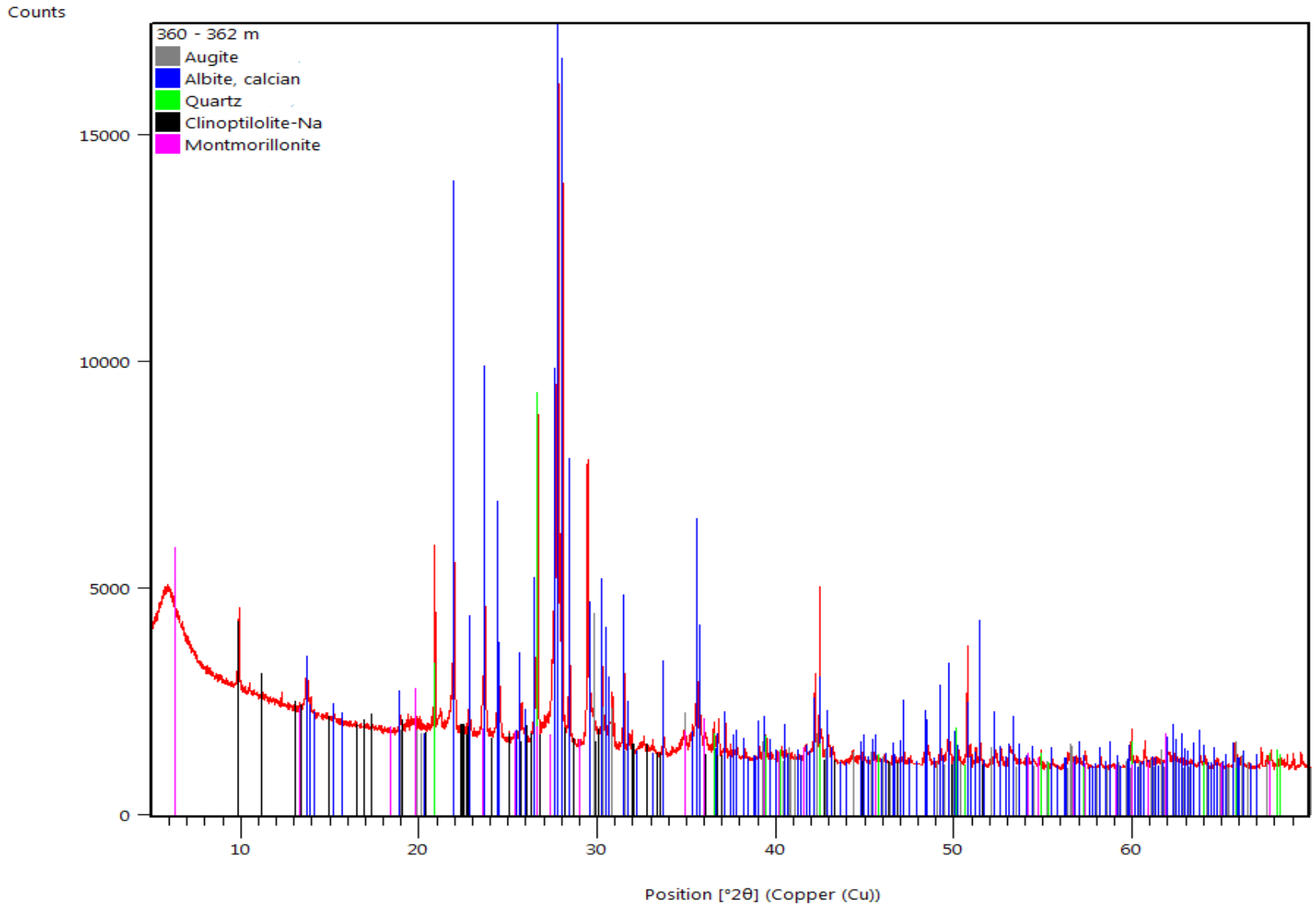

Figure A.76 X-ray diffraction pattern for Lourdes drill cuttings

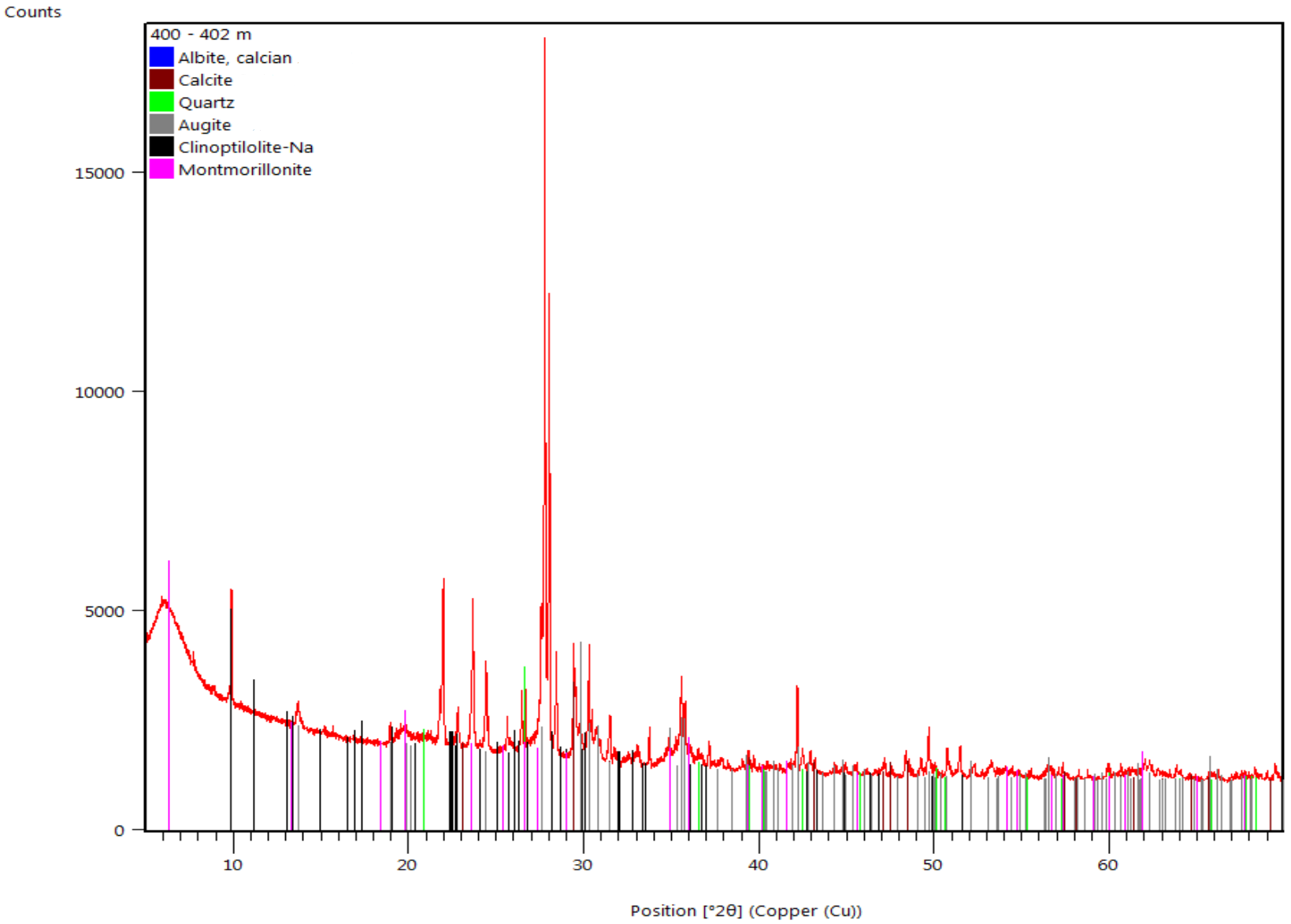

Figure A.77 X-ray diffraction pattern for Lourdes drill cuttings

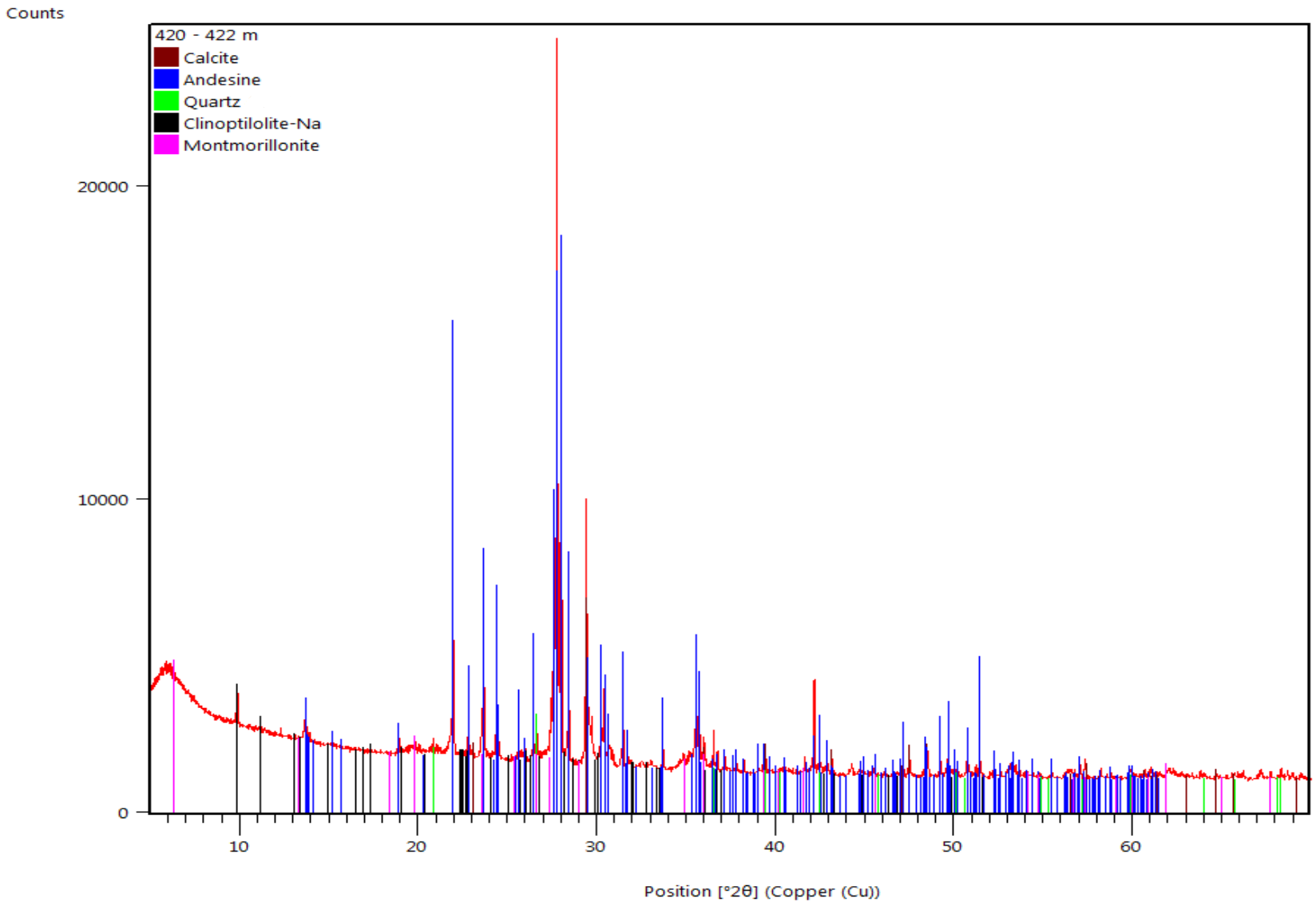

Figure A.78 X-ray diffraction pattern for Lourdes drill cuttings

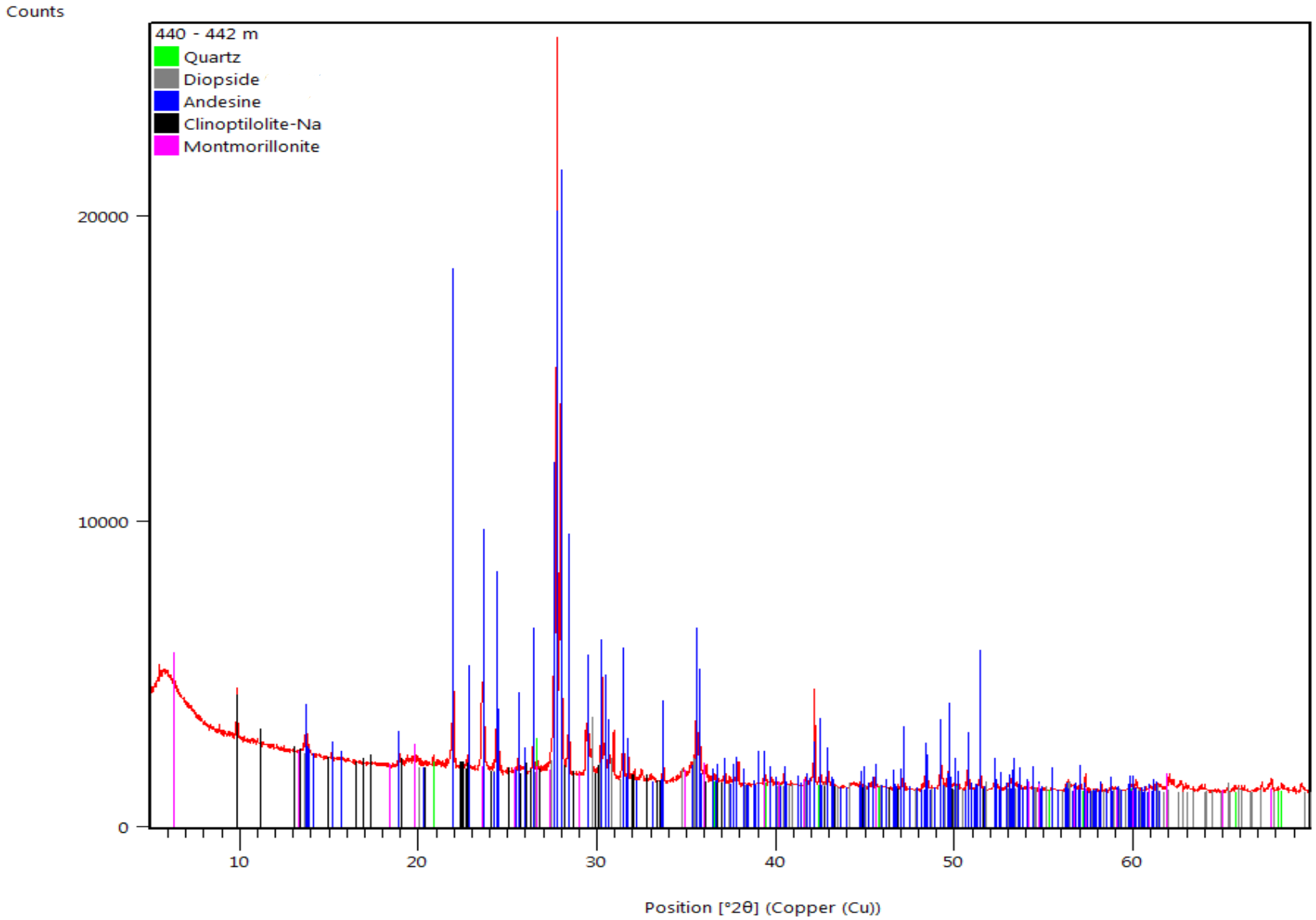

Figure A.79 X-ray diffraction pattern for Lourdes drill cuttings

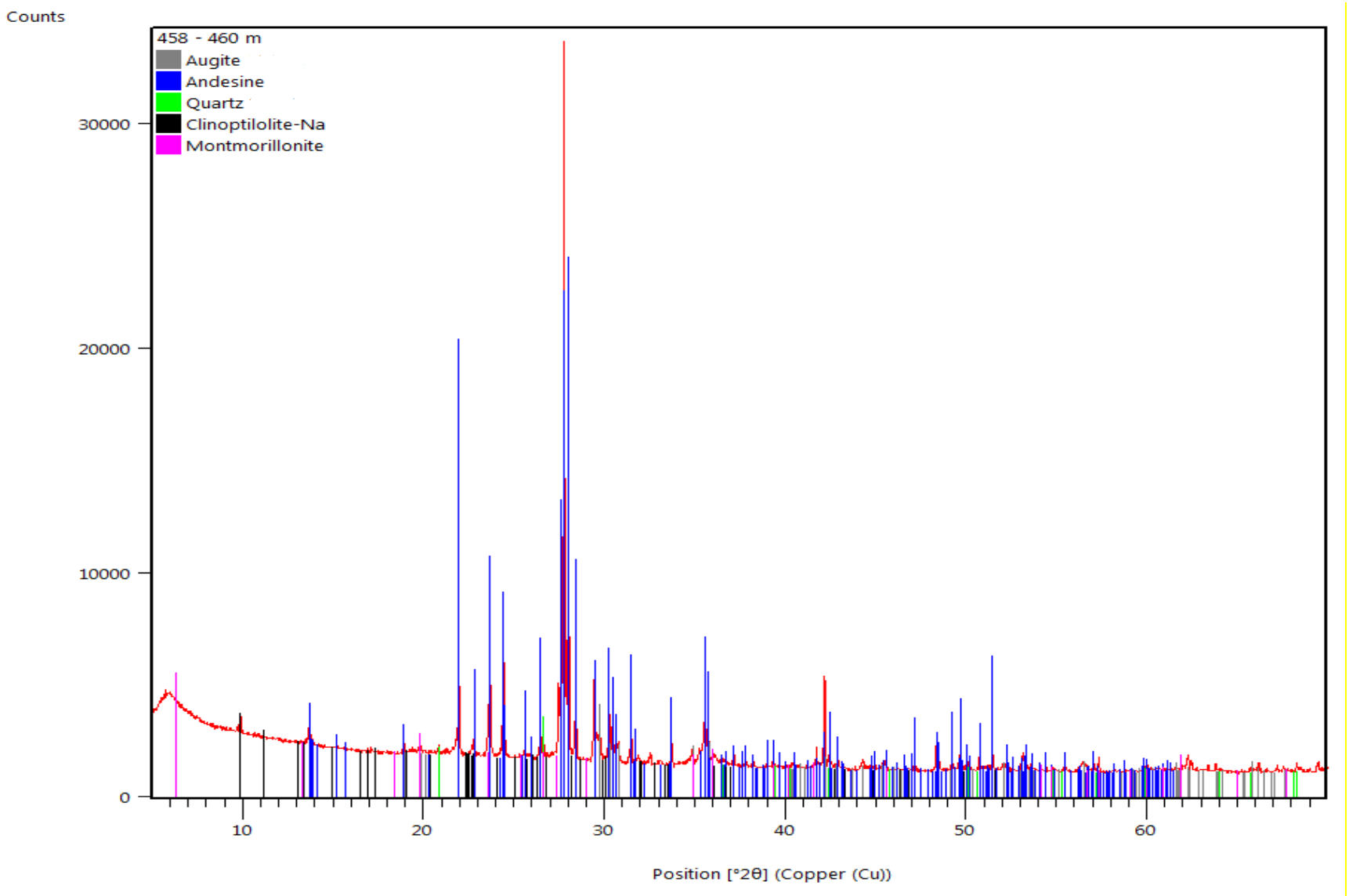

Figure A.80 X-ray diffraction pattern for Lourdes drill cuttings

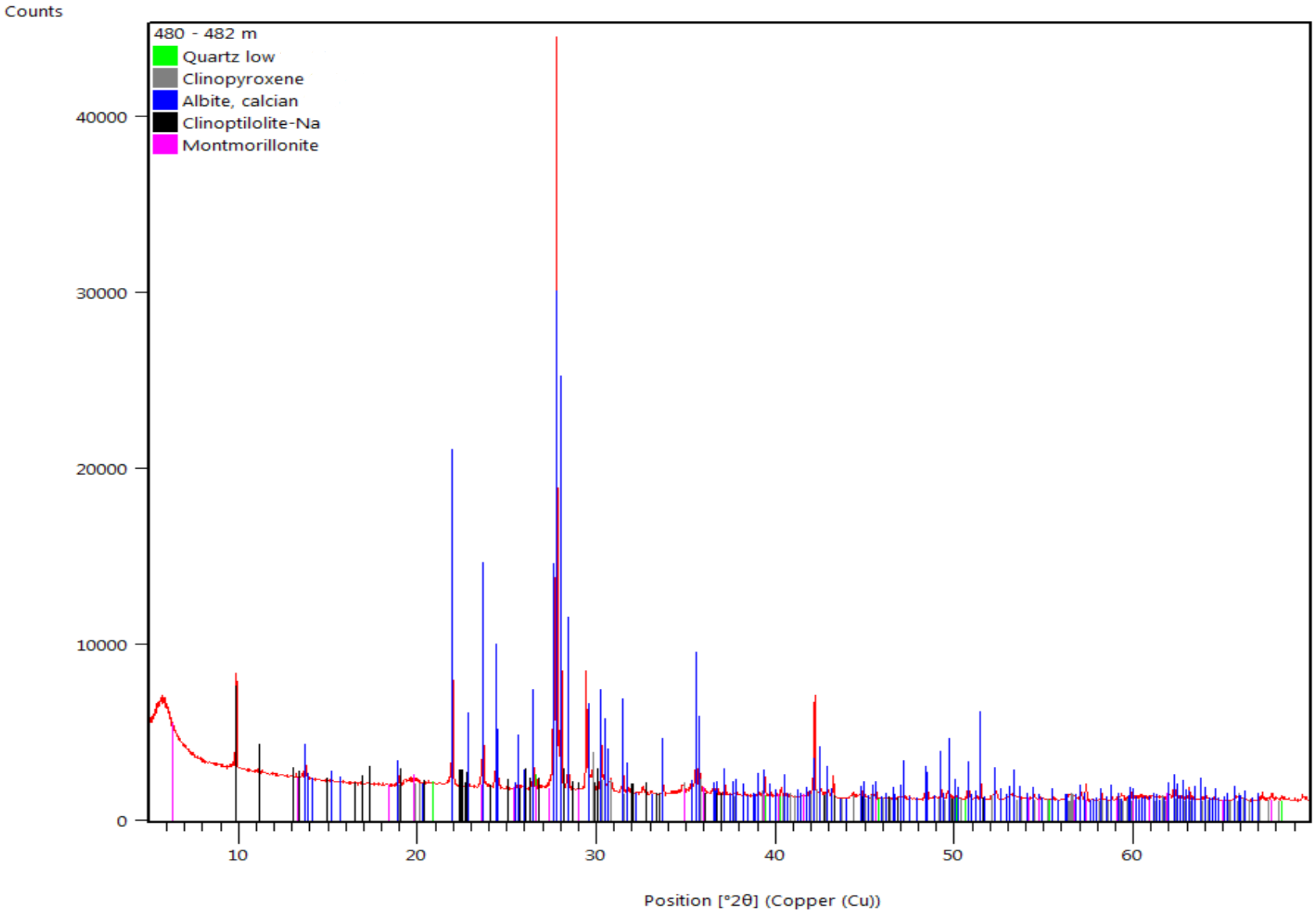

Figure A.81 X-ray diffraction pattern for Lourdes drill cuttings

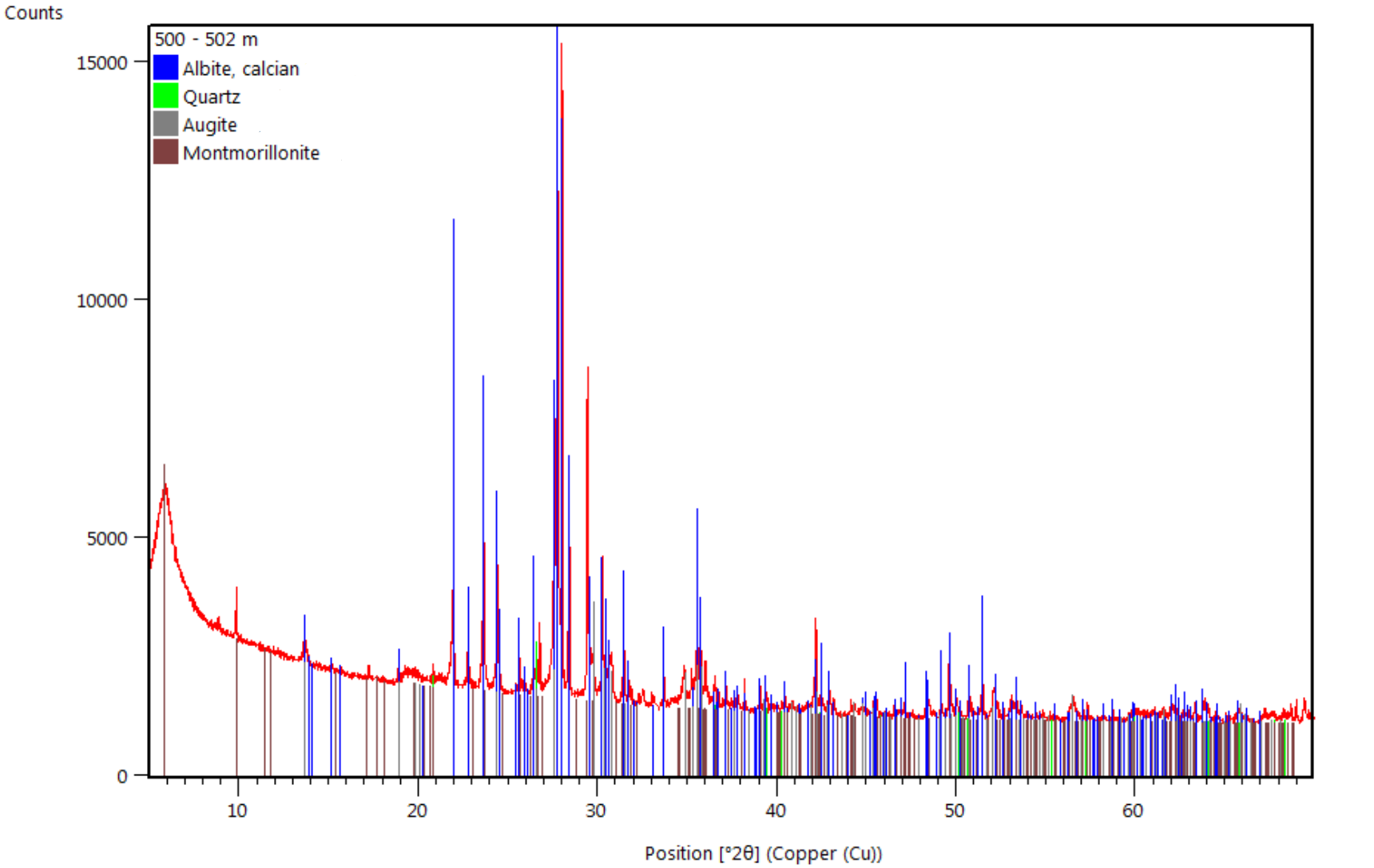

Figure A.82 X-ray diffraction pattern for Lourdes drill cuttings

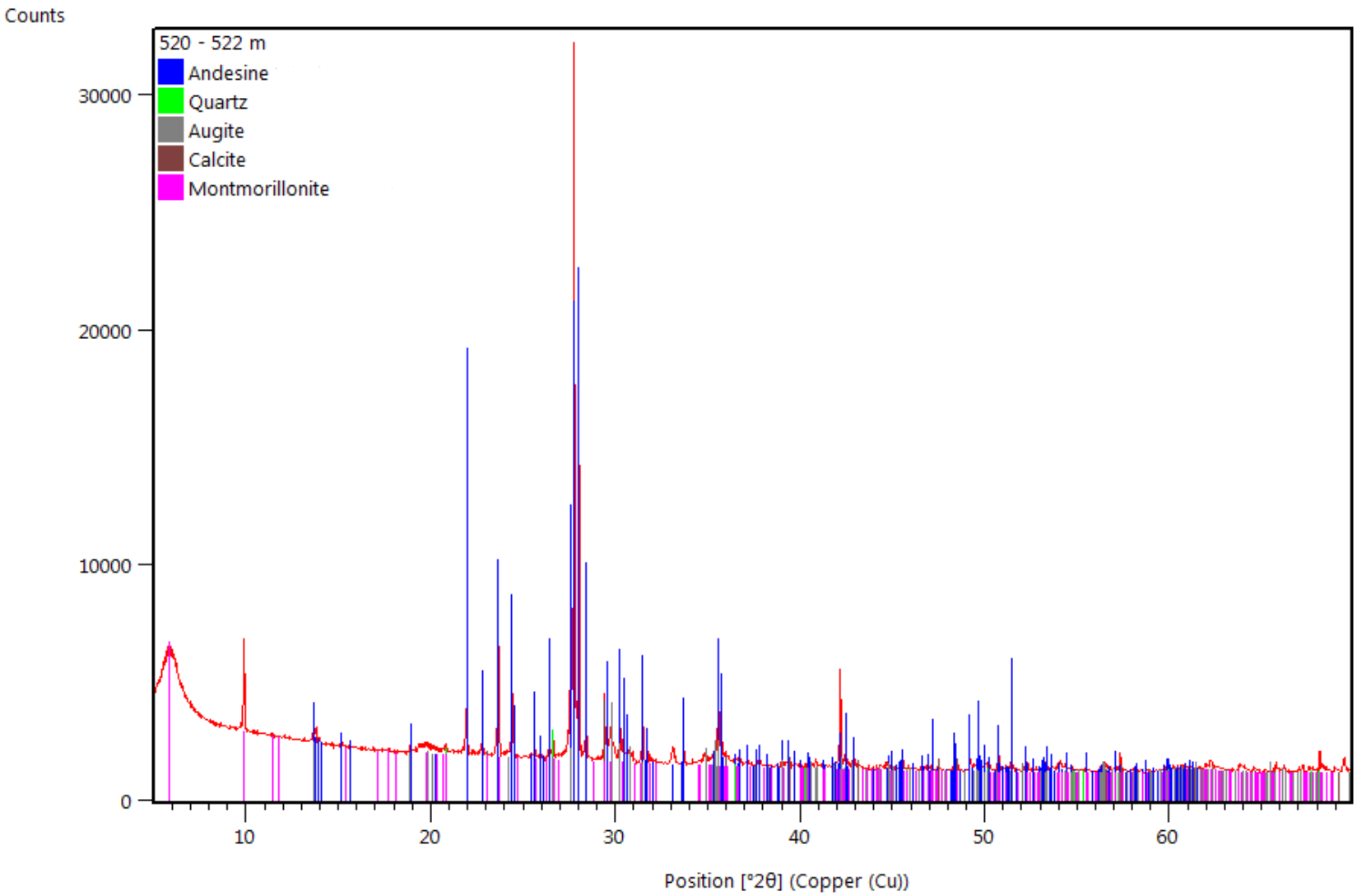

Figure A.83 X-ray diffraction pattern for Lourdes drill cuttings

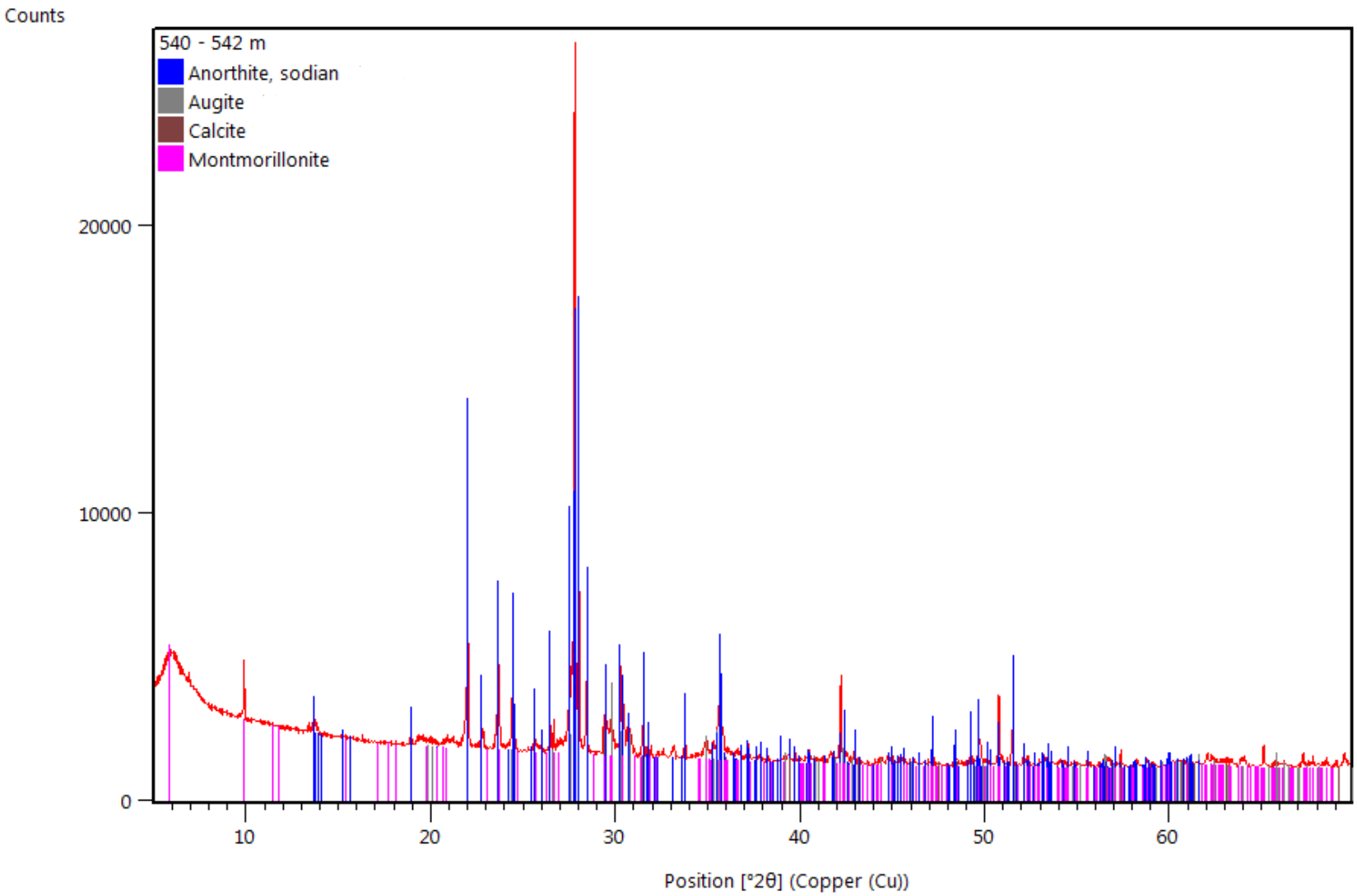

Figure A.84 X-ray diffraction pattern for Lourdes drill cuttings

Table A.85 Field rock samples: X-ray fluorescence results for major and trace elements. Values indicated as red were below quantification levels.

	Mg	Al	Si	P	S	Cl	K	Ca	Ti	V
	mg/kg	mg/kg	mg/kg	mg/kg	mg/kg	mg/kg	mg/kg	mg/kg	mg/kg	mg/kg
SAMPLE 4 - FINE SSF	4290	80900	3E+05	n.a	1520	56.4	21400	5710	3170	48.6
SAMPLE 4 - CONGLOMERADE	n.a	85900	3E+05	n.a	59200	n.a	32200	1210	625	49
SAMPLE 7 - IGNIMBRITE	n.a	71700	4E+05	n.a	155	95.7	40100	583	990	n.a

	Cr	Mn	Fe	Co	Ni	Cu	Zn	Ga	As	Rb
	mg/kg	mg/kg	mg/kg	mg/kg	mg/kg	mg/kg	mg/kg	mg/kg	mg/kg	mg/kg
SAMPLE 4 - FINE SSF	n.a	2910	26500	52.5	22.4	20.6	77	19.7	16.6	164
SAMPLE 4 - CONGLOMERADE	n.a	41.2	725	n.a	3.87	n.a	6.95	13.2	9.92	11.1
SAMPLE 7 - IGNIMBRITE	7.65	167	13500	41.9	n.a	10.5	79.2	21.9	6.77	169

	Sr	Y	Nb	Sn	Ba	Hf	Ta	W	Ir	Au
	mg/kg	mg/kg	mg/kg	mg/kg	mg/kg	mg/kg	mg/kg	mg/kg	mg/kg	mg/kg
SAMPLE 4 - FINE SSF	125	66.2	22.1	15.7	653	n.a	17.6	n.a	7.65	3.81
SAMPLE 4 - CONGLOMERADE	78.5	10.1	19.2	11.9	618	9.69	24.9	5.85	8.92	2.52
SAMPLE 7 - IGNIMBRITE	20.6	39.1	24.2	15.1	n.a	17.1	8.89	n.a	n.a	2.33

	Tl	Pb	O	Ra	Sc	Na	Zr	Re	Ar	Kr
	mg/kg	mg/kg	mg/kg	mg/kg	mg/kg	mg/kg	mg/kg	mg/kg	mg/kg	mg/kg
SAMPLE 4 - FINE SSF	4.06	20.7	6E+05	1.85	n.a	3790	2230	8.11	319	7.42
SAMPLE 4 - CONGLOMERADE	n.a	19.8	5E+05	n.a	n.a	n.a	1770	4.47	384	4.96
SAMPLE 7 - IGNIMBRITE	n.a	n.a	5E+05	n.a	n.a	21600	2390	n.a	157	3.43

Table A.86 Arrastres drill cuttings: X-ray fluorescence results for major elements

Majors	Mg Ka1	Al Ka1	Si Ka1	P Ka1	S Ka1	K Ka1	Ca Ka1	Ti Ka1	V Ka1	Cr Ka1	Mn Ka1	Fe Ka1
010 - 012 Arrastres 1	0.49	4.36	17.67	0.06	0.20	0.92	2.97	0.62	0.00	0.01	0.05	4.38
010 - 012 Arrastres 2	0.92	4.84	18.79	0.09	0.20	1.05	3.28	0.66	0.01	0.02	0.06	5.18
010 - 012 Arrastres 3	1.10	5.40	18.84	0.10	0.18	1.10	4.07	0.81	0.01	0.01	0.09	3.84
020 - 022 Arrastres 1	0.96	5.24	18.07	0.10	0.19	1.09	4.11	0.77	0.01	0.01	0.09	4.09
020 - 022 Arrastres 2	0.92	5.20	18.04	0.09	0.19	1.08	4.11	0.78	0.01	0.01	0.10	4.11
020 - 022 Arrastres 3	1.03	5.35	18.55	0.11	0.18	1.12	4.14	0.78	0.01	0.01	0.08	4.28
040 - 042 Arrastres 1	1.14	5.43	17.92	0.13	0.16	0.94	4.23	0.79	0.01	0.01	0.08	4.72
040 - 042 Arrastres 2	1.28	5.49	17.95	0.13	0.17	0.94	4.31	0.81	0.01	0.01	0.08	4.46
040 - 042 Arrastres 3	1.20	5.48	17.94	0.13	0.17	0.95	4.29	0.80	0.01	0.01	0.08	4.69
060 - 062 Arrastres 1	0.23	4.69	21.58	0.05	0.23	1.61	2.30	0.41	0.00	0.01	0.06	3.31
060 - 062 Arrastres 2	0.28	4.86	23.14	0.05	0.23	1.69	2.44	0.41	0.00	0.01	0.05	3.04
060 - 062 Arrastres 3	0.29	4.86	22.80	0.05	0.26	1.64	2.32	0.39	0.00	0.01	0.05	3.14
080 - 082 Arrastres 1		3.88	29.05	0.04	0.20	2.51	1.09	0.18	0.01	0.01	0.04	1.99
080 - 082 Arrastres 2		3.73	27.12	0.03	0.20	2.41	1.15	0.19	0.01	0.01	0.04	2.16
080 - 082 Arrastres 3		3.91	28.66	0.04	0.21	2.52	1.17	0.19	0.01	0.01	0.05	2.17
100 - 102 Arrastres 1		4.74	26.38	0.01	0.22	2.59	0.85	0.07	0.01	0.01	0.03	1.17
100 - 102 Arrastres 2	0.01	5.03	27.48	0.02	0.21	2.88	0.94	0.09	0.02	0.01	0.03	1.34
100 - 102 Arrastres 3		4.82	26.04	0.02	0.21	2.75	0.91	0.07	0.01	0.01	0.03	1.20
120 - 122 Arrastres 1	0.00	5.01	28.19	0.03	0.21	3.22	1.26	0.19	0.01	0.01	0.03	1.96
120 - 122 Arrastres 2	0.11	5.12	28.34	0.03	0.21	3.21	1.23	0.14	0.01	0.01	0.04	2.01
120 - 122 Arrastres 3	0.11	5.15	28.86	0.03	0.21	3.29	1.21	0.16	0.01	0.01	0.04	2.05
142 - 144 Arrastres 1	0.08	4.68	22.32	0.00	0.20	1.24	1.01	0.11	0.01	0.01	0.03	1.66
142 - 144 Arrastres 2	0.27	5.10	23.73	0.01	0.19	1.33	1.09	0.13	0.01	0.01	0.03	1.78
142 - 144 Arrastres 3	0.09	4.62	21.63	0.00	0.20	1.08	0.98	0.10	0.01	0.01	0.03	1.72
160 - 162 Arrastres 1		4.04	27.48	0.02	0.21	2.93	0.59	0.06	0.02	0.01	0.03	1.16
160 - 162 Arrastres 2		4.26	28.49	0.02	0.20	3.14	0.62	0.05	0.01	0.01	0.03	1.09
160 - 162 Arrastres 3		4.25	28.73	0.02	0.21	3.12	0.59	0.06	0.01	0.01	0.03	1.05
180 - 182 Arrastres 1	0.24	4.46	20.58	0.07	0.18	1.87	2.49	0.37	0.00	0.01	0.04	2.97
180 - 182 Arrastres 2	0.31	4.59	22.07	0.08	0.18	1.95	2.37	0.40		0.01	0.04	2.89

180 - 182 Arrastres 3	0.19	4.30	20.62	0.06	0.17	1.95	2.37	0.38	0.00	0.01	0.04	2.88
200 - 202 Arrastres 1	0.37	5.08	21.19	0.07	0.17	1.62	2.56	0.64		0.00	0.05	2.60
200 - 202 Arrastres 2	0.71	5.28	24.53	0.10	0.18	1.90	2.66	0.72	0.01	0.00	0.05	2.68
200 - 202 Arrastres 3	0.62	5.06	23.21	0.08	0.18	1.78	2.77	0.79	0.00	0.00	0.05	2.38
220 - 222 Arrastres 1	1.00	5.53	20.11	0.20	0.17	1.41	3.95	1.21	0.03		0.07	1.85
220 - 222 Arrastres 2	0.77	5.18	18.81	0.16	0.17	1.38	3.83	1.09	0.02		0.07	2.35
220 - 222 Arrastres 3	1.03	5.34	19.60	0.17	0.17	1.43	3.92	1.01	0.01		0.07	2.61
240 - 242 Arrastres 1	0.92	5.38	18.91	0.28	0.14	1.36	4.50	0.55	0.00	0.00	0.07	4.51
240 - 242 Arrastres 2	1.05	5.61	19.21	0.25	0.15	1.37	4.50	0.58	0.01	0.00	0.07	4.34
240 - 242 Arrastres 3	0.87	5.65	19.38	0.26	0.15	1.39	4.54	0.46	0.00	0.01	0.06	4.20
260 - 262 Arrastres 1	1.06	5.17	18.39	0.22	0.16	1.23	3.94	0.89	0.01	0.00	0.07	3.52
260 - 262 Arrastres 2	0.75	5.41	18.90	0.21	0.15	1.40	3.98	0.55	0.00	0.00	0.06	4.05
260 - 262 Arrastres 3	0.94	5.64	19.06	0.25	0.14	1.32	4.37	0.61	0.01	0.00	0.07	4.21
280 - 282 Arrastres 1	0.81	4.62	16.48	0.15	0.17	1.11	3.39	1.86	0.10		0.07	
280 - 282 Arrastres 2	0.91	4.97	17.60	0.14	0.17	1.17	3.50	1.44	0.04		0.07	1.05
280 - 282 Arrastres 3	0.73	5.32	18.59	0.15	0.16	1.39	3.77	1.09	0.01		0.06	2.44
300 - 302 Arrastres 1	1.09	4.91	17.08	0.21	0.15	1.01	3.53	2.00	0.13		0.09	
300 - 302 Arrastres 2	1.08	5.13	17.45	0.20	0.15	1.05	3.57	2.10	0.15		0.09	
300 - 302 Arrastres 3	1.36	5.83	19.37	0.27	0.15	1.20	4.20	1.32	0.04		0.09	1.71
320 - 322 Arrastres 1	1.14	5.43	18.44	0.19	0.16	1.22	3.77	1.88	0.10		0.08	
320 - 322 Arrastres 2	0.98	5.69	19.65	0.22	0.16	1.39	4.28	0.88	0.01	0.00	0.07	3.25
320 - 322 Arrastres 3	0.87	5.75	19.59	0.22	0.15	1.39	4.20	0.94	0.02		0.07	3.18
340 - 342 Arrastres 1	1.12	4.89	16.40	0.20	0.16	0.97	3.27	2.93	0.36		0.09	
340 - 342 Arrastres 2	1.12	4.87	16.39	0.18	0.16	0.96	3.27	2.90	0.35		0.09	
340 - 342 Arrastres 3	1.00	4.91	16.59	0.17	0.17	1.09	3.19	2.51	0.24		0.08	
360 - 362 Arrastres 1	1.09	5.74	19.17	0.18	0.15	1.24	4.37	0.96	0.01	0.00	0.07	3.01
360 - 362 Arrastres 2	1.03	5.64	18.83	0.20	0.15	1.24	4.45	0.90	0.01	0.00	0.07	3.28
360 - 362 Arrastres 3	0.91	5.68	19.13	0.20	0.14	1.25	4.41	1.03	0.02		0.07	2.79
380 - 382 Arrastres 1	1.17	5.23	17.78	0.13	0.14	1.02	3.73	1.14	0.02		0.07	2.43
380 - 382 Arrastres 2	1.43	5.53	18.69	0.16	0.16	1.12	3.92	1.13	0.02		0.07	2.51
380 - 382 Arrastres 3	1.63	5.76	19.31	0.17	0.16	1.18	4.10	1.05	0.02	0.00	0.07	2.79
404 - 406 Arrastres 1	0.28	4.93	26.34	0.06	0.20	2.47	1.89	0.40	0.00	0.01	0.04	2.61

404 - 406 Arrastres 2	0.30	4.99	25.04	0.06	0.20	2.19	1.98	0.58	0.00	0.01	0.05	2.58
404 - 406 Arrastres 3	0.27	5.04	26.01	0.06	0.20	2.38	1.98	0.41	0.00	0.01	0.05	2.61
424 - 426 Arrastres 1	0.11	4.37	22.83	0.04	0.20	2.31	1.75	0.54	0.00	0.01	0.04	2.45
424 - 426 Arrastres 2		4.24	22.58	0.03	0.20	2.45	1.63	0.36	0.00	0.01	0.04	2.37
424 - 426 Arrastres 3	0.07	4.24	22.55	0.04	0.20	2.38	1.75	0.34	0.00	0.01	0.05	2.48
440 - 442 Arrastres 1		4.49	25.47	0.02	0.23	3.05	1.16	0.13	0.01	0.01	0.03	1.30
440 - 442 Arrastres 2		4.25	23.98	0.02	0.21	2.85	1.16	0.11	0.01	0.01	0.03	1.53
440 - 442 Arrastres 3		4.40	25.14	0.02	0.21	2.97	1.12	0.08	0.01	0.01	0.03	1.22
460 - 462 Arrastres 1	0.35	4.81	19.71	0.09	0.19	1.67	3.20	0.52	0.00	0.01	0.05	3.58
460 - 462 Arrastres 2	0.47	4.74	19.68	0.10	0.18	1.66	3.21	0.53	0.00	0.01	0.05	3.59
460 - 462 Arrastres 3	0.47	4.79	19.99	0.10	0.18	1.68	3.21	0.52	0.00	0.01	0.05	3.60
480 - 482 Arrastres 1		4.33	24.71	0.03	0.22	2.82	1.71	0.18	0.01	0.01	0.03	1.92
480 - 482 Arrastres 2		4.34	24.68	0.03	0.21	2.86	1.73	0.19	0.01	0.01	0.03	2.11
480 - 482 Arrastres 3		4.60	25.28	0.03	0.21	2.95	1.76	0.17	0.01	0.01	0.03	1.85
500 - 502 Arrastres 1		4.62	27.85	0.04	0.22	3.39	1.95	0.17	0.01	0.01	0.03	1.48
500 - 502 Arrastres 2		4.87	28.42	0.04	0.22	3.51	1.88	0.18	0.01	0.01	0.03	1.56
500 - 502 Arrastres 3		4.74	28.32	0.04	0.22	3.55	1.82	0.16	0.01	0.01	0.03	1.34
RTC-W-220-1	0.94	5.00	31.76	0.10	2.52	2.44	0.18	0.28	0.09	0.01	0.02	2.78
RTC-W-220-2	0.74	4.95	31.32	0.10	2.46	2.41	0.17	0.27	0.09	0.01	0.02	2.83
RTC-W-220-3	0.85	5.02	31.39	0.10	2.39	2.41	0.20	0.28	0.09	0.01	0.02	2.85
RTC-W-220-4	0.66	4.97	31.08	0.09	2.39	2.38	0.18	0.27	0.09	0.01	0.02	2.86
RTC-W-220-5	0.78	5.06	31.49	0.09	2.40	2.44	0.18	0.28	0.10	0.01	0.02	2.77

Table A.87 Arrastres drill cuttings: X-ray Fluorescence results for trace element

Trace	BaLa1	CoKa1	NiKa1	CuKa1	ZnKa1	GaKa1	AsKa1
010 - 012 Arrastres 1	1.9E-01	6.6E-03	9.7E-03	1.2E-02	1.3E-02	1.9E-03	
010 - 012 Arrastres 2	1.4E-01	7.3E-03	9.9E-03	9.9E-03	1.3E-02	1.9E-03	4.9E-04
010 - 012 Arrastres 3	1.3E-01	7.0E-03	1.0E-02	1.1E-02	1.2E-02	2.2E-03	
020 - 022 Arrastres 1	2.7E-01	7.4E-03	9.4E-03	5.4E-03	1.2E-02	1.9E-03	
020 - 022 Arrastres 2	2.7E-01	7.5E-03	9.2E-03	4.7E-03	1.2E-02	1.7E-03	1.3E-04
020 - 022 Arrastres 3	1.3E-01	7.1E-03	9.6E-03	5.2E-03	1.3E-02	1.8E-03	4.1E-04
040 - 042 Arrastres 1	2.6E-01	8.7E-03	9.7E-03	9.6E-03	1.3E-02	2.0E-03	2.3E-04
040 - 042 Arrastres 2	3.2E-01	7.1E-03	9.4E-03	7.6E-03	1.2E-02	1.6E-03	1.7E-04
040 - 042 Arrastres 3	1.3E-01	5.2E-03	8.5E-03	6.1E-03	9.9E-03	1.1E-03	1.8E-04
060 - 062 Arrastres 1	1.4E-01	1.7E-03	4.9E-03	3.6E-03	1.3E-02	2.2E-03	6.4E-04
060 - 062 Arrastres 2	1.6E-01	3.0E-03	5.8E-03	4.4E-03	1.5E-02	2.3E-03	9.7E-04
060 - 062 Arrastres 3	1.3E-01	1.7E-03	4.9E-03	3.7E-03	1.3E-02	2.1E-03	1.3E-03
080 - 082 Arrastres 1	5.2E-02	9.2E-04	2.0E-03	2.7E-03	7.3E-03	1.7E-03	4.2E-04
080 - 082 Arrastres 2	8.3E-02	8.3E-04	1.9E-03	3.3E-03	7.7E-03	1.9E-03	
080 - 082 Arrastres 3	4.8E-02	8.4E-04	1.5E-03	2.7E-03	6.7E-03	1.5E-03	1.0E-05
100 - 102 Arrastres 1	4.9E-02	6.8E-04	7.3E-04	4.9E-03	8.8E-03	2.0E-03	1.0E-03
100 - 102 Arrastres 2		4.1E-04		6.9E-04	3.2E-03	6.7E-04	1.0E-03
100 - 102 Arrastres 3		7.8E-04	7.1E-04	3.4E-03	8.0E-03	2.0E-03	9.0E-04
120 - 122 Arrastres 1		7.8E-04	2.2E-03	2.6E-03	1.0E-02	2.2E-03	1.4E-03
120 - 122 Arrastres 2	5.8E-02	7.5E-04	1.6E-03	2.5E-03	1.0E-02	2.1E-03	1.9E-03
120 - 122 Arrastres 3	2.0E-02	6.2E-04	1.2E-03	2.2E-03	1.0E-02	2.2E-03	1.3E-03
142 - 144 Arrastres 1		8.7E-04	6.0E-04	1.1E-03	8.1E-03	1.9E-03	6.1E-04
142 - 144 Arrastres 2	2.1E-02	7.0E-04	1.7E-03	1.7E-03	8.8E-03	2.4E-03	9.6E-04
142 - 144 Arrastres 3	3.8E-02	6.0E-04	7.1E-04	1.2E-03	8.7E-03	2.3E-03	6.7E-04
160 - 162 Arrastres 1	4.7E-02	5.3E-04	4.4E-04	1.1E-03	6.2E-03	1.5E-03	7.6E-04
160 - 162 Arrastres 2		6.4E-04	3.8E-04	9.9E-04	5.8E-03	1.7E-03	1.0E-03
160 - 162 Arrastres 3	2.0E-02	4.3E-04	2.4E-04	1.4E-03	6.1E-03	1.7E-03	1.5E-03
180 - 182 Arrastres 1	1.2E-01	1.5E-03	2.9E-03	1.8E-03	6.9E-03	1.9E-03	5.5E-04
180 - 182 Arrastres 2	3.0E-02	1.5E-03	2.8E-03	1.6E-03	7.0E-03	1.8E-03	7.8E-04

180 - 182 Arrastres 3	1.5E-01	9.8E-04	2.5E-03	1.2E-03	6.1E-03	1.4E-03	3.0E-04
200 - 202 Arrastres 1	3.3E-01	2.8E-03	4.3E-03	2.1E-03	8.8E-03	2.4E-03	5.6E-04
200 - 202 Arrastres 2	1.1E-01	2.8E-03	4.3E-03	2.6E-03	9.9E-03	2.5E-03	7.8E-04
200 - 202 Arrastres 3	2.0E-01	4.6E-03	5.0E-03	3.4E-03	1.1E-02	2.9E-03	3.2E-04
220 - 222 Arrastres 1	3.7E-01	8.9E-03	6.9E-03	3.1E-03	1.3E-02	2.3E-03	
220 - 222 Arrastres 2	2.8E-01	8.1E-03	6.5E-03	3.2E-03	1.2E-02	2.5E-03	
220 - 222 Arrastres 3	4.7E-01	7.6E-03	6.3E-03	3.3E-03	1.3E-02	2.4E-03	
240 - 242 Arrastres 1	3.9E-01	8.4E-03	7.1E-03	3.2E-03	1.4E-02	2.4E-03	
240 - 242 Arrastres 2	2.7E-01	8.7E-03	7.0E-03	3.3E-03	1.4E-02	2.5E-03	
240 - 242 Arrastres 3	1.9E-01	9.5E-03	7.3E-03	3.2E-03	1.3E-02	2.4E-03	5.6E-06
260 - 262 Arrastres 1	4.6E-01	1.1E-02	7.7E-03	3.4E-03	1.6E-02	2.7E-03	
260 - 262 Arrastres 2	1.5E-01	1.3E-02	8.1E-03	3.3E-03	1.6E-02	2.2E-03	
260 - 262 Arrastres 3	2.0E-01	1.1E-02	7.6E-03	3.0E-03	1.6E-02	2.5E-03	
280 - 282 Arrastres 1	1.3E+00	2.4E-02	9.9E-03	5.6E-03	1.6E-02	3.0E-03	
280 - 282 Arrastres 2	1.3E+00	2.3E-02	9.9E-03	6.0E-03	1.6E-02	3.1E-03	
280 - 282 Arrastres 3	1.0E+00	2.2E-02	9.7E-03	5.3E-03	1.6E-02	2.8E-03	
300 - 302 Arrastres 1	6.4E-01	2.6E-02	1.0E-02	5.0E-03	2.0E-02	2.7E-03	
300 - 302 Arrastres 2	1.3E+00	3.1E-02	1.1E-02	4.9E-03	2.0E-02	3.0E-03	
300 - 302 Arrastres 3	1.1E+00	3.4E-02	1.1E-02	5.5E-03	2.0E-02	2.7E-03	
320 - 322 Arrastres 1	7.7E-01	2.6E-02	1.0E-02	4.8E-03	1.8E-02	3.0E-03	
320 - 322 Arrastres 2	1.0E+00	2.6E-02	1.0E-02	5.1E-03	1.7E-02	3.1E-03	
320 - 322 Arrastres 3	9.5E-01	2.2E-02	9.7E-03	4.4E-03	1.7E-02	2.8E-03	
340 - 342 Arrastres 1	1.5E+00	4.5E-02	1.2E-02	8.8E-03	2.1E-02	3.1E-03	
340 - 342 Arrastres 2	2.6E+00	7.1E-02	1.2E-02	9.1E-03	2.4E-02	2.9E-03	2.0E-04
340 - 342 Arrastres 3	1.6E+00	4.7E-02	1.2E-02	8.2E-03	2.0E-02	3.3E-03	1.3E-05
360 - 362 Arrastres 1	3.7E-01	8.3E-03	7.0E-03	3.7E-03	1.3E-02	2.2E-03	
360 - 362 Arrastres 2	2.8E-01	7.6E-03	7.1E-03	3.7E-03	1.3E-02	2.2E-03	
360 - 362 Arrastres 3	3.1E-02	7.6E-03	6.9E-03	3.9E-03	1.2E-02	2.2E-03	
380 - 382 Arrastres 1	3.2E-01	9.1E-03	8.3E-03	4.1E-03	1.1E-02	2.2E-03	1.6E-04
380 - 382 Arrastres 2	6.4E-01	9.0E-03	8.2E-03	4.0E-03	1.2E-02	2.3E-03	
380 - 382 Arrastres 3	3.9E-01	8.5E-03	8.2E-03	4.2E-03	1.2E-02	2.2E-03	6.9E-06
404 - 406 Arrastres 1	1.9E-01	1.9E-03	3.2E-03	1.9E-03	8.6E-03	2.1E-03	2.3E-03

404 - 406 Arrastres 2	7.0E-02	2.2E-03	4.1E-03	2.0E-03	8.8E-03	2.3E-03	1.7E-03
404 - 406 Arrastres 3	4.5E-01	3.3E-03	4.7E-03	2.2E-03	9.0E-03	2.5E-03	2.3E-03
424 - 426 Arrastres 1	0.112236	0.001022	0.002442	0.002739	0.007367	0.002116	0.001981
424 - 426 Arrastres 2	0.092335	0.001203	0.002443	0.00276	0.007002	0.001961	0.001824
424 - 426 Arrastres 3	0.128243	0.001047	0.002539	0.002861	0.007645	0.002156	0.001313
440 - 442 Arrastres 1	6.6E-02	1.3E-03	2.8E-03	9.8E-04	6.6E-03	2.0E-03	1.3E-03
440 - 442 Arrastres 2	2.7E-02	7.9E-04	1.1E-03	5.5E-04	4.8E-03	2.0E-03	1.7E-03
440 - 442 Arrastres 3	1.4E-01	9.1E-04	9.5E-04	1.1E-03	5.5E-03	2.0E-03	1.7E-03
460 - 462 Arrastres 1	0.044474	0.0032	0.004386	0.002391	0.010932	0.001918	0.000601
460 - 462 Arrastres 2	0.07408	0.003074	0.004492	0.00256	0.010506	0.001873	0.000872
460 - 462 Arrastres 3	0.055158	0.002884	0.004338	0.002496	0.010768	0.001877	0.000805
480 - 482 Arrastres 1	0.06954	0.000872	0.002038	0.003753	0.006476	0.001972	0.00133
480 - 482 Arrastres 2	0.027101	0.000792	0.001547	0.002867	0.005651	0.001615	0.001581
480 - 482 Arrastres 3		0.000741	0.00153	0.003333	0.006029	0.00199	0.001636
500 - 502 Arrastres 1	7.3E-02	5.6E-04	9.6E-04	4.5E-03	5.0E-03	1.8E-03	3.2E-03
500 - 502 Arrastres 2	1.7E-03	5.9E-04	9.3E-04	4.4E-03	4.7E-03	2.0E-03	1.9E-03
500 - 502 Arrastres 3	8.2E-02	7.3E-04	1.1E-03	4.4E-03	4.8E-03	1.8E-03	3.0E-03
RTC-W-220-1	8.4E-02	1.5E-03	1.4E-02	1.2E-02	8.3E-02	1.8E-03	2.0E-03
RTC-W-220-2	2.8E-01	1.6E-03	1.4E-02	1.2E-02	8.1E-02	1.7E-03	2.6E-03

Table A.88 Arrastres drill cuttings: X-ray Fluorescence results for trace element continued

Trace	PbLa1	ThLa1	RbKa1	U La1	SrKa1	Y Ka1	ZrKa1	NbKa1	MoKa1
010 - 012 Arrastres 1	1.2E-03	5.7E-04	6.4E-03		3.4E-02	4.6E-03	2.4E-02	1.0E-03	1.9E-03
010 - 012 Arrastres 2	1.3E-03	6.3E-04	7.0E-03	5.9E-04	3.3E-02	4.6E-03	2.4E-02	1.1E-03	2.6E-03
010 - 012 Arrastres 3	1.2E-03	6.0E-04	6.5E-03	8.6E-04	3.5E-02	4.7E-03	2.4E-02	1.1E-03	2.7E-03
020 - 022 Arrastres 1	1.1E-03	5.7E-04	6.3E-03		3.4E-02	4.2E-03	2.2E-02	1.0E-03	1.8E-03
020 - 022 Arrastres 2	1.1E-03	5.8E-04	6.9E-03		3.4E-02	4.3E-03	2.2E-02	8.8E-04	2.4E-03
020 - 022 Arrastres 3	1.2E-03	5.6E-04	6.4E-03		3.4E-02	4.1E-03	2.3E-02	1.0E-03	2.1E-03
040 - 042 Arrastres 1	1.3E-03	4.6E-04	5.1E-03		4.0E-02	4.0E-03	2.1E-02	9.6E-04	1.9E-03
040 - 042 Arrastres 2	1.0E-03	4.1E-04	5.0E-03		3.6E-02	3.4E-03	1.9E-02	9.6E-04	1.7E-03
040 - 042 Arrastres 3	9.2E-04	3.3E-04	4.3E-03		2.8E-02	2.8E-03	1.5E-02	1.1E-03	3.4E-04
060 - 062 Arrastres 1	1.5E-03	8.8E-04	1.1E-02		2.5E-02	3.8E-03	3.1E-02	1.3E-03	2.5E-03
060 - 062 Arrastres 2	1.6E-03	7.8E-04	9.6E-03		2.7E-02	4.2E-03	2.3E-02	1.3E-03	1.6E-03
060 - 062 Arrastres 3	1.7E-03	8.8E-04	1.1E-02		2.7E-02	4.1E-03	2.1E-02	1.4E-03	1.1E-03
080 - 082 Arrastres 1	1.2E-03	1.1E-03	1.5E-02	2.3E-04	1.2E-02	4.2E-03	2.0E-02	1.5E-03	9.1E-04
080 - 082 Arrastres 2	1.1E-03	1.1E-03	1.4E-02	8.0E-04	1.1E-02	3.7E-03	2.1E-02	1.5E-03	1.0E-03
080 - 082 Arrastres 3	1.0E-03	9.7E-04	1.3E-02	9.1E-05	1.1E-02	4.2E-03	1.9E-02	1.5E-03	1.1E-03
100 - 102 Arrastres 1	1.6E-03	1.5E-03	2.0E-02		5.2E-03	2.7E-03	1.5E-02	1.7E-03	
100 - 102 Arrastres 2	1.1E-03	8.1E-04	1.0E-02		1.9E-03	2.7E-03	8.4E-03	1.7E-03	
100 - 102 Arrastres 3	1.5E-03	1.5E-03	2.0E-02		3.8E-03	2.3E-03	2.1E-02	1.7E-03	
120 - 122 Arrastres 1	1.7E-03	1.7E-03	2.2E-02		1.1E-02	1.7E-03	2.0E-02	1.7E-03	
120 - 122 Arrastres 2	1.8E-03	1.7E-03	2.2E-02	1.5E-04	1.2E-02	1.7E-03	1.6E-02	1.7E-03	
120 - 122 Arrastres 3	1.7E-03	1.7E-03	2.2E-02	2.5E-04	1.2E-02	1.7E-03	1.6E-02	1.6E-03	
142 - 144 Arrastres 1	1.4E-03	8.1E-04	1.1E-02		6.2E-03	5.2E-03	1.9E-02	1.8E-03	
142 - 144 Arrastres 2	1.6E-03	8.7E-04	1.1E-02		6.4E-03	6.0E-03	2.6E-02	2.0E-03	4.9E-04
142 - 144 Arrastres 3	1.5E-03	8.8E-04	1.2E-02		6.3E-03	5.0E-03	1.7E-02	1.7E-03	
160 - 162 Arrastres 1	1.4E-03	1.9E-03	2.4E-02	1.1E-03	3.0E-03	1.1E-03	1.4E-02	1.6E-03	
160 - 162 Arrastres 2	1.5E-03	1.8E-03	2.4E-02	1.0E-03	2.7E-03	1.1E-03	1.4E-02	1.6E-03	
160 - 162 Arrastres 3	1.6E-03	1.8E-03	2.4E-02	7.5E-04	2.3E-03	1.2E-03	1.5E-02	1.7E-03	
180 - 182 Arrastres 1	1.4E-03	1.3E-03	1.7E-02	9.9E-04	1.6E-02	3.1E-03	2.0E-02	1.3E-03	1.5E-03
180 - 182 Arrastres 2	1.4E-03	1.3E-03	1.7E-02	1.4E-04	1.5E-02	3.3E-03	2.0E-02	1.4E-03	1.0E-03

180 - 182 Arrastres 3	1.1E-03	1.1E-03	1.5E-02	8.0E-04	1.4E-02	3.5E-03	1.6E-02	1.4E-03	2.0E-04
200 - 202 Arrastres 1	1.5E-03	1.0E-03	1.2E-02		2.2E-02	4.0E-03	2.3E-02	1.5E-03	1.4E-03
200 - 202 Arrastres 2	1.6E-03	1.0E-03	1.2E-02		2.2E-02	4.1E-03	2.4E-02	1.6E-03	7.5E-04
200 - 202 Arrastres 3	1.6E-03	9.3E-04	1.1E-02		2.2E-02	3.8E-03	2.7E-02	1.7E-03	1.7E-03
220 - 222 Arrastres 1	1.3E-03	6.8E-04	7.4E-03		3.3E-02	4.3E-03	2.8E-02	1.4E-03	2.5E-03
220 - 222 Arrastres 2	1.3E-03	7.1E-04	7.5E-03	2.8E-04	3.4E-02	4.1E-03	2.9E-02	1.5E-03	3.0E-03
220 - 222 Arrastres 3	1.2E-03	6.8E-04	8.0E-03		3.6E-02	4.5E-03	2.9E-02	1.4E-03	2.8E-03
240 - 242 Arrastres 1	1.3E-03	6.2E-04	6.6E-03		3.8E-02	4.6E-03	3.0E-02	1.4E-03	3.3E-03
240 - 242 Arrastres 2	1.3E-03	6.3E-04	6.9E-03		3.8E-02	4.6E-03	2.9E-02	1.4E-03	2.8E-03
240 - 242 Arrastres 3	1.3E-03	6.1E-04	6.8E-03		3.7E-02	4.7E-03	3.0E-02	1.3E-03	3.0E-03
260 - 262 Arrastres 1	1.2E-03	5.6E-04	5.7E-03		3.3E-02	4.6E-03	2.7E-02	1.3E-03	2.0E-03
260 - 262 Arrastres 2	1.2E-03	5.6E-04	6.2E-03		3.3E-02	4.3E-03	2.7E-02	1.3E-03	2.5E-03
260 - 262 Arrastres 3	1.3E-03	5.6E-04	5.9E-03		3.4E-02	4.5E-03	2.8E-02	1.3E-03	2.4E-03
280 - 282 Arrastres 1	1.5E-03	5.7E-04	5.8E-03		2.9E-02	4.1E-03	4.2E-02	1.8E-03	3.9E-03
280 - 282 Arrastres 2	1.4E-03	5.8E-04	5.9E-03		2.9E-02	4.1E-03	4.2E-02	1.9E-03	4.4E-03
280 - 282 Arrastres 3	1.4E-03	5.7E-04	5.9E-03		3.0E-02	4.9E-03	4.0E-02	1.8E-03	3.8E-03
300 - 302 Arrastres 1	1.4E-03	5.1E-04	5.0E-03		2.7E-02	4.5E-03	3.9E-02	1.9E-03	3.3E-03
300 - 302 Arrastres 2	1.5E-03	5.1E-04	4.2E-03		2.5E-02	4.5E-03	4.2E-02	2.0E-03	4.2E-03
300 - 302 Arrastres 3	1.4E-03	5.0E-04	4.8E-03		2.4E-02	4.3E-03	4.6E-02	2.1E-03	4.9E-03
320 - 322 Arrastres 1	1.4E-03	5.6E-04	5.6E-03		2.7E-02	4.0E-03	4.2E-02	2.1E-03	3.4E-03
320 - 322 Arrastres 2	1.4E-03	5.8E-04	5.0E-03		2.8E-02	3.9E-03	4.3E-02	2.0E-03	4.6E-03
320 - 322 Arrastres 3	1.4E-03	5.8E-04	5.8E-03		3.0E-02	4.0E-03	3.9E-02	1.9E-03	4.3E-03
340 - 342 Arrastres 1	1.5E-03	5.0E-04	4.0E-03		2.1E-02	3.8E-03	4.9E-02	2.3E-03	4.3E-03
340 - 342 Arrastres 2	1.5E-03	4.3E-04	3.6E-03		1.5E-02	3.8E-03	5.5E-02	2.7E-03	5.1E-03
340 - 342 Arrastres 3	1.6E-03	5.6E-04	4.7E-03		2.3E-02	4.1E-03	4.9E-02	2.2E-03	5.1E-03
360 - 362 Arrastres 1	1.1E-03	5.9E-04	6.8E-03		4.0E-02	4.5E-03	2.8E-02	1.3E-03	3.3E-03
360 - 362 Arrastres 2	1.1E-03	5.8E-04	6.2E-03		3.9E-02	4.4E-03	2.9E-02	1.3E-03	3.1E-03
360 - 362 Arrastres 3	1.1E-03	5.7E-04	6.7E-03		3.9E-02	4.4E-03	2.9E-02	1.3E-03	3.1E-03
380 - 382 Arrastres 1	1.2E-03	5.6E-04	6.7E-03		3.3E-02	4.0E-03	2.7E-02	1.3E-03	2.6E-03
380 - 382 Arrastres 2	1.2E-03	5.6E-04	6.3E-03		3.3E-02	4.7E-03	2.8E-02	1.2E-03	3.2E-03
380 - 382 Arrastres 3	1.2E-03	5.3E-04	5.6E-03	9.4E-05	3.3E-02	4.6E-03	2.8E-02	1.2E-03	3.1E-03
404 - 406 Arrastres 1	1.9E-03	1.2E-03	1.6E-02		1.2E-02	3.6E-03	2.0E-02	1.6E-03	3.5E-04

404 - 406 Arrastres 2	1.8E-03	1.2E-03	1.5E-02		1.3E-02	3.7E-03	2.1E-02	1.7E-03	6.0E-04
404 - 406 Arrastres 3	2.1E-03	1.2E-03	1.5E-02		1.4E-02	3.9E-03	2.3E-02	1.7E-03	1.0E-03
424 - 426 Arrastres 1	0.001746	0.001322	0.016985		0.006815	0.003736	0.016577	0.001797	
424 - 426 Arrastres 2	0.001749	0.001368	0.017864		0.007692	0.003069	0.017147	0.001589	
424 - 426 Arrastres 3	0.001675	0.001386	0.017661	0.000189	0.007883	0.003013	0.017533	0.001569	
440 - 442 Arrastres 1	1.6E-03	1.4E-03	1.8E-02	3.3E-04	7.3E-03	3.1E-03	1.8E-02	1.6E-03	4.2E-04
440 - 442 Arrastres 2	1.7E-03	1.5E-03	2.0E-02	5.0E-04	6.4E-03	2.5E-03	1.4E-02	1.6E-03	
440 - 442 Arrastres 3	1.7E-03	1.6E-03	2.0E-02		4.7E-03	2.2E-03	1.7E-02	1.7E-03	
460 - 462 Arrastres 1	0.001351	0.000944	0.011461	0.000249	0.026442	0.003866	0.021539	0.00139	0.001124
460 - 462 Arrastres 2	0.001375	0.000942	0.012043		0.025746	0.004102	0.023627	0.001394	0.00118
460 - 462 Arrastres 3	0.001407	0.000933	0.0119		0.025971	0.004083	0.021408	0.001446	0.001024
480 - 482 Arrastres 1	0.001618	0.001617	0.020513	0.000374	0.008603	0.001834	0.0168	0.001673	
480 - 482 Arrastres 2	0.001592	0.001466	0.019231	0.000334	0.010307	0.002925	0.014593	0.001648	
480 - 482 Arrastres 3	0.001685	0.001684	0.021344	0.000666	0.009623	0.001437	0.017134	0.001729	
500 - 502 Arrastres 1	2.0E-03	1.5E-03	2.0E-02	2.4E-04	1.1E-02	2.7E-03	1.4E-02	1.6E-03	
500 - 502 Arrastres 2	1.7E-03	1.5E-03	1.9E-02	5.8E-04	1.2E-02	2.5E-03	1.2E-02	1.6E-03	
500 - 502 Arrastres 3	2.0E-03	1.5E-03	2.0E-02		1.1E-02	3.0E-03	1.2E-02	1.7E-03	
RTC-W-220-1	1.7E-03	1.1E-03	1.3E-02	1.8E-03	5.9E-03	3.2E-03	1.1E-02	1.3E-03	7.4E-03
RTC-W-220-2	1.9E-03	1.1E-03	1.4E-02	1.7E-03	5.8E-03	3.3E-03	1.1E-02	1.3E-03	7.3E-03

Table A.89 Lourdes drill cuttings: X-ray Fluorescence results for major element

Majors	MgKa1	AlKa1	SiKa1	P Ka1	S Ka1
000 - 002 Lourdes 1	0.238447	5.15229	18.60317	0.052029	0.195803
000 - 002 Lourdes 2	0.325449	5.175692	18.76511	0.049553	0.211126
000 - 002 Lourdes 3	0.250224	5.376904	19.19744	0.05921	0.210848
020 - 022 Lourdes 1	0.143909	4.84564	21.20641	0.029311	0.221776
020 - 022 Lourdes 2	0.12805	4.677539	21.00386	0.020452	0.215629
020 - 022 Lourdes 3	0.108509	4.760353	21.29804	0.028122	0.20738
040 - 042 Lourdes 1	0.284155	5.661889	22.64366	0.038876	0.191674
040 - 042 Lourdes 2	0.191705	5.316404	22.19997	0.035143	0.214412
040 - 042 Lourdes 3	0.209732	5.452156	22.08115	0.031469	0.197591
060 - 062 Lourdes 1	0.138901	4.700972	19.92619	0.044601	0.18792
060 - 062 Lourdes 2	0.231512	4.862853	19.9913	0.043626	0.192353
060 - 062 Lourdes 3	0.231146	4.826306	20.01521	0.049329	0.199224
080 - 082 Lourdes 1	0.108581	4.067607	21.01082	0.040919	0.171737
080 - 082 Lourdes 2	0.069838	4.002416	21.12529	0.042163	0.165942
080 - 082 Lourdes 3	0.174774	4.021532	21.04132	0.040993	0.160095
100 - 102 Lourdes 1	0.122747	4.048063	19.11509	0.027559	0.167272
100 - 102 Lourdes 2	0.183532	4.1591	19.26408	0.026892	0.165653
100 - 102 Lourdes 3	0.21281	4.261624	19.85793	0.031999	0.167717
120 - 122 Lourdes 1	0.164607	4.602059	20.48174	0.032569	0.165695
120 - 122 Lourdes 2	0.145587	4.497628	20.20029	0.02535	0.194739
120 - 122 Lourdes 3	0.042087	4.091045	18.75457	0.021956	0.169873
140 - 142 Lourdes 1	0.20363	4.467691	21.05533	0.026558	0.163586
140 - 142 Lourdes 2	0.106554	4.450611	21.31714	0.027216	0.158335
140 - 142 Lourdes 3	0.04125	4.205198	20.34461	0.027862	0.155867
160 - 162 Lourdes 1	0.083319	4.584091	21.69139	0.030506	0.15979
160 - 162 Lourdes 2	0.179393	4.673981	21.97358	0.031254	0.166777
160 - 162 Lourdes 3	0.083714	4.32491	20.66871	0.021233	0.153696
180 - 182 Lourdes 1		4.012521	20.29854	0.013874	0.166388
180 - 182 Lourdes 2		3.937717	19.56111	0.007002	0.174425

180 - 182 Lourdes 3		4.136851	20.32384	0.010339	0.164823
200 - 202 Lourdes 1		4.413069	22.66482	0.009228	0.157145
200 - 202 Lourdes 2		4.316357	22.24113	0.009813	0.1664
200 - 202 Lourdes 3		4.581008	23.32961	0.01626	0.170653
220 - 222 Lourdes 1		4.479179	22.43427	0.013084	0.171354
220 - 222 Lourdes 2		4.532791	22.42747	0.01522	0.16862
220 - 222 Lourdes 3		4.571017	23.19094	0.02032	0.164308
240 - 242 Lourdes 1		4.231288	20.94296	0.00936	0.169109
240 - 242 Lourdes 2		4.333135	22.58516	0.013287	0.17765
240 - 242 Lourdes 3		4.368179	22.57778	0.013235	0.166318
260 - 262 Lourdes 1		4.319641	21.48452	0.009708	0.169445
260 - 262 Lourdes 2		4.216879	21.12597	0.010503	0.174992
260 - 262 Lourdes 3		4.166113	20.76185	0.006468	0.17332
280 - 282 Lourdes 1		4.343053	20.83226	0.002005	0.169567
280 - 282 Lourdes 2		4.567486	22.23138	0.00795	0.181363
280 - 282 Lourdes 3		4.723134	22.21429	0.010157	0.171165
300 - 302 Lourdes 1	0.530684	4.860862	18.09897	0.081469	0.134783
300 - 302 Lourdes 2	0.450798	4.622207	18.41165	0.075598	0.136233
300 - 302 Lourdes 3	0.543649	4.875995	18.67804	0.089909	0.142918
320 - 322 Lourdes 1	0.090988	4.837377	20.33774	0.036386	0.162387
320 - 322 Lourdes 2		3.030479	14.03028		0.140281
320 - 322 Lourdes 3	0.01778	4.597345	19.54999	0.026481	0.148848
340 - 342 Lourdes 1	0.333143	4.425133	17.44607	0.060913	0.144164
340 - 342 Lourdes 2	0.313657	4.679302	17.33798	0.067972	0.151923
340 - 342 Lourdes 3	0.375042	4.706354	17.76985	0.065752	0.142613
360 - 362 Lourdes 1	0.367117	4.683822	17.27413	0.08654	0.138654
360 - 362 Lourdes 2	0.417491	4.5495	17.67346	0.052716	0.152599
360 - 362 Lourdes 3	0.415602	4.692394	17.2487	0.053336	0.145609
380 - 382 Lourdes 1	0.197889	3.983431	17.26676	0.026163	0.159022
380 - 382 Lourdes 2	0.315628	4.152678	17.81876	0.02962	0.170408
380 - 382 Lourdes 3	0.343225	4.243208	18.07368	0.034636	0.162633
400 - 402 Lourdes 1	0.58305	4.069847	15.63327	0.056052	0.147803

400 - 402 Lourdes 2	0.550035	4.36205	15.74825	0.061678	0.162472
400 - 402 Lourdes 3	0.582812	4.04891	15.01843	0.049869	0.153532
420 - 422 Lourdes 1	0.408664	4.447973	15.88269	0.061111	0.140783
420 - 422 Lourdes 2	0.600597	4.57524	16.17045	0.063506	0.150939
420 - 422 Lourdes 3	0.471706	4.412618	15.7247	0.058677	0.149915
440 - 442 Lourdes 1	0.701387	4.61426	15.72336	0.054622	0.15595
440 - 442 Lourdes 2	0.919855	5.04958	16.64704	0.078323	0.146299
440 - 442 Lourdes 3	0.699171	4.620562	15.6703	0.062587	0.137727
458 - 460 Lourdes 1	0.591773	4.69553	15.69957	0.053661	0.152045
458 - 460 Lourdes 2	0.772491	5.088909	16.48064	0.073086	0.141573
458 - 460 Lourdes 3	0.857974	5.18791	16.71546	0.071173	0.15031
480 - 482 Lourdes 1	0.974529	4.577879	16.0191	0.070495	0.122243
480 - 482 Lourdes 2	1.059245	4.542803	16.38112	0.081252	0.124481
480 - 482 Lourdes 3	1.186711	4.633009	16.3908	0.075737	0.12099
500 - 502 Lourdes 1	1.021146	4.746574	15.37715	0.077789	0.134992
500 - 502 Lourdes 2	1.15225	4.850833	15.85699	0.092847	0.13282
500 - 502 Lourdes 3	0.864274	4.594035	15.41806	0.078678	0.133455
520 - 522 Lourdes 1	1.100626	4.448843	15.14795	0.081946	0.132799
520 - 522 Lourdes 2	1.037931	4.468893	15.13941	0.078527	0.132076
520 - 522 Lourdes 3	1.018604	4.416004	15.29682	0.086415	0.131025
540 - 542 Lourdes 1	0.656435	3.970082	14.29512	0.06155	0.139505
540 - 542 Lourdes 2	0.709471	3.989037	14.01407	0.058049	0.140142
540 - 542 Lourdes 3	0.893714	4.298524	14.85632	0.061212	0.147369
548 - 550 Lourdes 1	0.757663	4.186693	14.84547	0.064245	0.144596
548 - 550 Lourdes 2	1.081161	4.852687	16.05686	0.081533	0.137043
548 - 550 Lourdes 3	0.812865	4.431714	15.15095	0.071615	0.128067
RTC-W-220-6	0.753569	4.754989	30.43974	0.08789	2.366838
RTC-W-220-7	0.60229	4.727493	30.11072	0.082462	2.332471
RTC-W-220-8	0.695015	4.729598	30.13022	0.083178	2.401822

Table A.90 Lourdes drill cuttings X-ray fluorescence results for major elements continued

Majors	K Ka1	CaKa1	TiKa1	V Ka1	CrKa1	MnKa1	FeKa1
000 - 002 Lourdes 1	1.681881	4.202154	0.242089	0.007628	0.008067	0.034421	3.517262
000 - 002 Lourdes 2	1.664178	4.385637	0.258388	0.008139	0.008017	0.033061	3.573946
000 - 002 Lourdes 3	1.704541	4.267543	0.246763	0.007893	0.008132	0.033547	3.617011
020 - 022 Lourdes 1	2.092586	3.763477	0.295237	0.006907	0.008144	0.054283	2.720485
020 - 022 Lourdes 2	2.038352	3.730759	0.303839	0.003004	0.007769	0.049028	2.708655
020 - 022 Lourdes 3	2.108296	3.68536	0.305074	0.00408	0.007974	0.04859	2.644729
040 - 042 Lourdes 1	2.310197	2.081414	0.303435	0.007107	0.00866	0.044789	3.726098
040 - 042 Lourdes 2	2.343579	1.828438	0.267973	0.007222	0.008875	0.04085	3.671428
040 - 042 Lourdes 3	2.317969	1.891393	0.284358	0.006701	0.008744	0.045386	3.731429
060 - 062 Lourdes 1	1.880069	5.765817	0.245133	0.005779	0.008207	0.037166	3.141392
060 - 062 Lourdes 2	1.862392	6.694946	0.243825	0.004492	0.008223	0.033601	3.075333
060 - 062 Lourdes 3	1.852569	6.684623	0.241253	0.004542	0.008243	0.033817	3.104244
080 - 082 Lourdes 1	1.987358	6.312526	0.206994	0.005179	0.008352	0.03006	2.444966
080 - 082 Lourdes 2	1.914439	6.130382	0.192066	0.006804	0.008633	0.02992	2.518225
080 - 082 Lourdes 3	1.935048	6.384388	0.192896	0.0061	0.008994	0.030873	2.525049
100 - 102 Lourdes 1	1.951237	6.218643	0.186109	0.007138	0.008511	0.031872	2.383238
100 - 102 Lourdes 2	1.879579	6.553857	0.199886	0.007072	0.008344	0.033168	2.510531
100 - 102 Lourdes 3	1.973067	6.815536	0.217927	0.00548	0.007806	0.032652	2.434646
120 - 122 Lourdes 1	2.144685	5.34993	0.23322	0.004492	0.008166	0.037832	2.507955
120 - 122 Lourdes 2	1.973286	5.22983	0.218883	0.004042	0.007442	0.038794	2.521817
120 - 122 Lourdes 3	1.925331	5.093696	0.200848	0.00494	0.00789	0.035187	2.432781
140 - 142 Lourdes 1	2.23735	3.982227	0.228634	0.006922	0.008174	0.039078	2.565706
140 - 142 Lourdes 2	2.222288	3.98029	0.218504	0.007641	0.008734	0.038778	2.562348
140 - 142 Lourdes 3	2.148093	3.643937	0.211734	0.006721	0.00834	0.037097	2.549138
160 - 162 Lourdes 1	2.294438	3.853965	0.238519	0.006808	0.008428	0.039642	2.729306
160 - 162 Lourdes 2	2.291014	4.007025	0.246679	0.006812	0.008969	0.039317	2.768641
160 - 162 Lourdes 3	2.03175	3.430232	0.205433	0.009975	0.011344	0.042972	2.183556
180 - 182 Lourdes 1	2.231012	2.170456	0.191029	0.006291	0.010042	0.037551	2.313962
180 - 182 Lourdes 2	2.097274	2.071283	0.155289	0.008334	0.011584	0.040538	1.867486

180 - 182 Lourdes 3	2.173417	2.120067	0.150873	0.007658	0.009546	0.035851	2.215448
200 - 202 Lourdes 1	2.463624	1.465352	0.114713	0.009395	0.00985	0.032417	1.787864
200 - 202 Lourdes 2	2.42334	1.307297	0.133606	0.009248	0.010634	0.035371	1.833967
200 - 202 Lourdes 3	2.5453	1.448008	0.138918	0.008704	0.011079	0.036613	1.865741
220 - 222 Lourdes 1	2.319741	1.31687	0.167968	0.00525	0.009878	0.037433	2.071968
220 - 222 Lourdes 2	2.317144	1.32127	0.165963	0.006067	0.009982	0.037601	2.132584
220 - 222 Lourdes 3	2.408624	1.387593	0.173632	0.007057	0.010171	0.043148	2.144615
240 - 242 Lourdes 1	2.30675	1.419085	0.168825	0.009092	0.013826	0.040152	1.460371
240 - 242 Lourdes 2	2.442127	1.581175	0.136201	0.008063	0.011176	0.039553	1.802473
240 - 242 Lourdes 3	2.438023	1.578907	0.133525	0.007606	0.01081	0.039314	1.810699
260 - 262 Lourdes 1	2.246966	1.429888	0.160357	0.007495	0.010286	0.036234	2.20519
260 - 262 Lourdes 2	2.256294	1.385656	0.167029	0.008013	0.00997	0.039747	2.213716
260 - 262 Lourdes 3	2.151812	1.313303	0.146192	0.008406	0.01008	0.035906	2.177466
280 - 282 Lourdes 1	1.844147	1.392884	0.103446	0.008493	0.010055	0.025437	1.477793
280 - 282 Lourdes 2	2.021855	1.508174	0.117522	0.009363	0.010776	0.028205	1.517958
280 - 282 Lourdes 3	2.118857	1.475689	0.106414	0.010947	0.010461	0.041488	1.397026
300 - 302 Lourdes 1	1.414233	3.45238	0.4692	0.000405	0.006378	0.039282	3.347331
300 - 302 Lourdes 2	1.443712	3.077742	0.472141		0.005335	0.037114	3.055514
300 - 302 Lourdes 3	1.453011	3.436215	0.474529		0.00617	0.038388	3.081008
320 - 322 Lourdes 1	1.603137	2.918608	0.367074		0.007305	0.039989	2.360701
320 - 322 Lourdes 2	0.986754	1.676246	0.242383	0.014045	0.020051	0.053257	0.477456
320 - 322 Lourdes 3	1.434075	2.867811	0.388257		0.00636	0.03774	2.414656
340 - 342 Lourdes 1	1.275998	3.382472	0.522191		0.005071	0.041341	3.045165
340 - 342 Lourdes 2	1.286522	3.381938	0.537692		0.004204	0.042306	2.989075
340 - 342 Lourdes 3	1.27538	3.207457	0.55167		0.003649	0.045109	2.986867
360 - 362 Lourdes 1	1.207366	3.810011	0.654504		0.00238	0.048384	3.010744
360 - 362 Lourdes 2	1.248183	3.392352	0.59613		0.00162	0.04644	3.159457
360 - 362 Lourdes 3	1.2244	3.582469	0.640284		0.0019	0.049642	3.186996
380 - 382 Lourdes 1	1.35777	2.693005	0.474893		0.00513	0.046504	3.551746
380 - 382 Lourdes 2	1.352438	2.680157	0.465998		0.005303	0.047141	3.502716
380 - 382 Lourdes 3	1.376404	2.823987	0.485212		0.005073	0.050238	3.615508
400 - 402 Lourdes 1	0.879114	3.388329	0.766252			0.048569	3.338367

400 - 402 Lourdes 2	0.944534	3.489097	0.783415			0.052174	3.331552
400 - 402 Lourdes 3	0.853993	3.515666	0.768999		1.25E-05	0.053089	3.39179
420 - 422 Lourdes 1	1.013123	3.928137	0.776571			0.063616	3.109181
420 - 422 Lourdes 2	0.970093	4.598596	0.809918			0.059853	3.435728
420 - 422 Lourdes 3	0.928598	4.473521	0.819412			0.060672	3.444911
440 - 442 Lourdes 1	0.696691	3.800177	0.916988	0.000959		0.065686	3.437308
440 - 442 Lourdes 2	0.718191	4.492424	1.025526	0.00597		0.071731	3.085787
440 - 442 Lourdes 3	0.681258	3.942236	0.98609	0.002975		0.065187	3.147528
458 - 460 Lourdes 1	0.740714	3.47539	0.804054			0.058489	3.404307
458 - 460 Lourdes 2	0.865235	4.032048	0.884689	0.002738		0.06698	3.291052
458 - 460 Lourdes 3	0.863251	4.152195	0.894841	0.001736		0.067661	3.340067
480 - 482 Lourdes 1	0.604921	4.171444	0.899119	0.00485		0.061589	3.559447
480 - 482 Lourdes 2	0.59586	4.100753	0.90122	0.002554		0.060545	3.472655
480 - 482 Lourdes 3	0.584317	4.065765	0.885919	0.001149		0.058863	3.521534
500 - 502 Lourdes 1	0.65597	4.619086	1.066719	0.008267		0.069094	3.196476
500 - 502 Lourdes 2	0.658787	4.613423	1.030924	0.005253		0.067141	3.332716
500 - 502 Lourdes 3	0.649914	4.488701	0.998951	0.002703		0.065831	3.454014
520 - 522 Lourdes 1	0.410449	4.271684	1.086028	0.006215		0.073562	3.026476
520 - 522 Lourdes 2	0.423483	4.279211	1.052923	0.003817		0.071613	3.087525
520 - 522 Lourdes 3	0.412338	4.344808	1.163684	0.011408		0.075093	2.756131
540 - 542 Lourdes 1	0.678178	3.337558	0.80277			0.056932	3.733543
540 - 542 Lourdes 2	0.633541	3.28596	0.885012			0.057362	3.544727
540 - 542 Lourdes 3	0.736434	3.690492	0.89415			0.064411	3.387361
548 - 550 Lourdes 1	0.75399	3.601892	0.864675			0.060295	3.493537
548 - 550 Lourdes 2	0.771016	4.194472	0.980173	0.003287		0.068751	3.347468
548 - 550 Lourdes 3	0.771643	3.966185	0.962327	0.003168		0.063233	3.434218
RTC-W-220-6	2.442331	0.131747	0.269617	0.09363	0.010075	0.023193	2.825729
RTC-W-220-7	2.418874	0.12005	0.268604	0.093249	0.010155	0.02291	2.780955
RTC-W-220-8	2.43413	0.139391	0.262921	0.091573	0.010416	0.022992	2.801312

Table A.91 Lourdes drill cuttings: X-ray fluorescence results for trace elements

Trace	BaLa1	CoKa1	NiKa1	CuKa1	ZnKa1	GaKa1
000 - 002 Lourdes 1	1.4E-02	1.3E-03	3.4E-03	2.1E-03	9.1E-03	1.8E-03
000 - 002 Lourdes 2	5.5E-02	1.4E-03	3.9E-03	2.1E-03	9.1E-03	2.0E-03
000 - 002 Lourdes 3		1.3E-03	3.6E-03	2.2E-03	9.2E-03	1.7E-03
020 - 022 Lourdes 1		7.6E-04	2.7E-03	1.4E-03	7.6E-03	1.7E-03
020 - 022 Lourdes 2	4.1E-02	9.8E-04	2.5E-03	1.6E-03	7.9E-03	1.7E-03
020 - 022 Lourdes 3	3.3E-03	7.7E-04	2.1E-03	1.5E-03	7.4E-03	1.8E-03
040 - 042 Lourdes 1	6.7E-02	1.5E-03	3.0E-03	1.9E-03	1.0E-02	1.9E-03
040 - 042 Lourdes 2	5.3E-02	1.3E-03	3.2E-03	1.7E-03	9.6E-03	1.9E-03
040 - 042 Lourdes 3	1.1E-01	1.1E-03	3.3E-03	1.7E-03	9.7E-03	1.8E-03
060 - 062 Lourdes 1		9.3E-04	2.7E-03	1.9E-03	7.5E-03	1.8E-03
060 - 062 Lourdes 2	4.7E-02	9.9E-04	2.4E-03	1.9E-03	7.6E-03	1.8E-03
060 - 062 Lourdes 3	7.2E-02	1.0E-03	2.8E-03	1.6E-03	7.1E-03	2.0E-03
080 - 082 Lourdes 1	7.2E-02	8.0E-04	1.7E-03	1.4E-03	6.9E-03	1.4E-03
080 - 082 Lourdes 2	1.5E-01	7.9E-04	1.9E-03	1.7E-03	6.6E-03	1.5E-03
080 - 082 Lourdes 3	6.9E-02	9.9E-04	1.9E-03	1.7E-03	7.5E-03	1.4E-03
100 - 102 Lourdes 1	5.1E-02	5.9E-04	2.1E-03	1.2E-03	6.5E-03	1.4E-03
100 - 102 Lourdes 2	5.4E-02	5.4E-04	2.0E-03	1.3E-03	6.3E-03	1.5E-03
100 - 102 Lourdes 3	1.1E-01	7.7E-04	2.0E-03	1.3E-03	6.3E-03	1.4E-03
120 - 122 Lourdes 1	1.4E-01	8.2E-04	2.1E-03	1.3E-03	7.3E-03	1.4E-03
120 - 122 Lourdes 2	7.6E-02	9.0E-04	2.1E-03	1.2E-03	6.7E-03	1.6E-03
120 - 122 Lourdes 3	3.6E-02	9.2E-04	1.8E-03	1.2E-03	6.5E-03	1.7E-03
140 - 142 Lourdes 1	2.6E-02	5.9E-04	2.0E-03	1.3E-03	6.8E-03	1.7E-03
140 - 142 Lourdes 2	3.1E-02	6.7E-04	2.0E-03	1.3E-03	6.7E-03	1.6E-03
140 - 142 Lourdes 3	1.5E-01	8.8E-04	2.2E-03	1.3E-03	6.3E-03	1.7E-03
160 - 162 Lourdes 1	1.8E-01	1.2E-03	2.8E-03	1.3E-03	7.2E-03	1.6E-03
160 - 162 Lourdes 2		9.8E-04	2.6E-03	1.2E-03	6.8E-03	1.6E-03
160 - 162 Lourdes 3	1.3E-01	8.9E-04	2.7E-03	1.3E-03	6.9E-03	1.8E-03
180 - 182 Lourdes 1	2.3E-03	7.5E-04	1.7E-03	8.3E-04	5.8E-03	1.6E-03
180 - 182 Lourdes 2	4.8E-02	6.4E-04	1.4E-03	1.0E-03	6.1E-03	1.7E-03

180 - 182 Lourdes 3	7.6E-02	6.3E-04	1.7E-03	6.5E-04	5.7E-03	1.7E-03
200 - 202 Lourdes 1	1.2E-01	8.2E-04	8.4E-04	4.3E-04	4.6E-03	1.6E-03
200 - 202 Lourdes 2	1.9E-02	7.9E-04	1.2E-03	5.7E-04	4.3E-03	1.8E-03
200 - 202 Lourdes 3	6.0E-02	5.1E-04	1.1E-03	6.3E-04	4.3E-03	1.7E-03
220 - 222 Lourdes 1	1.1E-01	4.8E-04	6.8E-04	5.4E-04	5.5E-03	1.9E-03
220 - 222 Lourdes 2	1.1E-01	6.5E-04	1.1E-03	5.9E-04	5.5E-03	1.9E-03
220 - 222 Lourdes 3	5.4E-02	5.5E-04	1.1E-03	7.9E-04	5.9E-03	1.8E-03
240 - 242 Lourdes 1	8.1E-02	7.2E-04	8.1E-04	5.3E-04	4.8E-03	1.7E-03
240 - 242 Lourdes 2	7.8E-02	6.6E-04	1.0E-03	6.1E-04	5.1E-03	1.6E-03
240 - 242 Lourdes 3	7.7E-02	5.4E-04	1.0E-03	6.3E-04	4.8E-03	1.6E-03
260 - 262 Lourdes 1	1.1E-01	7.5E-04	1.0E-03	5.4E-04	5.8E-03	1.6E-03
260 - 262 Lourdes 2	9.1E-02	5.3E-04	1.2E-03	4.5E-04	6.1E-03	1.8E-03
260 - 262 Lourdes 3	1.3E-01	7.7E-04	1.3E-03	7.3E-04	6.0E-03	1.6E-03
280 - 282 Lourdes 1	6.5E-02	5.3E-04	3.2E-04	3.5E-04	3.7E-03	1.8E-03
280 - 282 Lourdes 2	1.6E-01	5.8E-04	7.0E-04	5.5E-04	4.1E-03	1.6E-03
280 - 282 Lourdes 3	7.1E-02	7.2E-04	8.1E-04	4.5E-04	3.9E-03	1.8E-03
300 - 302 Lourdes 1	1.4E-01	2.2E-03	5.4E-03	1.9E-03	7.4E-03	2.0E-03
300 - 302 Lourdes 2	1.2E-01	1.9E-03	5.5E-03	1.7E-03	6.9E-03	2.2E-03
300 - 302 Lourdes 3	1.2E-01	2.0E-03	5.6E-03	1.6E-03	7.5E-03	1.8E-03
320 - 322 Lourdes 1	1.3E-01	1.5E-03	3.5E-03	1.5E-03	5.4E-03	1.8E-03
320 - 322 Lourdes 2	1.8E-01	1.5E-03	3.4E-03	1.5E-03	5.4E-03	1.9E-03
320 - 322 Lourdes 3	1.8E-01	1.3E-03	3.4E-03	1.3E-03	5.3E-03	2.0E-03
340 - 342 Lourdes 1	1.0E-01	2.4E-03	5.2E-03	2.0E-03	7.7E-03	2.0E-03
340 - 342 Lourdes 2	1.7E-01	2.8E-03	6.0E-03	2.1E-03	7.6E-03	2.0E-03
340 - 342 Lourdes 3	2.3E-01	2.8E-03	5.6E-03	1.8E-03	7.5E-03	2.0E-03
360 - 362 Lourdes 1		3.3E-03	5.5E-03	1.8E-03	8.7E-03	1.9E-03
360 - 362 Lourdes 2	1.8E-01	3.6E-03	5.0E-03	1.6E-03	8.0E-03	2.0E-03
360 - 362 Lourdes 3	1.8E-01	3.2E-03	5.4E-03	1.7E-03	8.1E-03	2.0E-03
380 - 382 Lourdes 1	2.7E-02	2.5E-03	5.0E-03	1.6E-03	8.7E-03	1.9E-03
380 - 382 Lourdes 2	9.6E-02	2.6E-03	5.0E-03	1.7E-03	9.1E-03	1.8E-03
380 - 382 Lourdes 3	1.7E-01	3.0E-03	4.8E-03	1.5E-03	8.7E-03	1.9E-03
400 - 402 Lourdes 1	3.8E-01	5.0E-03	6.3E-03	2.0E-03	1.0E-02	1.9E-03

400 - 402 Lourdes 2	2.4E-01	5.1E-03	6.4E-03	2.1E-03	1.0E-02	1.9E-03
400 - 402 Lourdes 3	1.8E-01	4.2E-03	6.2E-03	1.8E-03	9.5E-03	2.0E-03
420 - 422 Lourdes 1	1.9E-01	4.9E-03	6.2E-03	3.6E-03	9.4E-03	2.1E-03
420 - 422 Lourdes 2	1.6E-01	4.7E-03	6.2E-03	3.7E-03	9.8E-03	2.2E-03
420 - 422 Lourdes 3	2.4E-01	4.9E-03	6.1E-03	3.9E-03	9.9E-03	2.1E-03
440 - 442 Lourdes 1	2.3E-01	5.7E-03	7.0E-03	4.0E-03	1.0E-02	2.0E-03
440 - 442 Lourdes 2	2.9E-01	6.7E-03	7.2E-03	3.7E-03	1.1E-02	2.1E-03
440 - 442 Lourdes 3	2.0E-01	6.2E-03	7.1E-03	4.2E-03	1.1E-02	2.0E-03
460 - 462 Lourdes 1	9.0E-02	5.3E-03	7.1E-03	2.6E-03	9.4E-03	2.1E-03
460 - 462 Lourdes 2	2.3E-01	5.4E-03	6.9E-03	2.5E-03	9.6E-03	2.0E-03
460 - 462 Lourdes 3	8.2E-03	5.0E-03	7.0E-03	2.8E-03	9.6E-03	2.1E-03
480 - 482 Lourdes 1	1.3E-01	5.3E-03	8.1E-03	3.8E-03	1.0E-02	1.8E-03
480 - 482 Lourdes 2	1.2E-01	5.4E-03	8.2E-03	4.0E-03	9.9E-03	1.7E-03
480 - 482 Lourdes 3	1.8E-01	5.6E-03	8.0E-03	4.4E-03	1.1E-02	1.9E-03
500 - 502 Lourdes 1	4.2E-01	6.6E-03	7.1E-03	2.7E-03	9.3E-03	1.9E-03
500 - 502 Lourdes 2	1.6E-01	7.4E-03	7.3E-03	3.1E-03	1.1E-02	2.1E-03
500 - 502 Lourdes 3	1.7E-01	7.0E-03	7.4E-03	3.1E-03	1.0E-02	2.0E-03
520 - 522 Lourdes 1	2.5E-01	6.7E-03	7.0E-03	4.1E-03	1.1E-02	1.9E-03
520 - 522 Lourdes 2	3.7E-01	6.5E-03	6.9E-03	3.0E-03	1.0E-02	2.0E-03
520 - 522 Lourdes 3	3.7E-01	7.9E-03	7.3E-03	4.6E-03	1.2E-02	2.0E-03
540 - 542 Lourdes 1	2.8E-01	7.4E-03	7.6E-03	4.0E-03	1.1E-02	2.0E-03
540 - 542 Lourdes 2	2.9E-01	7.3E-03	7.8E-03	4.0E-03	1.1E-02	2.1E-03
540 - 542 Lourdes 3	1.7E-01	7.3E-03	7.3E-03	3.3E-03	1.1E-02	2.0E-03
548 - 550 Lourdes 1	2.7E-01	7.5E-03	7.7E-03	3.0E-03	1.1E-02	1.9E-03
548 - 550 Lourdes 2	3.1E-01	7.3E-03	7.5E-03	3.5E-03	1.0E-02	2.0E-03
548 - 550 Lourdes 3	2.8E-01	7.0E-03	7.8E-03	3.9E-03	1.0E-02	2.1E-03

Table A.92 Lourdes drill cuttings: X-ray fluorescence results for trace elements continued

Trace	AsKa1	PbLa1	ThLa1	RbKa1	U La1	SrKa1
000 - 002 Lourdes 1	6.1E-04	1.3E-03	9.3E-04	1.2E-02	8.7E-05	2.5E-02
000 - 002 Lourdes 2	4.3E-04	1.3E-03	9.6E-04	1.2E-02	1.5E-04	2.6E-02
000 - 002 Lourdes 3	5.7E-04	1.2E-03	9.5E-04	1.2E-02		2.6E-02
020 - 022 Lourdes 1	5.7E-04	1.3E-03	1.2E-03	1.6E-02	5.8E-04	1.8E-02
020 - 022 Lourdes 2	5.6E-04	1.3E-03	1.2E-03	1.6E-02		1.7E-02
020 - 022 Lourdes 3	2.5E-04	1.2E-03	1.2E-03	1.5E-02	6.5E-04	1.8E-02
040 - 042 Lourdes 1	5.4E-04	1.3E-03	1.1E-03	1.5E-02		1.9E-02
040 - 042 Lourdes 2	5.0E-04	1.3E-03	1.2E-03	1.5E-02		1.8E-02
040 - 042 Lourdes 3	3.5E-04	1.2E-03	1.2E-03	1.5E-02		1.8E-02
060 - 062 Lourdes 1	2.7E-04	1.2E-03	1.1E-03	1.4E-02	3.7E-04	2.0E-02
060 - 062 Lourdes 2	4.2E-04	1.3E-03	1.2E-03	1.5E-02	4.2E-04	2.0E-02
060 - 062 Lourdes 3	5.8E-04	1.4E-03	1.2E-03	1.5E-02		1.9E-02
080 - 082 Lourdes 1	7.0E-04	1.2E-03	1.0E-03	1.3E-02	8.8E-04	2.2E-02
080 - 082 Lourdes 2	3.3E-04	1.1E-03	1.1E-03	1.3E-02	6.0E-04	2.2E-02
080 - 082 Lourdes 3	7.1E-04	1.2E-03	1.0E-03	1.3E-02	3.1E-04	2.1E-02
100 - 102 Lourdes 1	2.0E-04	1.0E-03	1.1E-03	1.4E-02	6.4E-04	2.1E-02
100 - 102 Lourdes 2	2.5E-04	1.1E-03	1.1E-03	1.4E-02	3.5E-04	2.0E-02
100 - 102 Lourdes 3	1.3E-04	1.0E-03	1.1E-03	1.4E-02		1.9E-02
120 - 122 Lourdes 1	1.9E-04	1.1E-03	1.1E-03	1.4E-02	7.0E-04	1.7E-02
120 - 122 Lourdes 2	1.0E-04	1.1E-03	1.1E-03	1.5E-02	1.4E-04	1.8E-02
120 - 122 Lourdes 3	2.7E-04	1.1E-03	1.1E-03	1.5E-02	6.0E-04	1.8E-02
140 - 142 Lourdes 1	8.4E-04	1.3E-03	1.2E-03	1.5E-02	7.0E-04	1.8E-02
140 - 142 Lourdes 2	6.4E-04	1.3E-03	1.2E-03	1.5E-02	2.7E-04	1.8E-02
140 - 142 Lourdes 3	7.9E-04	1.3E-03	1.2E-03	1.5E-02	6.4E-04	1.8E-02
160 - 162 Lourdes 1	9.5E-04	1.4E-03	1.2E-03	1.6E-02	1.6E-04	2.0E-02
160 - 162 Lourdes 2	6.1E-04	1.3E-03	1.1E-03	1.4E-02	8.3E-04	1.9E-02
160 - 162 Lourdes 3	6.2E-04	1.3E-03	1.2E-03	1.5E-02	9.3E-05	1.9E-02
180 - 182 Lourdes 1	4.9E-04	1.3E-03	1.3E-03	1.7E-02	6.0E-05	1.8E-02
180 - 182 Lourdes 2	7.1E-04	1.3E-03	1.3E-03	1.6E-02	5.1E-04	1.7E-02

180 - 182 Lourdes 3	4.9E-04	1.3E-03	1.2E-03	1.6E-02	2.1E-04	1.8E-02
200 - 202 Lourdes 1	7.9E-04	1.3E-03	1.2E-03	1.6E-02	1.0E-03	2.1E-02
200 - 202 Lourdes 2	1.9E-04	1.2E-03	1.3E-03	1.7E-02	9.0E-05	2.0E-02
200 - 202 Lourdes 3	5.9E-04	1.3E-03	1.2E-03	1.6E-02	9.1E-04	2.1E-02
220 - 222 Lourdes 1	2.9E-04	1.2E-03	1.3E-03	1.6E-02	7.9E-04	2.1E-02
220 - 222 Lourdes 2	5.0E-04	1.3E-03	1.2E-03	1.5E-02	9.5E-04	2.2E-02
220 - 222 Lourdes 3	3.5E-04	1.2E-03	1.2E-03	1.6E-02	1.2E-03	2.1E-02
240 - 242 Lourdes 1	6.3E-04	1.3E-03	1.3E-03	1.7E-02	6.3E-04	1.9E-02
240 - 242 Lourdes 2	3.8E-04	1.2E-03	1.3E-03	1.7E-02		2.0E-02
240 - 242 Lourdes 3	4.2E-04	1.2E-03	1.3E-03	1.7E-02	9.4E-04	2.0E-02
260 - 262 Lourdes 1	6.7E-04	1.3E-03	1.2E-03	1.6E-02	6.6E-04	2.2E-02
260 - 262 Lourdes 2	4.8E-04	1.2E-03	1.2E-03	1.6E-02	5.3E-04	2.2E-02
260 - 262 Lourdes 3	9.5E-04	1.4E-03	1.3E-03	1.6E-02	3.7E-04	2.1E-02
280 - 282 Lourdes 1		1.1E-03	1.1E-03	1.3E-02	1.3E-03	4.1E-02
280 - 282 Lourdes 2	4.9E-04	1.2E-03	1.1E-03	1.4E-02	1.2E-03	3.9E-02
280 - 282 Lourdes 3	3.7E-04	1.2E-03	1.1E-03	1.3E-02	7.9E-04	3.9E-02
300 - 302 Lourdes 1		1.1E-03	7.4E-04	8.8E-03	5.0E-04	4.2E-02
300 - 302 Lourdes 2		1.1E-03	7.3E-04	8.6E-03	4.3E-04	4.1E-02
300 - 302 Lourdes 3	7.9E-06	1.0E-03	7.1E-04	8.7E-03		4.1E-02
320 - 322 Lourdes 1	1.1E-04	1.1E-03	7.8E-04	9.4E-03	5.6E-04	4.3E-02
320 - 322 Lourdes 2	2.4E-05	1.1E-03	7.8E-04	9.5E-03	4.1E-04	4.5E-02
320 - 322 Lourdes 3		1.1E-03	7.5E-04	9.0E-03	2.6E-04	4.5E-02
340 - 342 Lourdes 1		1.2E-03	7.5E-04	9.0E-03	3.7E-04	4.2E-02
340 - 342 Lourdes 2		1.1E-03	7.1E-04	9.0E-03		4.1E-02
340 - 342 Lourdes 3		1.1E-03	7.2E-04	9.0E-03		4.1E-02
360 - 362 Lourdes 1		1.1E-03	6.5E-04	7.3E-03	5.9E-04	4.1E-02
360 - 362 Lourdes 2		1.0E-03	6.8E-04	8.7E-03		4.1E-02
360 - 362 Lourdes 3		1.1E-03	6.8E-04	8.1E-03	6.1E-05	4.1E-02
380 - 382 Lourdes 1	3.1E-04	1.3E-03	8.4E-04	1.1E-02		3.1E-02
380 - 382 Lourdes 2	4.2E-04	1.3E-03	8.2E-04	1.1E-02		3.0E-02
380 - 382 Lourdes 3	6.2E-04	1.3E-03	8.3E-04	1.0E-02		3.0E-02
400 - 402 Lourdes 1		1.0E-03	5.6E-04	6.7E-03		3.8E-02

400 - 402 Lourdes 2	1.8E-04	1.2E-03	5.6E-04	6.9E-03		3.9E-02
400 - 402 Lourdes 3		1.1E-03	5.3E-04	6.1E-03	4.5E-04	3.8E-02
420 - 422 Lourdes 1		1.1E-03	5.7E-04	6.4E-03	3.4E-04	4.0E-02
420 - 422 Lourdes 2		1.1E-03	5.8E-04	7.4E-03		3.9E-02
420 - 422 Lourdes 3	2.0E-04	1.2E-03	6.0E-04	6.9E-03	1.2E-04	4.0E-02
440 - 442 Lourdes 1	6.0E-05	1.1E-03	4.5E-04	4.9E-03	2.2E-04	4.1E-02
440 - 442 Lourdes 2		1.1E-03	4.4E-04	5.1E-03		4.2E-02
440 - 442 Lourdes 3	1.0E-04	1.2E-03	4.5E-04	5.0E-03		4.1E-02
460 - 462 Lourdes 1		9.5E-04	5.6E-04	6.8E-03		4.0E-02
460 - 462 Lourdes 2		1.0E-03	5.4E-04	6.2E-03		4.1E-02
460 - 462 Lourdes 3		1.0E-03	5.5E-04	6.6E-03		4.2E-02
480 - 482 Lourdes 1		1.1E-03	4.3E-04	4.8E-03	1.3E-04	4.3E-02
480 - 482 Lourdes 2	8.1E-05	9.9E-04	4.4E-04	5.1E-03		4.3E-02
480 - 482 Lourdes 3	8.8E-06	1.0E-03	4.2E-04	4.6E-03	1.1E-04	4.3E-02
500 - 502 Lourdes 1		8.9E-04	4.0E-04	4.7E-03	3.7E-05	4.2E-02
500 - 502 Lourdes 2		9.3E-04	4.3E-04	4.9E-03		4.2E-02
500 - 502 Lourdes 3		1.0E-03	3.9E-04	4.1E-03	8.5E-05	4.4E-02
520 - 522 Lourdes 1		9.5E-04	3.0E-04	3.2E-03		4.5E-02
520 - 522 Lourdes 2		9.0E-04	3.1E-04	3.4E-03		4.6E-02
520 - 522 Lourdes 3		9.5E-04	3.0E-04	3.2E-03		4.5E-02
540 - 542 Lourdes 1		1.1E-03	3.8E-04	4.1E-03		4.5E-02
540 - 542 Lourdes 2		1.0E-03	3.9E-04	4.2E-03		4.3E-02
540 - 542 Lourdes 3		9.9E-04	4.4E-04	4.6E-03	6.5E-04	4.4E-02
548 - 550 Lourdes 1	1.4E-05	1.1E-03	4.2E-04	5.0E-03		4.3E-02
548 - 550 Lourdes 2		1.0E-03	4.1E-04	4.2E-03	2.3E-04	4.3E-02
548 - 550 Lourdes 3	1.7E-04	1.1E-03	4.2E-04	4.2E-03		4.3E-02

Table A.93 Lourdes drill cuttings: X-ray fluorescence results for trace elements

Trace	Y Ka1	ZrKa1	NbKa1	MoKa1
000 - 002 Lourdes 1	3.5E-03	2.1E-02	1.3E-03	9.3E-04
000 - 002 Lourdes 2	3.7E-03	2.2E-02	1.3E-03	1.6E-03
000 - 002 Lourdes 3	3.8E-03	2.0E-02	1.4E-03	1.1E-03
020 - 022 Lourdes 1	3.4E-03	2.6E-02	1.5E-03	1.8E-03
020 - 022 Lourdes 2	3.5E-03	2.7E-02	1.5E-03	1.5E-03
020 - 022 Lourdes 3	3.6E-03	2.7E-02	1.5E-03	2.3E-03
040 - 042 Lourdes 1	3.9E-03	2.3E-02	1.5E-03	1.0E-03
040 - 042 Lourdes 2	3.8E-03	2.3E-02	1.5E-03	1.1E-03
040 - 042 Lourdes 3	3.8E-03	2.3E-02	1.4E-03	1.0E-03
060 - 062 Lourdes 1	3.6E-03	2.0E-02	1.4E-03	6.2E-04
060 - 062 Lourdes 2	3.4E-03	2.0E-02	1.4E-03	7.0E-04
060 - 062 Lourdes 3	3.5E-03	2.0E-02	1.4E-03	6.7E-04
080 - 082 Lourdes 1	3.3E-03	2.0E-02	1.2E-03	1.2E-03
080 - 082 Lourdes 2	3.3E-03	1.8E-02	1.2E-03	8.8E-04
080 - 082 Lourdes 3	3.5E-03	1.9E-02	1.3E-03	1.1E-03
100 - 102 Lourdes 1	3.6E-03	1.7E-02	1.2E-03	1.0E-03
100 - 102 Lourdes 2	3.4E-03	2.1E-02	1.3E-03	9.5E-04
100 - 102 Lourdes 3	3.6E-03	1.9E-02	1.3E-03	6.1E-04
120 - 122 Lourdes 1	3.2E-03	2.2E-02	1.3E-03	1.0E-03
120 - 122 Lourdes 2	3.4E-03	2.2E-02	1.3E-03	1.1E-03
120 - 122 Lourdes 3	3.3E-03	2.0E-02	1.3E-03	1.2E-03
140 - 142 Lourdes 1	3.2E-03	2.1E-02	1.4E-03	8.5E-04
140 - 142 Lourdes 2	3.5E-03	2.0E-02	1.4E-03	9.4E-04
140 - 142 Lourdes 3	3.4E-03	2.1E-02	1.4E-03	9.5E-04
160 - 162 Lourdes 1	3.6E-03	2.3E-02	1.5E-03	1.5E-03
160 - 162 Lourdes 2	3.4E-03	2.1E-02	1.4E-03	7.7E-04
160 - 162 Lourdes 3	3.3E-03	2.3E-02	1.5E-03	9.2E-04
180 - 182 Lourdes 1	3.3E-03	2.0E-02	1.5E-03	8.7E-04

180 - 182 Lourdes 2	3.2E-03	1.8E-02	1.3E-03	5.6E-04
180 - 182 Lourdes 3	3.4E-03	1.9E-02	1.4E-03	6.7E-04
200 - 202 Lourdes 1	3.3E-03	2.0E-02	1.3E-03	1.3E-03
200 - 202 Lourdes 2	3.3E-03	1.7E-02	1.3E-03	6.0E-04
200 - 202 Lourdes 3	3.3E-03	1.8E-02	1.4E-03	8.5E-04
220 - 222 Lourdes 1	3.2E-03	2.0E-02	1.4E-03	1.4E-03
220 - 222 Lourdes 2	3.2E-03	1.8E-02	1.4E-03	1.1E-03
220 - 222 Lourdes 3	3.0E-03	2.3E-02	1.4E-03	1.8E-03
240 - 242 Lourdes 1	3.0E-03	1.6E-02	1.4E-03	2.8E-04
240 - 242 Lourdes 2	3.2E-03	1.6E-02	1.3E-03	2.2E-04
240 - 242 Lourdes 3	3.0E-03	1.7E-02	1.4E-03	4.6E-04
260 - 262 Lourdes 1	3.2E-03	1.7E-02	1.3E-03	4.4E-04
260 - 262 Lourdes 2	3.2E-03	1.7E-02	1.4E-03	7.7E-04
260 - 262 Lourdes 3	3.1E-03	1.7E-02	1.4E-03	5.1E-04
280 - 282 Lourdes 1	3.3E-03	1.2E-02	1.2E-03	1.1E-03
280 - 282 Lourdes 2	3.0E-03	1.3E-02	1.2E-03	5.7E-04
280 - 282 Lourdes 3	3.1E-03	1.3E-02	1.2E-03	5.3E-04
300 - 302 Lourdes 1	3.9E-03	2.5E-02	1.2E-03	2.7E-03
300 - 302 Lourdes 2	3.8E-03	2.5E-02	1.1E-03	2.3E-03
300 - 302 Lourdes 3	4.0E-03	2.4E-02	1.2E-03	2.3E-03
320 - 322 Lourdes 1	3.4E-03	2.1E-02	1.1E-03	1.9E-03
320 - 322 Lourdes 2	3.5E-03	2.1E-02	1.2E-03	2.2E-03
320 - 322 Lourdes 3	3.5E-03	1.9E-02	1.1E-03	1.7E-03
340 - 342 Lourdes 1	4.1E-03	2.5E-02	1.2E-03	2.5E-03
340 - 342 Lourdes 2	4.1E-03	2.5E-02	1.2E-03	2.9E-03
340 - 342 Lourdes 3	4.2E-03	2.5E-02	1.2E-03	2.7E-03
360 - 362 Lourdes 1	3.9E-03	2.7E-02	1.2E-03	3.3E-03
360 - 362 Lourdes 2	4.6E-03	2.3E-02	1.1E-03	2.5E-03
360 - 362 Lourdes 3	3.8E-03	2.6E-02	1.2E-03	2.6E-03
380 - 382 Lourdes 1	3.9E-03	2.2E-02	1.2E-03	1.6E-03
380 - 382 Lourdes 2	3.9E-03	2.3E-02	1.3E-03	1.7E-03
380 - 382 Lourdes 3	3.7E-03	2.1E-02	1.3E-03	1.3E-03

400 - 402 Lourdes 1	4.1E-03	2.5E-02	1.1E-03	2.4E-03
400 - 402 Lourdes 2	4.4E-03	2.6E-02	1.1E-03	3.1E-03
400 - 402 Lourdes 3	3.9E-03	2.5E-02	1.1E-03	3.1E-03
420 - 422 Lourdes 1	4.6E-03	2.5E-02	1.1E-03	3.1E-03
420 - 422 Lourdes 2	4.3E-03	2.6E-02	1.1E-03	2.9E-03
420 - 422 Lourdes 3	3.9E-03	2.6E-02	1.1E-03	2.5E-03
440 - 442 Lourdes 1	4.0E-03	2.4E-02	1.1E-03	3.0E-03
440 - 442 Lourdes 2	4.2E-03	2.5E-02	1.0E-03	3.5E-03
440 - 442 Lourdes 3	3.9E-03	2.8E-02	1.0E-03	3.4E-03
460 - 462 Lourdes 1	4.2E-03	2.5E-02	1.0E-03	2.8E-03
460 - 462 Lourdes 2	3.9E-03	2.4E-02	1.1E-03	2.5E-03
460 - 462 Lourdes 3	4.5E-03	2.4E-02	1.1E-03	2.9E-03
480 - 482 Lourdes 1	3.8E-03	2.5E-02	1.0E-03	3.0E-03
480 - 482 Lourdes 2	3.8E-03	2.3E-02	1.1E-03	3.0E-03
480 - 482 Lourdes 3	3.9E-03	2.3E-02	1.0E-03	3.0E-03
500 - 502 Lourdes 1	3.7E-03	2.1E-02	9.2E-04	2.7E-03
500 - 502 Lourdes 2	3.9E-03	2.1E-02	9.4E-04	2.5E-03
500 - 502 Lourdes 3	3.8E-03	2.1E-02	9.3E-04	2.6E-03
520 - 522 Lourdes 1	4.0E-03	2.2E-02	9.4E-04	2.1E-03
520 - 522 Lourdes 2	4.0E-03	1.9E-02	9.5E-04	2.1E-03
520 - 522 Lourdes 3	4.2E-03	2.2E-02	1.0E-03	2.2E-03
540 - 542 Lourdes 1	3.9E-03	2.2E-02	1.0E-03	2.3E-03
540 - 542 Lourdes 2	4.3E-03	2.4E-02	1.0E-03	2.8E-03
540 - 542 Lourdes 3	4.0E-03	2.4E-02	9.9E-04	2.9E-03
548 - 550 Lourdes 1	4.3E-03	2.3E-02	9.8E-04	2.7E-03
548 - 550 Lourdes 2	4.2E-03	2.3E-02	1.0E-03	2.4E-03
548 - 550 Lourdes 3	4.2E-03	2.3E-02	1.1E-03	2.4E-03